

Report

P-17-20

March 2019



Hydraulic interference tests in KFR27, KFR103, and KFR105

Site investigation SDM-PSU

Johan Harrström

Sofia Hedberg

Johan Öhman

SVENSK KÄRNBRÄNSLEHANTERING AB

SWEDISH NUCLEAR FUEL
AND WASTE MANAGEMENT CO

Box 3091, SE-169 03 Solna
Phone +46 8 459 84 00
skb.se

SVENSK KÄRNBRÄNSLEHANTERING

ISSN 1651-4416

SKB P-17-20

ID 1586231

March 2019

Hydraulic interference tests in KFR27, KFR103, and KFR105

Site investigation SDM-PSU

Johan Harrström, Sofia Hedberg, Johan Öhman
Geosigma AB

Keywords: Interference test, KFR27, KFR103, KFR105, Transient, Hydraulic response, SBA structures, SFR.

This report concerns a study which was conducted for Svensk Kärnbränslehantering AB (SKB). The conclusions and viewpoints presented in the report are those of the authors. SKB may draw modified conclusions, based on additional literature sources and/or expert opinions.

Data in SKB's database can be changed for different reasons. Minor changes in SKB's database will not necessarily result in a revised report. Data revisions may also be presented as supplements, available at www.skb.se.

A pdf version of this document can be downloaded from www.skb.se.

© 2019 Svensk Kärnbränslehantering AB

Abstract

This report includes the execution, analysis and results of hydraulic interference tests. The tests were carried out between December 2015 to April 2016, to build confidence in previously modelled hydraulic connections, so-called SBA structures, within the SDM-PSU site investigation. The interference tests were performed in five borehole intervals that have been selected based on previously modelled structural intercepts, two intervals of KFR27, two intervals of KFR103, and one interval in borehole KFR105. Hydraulic responses to the pumping could be observed in surrounding packed-off borehole intervals, which are continuously monitored in terms of groundwater level (or more precisely, Point-Water Head; PWH). The identified responses are characterized in terms of response indices and hydraulic properties based on transient evaluation. Finally, the interpreted results are presented in terms of a response matrix together with 3D-images of modelled hydraulic structures.

The uppermost interference test in KFR27 (47.0–57.0 m) targeted the structure SBA1; although the test yielded a few responses in nearby borehole sections, none supported the structure SBA1. The lower test in KFR27 (189.4–194.4 m) targeted the structure SBA6, which was confirmed by distinct and fast responses in the observation intervals associated to the target structure. Both of the tests conducted in KFR103 (83.5–93.5 m and 177.0–187.0 m, respectively), confirmed the expected responses according to the modelled structures. The strongest and most rapid response to the shallow KFR103 test (83.5–93.5 m) occurred in KFR27:2, while the strongest and most rapid responses in the deep KFR103 test (177.0–187.0 m) occurred in HFR106:2 and KFR106:2. For the single test in KFR105 (120.0–137.0 m), the strongest and most rapid responses occurred in KFR103:2.

The interference test in KFR27 necessitated the de-installation of its monitoring system. The removal of the deepest packer (109–110 m borehole length) caused a large-scale disturbance that could be monitored in several borehole sections that are associated to the structure SBA6. This unintentional interference confirms the conceptualization of the investigated area, where the vertical hydraulic connectivity is interpreted to be limited.

Sammanfattning

Denna rapport innefattar utförande, analys och resultat från de hydrauliska interferenstester som utfördes mellan december 2015 och april 2016 i syfte att bekräfta de hydrauliska förbindelser, så kallade SBA-strukturer, som modellerats inom platsundersökningsområdet för SDM-PSU. Interferenstesterna utfördes i fem borrhålsintervall som valts ut utgående från tolkade skärningspunkter med identifierade hydrauliska strukturer (två sektioner i KFR27, två i KFR103 och en i KFR105). Hydrauliska responser till pumpningen kunde observeras i omgivande borrhålssektioner, vilka övervakas kontinuerligt med avseende på grundvattennivå (*Eng.* Point-Water Head; PWH).

För utvärdering av hydrauliska parametrar och responsindex för de responderande observationssektionerna tillämpades transient tolkningsmetodik. Slutligen sammanställdes en sammanfattande responsmatris och 3D-bilder för responserna i observationssektionerna.

Den översta interferenstesten i KFR27 (47,0–57,0 m) avsåg strukturen SBA1. Trots ett flertal responser i omkringliggande borrhålssektioner uteblev stöd för den avsedda strukturen SBA1. Däremot bekräftade den undre testen i KFR27 (189,4–194,4 m) strukturen SBA6 med distinkta, snabba responser i de observationssektioner som förknippas med strukturen. Båda testerna i KFR103 (83,5–93,5 m samt 177,0–187,0 m) bekräftade de avsedda strukturerna (SBA2-5). Den snabbaste och mest distinkta responsen i det övre testet av KFR103 (83,5–93,5 m) erhöles i KFR27:2, medan den snabbaste och mest distinkta responsen i det undre testet (177,0–187,0 m) erhöles i HFR106:2 and KFR106:2. Den snabbaste och mest distinkta responsen i testet KFR105 (120,0–137,0 m) erhöles i KFR103:2.

Vid förberedelserna inför interferenstest avinstallerades det befintliga övervakningssystemet i KFR27, varvid avinstallation av den understa manscheten (109–110 m borrhålslängd) orsakade en storskalig störning som kunde observeras i flera borrhålssektioner och förknippas med strukturen SBA6. Denna oavsiktliga interferens styrker tolkningen av att den vertikala förbindelsen i det undersökta området är begränsad.

Contents

1	Introduction	7
2	Objective and scope of work	9
3	Methodology and evaluation	11
3.1	General method of test evaluation	11
3.2	Data filtering	11
3.3	Pumping boreholes	14
3.4	Observation boreholes	14
3.5	Response analysis	15
4	Execution of the hydraulic interference tests	17
4.1	Test procedure	17
4.1.1	Procedure and equipment in KFR27 and KFR103	17
4.1.2	Procedure in KFR105	19
4.1.3	Monitoring equipment in observation boreholes	19
4.2	Description of test performance	19
4.2.1	Interference test in KFR27: 47.00–57.00 m	19
4.2.2	Interference test in KFR27: 189.40–194.40 m	20
4.2.3	Interference test in KFR103: 83.50–93.50 m	20
4.2.4	Interference test in KFR103: 177.00–187.00 m	20
4.2.5	Interference test in KFR105: 120.00–137.00 m	20
5	Results of the interference tests	21
5.1	Response analysis of the observation sections	22
5.2	Transient evaluation of the interference tests	27
5.3	Interference test in KFR27: 47.0–57.0 m	27
5.4	Interference test in KFR27: 189.4–194.4 m	29
5.5	Interference test in KFR103: 83.5–93.5 m	30
5.6	Interference test in KFR103: 177.0–187.0 m	32
5.7	Interference test in KFR105: 120.0–137.0 m	33
6	Summary of results	35
	References	45
Appendix 1	Linear plots of hydraulic pressure versus time for pumping boreholes and hydraulic head versus time for responding observation sections, together with barometric pressure and sea level data	47
Appendix 2	Hydraulic interference test diagrams	95
Appendix 3	Observation borehole sections	121
Appendix 4	Filtered and non-filtered responses in observation sections	125

1 Introduction

The final repository for low and intermediate level radioactive operational waste (SFR) was constructed and taken into operation in 1987. An investigation program for an extension of SFR (Projekt Utbyggnad SFR; PSU) was initiated by the Swedish Nuclear Fuel and Waste Management Company (SKB) in 2008 (SKB 2008). The interpretation of conducted investigations resulted in a conceptual Site Descriptive Model (SDM) of the bedrock hosting SFR (SKB 2012).

The SDM included six so-called Shallow Bedrock Aquifer structures (SBA) (Öhman et al. 2012). To build confidence in the existence of the SBA structures interference tests were conducted between December 2015 to April 2016 in five selected borehole intervals; two intervals in KFR27, two intervals in KFR103, and one interval in KFR105. KFR27 and KFR103 are subvertical boreholes drilled from the surface whereas KFR105 is a sub-horizontal, underground borehole drilled from the SFR-tunnel (Nedre ByggTunnel; NBT) at a depth of about 106 m below sea level.

Pressure responses during the interference tests were recorded by borehole loggers connected to SKB's Hydro Monitoring System (HMS) or by other, non-connected, loggers installed in the nearby boreholes. This report describes the execution, analysis and results of the hydraulic interference tests. Data and results are also available in the SKB database, Sicada.

Table 1-1. Controlling documents for performance of the activity.

Activity plan	Number	Version
Injektions- och interferenstester i KFR27, KFR103, KFR105	AP SFR-15-002	1.1
Method descriptions	Number	Version
Metodinstruktion för analys av injektions- och enhålspumptester	SKB MD 320.004	2.0
Metodbeskrivning för hydrauliska enhålspumptester	SKB MD 321.003	2.0
Metodbeskrivning för interferenstester	SKB MD 330.003	2.0

This work was carried out in accordance with specified controlling documents and activity plan (AP SFR-15-002). It is noted that an additional interference test was run in KFR103 at position 177.0–187.0 m borehole length. Hydraulic responses from the interference tests were monitored in the following packed-off borehole sections: KFR04, KFR05, KFR07B, KFR13, KFR27, KFR55, KFR101, KFR102A, KFR102B, KFR103, KFR104, KFR105, KFR106, HFR101, HFR102, HFR105, HFR106, HFM34, HFM35, KFM11A (Figure 1-1). Monitored sections are specified in Appendix 3.

Table 1-2. Data for the boreholes used for interference tests.

Borehole	Depth (m)	Diameter (m)	Inclination (° from horizontal)
KFR27	501.64	0.076	87.4
KFR103	200.5	0.076	54
KFR105	306.8	0.076	10

2 Objective and scope of work

The objective of the interference tests was to investigate previously modelled hydraulic connection in so-called SBA-structures (Shallow Bedrock Aquifer) at the SFR-site (Odén et al. 2014). The following investigations are presented in the presented report

- 1) Five constant-flow rate hydraulic interference tests in packed-off sections of KFR27, KFR103 and KFR105, Figure 2-1).
- 2) Hydraulic responses in surrounding borehole sections during within the SFR Regional model domain caused by the interference tests.

Hydraulic properties and response indices were determined for observed responses that fulfill the response criterion (i.e. the maximum drawdown, $s_p \geq 0.1$ m). Finally, a resulting response matrix was prepared for the interference tests. Technical data for the pumping tests in boreholes KFR27, KFR103 and KFR105 are presented in table 2-1.

The pumping time for each test was about 72 hours followed by a recovery period of the same magnitude. The interference tests were designed according to results from previous investigations concerning the SBA-structures of interest (Walger et al. 2010).

The array of analysed observation borehole sections in the five interference tests are listed in Appendix 3. Data from HMS (Hydro Monitoring System) was extracted to provide information about the water level conditions prior to, during, and after the interference tests. HMS monitors the water level continuously in the boreholes (i.e. or, more precisely, point-water head). In most boreholes the upper part has a casing to a certain length. This casing length is included in the upper section.

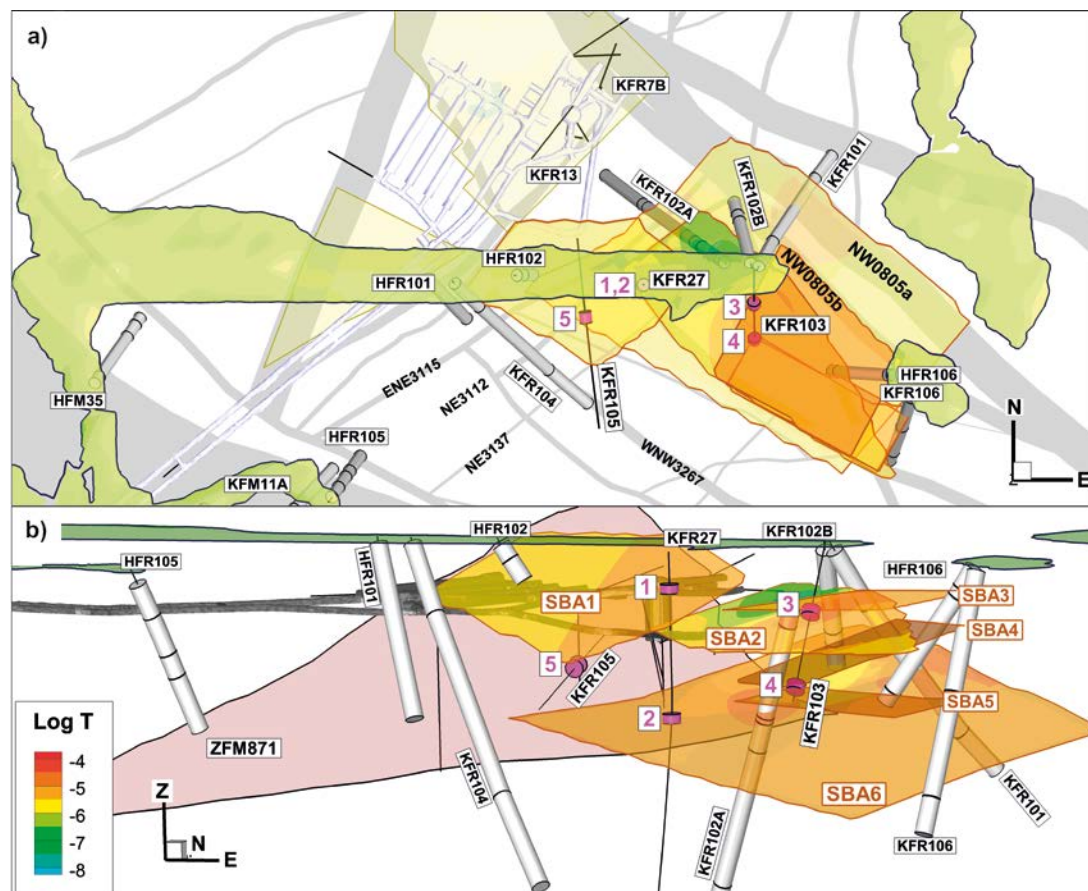


Figure 2-1. Overview of the interference-test setup (packed-off intervals indicated by pink cylinders), target SBA structures (contoured by modelled transmissivity), and observation borehole sections (white cylinders); a) top view, b) view towards northwest.

3 Methodology and evaluation

3.1 General method of test evaluation

Standard methods were used for transient evaluation of responses to constant-flow interference tests that rely on the approximation of the rock mass as an equivalent porous medium. The hydraulic properties (e.g. transmissivity and storativity) of the pumped sections were also evaluated according to theories for single-hole tests in an equivalent porous medium where the pumped flow is assumed to be uniformly distributed in the test section. The transient evaluation of the flow/pressure history accounted for wellbore storage effects and skin.

The transient analyses employ the software AQTESOLV Pro v. 4.5 (Hydrosolve, Inc.) that enables both manual and automatic type curve matching. The analysis was carried out as an iterative process of manual type-curve matching and automatic non-linear regression. The estimation of the hydraulic parameters was normally based on the identified pseudo-radial flow regime and associated flow regimes during the tests, e.g. pseudo spherical (leaky) flow. The flow regimes were derived from diagnostic analysis of the transient responses.

3.2 Data filtering

All monitored hydraulic head data (i.e. point water head, PWH) in the observation borehole sections involve an automatic correction for atmospheric pressure changes in HMS by subtracting the barometric pressure from the total pressure. Except for the test in KFR105, the pressure in the pumping boreholes has not been corrected for atmospheric pressure changes. Such effects generally have a little effect on the drawdown in the pumping borehole.

As the interference tests were performed below sea level, the monitored groundwater levels were strongly affected by fluctuations in sea levels and changes in air pressure (see Öhman et al. 2012, Figure 3-1). This background noise in monitored head may complicate the identification of responses and the estimation of the response time lag, dt_L (s). The background noise was reduced by means of a multiple-regression approach.

The correlation between monitored levels and sea level/air pressure depends on the depth of borehole sections (Figure 3-1), where the top-located sections (open) are considerably more correlated to the sea level compared to the deeper located sections in the same borehole. Deep-located sections are more negatively correlated to the air pressure, which is due to an underlying assumption of full barometer effect in the automatic computed groundwater level (i.e. an unrealistic assumption in the instantaneous air-pressure subtraction from the monitored total pressure). Note that even if the sea level is partly influenced by air pressure (mesoscale weather phenomena), it is also affected by wind, wind direction, and tide.

The sea level and air pressure varied substantially during the interference tests, c. 0.1–0.3 m, relative to the response criteria for drawdown, set to $s_p = 0.1$ m (Figure 3-2). For that reason the interpretation of the responses and test results was performed in two steps: 1) direct interpretation of pressure levels with “manual” consideration to sea level/air pressure changes and 2) interpretation on de-trended time series, where the influence from sea level/air pressure are reduced by multiple regression (Figure 3-3) to get a higher resolution on eventual responses.

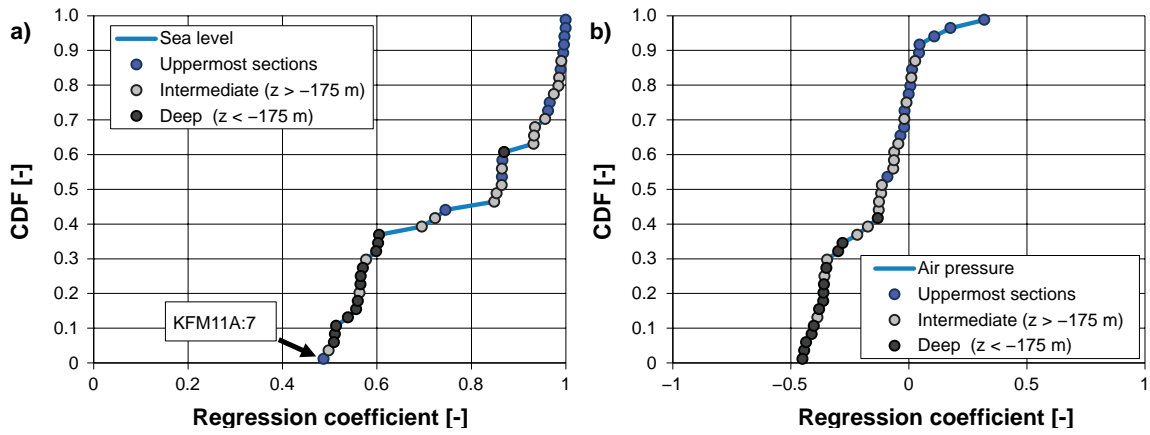


Figure 3-1. Multiple regression between groundwater pressure and environmental factors during a previous two months period (based on monitored pressure in 42 borehole sections). Regression coefficients for a) sea level and b) barometer pressure. The top sections are most influenced by the sea level (blue dots), whereas the deepest sections are negative correlated to air-pressure (i.e. assumptions of full barometer effect). Note that the top section in KFM11A, which is drilled from Stora Aspehällan, has a small correlation to the sea level.

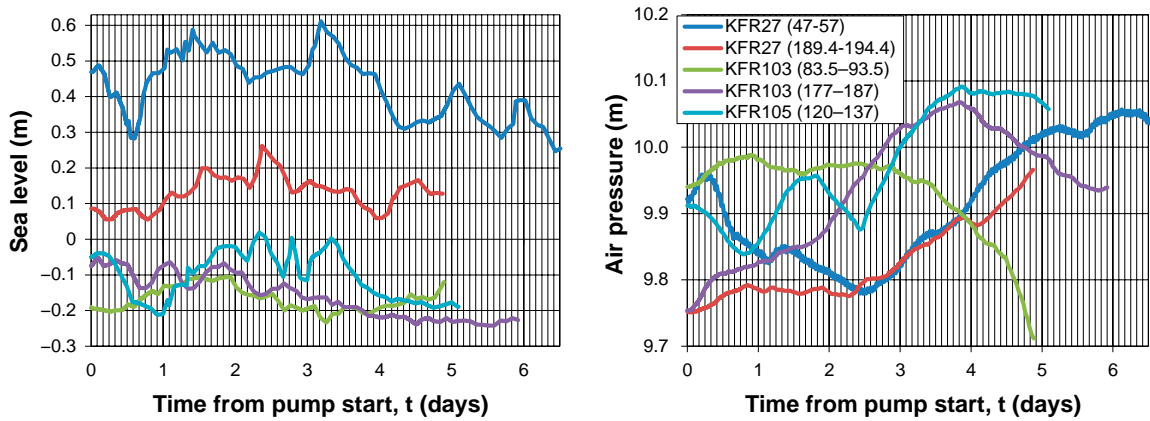


Figure 3-2. Fluctuations in sea level and changes in air pressure during the interference tests.

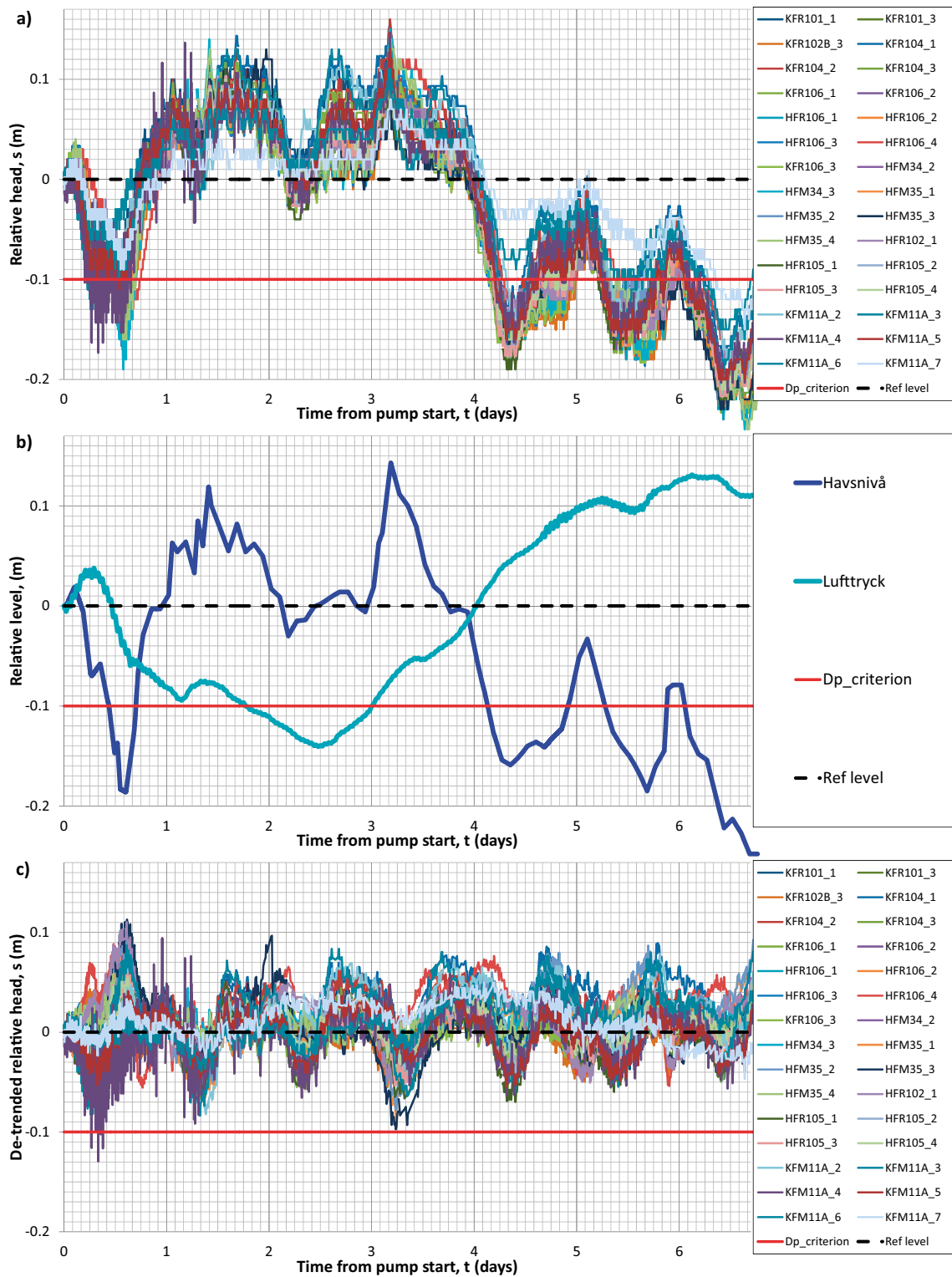


Figure 3-3. Principle for filtering data from components from variations in sea level and air pressure, demonstrated for non-responding sections for the test in KFR27 (47–57 m); a) monitored pressure levels, b) sea levels and air pressure, and c) filtered pressure based on multiple regression.

3.3 Pumping boreholes

Prior to the transient analysis, interpretation of the transmissivity based on the assumption of stationary conditions in the pumping boreholes was performed according to Moye's formula (Equation 3-1).

$$T_M = \frac{Q_p \cdot \rho_w \cdot g}{dp_p} \cdot C_M \quad \text{Equation 3-1}$$

$$C_M = \frac{1 + \ln\left(\frac{L_w}{2r_w}\right)}{2\pi}$$

Q_p = flow rate by the end of the flow period (m^3/s)

ρ_w = density of water (kg/m^3)

g = acceleration of gravity (m/s^2)

C_M = geometrical shape factor (-)

$dp_p = p_p - p_i$ (Pa)

r_w = borehole radius (m)

L_w = section length (m)

The transmissivity and skin factor of the pumping borehole were obtained from transient analysis based on the diagnostic analysis of flow regimes. The storativity, S [-], was estimated according to Equation 3-2. This is an empirical regression relationship between storativity and transmissivity (Rhén et al. 1997) in which the transmissivity, T , has the unit [m^2/s].

$$S = 0.0007 \cdot T^{0.5} \quad \text{Equation 3-2}$$

The wellbore storage coefficient, C_{WBS} [m^3/Pa], in an isolated pumping borehole section can be obtained from the estimated fictive casing radius, $r(c)$ [m], in an equivalent open test system according to Equation 3-3.

$$C_{WBS} = \frac{r(c)^2}{g} \quad \text{Equation 3-3}$$

The radius of influence at a certain time during the test may be estimated from Jacob's approximation of the Theis' well function according to Equation 3-4. This approximation assumes a cylindrical flow regime in a completely penetrating well in a horizontal porous medium.

$$r_i = \sqrt{\frac{2.25 \cdot T \cdot t}{S}} \quad \text{Equation 3-4}$$

Where r_i [m] is the radius of influence at time t [s] after start of pumping, usually at stop of pumping.

3.4 Observation boreholes

Data from all the observation borehole sections considered were included in the diagnostic analysis, where linear plots of head versus time were studied to identify potential responses. However, only responses where the maximum drawdown, s_p (m), exceeds 0.1 m were included in the analysis. Corresponding diagrams of air pressure and sea-level fluctuations were also used in the diagnostic analysis to assist the identification of responding sections. After a first inspection of non-filtered data, all further analyses were made on de-trended data (i.e. where the noise from sea and air-pressure fluctuation is reduced).

The observation sections were divided into three groups: responding sections, low-confidence responding sections, and non-responding sections. The first group, responding sections, exhibits clear response and recovery phases and fulfills the response criterion ($s_p \geq 0.1$ m). A few sections with clear responses, but with a maximum drawdown barely below 0.1 m, were also included in this group of responding sections. The second group, of low-confidence responses, includes observations that either do not fulfill the response criterion or do not exhibit clear recovery. No further analysis was made for these sections. The last group, non-responding sections, refer to sections where no response at all could be seen.

In the transient evaluation of hydraulic properties for clear responses, standard methods were employed to determine transmissivity and storativity (Kruseman and de Ridder 1991). Transient evaluation of hydraulic parameters was performed for the pumped borehole sections and for a few selected responses of particular interest. The apparent hydraulic diffusivity of responses (i.e. pressure-propagation rate) can usually be estimated from the response time dt_L , defined for a standard drawdown criterion of 0.01 m. However, the standard drawdown criterion was not applicable owing to the prevailing noise level in monitored head, and therefore it was not meaningful to calculate hydraulic diffusivity (T/S) from these parameters in this case.

The evaluation of the dominating transient flow regimes, i.e. pseudo-linear flow (PLF), pseudo-radial flow (PRF), and pseudo-spherical flow (PSF), and outer hydraulic boundary conditions was mainly based on diagnostic plots with logarithmic scaling. In particular, PRF is reflected by a constant (horizontal) derivative, whereas apparent No-Flow- (NFB) and Constant-Head Boundaries (CHB) are characterized by a rapid increase and decrease in the derivative, respectively. Based on the diagnostic analysis, relevant models were selected for the transient evaluation of the responses.

3.5 Response analysis

Responding sections where the drawdown, s_p [m], exceeds the response criterion ($s_p > 0.1$ m) are evaluated by means of so-called response indices 1 and 2-new (defined below). These indices represent the speed of propagation rate and strength of the responses, respectively, which in turn are assumed to characterize the hydraulic connection between the pumping and the observation sections. Index 1 is directly related to the hydraulic diffusivity (T/S) of the formation. The apparent hydraulic diffusivity ($D_a = T_o/S_o$) is also evaluated based on transient evaluation of the responses. The maximal drawdown, s_p [m], occurred in several observation sections long after the pumping had stopped indicating a fracture system which is remotely connected to the pumped sections.

The response time, dt_L [s], is defined as the time lag after start of pumping until the response exceeds 0.1 m in the observation section. This criterion was used for calculating the response indices. The pumping flow rate, Q_p [m³/s], was used in combination with the response time (dt_L), spherical distance between the pumped borehole section and the responding borehole section, r_s [m], and maximum drawdown s_p [m] to calculate the response indices 1 and 2-new. The spherical distance is calculated from the midpoints of the pumped borehole section and the observation sections. The response indices were calculated as follows:

Index 1 [m²/s]:

Normalized spherical distance (r_s) with respect to the response time dt_L ($s = 0.1$ m).

$$Index\ 1 = \frac{r_s^2}{dt_L} \quad \text{Equation 3-5}$$

Index 2 new [s/m²]:

Normalized maximum drawdown (s_p) with respect to the pumping rate by the end of the flow period (Q_p), also considering the distance (r_s) assuming $r_0 = 1$ m (fictive borehole radius).

$$Index\ 2\ new = \frac{s_p}{Q_p} \cdot \ln\left(\frac{r_s}{r_0}\right) \quad \text{Equation 3-6}$$

The classification of the response indices is given in Table 3-1 below.

Table 3-1. Classification of response indices based on $s_p = 0.1$ m according to SKB MD 330.003.

	Limits	Classification	Colour code
Index 1 [m²/s]	Index 1 > 100 m ² /s	Excellent	Red
	10 < Index 1 ≤ 100 m ² /s	High	Yellow
	1 < Index 1 ≤ 10 m ² /s	Medium	Green
	Index 1 ≤ 1 m ² /s	Low	Blue
	$s_p < 0.1$ m	Below limit	Light blue
Index 2 [s/m²]	Index 2 new > 5×10^5 s/m ²	Excellent	Red
	$5 \times 10^4 < \text{Index 2 new} \leq 5 \times 10^5$ s/m ²	High	Yellow
	$5 \times 10^3 < \text{Index 2 new} \leq 5 \times 10^4$ s/m ²	Medium	Green
	Index 2 new ≤ 5×10^3 s/m ²	Low	Blue
	$s_p < 0.1$ m	Below limit	Light blue

4 Execution of the hydraulic interference tests

The boreholes used in this project are all part of the ongoing monitoring programme at SFR. Thus, prior to an interference test, the installed packer system and monitoring equipment must be removed from the active borehole. The packer system and the monitoring equipment were re-installed after the completion of each interference test.

Severe corrosion damage to the installed equipment was discovered during de-installation of the packer system in KFR103. This finding suggested, retrospectively, that its head monitoring was out of order during the previous interference tests performed in KFR27. Therefore, a complementary interference test in KFR103, in the interval 177–187 m, was performed to examine if the structure SBA6 forms a hydraulic connection between KFR27 and KFR103.

4.1 Test procedure

The hydraulic interference tests were performed as pumping tests in different sections of boreholes KFR27, KFR103 and KFR105. In order to test the SBA-structures, pumping was made at specific levels or in the boreholes. Several boreholes in the vicinity of KFR27, KFR103 and KFR105 were utilized to collect hydraulic head response data before, during and after each period of pumping. A list of all observation sections used in these interference tests are listed in Appendix 3.

4.1.1 Procedure and equipment in KFR27 and KFR103

The PSS2-container and associated equipment were used for the interference tests in KFR27 and KFR103 (Figure 4-1). The container is placed on pallets in order to obtain a suitable working level in relation to the borehole casing. The hoisting rig is of a hydraulic chain-feed type. The jaws, holding the pipe string, are opened hydraulically and closed mechanically by springs. The rig is equipped with a load transmitter and the load limit may be adjusted. The maximum load is 22 kN. The packers and the test valve are operated hydraulically by water filled pressure vessels. Expansion and release of packers, as well as opening and closing of the test valve, is done using magnetic valves controlled by the software in the data acquisition system (schematic drawing of the equipment in the pumping borehole in Figure 4-2). The pipe string consists of aluminum pipes of 3 m length, connected by stainless steel taps sealed with double o-rings. Pressure is measured within (P) the test section, which is isolated by two packers. The hydraulic connection between the pipe string and the test section can be closed or opened by a test valve operated by the measurement system. The length of the test section was ten meters (except in KFR105, which employed a 17 m monitoring section, KFR105:4).

Equipment specifications concerning pumping and monitoring of the pumping boreholes are:

- Reciprocating compressor: Atlas Copco, with working pressure between 9 and 11 bar.
- Absolute pressure transducer: Druck PTX 161/D sg, ± 0.25 % accuracy.
- Flow meter: Krohne, DN40, nominal flow: 30–900 L/min, ± 1.14 % accuracy by 15 L/min, ± 12.3 % accuracy by 1.5 L/min.

The interference tests were performed as air-lift pumping tests. High-pressure compressed air was conducted through a small hose into the pipe string, which resulted in water flow from the section and up through the pipe string. The integrated water tank in the PSS-container was used to obtain an equalized flow. The pumping phase was instantaneously stopped by closing the test valve, which prevent the water to flow inside the pipe string. The drawdown and recovery as well as the flow rate in the pumping boreholes were monitored. The aim was to maintain a constant flow rate during a c. three days long pump period accompanied by an at least equally long recovery period.

The equipment above was checked before arrival on site. Also, functionality checks of the equipment were performed during on site establishment where the pressure transducers, flow meters and packer pressures were checked for reasonable values. During the first deep test in KFR27 (189.4–194.4 m), the air compressor broke down after only a few hours of pumping. After reparation of the compressor the test was restarted.

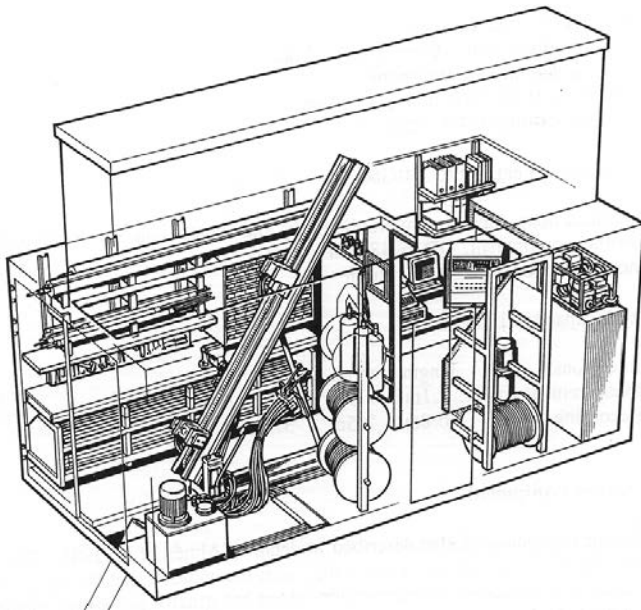


Figure 4-1. Outline of the PSS2 container with equipment.

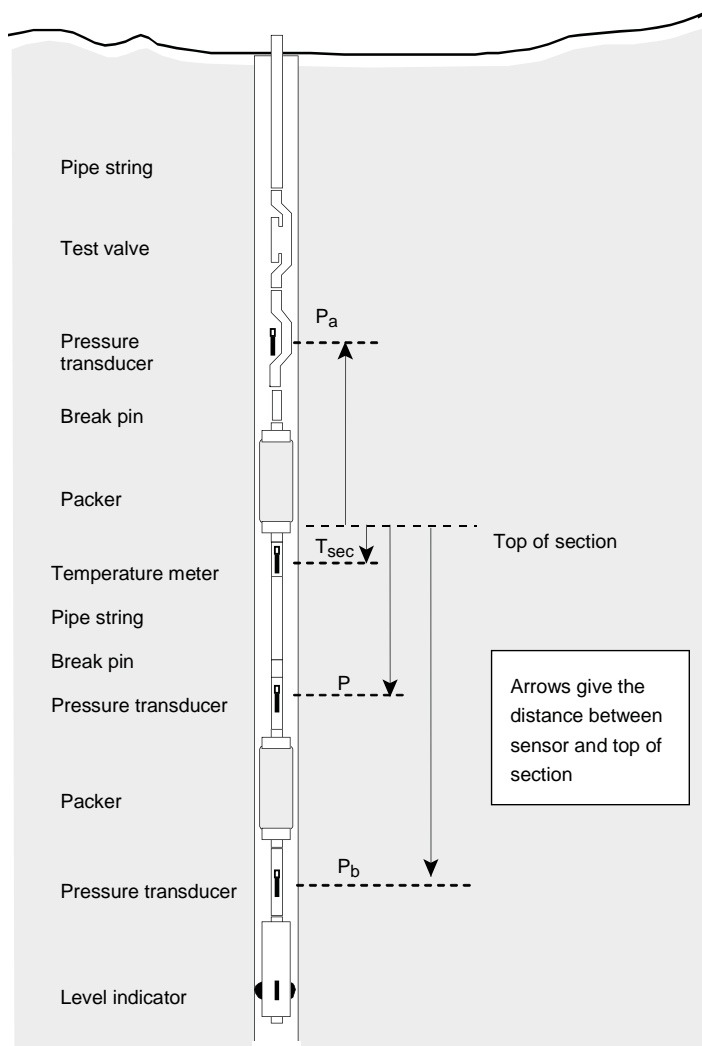


Figure 4-2. Schematic drawing of the down-hole equipment in the PSS2 system. In this project neither P_a nor P_b were used.

4.1.2 Procedure in KFR105

The interference test in the borehole section KFR105:4 in the SFR tunnel was performed using the permanently installed packer system in the borehole. Due to the hydrostatic pressure in KFR105 the test could be performed without pumping equipment. By opening a valve, the pumping section were connected to the atmospheric pressure in the tunnel. This resulted in a flow from the higher pressure inside the section to the lower pressure inside the SFR-tunnel. An interference test was consequently induced.

Equipment specifications concerning flow monitoring of the pumping boreholes are:

- Flow meter: Krohne, DN40, nominal flow: 30–900 L/min, ± 1.14 % accuracy by 15 L/min, ± 12.3 % accuracy by 1.5 L/min.

The pressure in the pumping section was monitored with the equipment of SKB's hydro monitoring system (HMS), see Section 4.1.3.

4.1.3 Monitoring equipment in observation boreholes

The interference tests utilize the ongoing monitoring of installed borehole sections at SFR which are part of the HMS monitoring programme at SFR (observation sections specified in Appendix 3). Each section is isolated by use of packers, expanded with nitrogen gas, strategically isolating specific lengths within boreholes. The isolated sections are hydraulically connected to water-level standpipes by polyamide tubes and lead-through pipes in the packers. The water-level standpipes are installed above the uppermost packer enabling easy pressure gauge maintenance and manual level measurements for each observation section.

The Point-Water Head (PWH) of each monitored borehole section is calculated based on measured total pressure, air-pressure correction (assuming full barometric effect) and known groundwater density in the standpipe.

4.2 Description of test performance

Below, the performance of each interference test is discussed with special reference to the drawdown and flow-rate conditions in the pumped borehole sections. The total drawdown and final flow rate (Q_p) in the pumped boreholes together with the duration of the pumping tests are shown in Table 4-1.

Table 4-1. Overview of the conditions for the five interference tests.

Test	Structure	borehole	Section (mbl)	Drawdown (m)	Flow rate (m ³ /s)	Pumping time (s)
1	SBA1	KFR27	47.0–57.0	7.70	4.1E–05	411 600
2	SBA6	KFR27	189.4–194.4	6.53	8.7E–05	248 520
3	SBA2-3	KFR103	83.5–93.5	3.12	4.5E–05	249 780
4 ¹⁾	SBA4-5 (SBA6)	KFR103	177.0–187.0	7.24	4.5E–05	345 420
5	Central block	KFR105	120.0–137.0	78.40	8.8E–05	267 360

1) The pumped borehole intercept has been interpreted as intercepted by SBA4-5. The primary objective of the test is to examine if KFR103 is hydraulically connected to SBA6, as the borehole instrumentation was not operative during the two preceding tests 1 and 2 (due to corrosion of the equipment).

4.2.1 Interference test in KFR27: 47.00–57.00 m

Pumping was performed during the period 2015-12-09 (16:30) to 2015-12-14 (10:50), see Figure A1-2. The final pumping rate was 2.5 L/min (4.1E–05 m³/s). The pumping rate was stable during the entire pumping phase. During the second day of pumping, water sampling was made from the pumped water, which is seen as a disturbance in the flow. The total drawdown in the pumping borehole was c. 7.7 m (76 kPa). The drawdown was stable throughout the test.

4.2.2 Interference test in KFR27: 189.40–194.40 m

Pumping was performed during the period 2016-02-23 (14:08) to 2016-02-26 (11:10), see Figure A1-18. The final pumping rate was 5.2 L/min ($8.7\text{E-}05\text{ m}^3/\text{s}$). The pumping rate was stable during the entire pumping phase. During the second day of pumping, water sampling was made from the pumped water, which is seen as a disturbance in the flow. The total drawdown in the pumping borehole was c. 6.5 m (64 kPa). The drawdown was very fast and stable throughout the test.

4.2.3 Interference test in KFR103: 83.50–93.50 m

Pumping was performed during the period 2016-04-01 (16:30) to 2016-04-04 (11:10), see Figure A1-34. The final pumping rate was 2.6 L/min ($4.5\text{E-}05\text{ m}^3/\text{s}$). The pumping rate was smoothly decreasing during the pumping phase from a rate of about 5.0 l/min at the beginning. The total drawdown in the pumping borehole was c. 3.1 m (31 kPa). The drawdown was stable throughout the test.

4.2.4 Interference test in KFR103: 177.00–187.00 m

Pumping was performed during the period 2016-04-07 (13:53) to 2016-04-11 (13:50), see Figure A1-59. The final pumping rate was 2.8 L/min ($4.5\text{E-}05\text{ m}^3/\text{s}$). The pumping rate was smoothly decreasing during the pumping phase from a rate of about 6.0 l/min at the beginning. The total drawdown in the pumping borehole was c. 7.2 m (71 kPa). The drawdown was stable throughout the test.

4.2.5 Interference test in KFR105: 120.00–137.00 m

Pumping was performed during the period 2016-04-26 (12:10) to 2016-04-29 (14:26), see Figure A1-78 and A1-79. The final pumping rate was 5.3 L/min ($8.8\text{E-}05\text{ m}^3/\text{s}$). The pumping rate was stable during the pumping phase. The total drawdown in the pumping borehole was c. 78.4 m (769 kPa). The drawdown was quick and stable throughout the test.

5 Results of the interference tests

The interference test results are divided into a response analysis and a transient evaluation. A summary of all results, including a stationary analysis, are presented in Section 6. Responses are presented in appendix 4 (i.e. both raw and de-trended head data). Measurements of air pressure and the local sea water level together with the observed pressure in the pumped boreholes and hydraulic head in all responding observation borehole sections are shown in linear (HMS)-diagrams in Appendix 1.

The de-installation (2015-11-23) and re-installation (2016-03-30) of the monitoring system in KFR27 caused an unintentional large-scale disturbance that can be observed in several monitored sections (Table 5-1, Figure 5-1). Even at the start of the first pumping test, sixteen days after de-installation, several of the monitoring sections had not yet reached full equilibrium. Thus, the first test in KFR103, which started only two days after the re-installation of KFR27, is subject to a large-scale recovery trend (see more in Section 5.1 and in Odén and Öhman 2017). No such disturbances were observed from the de-installation and re-installation in KFR103. Similarities, but in smaller scale, with responses in other monitoring sections could also be observed by inflating and deflating the packers for the test equipment during injection tests in KFR27.

For KFR105, the interference test was performed within the installed monitoring sections and de-installation of the equipment for the following injection tests were done after finishing the interference test.

Table 5-1. Monitoring sections affected by de- and re-installation of the monitoring equipment in KFR27.

Section	Section (mbI TOC)	Comment
KFR102B:1	146.0–180.8	No data from de-installation, from re-installation affected at the tests in KFR103.
KFR102B:2	128.0–145.0	
KFR102A:1	444.0–600.83	Not obvious, but probably affected. It takes about two weeks for stabilization, both tests in KFR103 affected
KFR102A:2	423.0–443.0	
KFR102A:3	255.0–422.0	Clearly affected, It takes about two weeks for stabilization, both tests in KFR103 affected
KFR102A:4	220.0–254.0	
KFR102A:5	214.0–219.0	
KFR102A:6	185.0–213.0	
KFR102A:7	103.0–184.0	Re-installation: Not obvious, but could probably affected. De-installation: no clear response.
KFR102A:8	0–102.0	
KFR101:1	279.5–341.8	Not obvious, but probably affected.
KFR101:2	91.0–278.5	Affected
KFR106:1	260.0–300.1	Slow response, but possible affected
KFR105:1	265.0–303.0	Not clearly affected, but possible.
KFR105:2	170.0–264.0	Affected. Pressure increase by re-installation and decrease by de-installation. The change in pressure is small, about 5 kPa.
KFR105:3	138.0–169.0	
KFR105:4	120.0–137.0	

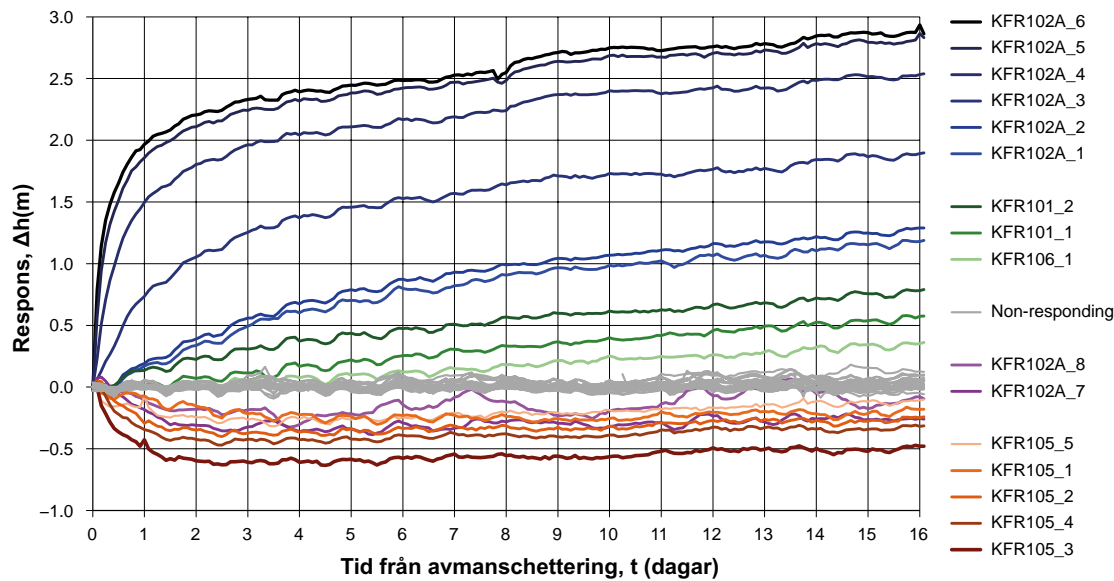


Figure 5-1. Hydraulic responses to de-installation of KFR27 (2015-11-23). No data available for KFR102B and KFR103.

5.1 Response analysis of the observation sections

The interpreted response speeds (i.e. Index 1) must be considered as rough estimates for many of the observation sections, as the fluctuations in head data complicate a rigorous determination of response time. The maximum drawdown does not always coincide with the stop of pumping, which may reflect the delay of indirect, poorly connected flow paths also seen in previous interference tests in SFR (Walger et al. 2010). The drawdown in the observation sections is determined as the maximum value, even if it occurs after the stop of pumping. The response diagram can be used to identify the observation sections with the most distinct responses.

Data from the evaluation of the responding sections from each interference test, such as distances, drawdown, time-lag and interpreted response indices are presented in Table 5-2.

As described earlier, the observation sections were divided into three categories: 1) responding sections, 2) low-confidence responses, and 3) non-responding sections (Section 3.4). Two sections (HFR106:3 and KFR102B:3) showed a clear response to the pumping in KFR103, and hence were included in the responding group, in spite of not fulfilling the response criterion, $s_p \geq 0.1$ m (i.e. unfortunately, this implies that hydraulic properties and indices cannot be defined).

The response time (dt_r) was estimated as the elapsed time where the drawdown in a monitored bore-hole section exceeds of 0.1 m (Table 5-2; Appendix 1). In some cases, fluctuations in monitored head (e.g. due to tidal effects) complicated an accurate determination of dt_r . It was possible, however, to make an approximate estimate from the drawdown curves. The estimated parameters were used to determine the two response indices (Section 1; Table 5-2), which serve as proxies for a joint characterization of speed and strength of responses (Figure 5-2 to Figure 5-6).

The upper right corner in the diagrams may be assumed to reflect well-connected responses, with high hydraulic diffusivities and distinct responses. On the other hand, delayed and small responses in the lower left corner may be assumed to reflect comparatively weak hydraulic connections. However, the magnitude of responses (i.e. Index 2-new) is primarily dominated by the presence of upstream hydraulic boundaries (Knudby and Carrera 2006), where no-flow boundaries enhance drawdown, while constant-head boundaries dampen the observed drawdown. Likewise, slow responses (i.e. Index 1) indicate poor connectivity or the presence of an apparent storativity term (e.g., dampening of a constant-head boundary).

The first test, in the upper part of KFR27 (47.0–57.0 m), gives Medium- to Low-speed indexed responses in KFR102A:3-8 and KFR105:2-4 (Figure 5-2). No response in HFR102 (i.e. which disqualifies SBA1). Note that the monitoring systems in KFR102B and KFR103 were out of order during this test (i.e. owing to corrosion damage).

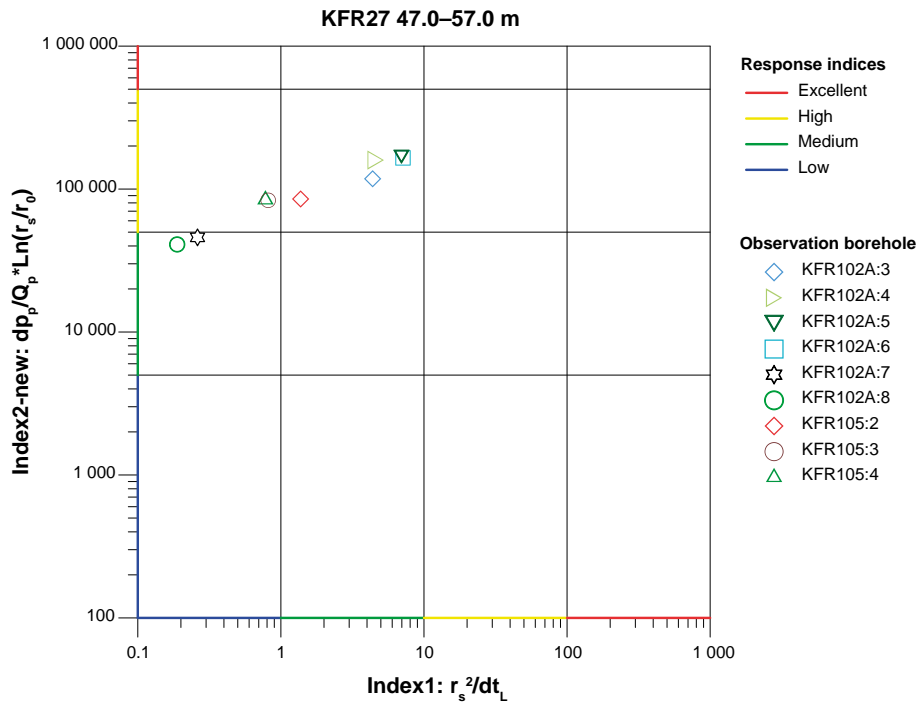


Figure 5-2. Cross plot of the response indices for the responding observation sections during the interference test in KFR27: 47.0–57.0 m.

The second test, targeting the deeper SBA6 intercept in KFR27 (189.4–194.4 m), induces High-speed indexed responses in borehole sections associated to SBA6 intercepts (Figure 5-3). Medium-speed indexed responses are also observed in other borehole sections of KFR101, KFR102A, KFR102B, and KFR105. Notably, a low-confidence response is observed in KFR106:1. Also, no response is observed in KFR104, which supports the suggested termination of SBA6. Note that the monitoring system in KFR103 was out of order during this test (i.e. owing to corrosion damage).

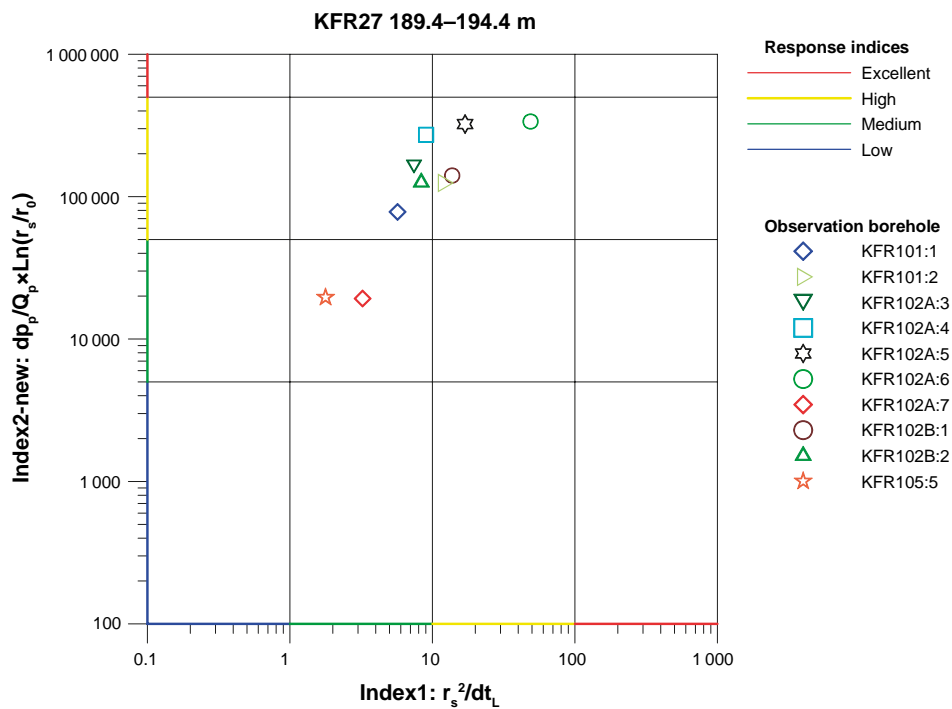


Figure 5-3. Cross plot for the response indices for the responding observation sections during the interference test in KFR27: 189.4–194.4 m.

The two tests in KFR103 (Figure 5-4 and 5-5) induce clear responses in several observation sections, but also many low-confidence responding sections. These sections coinciding by the sections affected by the de-installation in KFR27 (see Section 5).

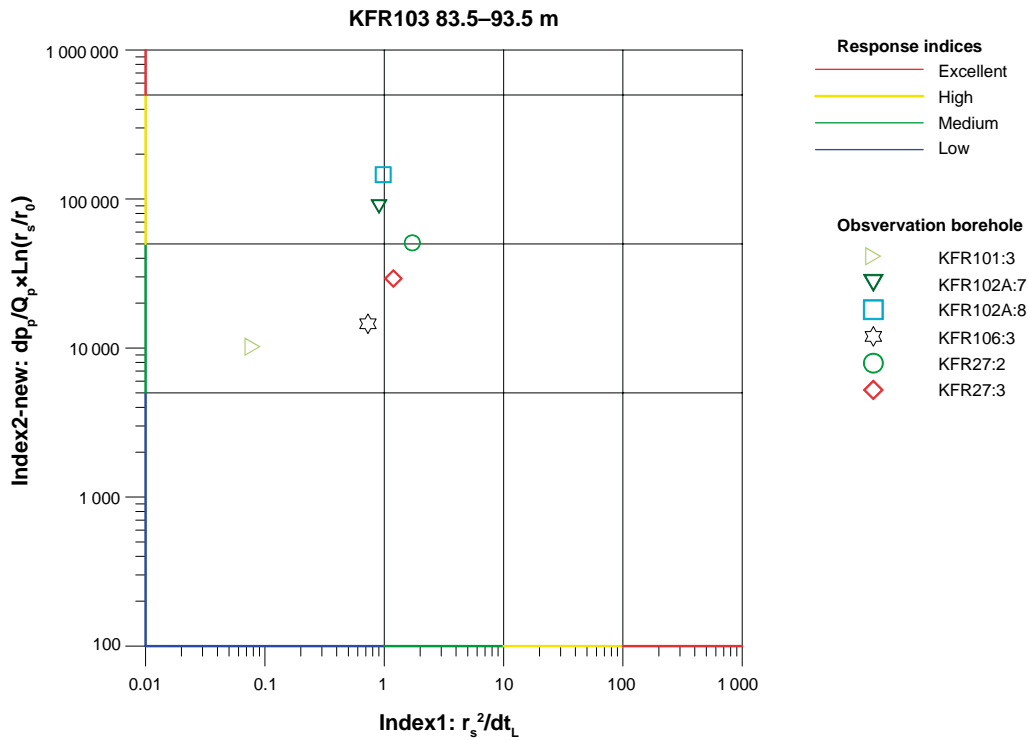


Figure 5-4. Cross plot of the response indices for the responding observation sections during the interference test in KFR103: 83.5–93.5 m.

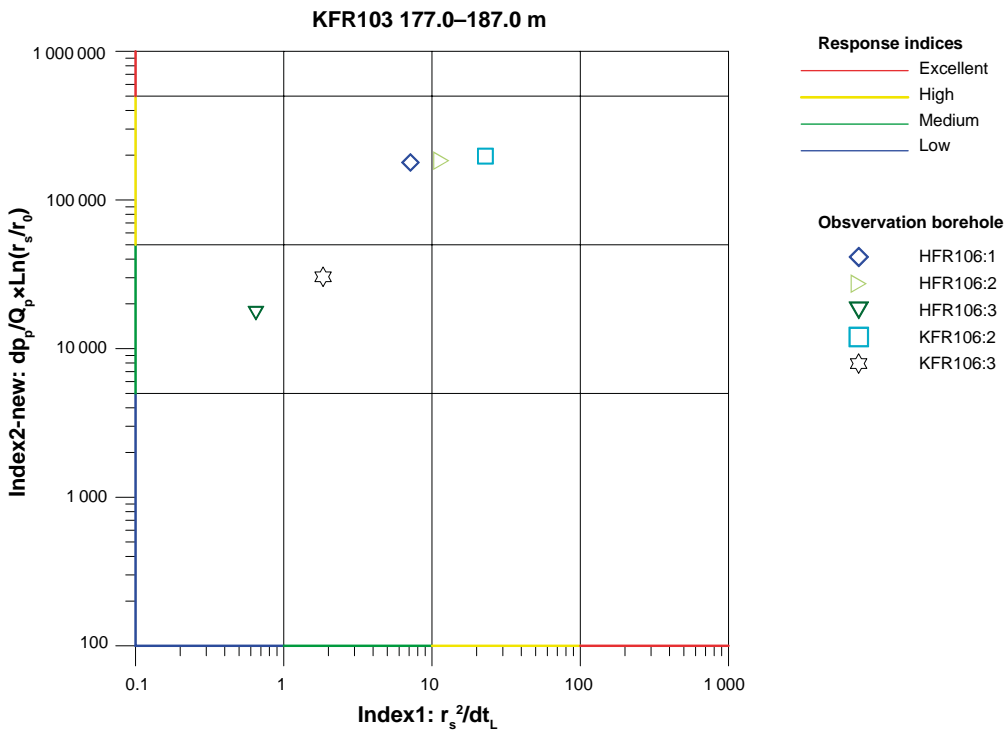


Figure 5-5. Cross plot of the response indices for showing the responding observation sections during the interference test in KFR103: 177.0–187.0 m.

The test in KFR105 have no sections showing high responses due to Index 1 and only one section with a high response due to Index 2 new (Figure 5-6).

An analysis of responses in the observation borehole sections was undertaken and compiled in terms of a response matrix (Table 6-4). All response analysis was made on de-trended head data (PWH), where the noise from sea-level and air pressure fluctuation has been reduced.

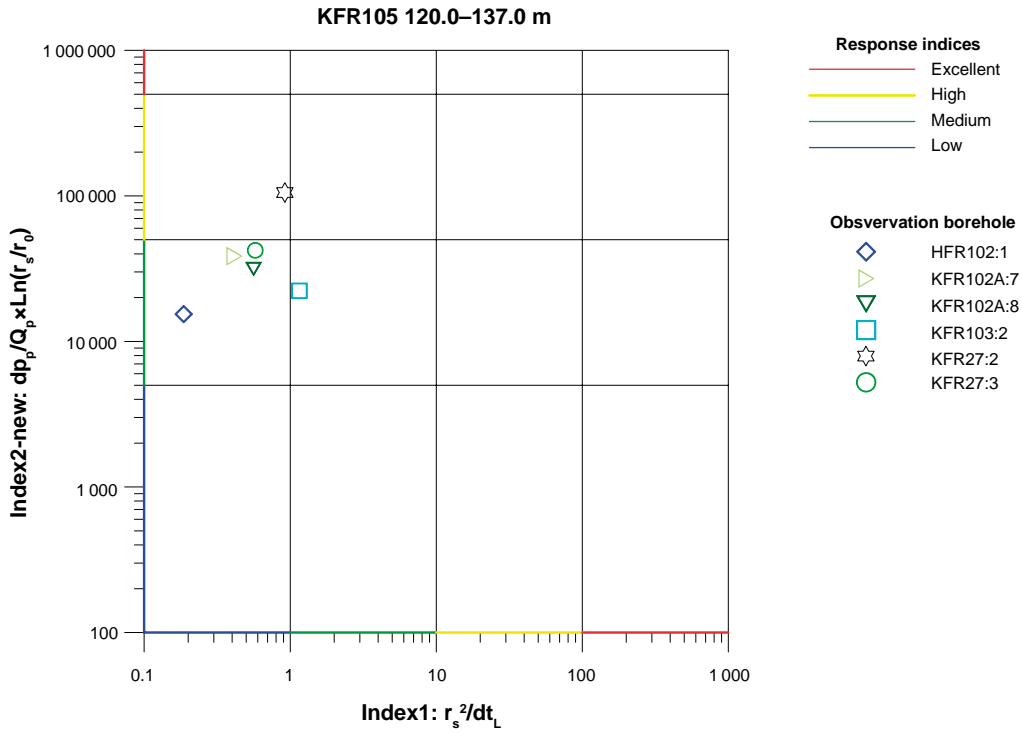


Figure 5-6. Cross plot of the response indices for the responding observation sections during the interference test in KFR105: 120.0–137.0 m.

Table 5-2. Analysis of responses in the observation sections during interference tests.

Pumped borehole	Section (mbl TOC)	Observation borehole ID: section	Section (mbl TOC)	Distance (m)	Qp (m ³ /s)	s _p (m)	dt _t [s = 0.1 m] (s)	Index 1: r _s ² /dt _t [s = 0.1 m] (m ² /s)	Index 1 classification*	Index 2_new: s _p /Q _p *ln(r _j /r ₀) (s/m ²)	Index 2_new classification*
KFR27	47.00–57.00	KFR102A:3	255.00–422.00	276.0	4.10E–05	0.86	17400	4.38	M	117951	H
KFR27	47.00–57.00	KFR102A:4	220.00–254.00	193.8	4.10E–05	1.24	8160	4.60	M	159363	H
KFR27	47.00–57.00	KFR102A:5	214.00–219.00	179.4	4.10E–05	1.33	4620	6.96	M	168428	H
KFR27	47.00–57.00	KFR102A:6	185.00–213.00	168.1	4.10E–05	1.32	3960	7.14	M	165073	H
KFR27	47.00–57.00	KFR102A:7	103.00–184.00	141.1	4.10E–05	0.38	76200	0.26	L	45895	M
KFR27	47.00–57.00	KFR102A:8	0.00–102.00	140.3	4.10E–05	0.34	104400	0.19	L	41016	M
KFR27	47.00–57.00	KFR105:2	170.00–264.00	183.8	4.10E–05	0.67	24600	1.37	M	85248	H
KFR27	47.00–57.00	KFR105:3	138.00–169.00	141.7	4.10E–05	0.69	24600	0.82	L	83404	H
KFR27	47.00–57.00	KFR105:4	120.00–137.00	129.8	4.10E–05	0.71	21600	0.78	L	84302	H
KFR27	189.40–194.40	KFR101:1	279.50–341.76	340.8	8.74E–05	1.17	20400	5.69	M	78110	H
KFR27	189.40–194.40	KFR101:2	91.00–278.50	266.6	8.74E–05	1.96	5700	12.47	H	125247	H
KFR27	189.40–194.40	KFR102A:3	255.00–422.00	156.6	8.74E–05	2.82	3300	7.43	M	162759	H
KFR27	189.40–194.40	KFR102A:4	220.00–254.00	106.6	8.74E–05	5.08	1260	9.02	M	271544	H
KFR27	189.40–194.40	KFR102A:5	214.00–219.00	105.8	8.74E–05	6.05	660	16.96	H	322874	H
KFR27	189.40–194.40	KFR102A:6	185.00–213.00	108.3	8.74E–05	6.28	240	48.85	H	336804	H
KFR27	189.40–194.40	KFR102A:7	103.00–184.00	132.2	8.74E–05	0.34	5400	3.24	M	19273	M
KFR27	189.40–194.40	KFR102B:1	146.00–180.08	197.1	8.74E–05	2.32	2820	13.77	H	140524	H
KFR27	189.40–194.40	KFR102B:2	128.00–145.00	199.0	8.74E–05	2.08	4740	8.36	M	126154	H
KFR27	189.40–194.40	KFR105:5	4.00–119.00	120.9	8.74E–05	0.36	8220	1.78	M	19588	M
KFR103	83.50–93.50	HFR106:3	36.00–46.00	240.8	4.47E–05	< 0.10	-	-	B	-	B
KFR103	83.50–93.50	KFR101:3	0.00–90.00	83.2	4.47E–05	0.10	87780	0.08	L	10234	M
KFR103	83.50–93.50	KFR102A:7	103.00–184.00	118.0	4.47E–05	0.83	15420	0.90	L	89032	H
KFR103	83.50–93.50	KFR102A:8	0.00–102.00	71.0	4.47E–05	1.53	5160	0.98	L	145753	H
KFR103	83.50–93.50	KFR102B:3	0.00–127.00	94.5	4.47E–05	< 0.07	-	-	B	-	B
KFR103	83.50–93.50	KFR106:3	0.00–142.00	290.9	4.47E–05	0.11	115980	0.73	L	14583	M
KFR103	83.50–93.50	KFR27:2	47.00–109.00	174.3	4.47E–05	0.44	17700	1.72	M	50791	H
KFR103	83.50–93.50	KFR27:3	0.00–46.00	181.3	4.47E–05	0.25	27600	1.19	M	29294	M
KFR103	177.00–187.00	HFR106:1	175.00–190.40	134.3	4.50E–05	1.64	2520	7.15	M	178931	H
KFR103	177.00–187.00	HFR106:2	47.00–174.00	184.3	4.50E–05	1.59	2940	11.55	H	183922	H
KFR103	177.00–187.00	HFR106:3	36.00–46.00	243.0	4.50E–05	0.14	91020	0.65	L	17316	M
KFR103	177.00–187.00	KFR106:2	143.00–259.00	274.9	4.50E–05	1.58	3300	22.90	H	197511	H
KFR103	177.00–187.00	KFR106:3	0.00–142.00	273.0	4.50E–05	0.24	40440	1.84	M	30441	M
KFR105	120.00–137.00	HFR102:1	28.00–55.04	146.7	8.77E–05	0.27	115440	0.19	L	15429	M
KFR105	120.00–137.00	KFR102A:7	103.00–184.00	219.2	8.77E–05	0.63	114900	0.42	L	38685	M
KFR105	120.00–137.00	KFR102A:8	0.00–102.00	254.4	8.77E–05	0.50	115200	0.56	L	31454	M
KFR105	120.00–137.00	KFR103:2	79.00–177.00	263.5	8.77E–05	0.35	60000	1.16	M	22285	M
KFR105	120.00–137.00	KFR27:2	47.00–109.00	115.8	8.77E–05	1.95	14580	0.92	L	105541	H
KFR105	120.00–137.00	KFR27:3	0.00–46.00	149.3	8.77E–05	0.74	38700	0.58	L	42282	M

* E = Excellent; H = High; M = Medium; L = Low, B = Below limit (s < 0.1 m)

5.2 Transient evaluation of the interference tests

Hydraulic properties were evaluated for the pumped borehole sections based on type-curve fitting of analytical models to transient flow histories and for selected responses of special interest. The transient analysis was made on de-trended data. Test diagrams together with the transient evaluation in the responding observation borehole sections are shown in Appendix 2. In the transient analysis of the responses, the reference time ($t_0 = 0$ s) and initial drawdown ($s(t_0) = 0$ m) are initialized by the actual start of pumping and the actual head in the observation borehole sections at this time, respectively.

Earlier interference tests at SFR (Walger et al. 2010) yielded responses where the drawdown continues to reach its maximum after the stop of pumping. For this reason it was decided to apply both the flow and recovery periods in the transient type-curve evaluation of responses (i.e. as a joint sequence). For the pumped sections, in contrary, the flow and recovery periods were analyzed separately. The time delay is assumed to represent limitations in the hydraulic connection between the observation section and the pumped borehole interval. For well-connected flow paths, the delay (normalized by the distance) is usually small.

In most of the cases, the drawdown derivative first indicated flow regimes with a transition period. In some cases, this transition turned into a clear Pseudo Radial Flow period (PRF) at some point and in many of the responses a period of Pseudo Spherical Flow period (PSF) occurred that often lasted until the onset of the recovery period. Their method was applied to evaluate responses characterized by PRF or only a transition period, while Hantush-Jacob's method was applied for those exhibiting pseudo-spherical (leaky) flow at the end. The corresponding methods were applied for the pumped borehole intervals, but also taking into account wellbore storage and skin effects (see Section 3.3).

The estimated transmissivity T_o , storativity S_o of the transient evaluated observation sections are listed Table 6-3 in section 6 and the estimated transmissivity of the pumped borehole intervals is shown in Table 6-2. The estimations of T_o and S_o are based on the assumption of an equivalent porous medium and may thus not always represent the specific flow paths between the observation sections and the pumping borehole, particularly for observation sections with bad hydraulic connection to the pumping borehole. Instead, the hydraulic diffusivity T/S may be more representative for the specific pathways between the boreholes.

Regarding the observation sections with the highest transmissivities, the transient evaluation is based on the early drawdown response in the sections. Some of these sections have a rather low apparent hydraulic diffusivity, D_a according to Table 6-3, indicating a relatively weak hydraulic connection to the pumping borehole section. Thus, the separation into T_o and S_o may be uncertain for these sections.

Observation sections with a high estimated apparent hydraulic diffusivity in Table 6-3 generally have low estimated values on the storativity S_o . Estimated T_o -values from the observation sections with good hydraulic connection to the pumping borehole section are normally strongly influenced by the transmissivity of the latter section.

5.3 Interference test in KFR27: 47.0–57.0 m

A linear diagram of pressure and flow rate versus time in the pumping borehole interval 47.0–57.0 m is presented in Appendix 1, Figure A1-2. The actual start and stop times of the pumping tests are shown in Table 2-1. The air pressure and sea water level are shown in Figure A1-1. Both air pressure and sea level are changing during the pumping period, with a decrease in air pressure and increase in sea levels during the first three pumping days.

Transient evaluation as described in Chapter 3 was made of both the observed drawdown and pressure recovery in the pumping borehole interval considering wellbore storage and skin effects, see Figures A2-1a to A2-2b. The Interpreted flow regime during the pumping is a long period of PRF possibly turning towards a Constant Head Boundary at the end. The recovery period shows similar flow regime but is preceded by a longer transition period towards the PRF.

The estimated transmissivity from the transient analysis of the pumping borehole (1.08×10^{-5} m²/s) during the actual pumping test is slightly greater than the stationary analysis T_M (4.61×10^{-6} m²/s) and

the estimated transmissivity T_f from the flow logging ($3.5 \times 10^{-6} \text{ m}^2/\text{s}$ for a conductive fracture identified at c. 49.84–54.85 m), see Table 6-2. The strongest and most rapid responses occurred in KFR102A:3-6 and KFR105:2 (Table 6-4).

All of these sections showed a medium response due to Index 1 and a high response due to Index 2 new. Other sections showing a response were KFR102A:7-8 and KFR105:3-4. Low confidence responses were found in KFR101:2, KFR102A:1-2, KFR105:1 and KFR105:5. The shortest distances to the responding observation sections together with the estimated hydraulic parameters from the observation borehole sections are presented in Table 5-2.

No data was available for observation sections in KFR102B:1-2 and KFR103 due to non-functioning monitoring equipment. For HFR101, the drawdown curve was incountious and not usable for response evaluation. For these observation sections no evaluations were proformed. In KFM11A:1, a pressure decrease is explained by that the equipment was lifted shortly before teststart. A decrease in pressure could be seen also before test start and for that reason the section is classified as non-responding.

For the interference test in KFR27, 47.0–57.0 m, transient evaluation was made for one section: KFR102A:8 and a cross-plot of the estimated transmissivity T_o and storativity S_o from the transient evaluated response in the observation section is shown in Figure 5-7.

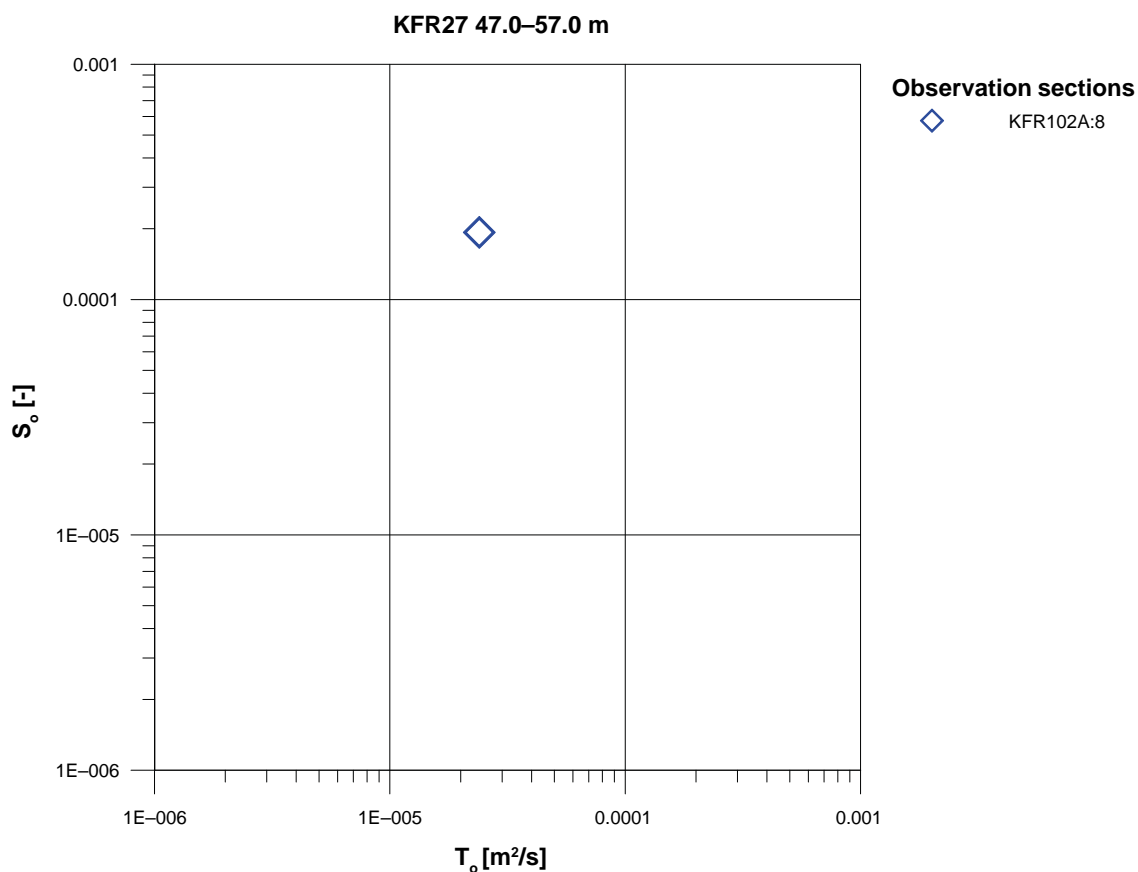


Figure 5-7. Estimated transmissivity and storativity from transient evaluation of the transient evaluated responding sections during the interference test in KFR27 47.0–57.0 m.

5.4 Interference test in KFR27: 189.4–194.4 m

A linear diagram of pressure and flow rate versus time in the pumping borehole interval 189.4–194.4 m is presented in Appendix 1, Figure A1-18. The actual start and stop times of the pumping tests are shown Table 2-1. The air pressure and sea water level are shown in Figure A1-17. The air pressure is increasing during the pumping period and the increase starts a day before start of pumping and proceeds three days after stop of pumping. The sea level is showing a varying behavior with a variance of ca 0.1 m throughout the test. During the recovery phase the sea level has a small decreasing trend with the same variance.

Transient evaluation as described in Chapter 3 was made of both the observed drawdown and pressure recovery in the pumping borehole interval, considering wellbore storage and skin effects, see Figures A2-4a to A2-5b. The flow in the pumping section starts with a wellbore storage effect (WBS) followed by a transition to a PRF at the end of the pumping.

The estimated transmissivity from the transient analysis of the pumping borehole ($6.04 \times 10^{-6} \text{ m}^2/\text{s}$) are in the same order as the transmissivity obtained from the flow logging ($6.10 \times 10^{-6} \text{ m}^2/\text{s}$ for a conductive fracture identified at c. 189.42–194.42 m), see Table 6-2. The value from the stationary analysis T_M is larger ($4.12 \times 10^{-5} \text{ m}^2/\text{s}$). The strongest and most rapid responses occurred in KFR101:2, KFR102A:5-6 and KFR102B:1 (Table 6-4).

All of these sections showed a large and fast response for both Index 1 and Index 2 new. Other sections showing a clear response were KFR101:1, KFR102A:3-4, KFR102A:7, KFR102B:3 and KFR105:5. Low confidence responses were found in KFR102A:1-2, KFR102A:8 and KFR106:1. The shortest distances to the responding observation sections together with the estimated hydraulic parameters from the observation borehole sections are presented in Table 5-2.

No data was available for observation sections in KFR103 due to non-functioning monitoring equipment. KFR102B which was no-functioning during the previous test in KFR27, 47.0–57.0 m, were lifted and re-installed before the test in KFR27 189.4–194.4 m. Data from KFM11A:1 was not available in Sicada for the testperiods when the data filtering and test evaluation were performed. A later evaluation of pressure data indicated though that there was no response in KFM11A:1. For HFR101 data was uncontinuous? and not suitable to use for evaluation.

For the interference test in KFR27 189.4–194.4 m, transient evaluation was made for the following sections: KFR102A:6, KFR101:2, KFR102B:1 and KFR106:1. A cross-plot of the estimated transmissivity T_o and storativity S_o from the transient evaluated responses in the observation sections is shown in Figure 5-8.

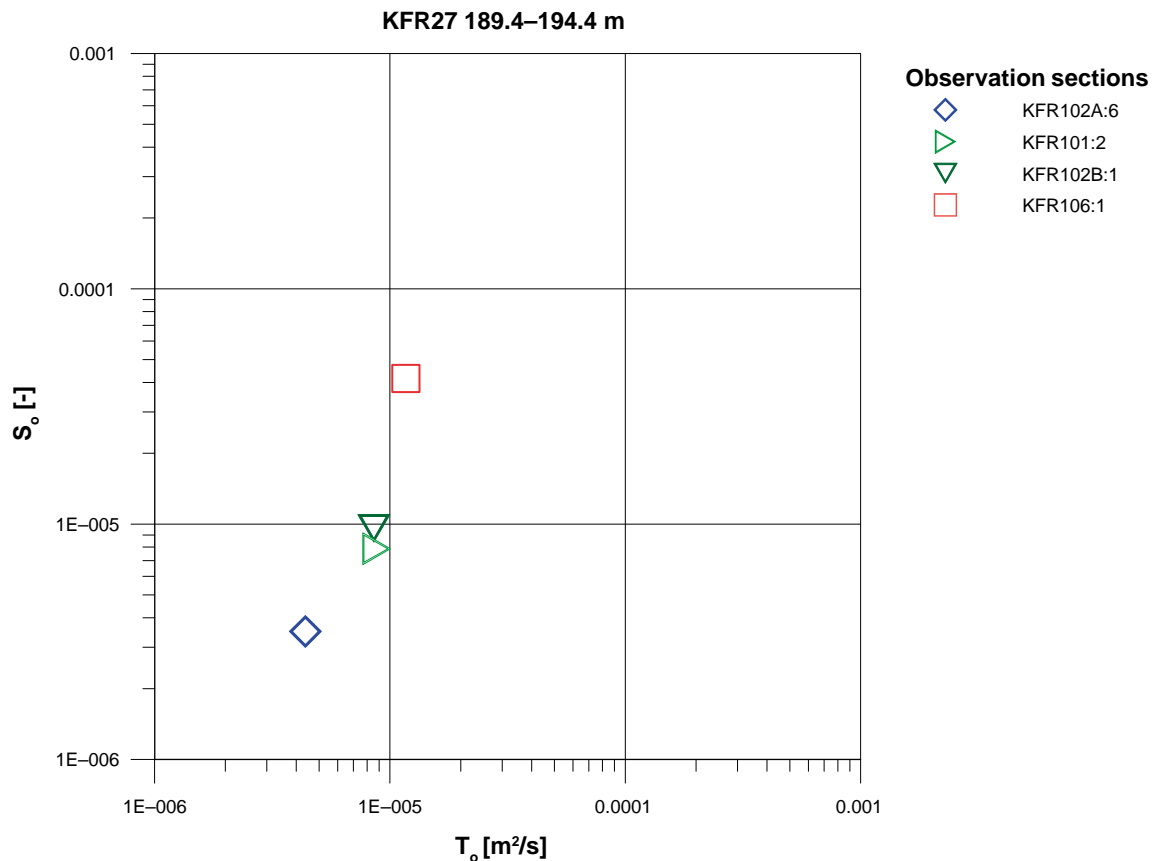


Figure 5-8. Estimated transmissivity and storativity from transient evaluation of the transient evaluated responding sections during the interference test in KFR27 189.4–194.4 m.

5.5 Interference test in KFR103: 83.5–93.5 m

A linear diagram of pressure and flow rate versus time in the pumping borehole interval 83.5–93.5 m is presented in Appendix 1, Figure A1-34. The actual start and stop times of the pumping tests are shown in Table 2-1. The air pressure and sea water level are shown in Figure A1-33. The air pressure was increasing during the flow period and decreasing during the recovery period, in total, a change of about 3 kPa up and down. The sea level is varying within 0.1 m without a clear trend during the test.

Transient evaluation as described in Chapter 3 was made of both the observed drawdown and pressure recovery in the pumping borehole interval considering wellbore storage and skin effects, see Figures A2-10a to A2-11b. The response in the pumped section was relatively small and the drawdown indicating a more or less stationary flow regime (PSS) while the recovery shows a period of PSF followed by a PSS at the end.

The estimated transmissivity from the transient analysis of the pumping borehole ($1.54 \times 10^{-5} \text{ m}^2/\text{s}$) is in the same magnitude as from the stationary analysis T_M ($1.30 \times 10^{-5} \text{ m}^2/\text{s}$) and the estimated transmissivity of the pumped section from the flow logging ($1.5 \times 10^{-5} \text{ m}^2/\text{s}$ for a conductive fracture identified at c. 84.95–94.95 m), see Table 6-2. The strongest and most rapid responses occurred in KFR27:2 (Table 6-4). This section showed a medium response due to Index 1 and high response due to Index 2 new. Other sections showing a response were HFR106:3, KFR101:3, KFR102A:7-8, KFR102B:3, KFR106:3 and KFR27:3. Low confidence responses were found in HFR106:1-2, KFR101:1-2, KFR102A:1-6, KFR102B:1-2, KFR105:2-4, KFR106:2 and KFR27:1. The shortest distances to the responding observation sections together with the estimated hydraulic parameters from the observation borehole sections are presented in Table 5-2.

Data from KFM11A:1 were not available in Sicada for the testperiod when the data filtering and test evaluation were performed. A later evaluation of pressure data indicated, though, that there was no response in KFM11A:1. Several observation sections were affected, or possible affected, by the re-installation in KFR27 (i.e. KFR102B:1-2, KFR102A:1-8, and KFR101:1-2, KFR105:2-4).

The influence from packer re-installation in KFR27 is manifested as a long-term drawdown trend, but lacking recovery phase. Of these sections, KFR102A:7-8 are considered true responses. This implies, in turn, that many of the “low-confidence” responses can be written off as super-imposed drawdown from SFR (via the extension of ZFM871) that is successively recovering via the deep section in KFR27.

For the interference test in KFR103, 83.5–93.5 m, transient evaluation was made for responses in the following sections: HFR106:3, KFR102A:8, KFR27:2, KFR106:3, and KFR101:3. A cross-plot of the estimated transmissivity T_o and storativity S_o from the transient evaluated responses in the observation sections is shown in Figure 5-9. The estimations of T_o and S_o are based on the assumption of an equivalent porous medium and may thus not always represent the specific flow paths between the observation sections and the pumping borehole, particularly for observation sections with bad hydraulic connection to the pumping borehole.

Regarding the observation sections with the highest transmissivities in Figure 5-9, the transient evaluation is based on the early drawdown response in the sections. Some of these sections have a rather low apparent hydraulic diffusivity (D_a) according to Table 6-3, indicating a relatively weak hydraulic connection to the pumping borehole section. Thus, the separation into T_o and S_o may be uncertain for these sections.

Observation sections with a high estimated hydraulic diffusivity in Table 6-3 generally have low estimated values on the storativity S_o . Estimated T_o -values from the observation sections with good hydraulic connection to the pumping borehole section are normally strongly influenced by the transmissivity of the latter section.

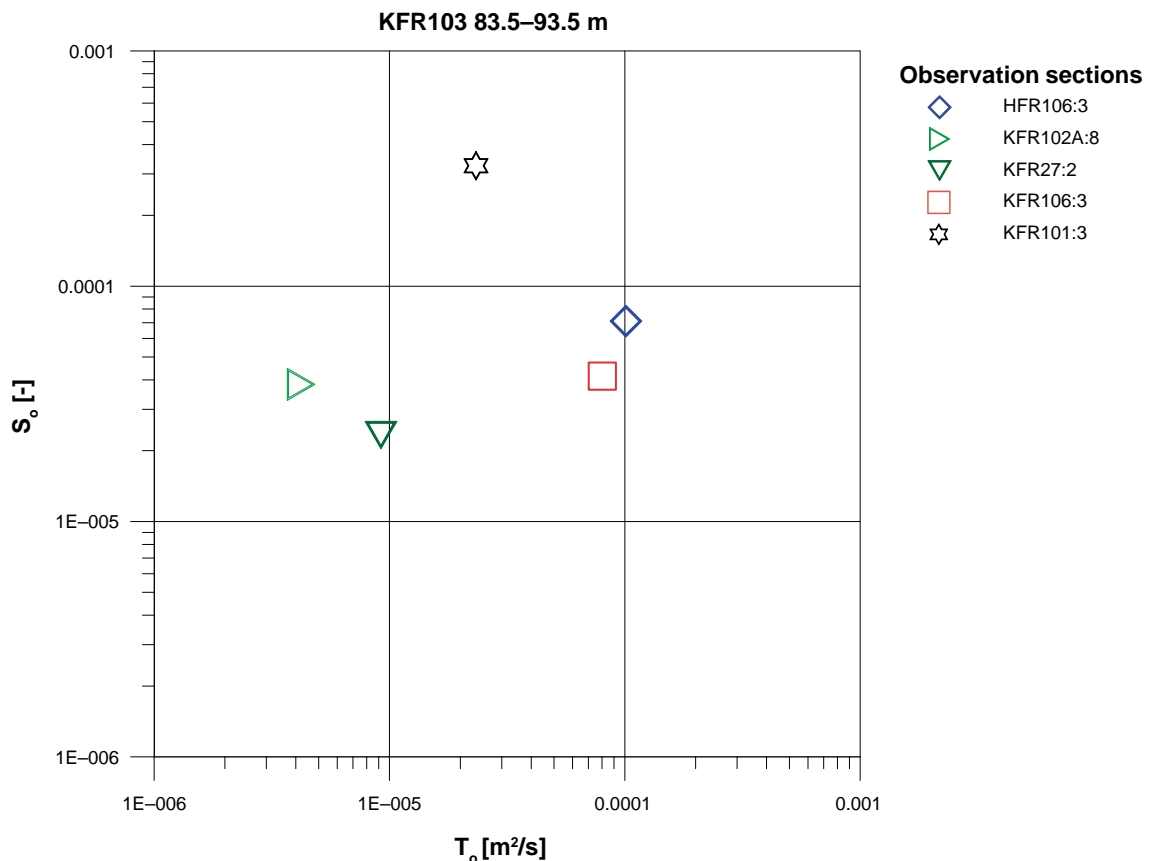


Figure 5-9. Estimated transmissivity and storativity from transient evaluation of the transient evaluated responding sections during the interference test in KFR103 83.5–93.5 m.

5.6 Interference test in KFR103: 177.0–187.0 m

A linear diagram of pressure and flow rate versus time in the pumping borehole interval 177.0–187.0 m is presented in Appendix 1, Figure A1-59. The actual start and stop times of the pumping tests are shown in Table 2-1. The air pressure and sea water level are shown in Figure A1-58. The air pressure was increasing during the flow period, in total a change of about 4 kPa starting one day before pumping start. During the recovery period, the air pressure was decreasing. The sea level was varying but decreasing during the end of the pumping period and recovery period.

Transient evaluation as described in Chapter 3 was made of both the observed drawdown and pressure recovery in the pumping borehole interval considering wellbore storage and skin effects, see Figures A2-17a to A2-18b. The flow regime during the pumping indicates a period of PRF followed by a transition period. The flow decreases after about 20000 seconds which can be seen in Figure A2-17a. Recovery starts with a transition period turning into a PRF that dominates the period.

The estimated transmissivity from the transient analysis of the pumping borehole ($5.70 \times 10^{-6} \text{ m}^2/\text{s}$) is similar to the stationary analysis T_M ($5.28 \times 10^{-6} \text{ m}^2/\text{s}$). The estimated transmissivity from the earlier flow logging is slightly greater ($1.0 \times 10^{-5} \text{ m}^2/\text{s}$ for a conductive fracture identified at c. 180.02–185.02 m), see Table 6-2. The strongest and most rapid responses occurred in HFR106:2 and KFR106:2 (Table 6-4). These sections showed a clear response due to both Index 1 and Index 2 new. Other sections showing a response were HFR106:1, HFR106:3, KFR106:3, and KFR27:2-3. Low confidence responses were found in KFR101:1-2, KFR102A:1-6, KFR102B:1-2, KFR106:1 and KFR27:1. The shortest distances to the responding observation sections together with the estimated hydraulic parameters from the observation borehole sections are presented in Table 5-2.

Data from KFM11A:1 were not available in Sicada for the testperiod when the data filtering and test evaluation were performed. A later evaluation of pressure data indicated that there was no response in KFM11A:1. Several observation sections were affected or possibly affected by the re-installation of packers in KFR27 prior the tests in KFR103 (i.e. KFR101:1-2, KFR102A:1-8, KFR102B:1-2, and, KFR105:1-4) seen in Figure 5-10.

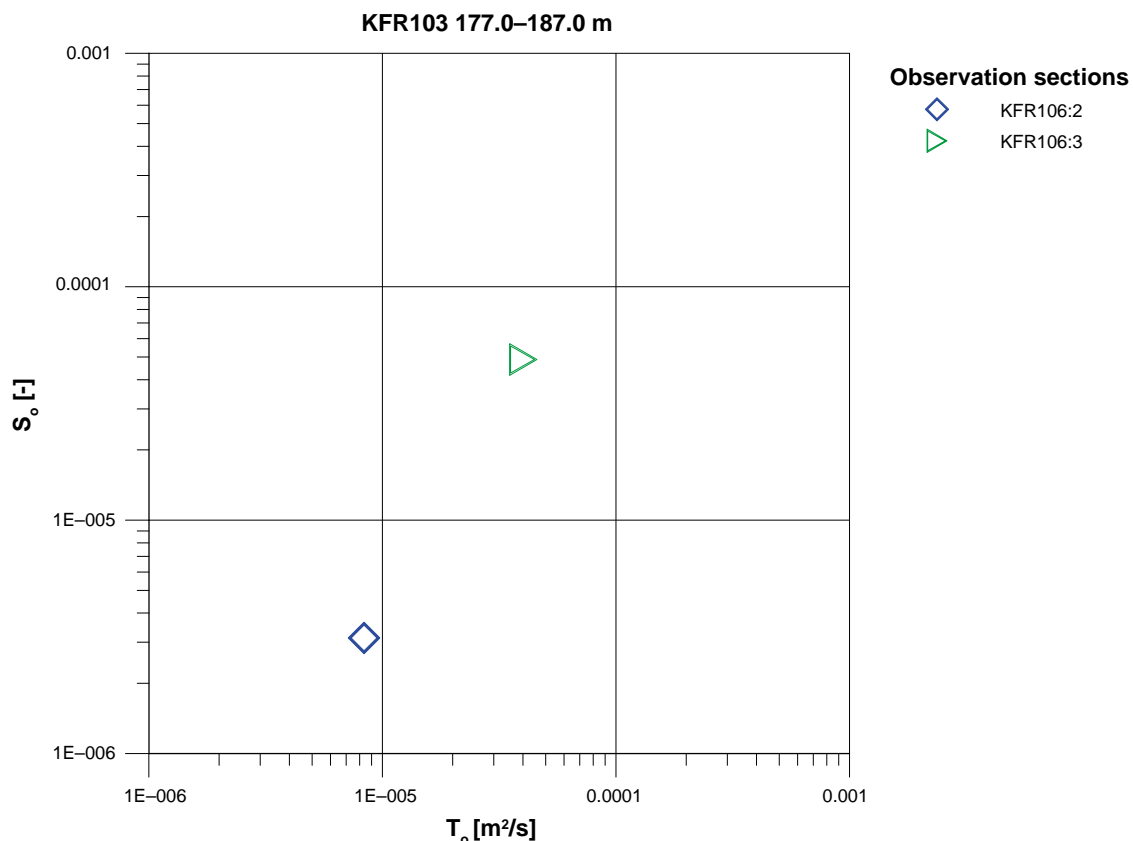


Figure 5-10. Estimated transmissivity and storativity from transient evaluation of the transient evaluated responding sections during the interference test in KFR103 177.0–187.0 m.

The influence from packer re-installation in KFR27 was manifested as a long-term drawdown trend, but lack of corresponding recovery phase. Of these sections, KFR102A:7-8 and KFR105:1-4 are judged to be non-responding sections. This implies, in turn, that many of the “low-confidence” responses can be written off as super-positioned drawdown from SFR (via the extension of ZFM871) that is successively recovering via the deep section in KFR27.

For the interference test in KFR103, 177.0–187.0 m transient evaluation was made for the following sections: KFR106:2 and KFR106:3. A cross-plot of the estimated transmissivity T_o and storativity S_o from the transient evaluated responses in the observation sections is shown in Figure 5-10.

The estimations of T_o and S_o are based on the assumption of an equivalent porous medium and may thus not always represent the specific flow paths between the observation sections and the pumping borehole, particularly for observation sections with bad hydraulic connection to the pumping borehole. Instead, the hydraulic diffusivity T/S may be more representative for the specific pathways between the boreholes.

Regarding the observation sections with the highest transmissivities in Figure 5-10, the transient evaluation is based on the early drawdown response in the sections. Some of these sections have a rather low apparent hydraulic diffusivity (D_a) according to Table 6-3, indicating a relatively weak hydraulic connection to the pumping borehole section. Thus, the separation into T_o and S_o may be uncertain for these sections.

Observation sections with a high estimated hydraulic diffusivity in Table 6-3 generally have low estimated values on the storativity S_o . Estimated T_o -values from the observation sections with good hydraulic connection to the pumping borehole section are normally strongly influenced by the transmissivity of the latter section.

5.7 Interference test in KFR105: 120.0–137.0 m

A linear diagram of pressure and flow rate versus time in the pumping borehole interval 120.0–137.0 m is presented in Appendix 1, Figure A1-78. The actual start and stop times of the pumping tests are shown in Table 2-1. The air pressure and sea water level are shown in Figure A1-77. The air pressure was increasing during the test period, with the strongest increase during the recovery phase, in total an increase of about 2.5 kPa. The sea level was relatively stable during the pumping period.

Transient evaluation as described in Chapter 3 was made of both the observed drawdown and pressure recovery in the pumping borehole interval considering wellbore storage and skin effects, see Figures A2-21a to A2-22b. The flow regime during pumping as well as recovery shows shorter periods of PRF turning into a PSS at the end. The estimated transmissivity from the transient analysis of the pumping borehole ($1.98 \times 10^{-6} \text{ m}^2/\text{s}$) is similar to the stationary analysis T_M ($1.14 \times 10^{-6} \text{ m}^2/\text{s}$). The estimated transmissivity from the earlier flow logging is slightly smaller ($6.5 \times 10^{-7} \text{ m}^2/\text{s}$ for a conductive fracture identified at c. 132.9–137.9 m), see Table 6-2.

The strongest and most rapid responses occurred in KFR103:2 (Table 6-4). This section showed a medium response due to both Index 1 and Index 2 new. Other sections showing a response were HFR102:1, KFR102A.7-8 and KFR27:2-3. Low confidence responses were found in HFR102:2, KFR102A:3-6, KFR103:1 and KFR27:1. The shortest distances to the responding observation sections together with the estimated hydraulic parameters from the observation borehole sections are presented in Table 5-2.

Data from HFR101:1 and KFM11A:1 were not available in Sicada for the testperiod when the data filtering and test evaluation were performed. A later evaluation of pressure data indicated though that there was no response in these sections. For the interference test in KFR105, 120.0–137.0 m transient evaluation was made for following sections: KFR102A:8 and KFR27:2. A cross-plot of the estimated transmissivity T_o and storativity S_o from the transient evaluated responses in the observation sections is shown in Figure 5-11.

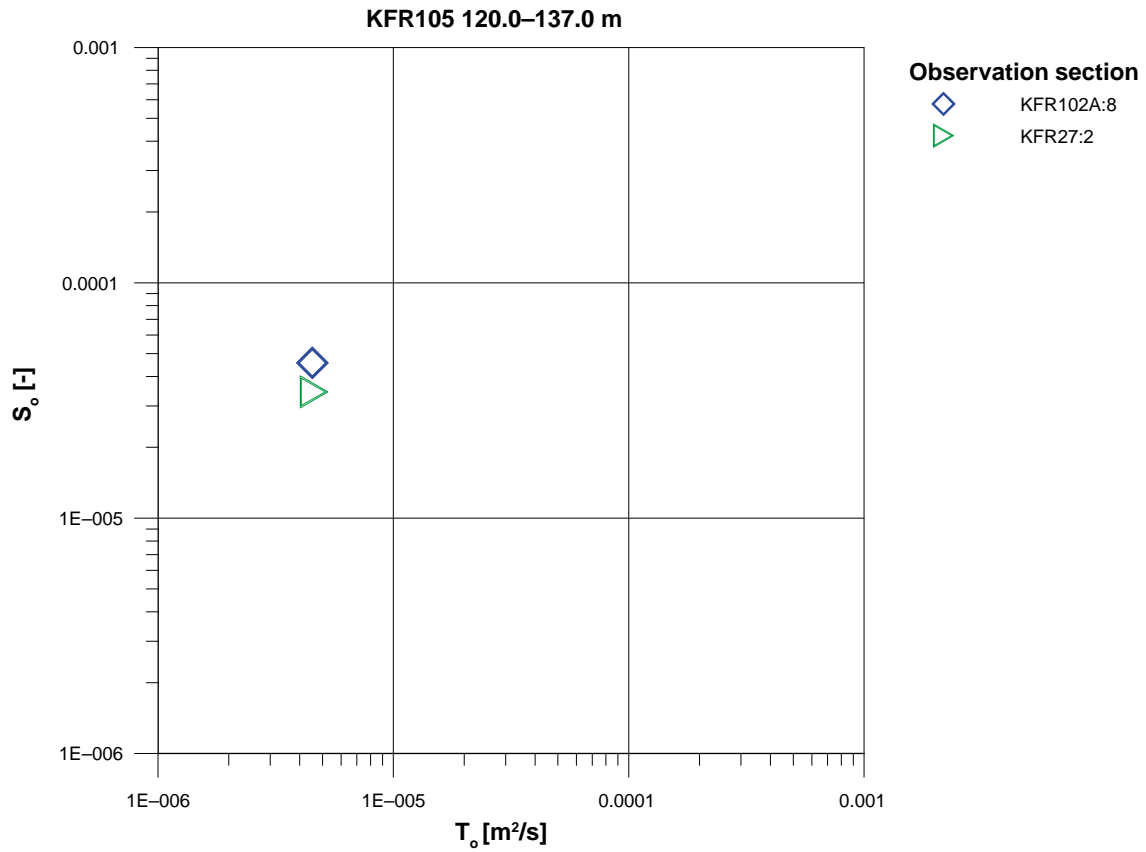


Figure 5-11. Estimated transmissivity and storativity from transient evaluation of the transient evaluated responding sections during the interference test in KFR105 120.0–137.0 m.

6 Summary of results

The five performed interference tests were conducted in order to clarify the existence of modelled hydraulic SBA-structures in the SFR site investigation. Hydraulic parameters for both pumping sections as well as the responding sections were calculated together with an evaluation of the responses.

Drawdown in pumping sections ranged from 3 to 8 meters for the pumped surface boreholes. In KFR105, situated in the tunnel, the drawdown was more than 78 m. Evaluated transmissivities (T_T) ranged between $1.1E-05$ and $6.0E-06$ and the drawdowns indicated flow of either pseudo-radial or pseudo-spherical flow. The evaluation of the pumped sections showed good agreement with earlier performed PFL-logging.

The responses in the observation sections were also evaluated transient and the transmissivities were in the same range as for the pumped sections. The only exception is the response in HFR106:3 during pumping in KFR103 83.5–93.5 m where T_o was estimated to $1.0E-04$. The apparent hydraulic diffusivity ($D_a = T_o/S_o$) was calculated and a low value indicate a weak connection to the pumped section. The identified flow regimes in the responding sections indicated either pseudo-radial or pseudo-spherical flow and no hydraulic borders were seen.

The estimated transmissivity of the observation sections may be more weighted towards the hydraulic properties close to the pumping borehole. In addition, the estimated transmissivity of some observation sections may be overestimated from interference tests due to poor hydraulic connection to the pumping borehole.

A compilation of measured test data from the pumping boreholes during the interference tests is shown in Table 6-1 to 6-3, estimated hydraulic parameters for the pumping borehole sections and responding observation borehole sections respectively, are presented.

Nomenclature used:

h_i = initial hydraulic head

h_p = ground water level at the end of pumping

dh_p = hydraulic head change at the end of pumping

h_f = hydraulic head at the stop of recovery

Q_p = flow rate at stop of pumping

Q_m = medium flow rate during the flow period

V_p = volume pumped during the test

Q/s = specific flow for the pumping/injection borehole

T_M = steady state transmissivity from Moye's equation

T_T = transmissivity from transient evaluation of single-hole test

S^* = assumed storativity by the estimation of the skin factor in single hole tests

C = wellbore storage coefficient

ξ = skin factor

s_p = drawdown

T_o = transmissivity of an observation section from transient evaluation of interference test

S_o = storativity of an observation section from transient evaluation of interference test

T_o/S_o = hydraulic diffusivity of an observation section (m^2/s)

K'/b' = leakage coefficient from transient evaluation of interference test

Table 6-1. Test data from pumped borehole intervals during the interference tests.

Pumping borehole ID	Section (mbl TOC)	Test Type ¹⁾	h _i (m)	h _p (m)	h _r (m)	dh _p (m)	Q _p (m ³ /s)
KFR27	47.0–57.0	1B	55.25	47.50	55.35	7.75	4.1E–05
KFR27	189.4–194.4	1B	195.31	188.79	194.80	6.52	8.7E–05
KFR103	83.5–93.5	1B	76.81	73.69	76.55	3.12	4.5E–05
KFR103	177.0–187.0	1B	152.09	144.85	151.48	7.24	4.5E–05
KFR105	120.0–137.0	1B	134.90	56.50	134.35	78.40	8.8E–05

1) 1B: Pumping test-submersible pump, 2: Interference test (observation borehole during pumping in another borehole).

Table 6-2. Calculated hydraulic parameters from the single-hole pumping tests during the interference tests.

Pumping borehole ID	Section (mbl TOC)	Q/s (m ² /s)	T-fa (PFL) (m ² /s)	TM (m ² /s)	TT (m ² /s)	ζ (–)	C (m ² / Pa)	S* (–)	r _i (m)	Transient model type	Use period for transient evaluation
KFR27	47.0–57.0	4.9E–06	3.5E–006	4.6E–06	1.1E–05	4.02	2.0E–09	2.3E–06	2085	PRF	Drawdown
KFR27	189.4–194.4	1.4–05	6.1E–006	1.1E–05	6.0E–06	–7.64	1.8E–05	1.7E–06	1401	PRF	Recovery
KFR103	83.5–93.5	1.4–05	1.5E–005	1.3E–05	1.5E–05	–3.02	1.9E–06	2.7E–06	1777	PSF	Recovery
KFR103	177.0–187.0	6.2E–06	1.0E–005	5.8E–06	5.7E–06	–5.42	2.1E–07	1.7E–06	1614	PRF	Recovery
KFR105	120.0–137.0	1.1E–06	6.5E–007	1.1E–06	2.0E–06	2.07	8.7E–10	9.9E–07	1100	PSF	Recovery

Table 6-3. Calculated hydraulic parameters from the transient evaluated responding observation sections during the interference tests.

Pumping borehole ID	Section (mbl TOC)	Observation borehole ID: section	Section (mbl TOC)	Distance (m)	S _p (m)	T _o (m ² /s)	S _o (–)	D _s = T _o /S _o (m ² /s)	Transient model type
KFR27	47.0–57.0	KFR102A:8	0–102.0	140.3	0.34	2.4E–05	1.9E–04	0.12	PRF
KFR27	189.4–194.4	KFR102A:6	185.0–213.0	108.3	6.28	4.4E–06	3.5E–06	1.25	PRF
KFR27	189.4–194.4	KFR101:2	91.0–278.5	266.6	1.96	8.8E–06	7.9E–06	1.12	PSF
KFR27	189.4–194.4	KFR102B:1	146.0–180.1	197.1	2.32	8.6E–06	9.6E–06	0.89	PRF
KFR27	189.4–194.4	KFR106:1	260.0–300.1	475.4	0.31	1.2E–05	4.2E–05	0.28	PRF
KFR103	83.5–93.5	HFR106:3	36.0–46.0	240.8	0.10	1.0E–04	7.1E–05	1.42	PSF
KFR103	83.5–93.5	KFR102A:8	0–102.0	71.0	1.53	4.2E–06	3.8E–05	0.11	PSF
KFR103	83.5–93.5	KFR27:2	47.0–109.0	174.3	0.44	9.2E–06	2.3E–05	0.40	PSF
KFR103	83.5–93.5	KFR106:3	0–142.0	290.9	0.11	8.0E–05	4.2E–05	1.93	PSF
KFR103	83.5–93.5	KFR101:3	0–90.0	83.2	0.10	2.3E–05	3.3E–04	0.07	PSF
KFR103	177.0–187.0	KFR106:2	143.0–259.0	274.9	1.58	8.4E–06	3.1E–06	2.67	PSF
KFR103	177.0–187.0	KFR106:3	0–142.0	273.0	0.24	4.0E–05	4.9E–05	0.82	PSF
KFR105	120.0–137.0	KFR102A:8	0–102.0	254.4	0.50	4.5E–06	4.6E–05	0.10	PSF
KFR105	120.0–137.0	KFR27:2	47.0–109.0	115.8	1.95	4.6E–06	3.4E–05	0.13	PSF

The observed responses to the five interference tests, as characterized by indices for propagation rate and strength (classification according to Table 5-2), are compiled in matrix form in Table 6-4 and also shown in cross-plots in Section 5.1. One unexpected result of the interference tests was that the removal and re-installation of packers in KFR27 caused a long-time response in several observation sections associated to the SBA2 and SBA6 structures. According to Öhman et al. (2012) the entire borehole KFR27 lies inside the modelled geometric bounds of a steeply dipping deformation zone called ZFMWNW0835. There are also two distinct so-called target intercepts, one below 320 m and one between -105 and -117 m. The deeper one has a strong hydraulic signature of the zone whilst the upper one doesn't.

Different boreholes have different geometric sampling bias versus different sets and can therefore not be directly compared. Terzaghi weighting reduces these artefacts and provides more directly comparable fracture intensity estimates; however, it cannot fully eliminate the geometrical artefacts, particularly for fractures that are almost parallel to the borehole (Öhman et al. 2012). This can be seen in two boreholes: the steep borehole KFR27 (average inclination of -86°), which has a strong sampling bias against steep fractures and the sub-horizontal KFR105 (average inclination of -10°), which has a strong bias against horizontal/gently dipping fractures. This is also more thoroughly discussed in the report TD15, Complementary simulation cases in support of SR-PSU (Odén and Öhman 2017).

The resulting response indices for each test, presented in Table 6-4 is summarized below together with a comparison of the responses to the modelled structures within the SFR-site:

Interference test 1, KFR27 (47–57 m), targeting SBA1: responses observed in KFR102A and KFR105, classified as Low- to Medium in propagation rate, and High- to Medium in strength. The interference test does not confirm the modelled structure SBA1. A few low- confidence responses are also noted, associated to packer de-installation in KFR27.

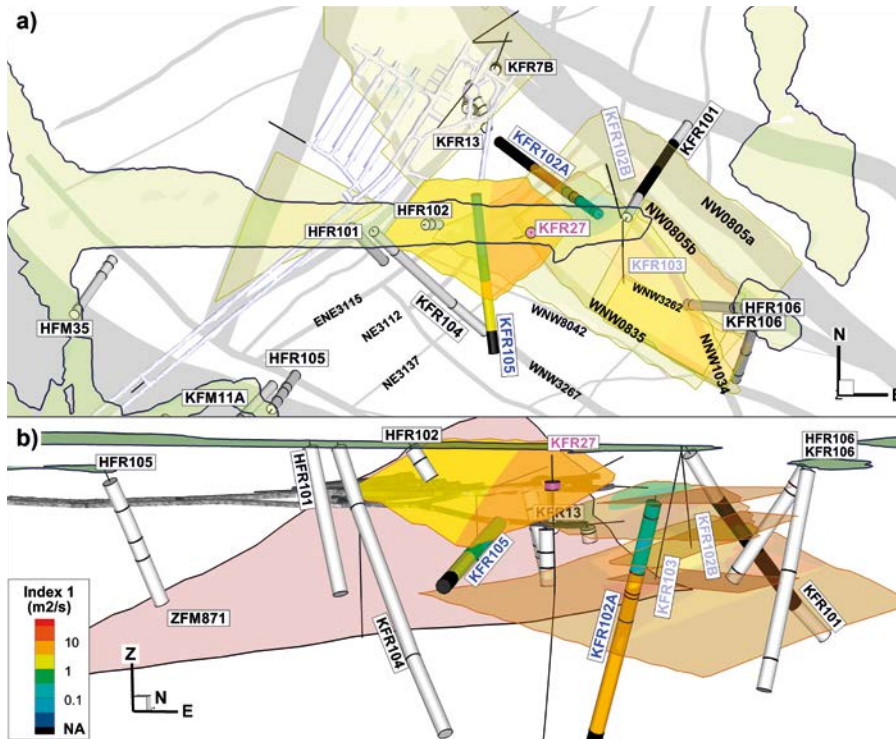


Figure 6-1. Index 1 from the interference test in KFR27, 47–57 m. Non-responding sections in white and low-confidence responses in black.

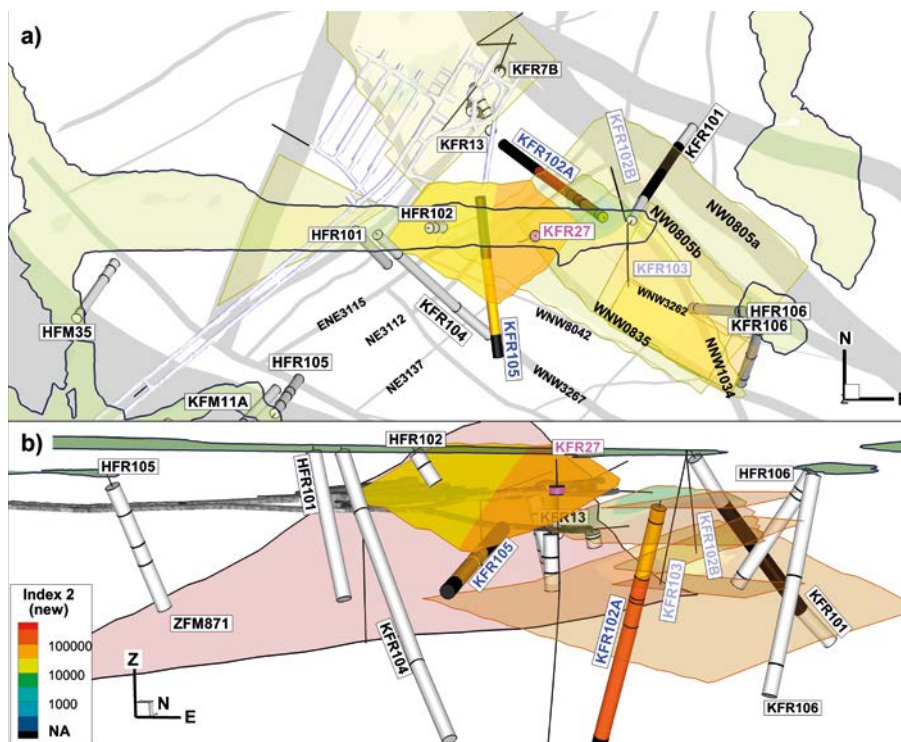


Figure 6-2. Index 2 from the interference test in KFR27, 47–57 m. Non-responding sections in white and low-confidence responses in black.

Interference test 2, KFR27 (189.4–194.4 m), targeting SBA6: responses observed in KFR101, KFR102A, KFR102B and KFR105, classified as Medium- to High in propagation rate and in strength. Responses seen in KFR102A:1, 2 and 8 and KFR106:1 are classified as low confident which indicate some response but not in a significant level. Responses in KFR101, KFR102A, and KFR102B confirm connections in the SBA6 structure. Potential connection to KFR103 could not be evaluated due to malfunctioning downhole equipment. The low-confidence response in KFR106 is potentially indirect. Response in KFR105:5 is in the most upper section in the borehole.

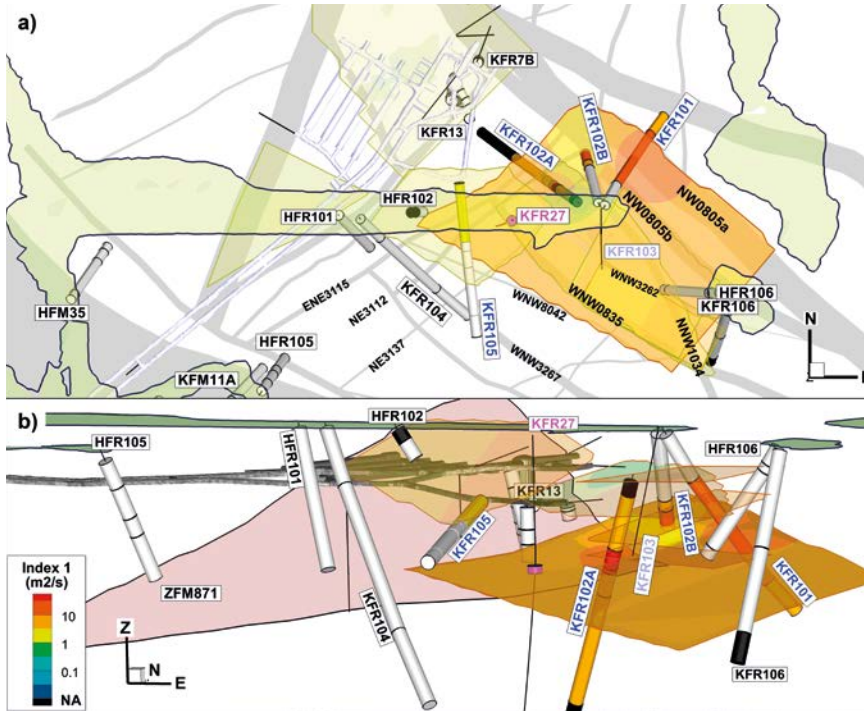


Figure 6-3. Index 1 from the interference test in KFR27, 189.4–194.4 m. Non-responding sections in white and low-confidence responses in black.

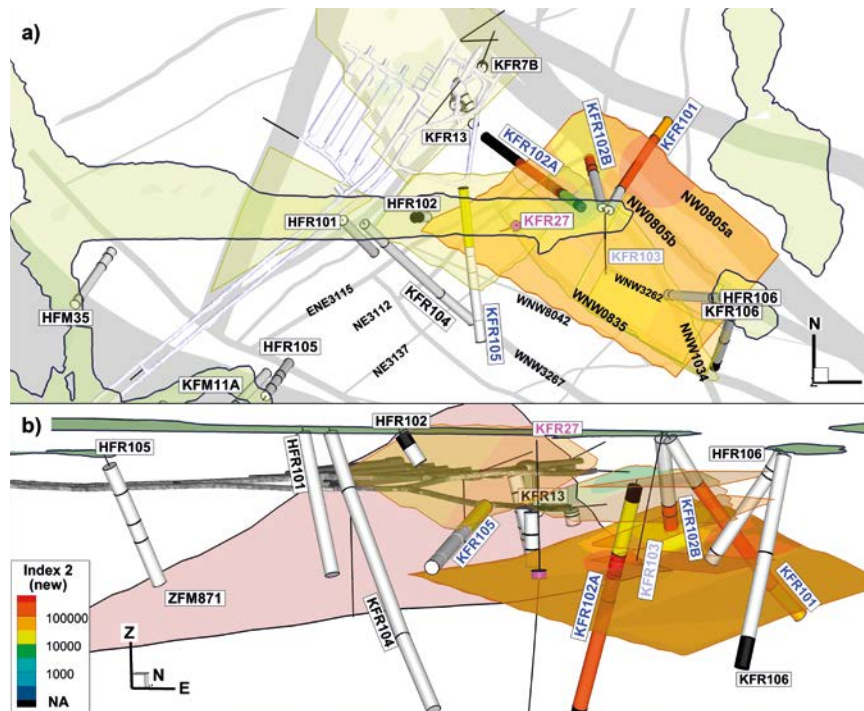


Figure 6-4. Index 2 from the interference test in KFR27, 189.4–194.4 m. Non-responding sections in white and low-confidence responses in black.

Interference test 3, KFR103 (83.5–93.5 m), targeting SBA2-3: responses observed in shallow bore-hole sections: KFR101:3, KFR102A:7-8, KFR106:3 and KFR27:2-3 classified as Low- to Medium in propagation rate, and High- to Medium in strength. The shallow responses are in line with expectations from the modelled geometry of SBA2 and SBA3. A pattern of low-confidence responses (HFR106:1-2, KFR101:1-2, KFR102A:1-6, KFR102B:1-2, KFR105:2-4, KFR106:2, and KFR27:1) is associated to the re-installation of the packer system in KFR27.

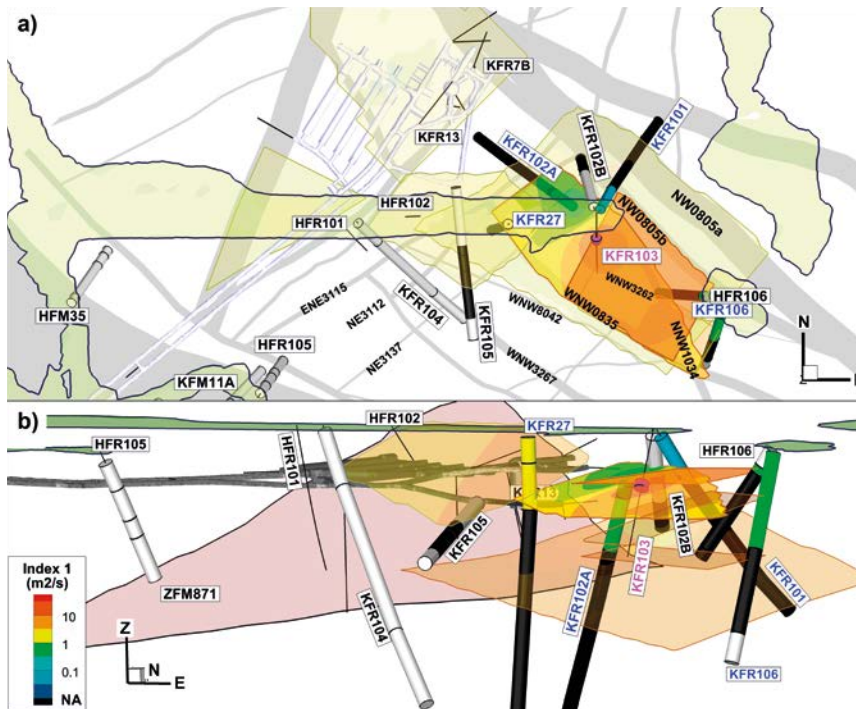


Figure 6-5. Index 1 from the interference test in KFR103, 83.5–93.5 m. Non-responding sections in white and low-confidence responses in black

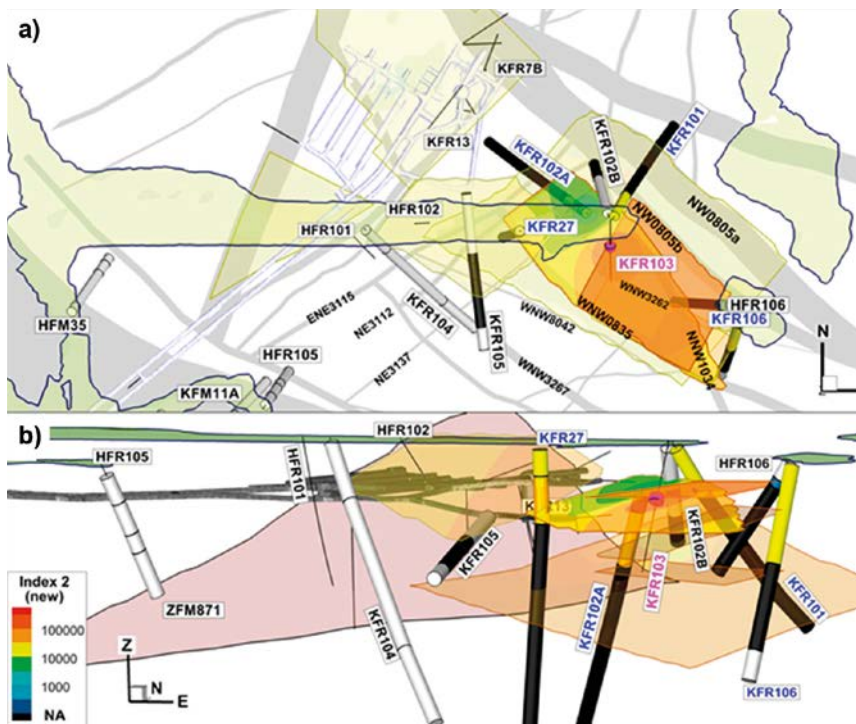


Figure 6-6. Index 2 from the interference test in KFR103, 83.5–93.5 m. Non-responding sections in white and low-confidence responses in black.

Interference test 4, KFR103 (177–187 m), targeting SBA4-5 (and SBA6): responses observed in HFR106:1-3 and KFR106:2-3, classified as Low- to High in propagation rate, and High- to Medium in strength. The responses are in line with expectations from the modelled geometry of SBA4 and SBA5. The same pattern of low-confidence responses, as in the shallow KFR103 test, reinforcing the association to the re-installation of the packer system in KFR27. This might be indicating some connection to SBA6.

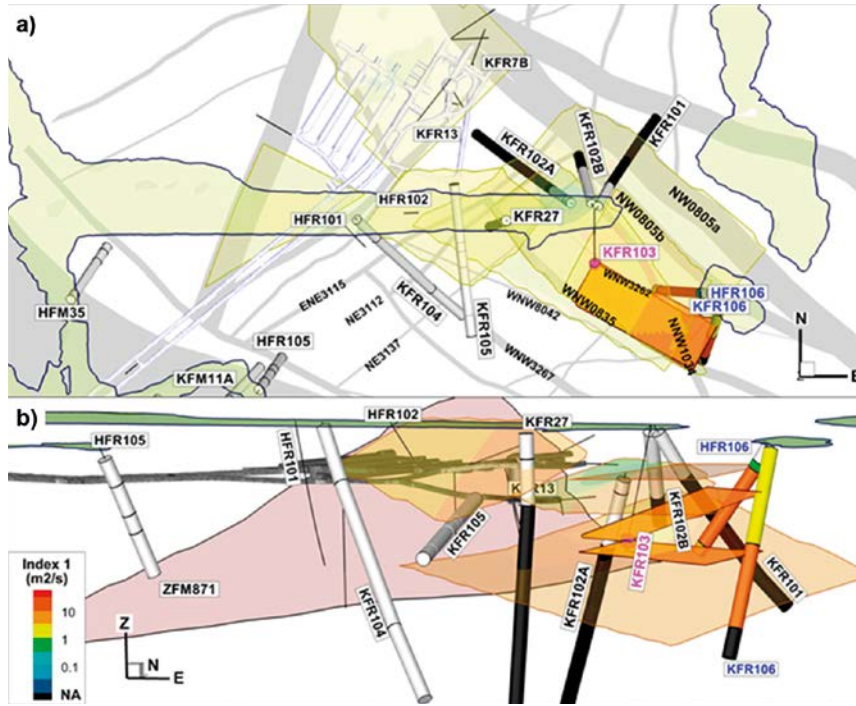


Figure 6-7. Index 1 from the interference test in KFR103, 177.0–187.0 m. Non-responding sections in white and low-confidence responses in black.

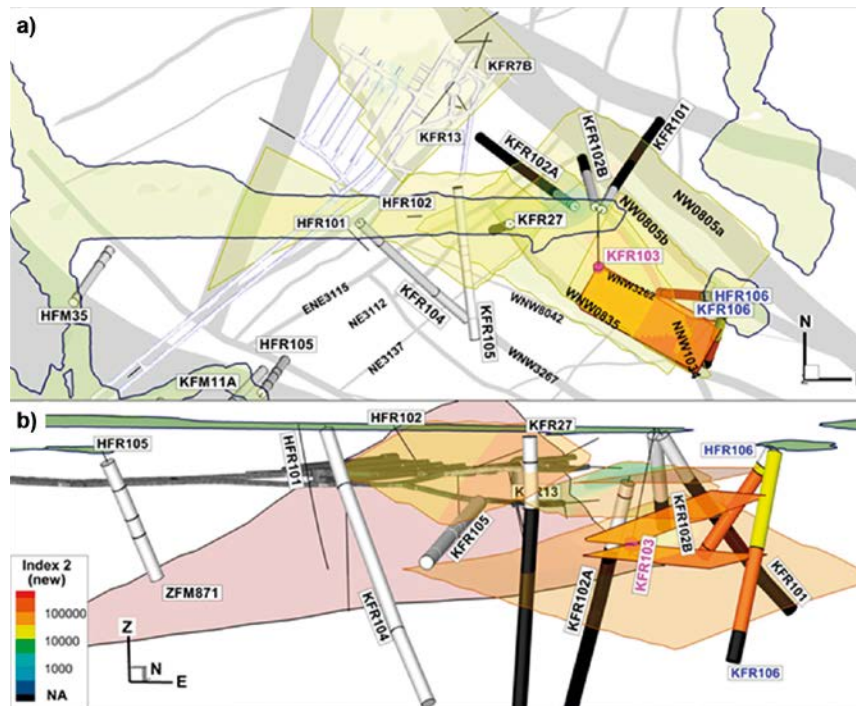


Figure 6-8. Index 2 from the interference test in KFR103, 177.0–187.0 m. Non-responding sections in white and low-confidence responses in black.

Interference test 5, KFR105 (120–137 m), permanently installed section in underground borehole from the SFR tunnel: responses observed in HFR102:1, KFR102A:7-8, KFR103:2 and KFR27:2-3, classified as Low- to Medium in propagation rate, and High- to Medium in strength. Confirms the observed patterns of the earlier KFR105 test (Walger et al. 2010). Additionally, the test demonstrates an absence of responses in KFR104, which confirms the conceptual model of less hydraulic connection towards the Central Block (Öhman et al. 2012).

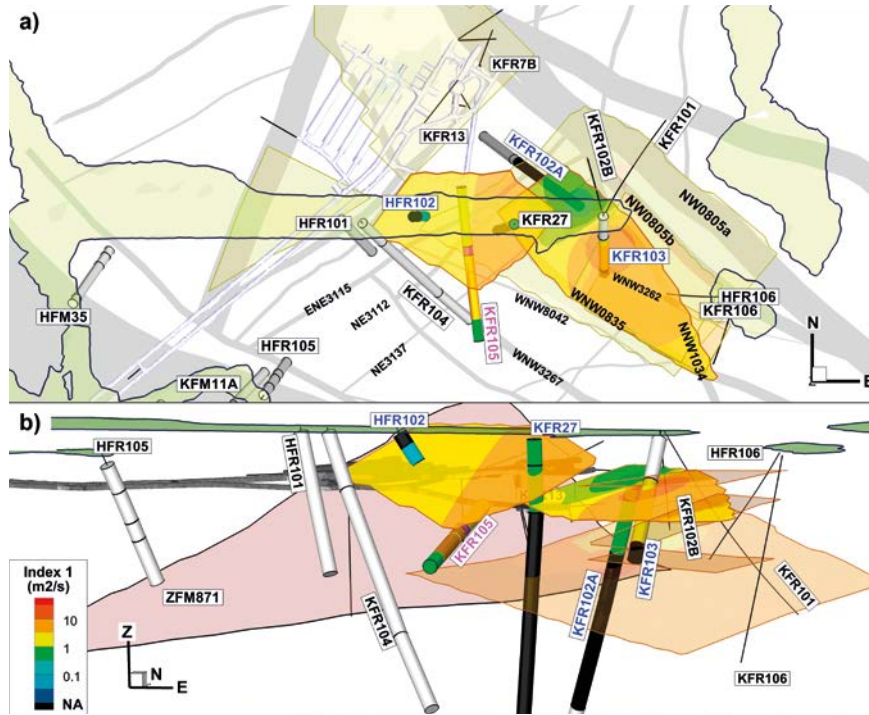


Figure 6-9. Index 1 from the interference test in KFR105, 120.0–137.0 m. Non-responding sections in white and low-confidence responses in black.

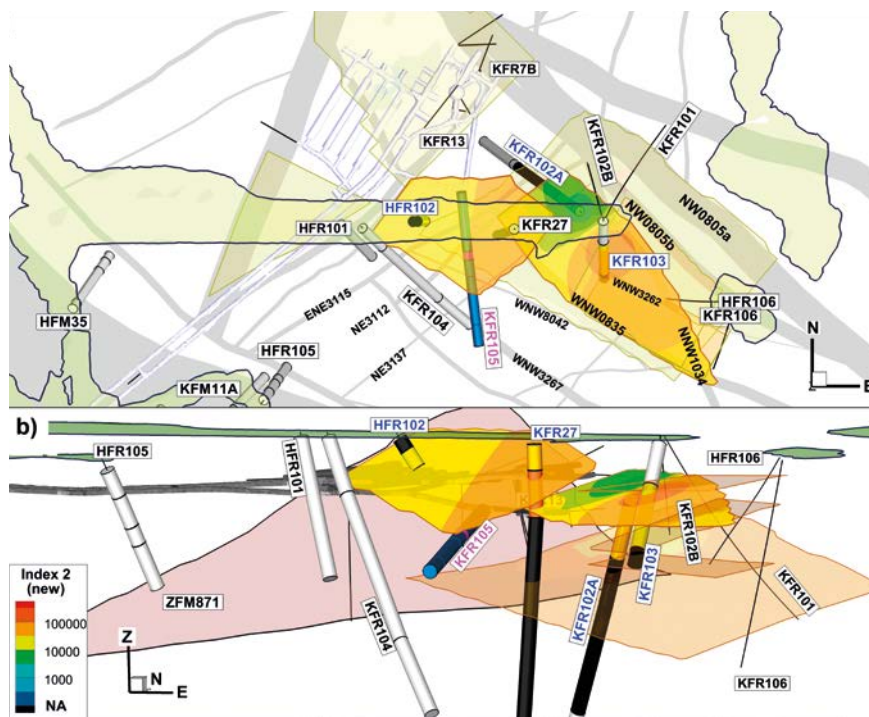


Figure 6-10. Index 2 from the interference test in KFR105, 120.0–137.0 m. Non-responding sections in white and low-confidence responses in black.

According to AP SFR-15-002 boreholes HFM16, KFM08A, B, C and KFM06A, B, C was checked for responses to the interference tests performed in this project and no responding sections were found in these boreholes.

Table 6-4. Response matrix with Index 1 and Index 2 new for the responding observation sections included in the interference tests. E = Excellent; H = High; M = Medium; L = Low, B = Below limit, sections were $s < 0.1$ m. LC = Low confidence responses, N = Non-responding sections.

Observation borehole section	Pumping Hole	KFR27		KFR27		KFR103		KFR103		KFR105	
	Section (m.b. TOC)	47.00–57.00		189.40–194.40		83.50–93.50		177.00–187.00		120.00–137.00	
	Flow rate (L/min)	2.46		5.24		2.68		2.70		5.26	
	Drawdown (m)	7.70		6.53		3.12		7.24		78.40	
	Response indices	1	2 new	1	2 new	1	2 new	1	2 new	1	2 new
	Interval (m)										
HFM34:2	22.00–90.00	N	N	N	N	N	N	N	N	N	N
HFM34:3	0.00–21.00	N	N	N	N	N	N	N	N	N	N
HFM35:1	182.00–200.75	N	N	N	N	N	N	N	N	N	N
HFM35:2	151.00–181.00	N	N	N	N	N	N	N	N	N	N
HFM35:3	34.00–150.00	N	N	N	N	N	N	N	N	N	N
HFM35:4	0.00–33.00	N	N	N	N	N	N	N	N	N	N
HFR102:1	28.00–55.04	N	N	N	N	-	-	-	-	L	M
HFR102:2	0.00–27.00	N	N	N	N	-	-	-	-	LC	LC
HFR105:1	134.00–200.50	N	N	N	N	N	N	N	N	N	N
HFR105:2	107.00–133.00	N	N	N	N	N	N	N	N	N	N
HFR105:3	61.00–106.00	N	N	N	N	N	N	N	N	N	N
HFR105:4	0.00–60.00	N	N	N	N	N	N	N	N	N	N
HFR106:1	175.00–190.40	N	N	N	N	LC	LC	M	H	-	-
HFR106:2	47.00–174.00	N	N	N	N	LC	LC	H	H	-	-
HFR106:3	36.00–46.00	N	N	N	N	B	B	L	M	-	-
HFR106:4	0.00–35.00	N	N	N	N	N	N	N	N	-	-
KFM11A:1	711.00–851.21	N	N	N	N	N	N	N	N	N	N
KFM11A:2	690.00–710.00	N	N	N	N	N	N	N	N	N	N
KFM11A:3	457.00–689.00	N	N	N	N	N	N	N	N	N	N
KFM11A:4	446.00–456.00	N	N	N	N	N	N	N	N	N	N
KFM11A:5	361.00–445.00	N	N	N	N	N	N	N	N	N	N
KFM11A:6	131.00–360.00	N	N	N	N	N	N	N	N	N	N
KFM11A:7	0.00–130.00	N	N	N	N	N	N	N	N	N	N
KFR04:1	84.09–100.50	N	N	N	N	-	-	-	-	-	-
KFR04:2	44.09–83.09	N	N	N	N	-	-	-	-	-	-
KFR04:3	28.09–43.09	N	N	N	N	-	-	-	-	-	-
KFR04:4	5.09–27.09	N	N	N	N	-	-	-	-	-	-
KFR05:1	97.15–131.00	N	N	N	N	-	-	-	-	-	-
KFR05:2	80.15–96.15	N	N	N	N	-	-	-	-	-	-
KFR05:3	57.15–79.15	N	N	N	N	-	-	-	-	-	-
KFR05:4	12.15–56.15	N	N	N	N	-	-	-	-	-	-
KFR101:1	279.50–341.76	N	N	M	H	LC	LC	LC	LC	-	-
KFR101:2	91.00–278.50	LC	LC	H	H	LC	LC	LC	LC	-	-
KFR101:3	0.00–90.00	N	N	N	N	L	M	N	N	-	-
KFR102A:1	444.00–600.83	LC	LC	LC	LC	LC	LC	LC	LC	N	N
KFR102A:2	423.00–443.00	LC	LC	LC	LC	LC	LC	LC	LC	N	N
KFR102A:3	255.00–422.00	M	H	M	H	LC	LC	LC	LC	LC	LC
KFR102A:4	220.00–254.00	M	H	M	H	LC	LC	LC	LC	LC	LC
KFR102A:5	214.00–219.00	M	H	H	H	LC	LC	LC	LC	LC	LC
KFR102A:6	185.00–213.00	M	H	H	H	LC	LC	LC	LC	LC	LC
KFR102A:7	103.00–184.00	L	M	M	M	L	H	N	N	L	M
KFR102A:8	0.00–102.00	L	M	LC	LC	L	H	N	N	L	M
KFR102B:1	146.00–180.08	-	-	H	H	LC	LC	LC	LC	-	-
KFR102B:2	128.00–145.00	-	-	M	H	LC	LC	LC	LC	-	-
KFR102B:3	0.00–127.00	N	N	N	N	B	B	N	N	-	-

Observation borehole section	Pumping Hole	KFR27		KFR27		KFR103		KFR103		KFR105		
	Section (m.b. TOC)	47.00–57.00		189.40–194.40		83.50–93.50		177.00–187.00		120.00–137.00		
	Flow rate (L/min)	2.46		5.24		2.68		2.70		5.26		
	Drawdown (m)	7.70		6.53		3.12		7.24		78.40		
	Response indices	1	2 new	1	2 new	1	2 new	1	2 new	1	2 new	
	Interval (m)											
KFR103:1	178.00–200.50	-	-	-	-	-	-	-	-	-	LC	LC
KFR103:2	79.00–177.00	-	-	-	-	-	-	-	-	-	M	M
KFR103:3	0.00–78.00	-	-	-	-	-	-	-	-	-	N	N
KFR104:1	333.00–454.57	N	N	N	N	N	N	N	N	N	N	N
KFR104:2	98.00–332.00	N	N	N	N	N	N	N	N	N	N	N
KFR104:3	0.00–97.00	N	N	N	N	N	N	N	N	N	N	N
KFR105:1	265.00–303.00	LC	LC	N	N	N	N	N	N	N	-	-
KFR105:2	170.00–264.00	M	H	N	N	LC	LC	N	N	N	-	-
KFR105:3	138.00–169.00	L	H	N	N	LC	LC	N	N	N	-	-
KFR105:4	120.00–137.00	L	H	N	N	LC	LC	N	N	N	-	-
KFR105:5	4.00–119.00	LC	LC	M	M	N	N	N	N	N	-	-
KFR106:1	260.00–300.13	N	N	LC	LC	N	N	LC	LC	N	-	-
KFR106:2	143.00–259.00	N	N	N	N	LC	LC	H	H	N	-	-
KFR106:3	0.00–142.00	N	N	N	N	L	M	M	M	N	-	-
KFR13:1	53.75–76.60	N	N	N	N	-	-	-	-	-	-	-
KFR13:2	33.75–52.75	N	N	N	N	-	-	-	-	-	-	-
KFR13:3	3.75–32.75	N	N	N	N	-	-	-	-	-	-	-
KFR55:1	48.53–61.89	N	N	N	N	-	-	-	-	-	-	-
KFR55:2	39.53–47.53	N	N	N	N	-	-	-	-	-	-	-
KFR55:3	21.53–38.53	N	N	N	N	-	-	-	-	-	-	-
KFR55:4	7.53–20.53	N	N	N	N	-	-	-	-	-	-	-
KFR07B:1	3.40–7.60	N	N	N	N	-	-	-	-	-	-	-
KFR07B:2	8.60–21.10	N	N	N	N	-	-	-	-	-	-	-
HFR101:1	0.00–209.30	N	N	N	N	-	-	-	-	-	N	N
KFR27:1	110.00–501.64	-	-	-	-	LC	LC	LC	LC	LC	LC	LC
KFR27:2	47.00–109.00	-	-	-	-	M	H	N	N	L	H	H
KFR27:3	0.00–46.00	-	-	-	-	M	M	N	N	L	M	M

References

SKB's (Svensk Kärnbränslehantering AB) publications can be found at www.skb.com/publications. SKBdoc documents will be submitted upon request to document@skb.se.

Knudby C, Carrera J, 2006. On the use of apparent hydraulic diffusivity as indicator of connectivity. *Journal of Hydrology* 329, 377-389.

Kruseman G P, de Ridder N A, 1991. Analysis and evaluation of pumping test data. 2nd ed. Wageningen, The Netherlands: International Institute for Land Reclamation and Improvement. (ILRI publication 47)

Odén M, Öhman J, 2017. TD15 Complementary simulation cases in support of SR-PSU. SKBdoc 1578373 ver 1.0, Svensk Kärnbränslehantering AB.

Odén M, Follin S, Öhman J, Vidtsrand P, 2014. SR-PSU Bedrock hydrogeology. Groundwater flow modelling methodology, setup and results. SKB R-13-25, Svensk Kärnbränslehantering AB.

Rhén I (ed), Gustafson G, Stanfors R, Wikberg P, 1997. Äspö HRL – Geoscientific evaluation 1997/5. Models based on site characterization 1986–1995. SKB TR 97-06, Svensk Kärnbränslehantering AB.

SKB, 2008. Geovetenskapligt undersökningsprogram för utbyggnad av SFR. SKB R-08-67, Svensk Kärnbränslehantering AB. (In Swedish.)

SKB, 2013. Site description of the SFR area at Forsmark at completion of the site investigation phase. SDM-PSU Forsmark. SKB TR-11-04, Svensk Kärnbränslehantering AB.

Walger E, Ludvigson J-E, Gentzschein B, 2010. SFR Site investigation. Evaluation of selected interference tests and pressure responses during drilling at SFR. SKB P-10-43, Svensk Kärnbränslehantering AB.

Öhman J, Bockgård N, Follin S, 2012. Bedrock hydrogeology. Site investigation SFR. SKB R-11-03, Svensk Kärnbränslehantering AB.

Linear plots of hydraulic pressure versus time for pumping boreholes and hydraulic head versus time for responding observation sections, together with barometric pressure and sea level data

A1.1 Interference test in KFR27: 47–57 m

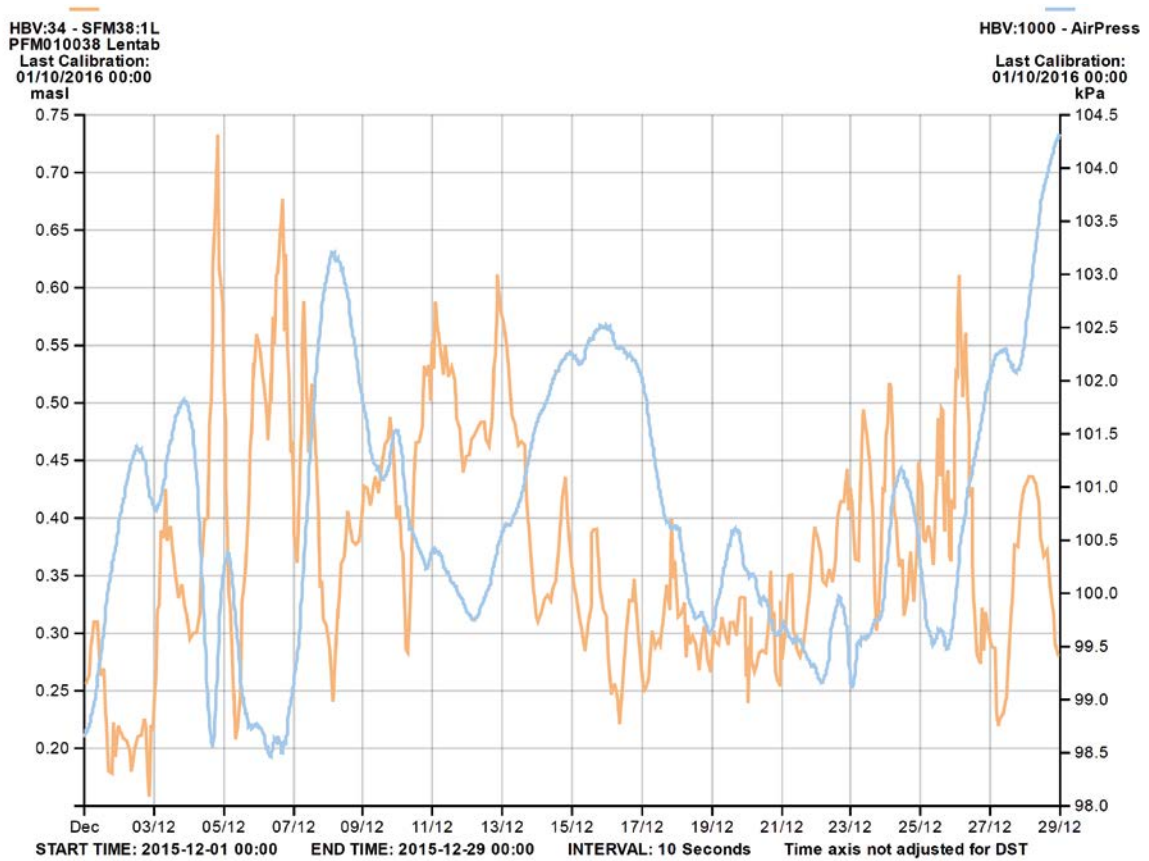


Figure A1-1. Registered air pressure (blue line) and sea water level (orange line) at SFR during the interference test period in KFR27: 47–57 m, with data from circa ten days before and ten days after. Each parameter has its own Y-scale. Pumping period occurred between 2015-12-09 and 2015-12-14.

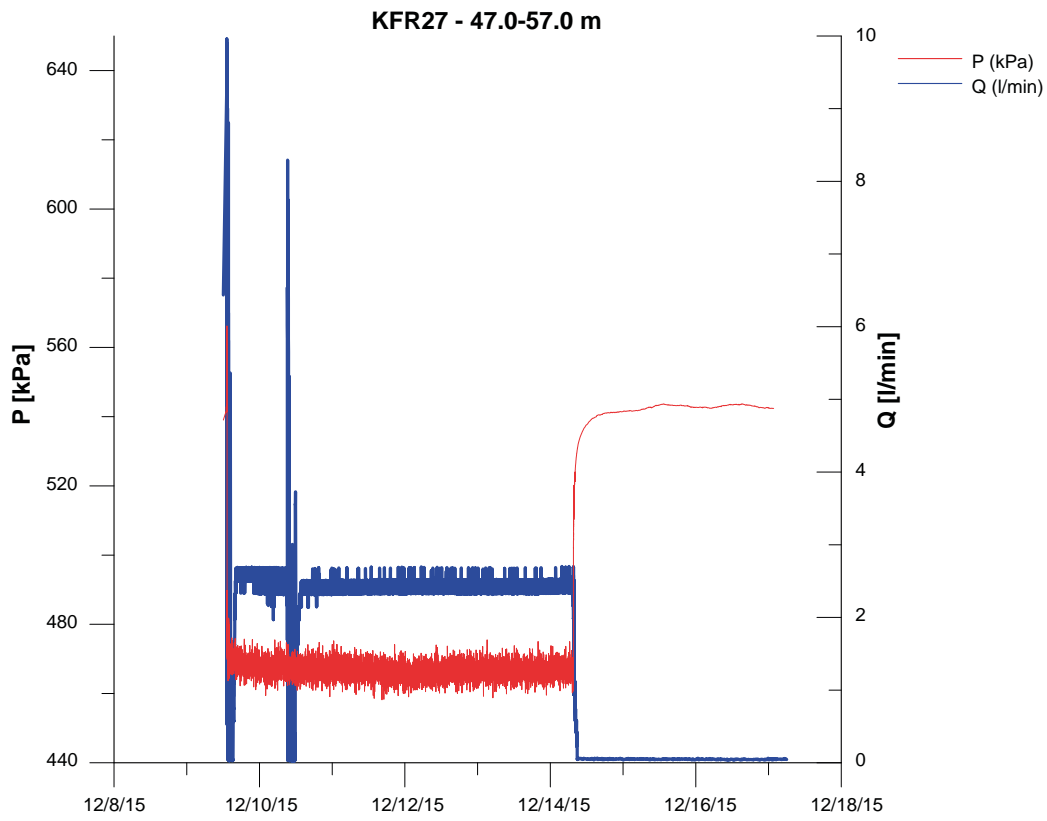


Figure AI-2. Linear plot of observed pressure and pumped flow versus time in the pumping borehole KFR27 47: 0–57.0 m during the interference pumping test.

A1.1.1 Responses in observation sections for test in KFR27: 47–57 m

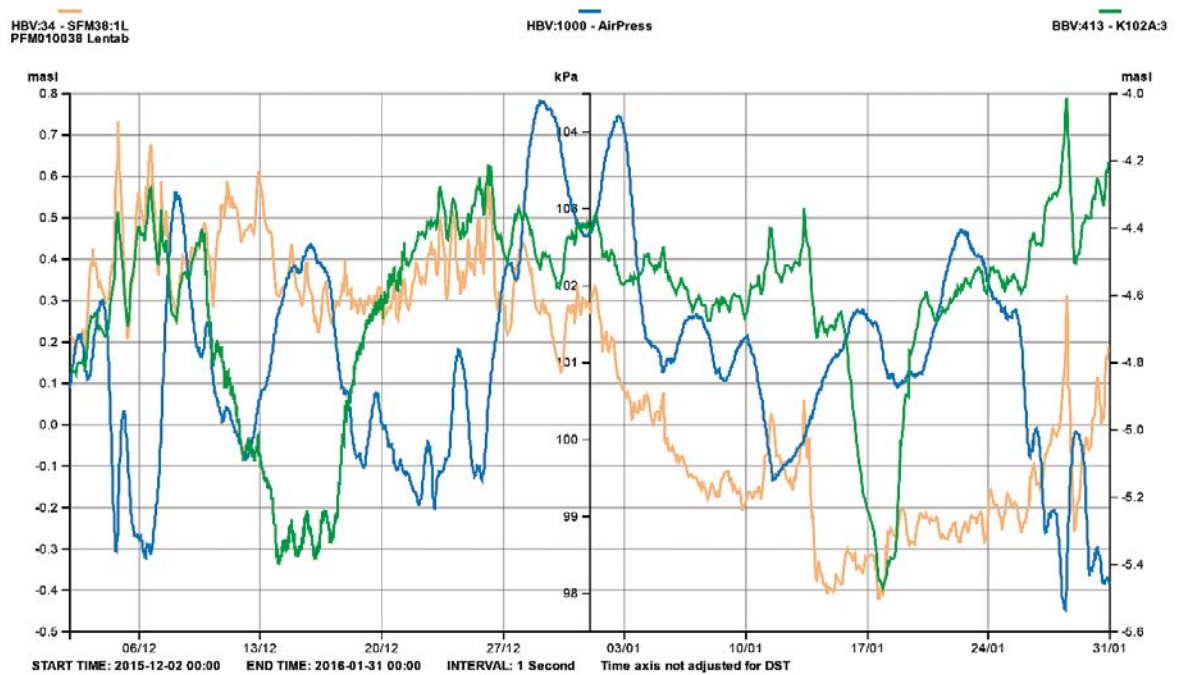


Figure A1-3. Linear plot of observed head versus time in the observation borehole KFR102A:3 during the interference pumping tests in KFR27: 47.0–57.0 m. Pumping period occurred between 2015-12-09 and 2015-12-14.

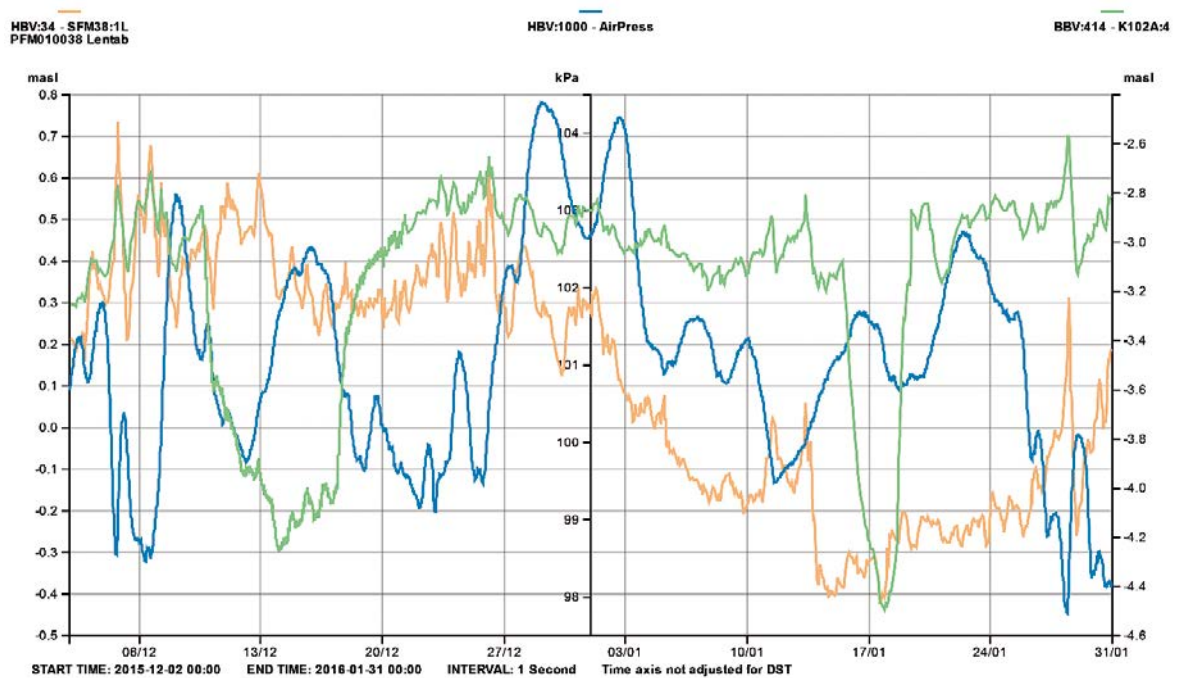


Figure A1-4. Linear plot of observed head versus time in the observation borehole KFR102A:4 during the interference pumping tests in KFR27: 47.0–57.0 m. Pumping period occurred between 2015-12-09 and 2015-12-14.

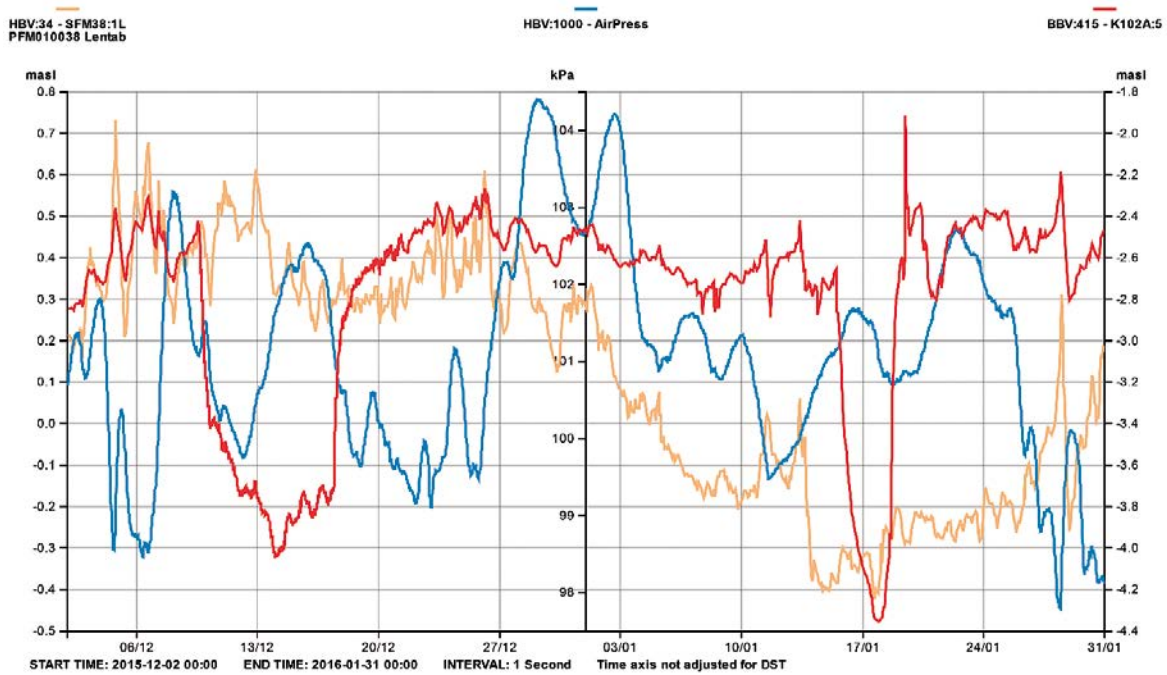


Figure A1-5. Linear plot of observed head versus time in the observation borehole KFR102A:5 during the interference pumping tests in KFR27: 47.0–57.0 m. Pumping period occurred between 2015-12-09 and 2015-12-14.

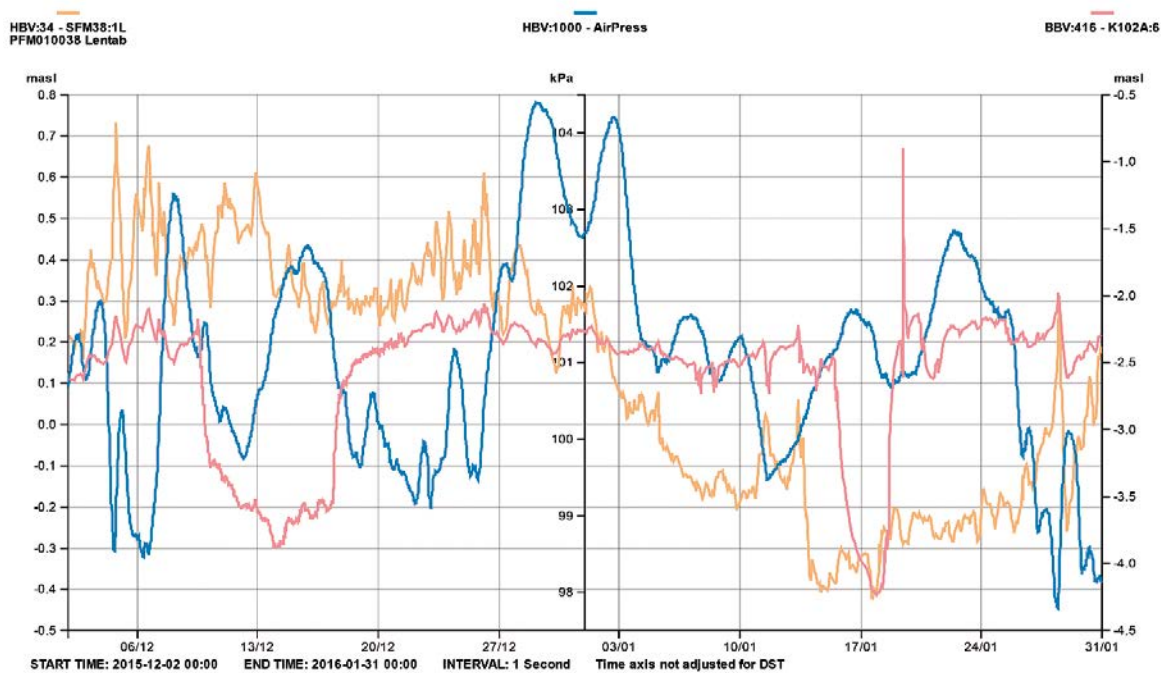


Figure A1-6. Linear plot of observed head versus time in the observation borehole KFR102A:6 during the interference pumping tests in KFR27: 47.0–57.0 m. Pumping period occurred between 2015-12-09 and 2015-12-14.

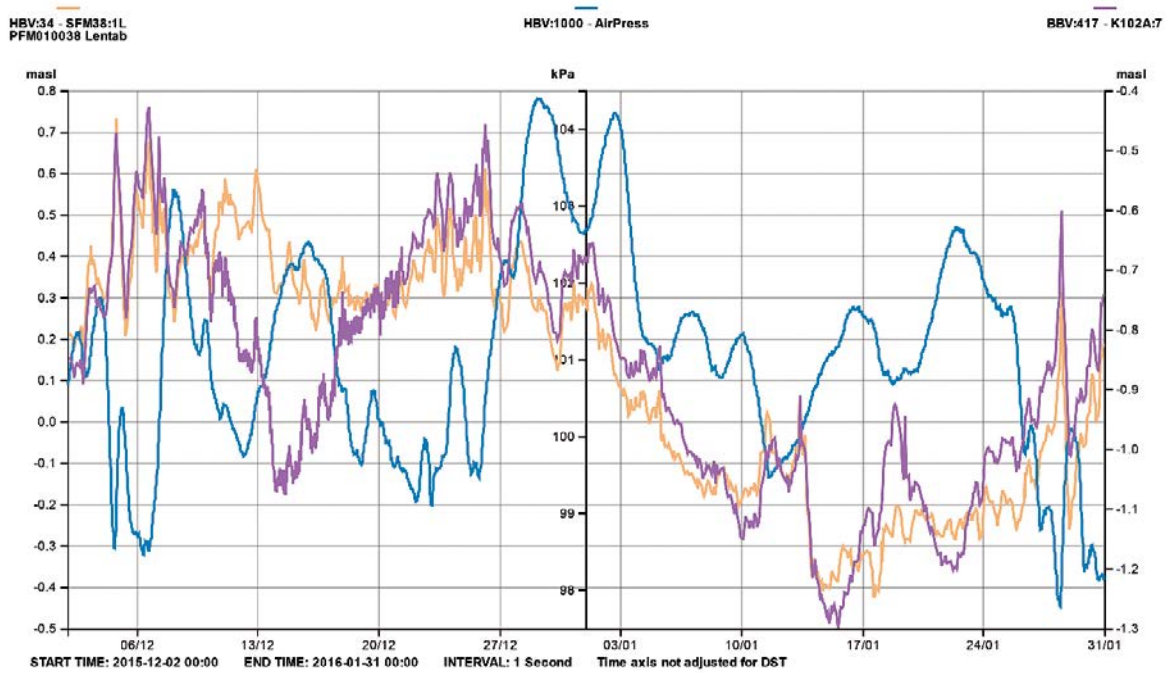


Figure A1-7. Linear plot of observed head versus time in the observation borehole KFR102A:7 during the interference pumping tests in KFR27: 47.0–57.0 m. Pumping period occurred between 2015-12-09 and 2015-12-14.

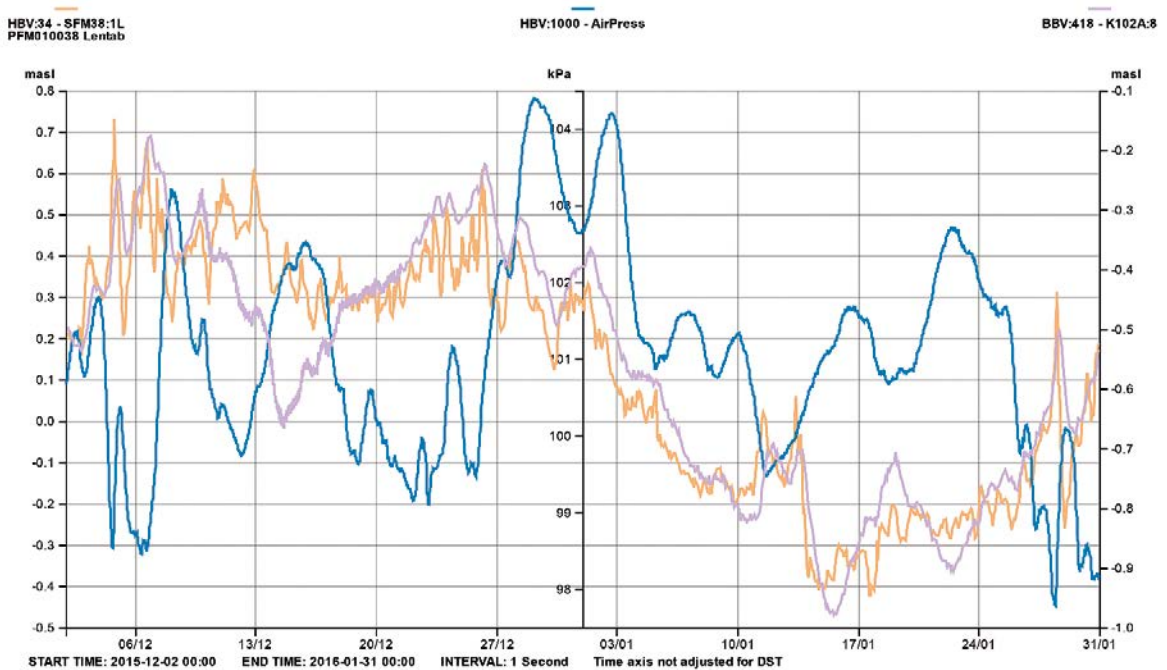


Figure A1-8. Linear plot of observed head versus time in the observation borehole KFR102A:8 during the interference pumping tests in KFR27: 47.0–57.0 m. Pumping period occurred between 2015-12-09 and 2015-12-14.

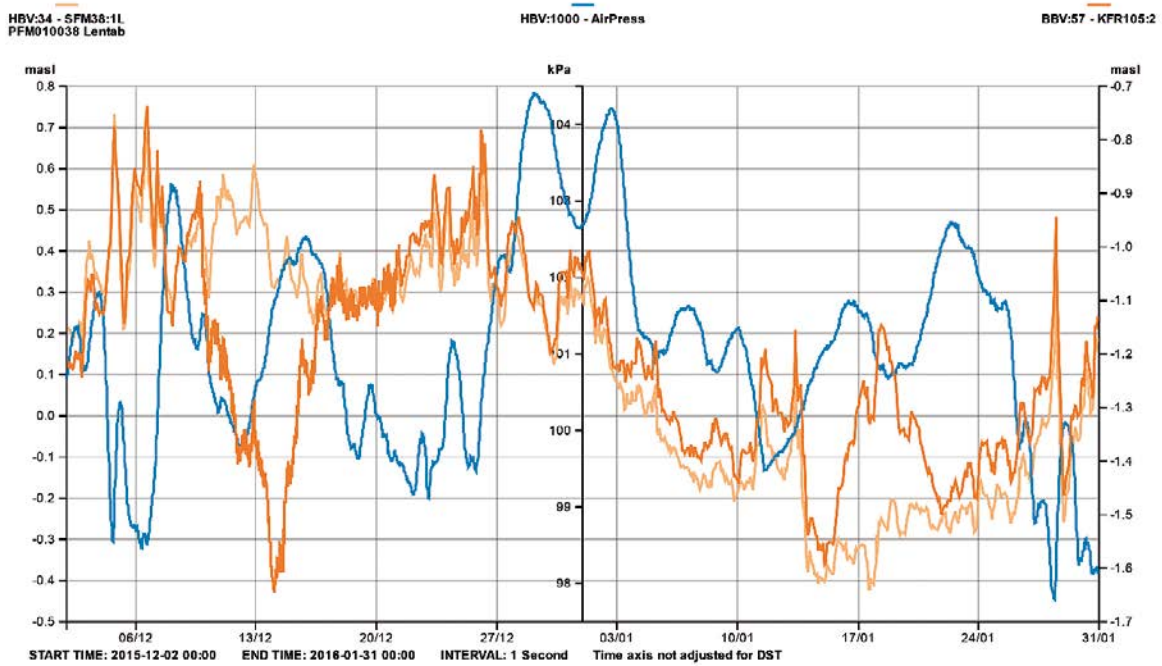


Figure A1-9. Linear plot of observed head versus time in the observation borehole KFR105:2 during the interference pumping tests in KFR27: 47.0–57.0 m. Pumping period occurred between 2015-12-09 and 2015-12-14.

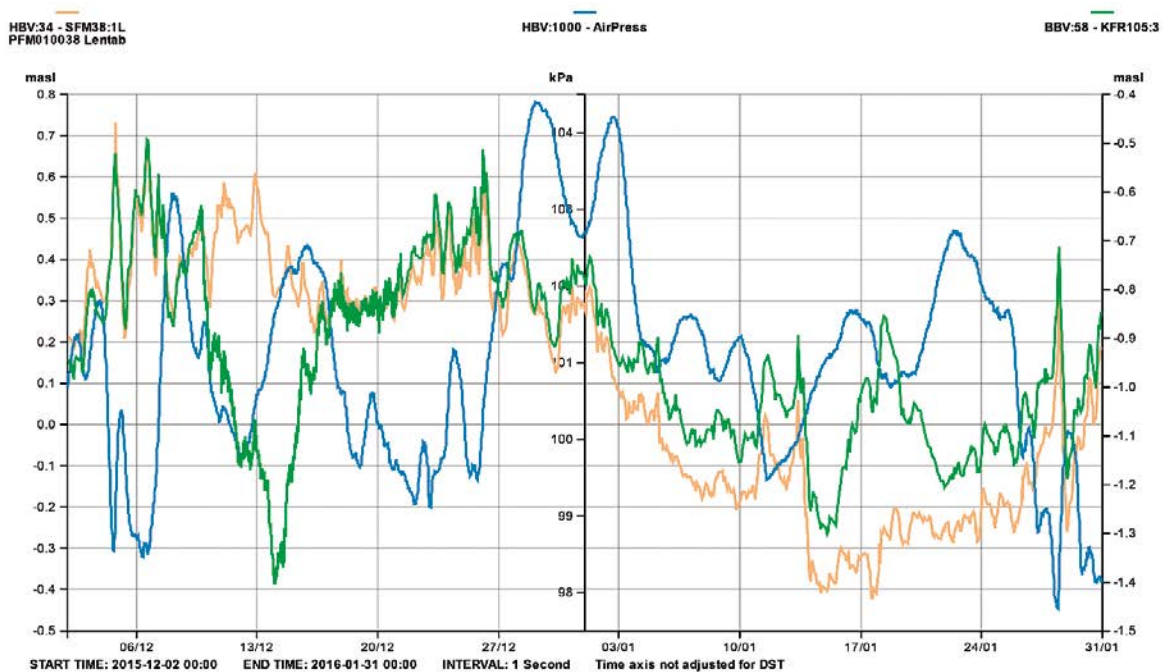


Figure A1-10. Linear plot of observed head versus time in the observation borehole KFR105:3 during the interference pumping tests in KFR27: 47.0–57.0 m. Pumping period occurred between 2015-12-09 and 2015-12-14.

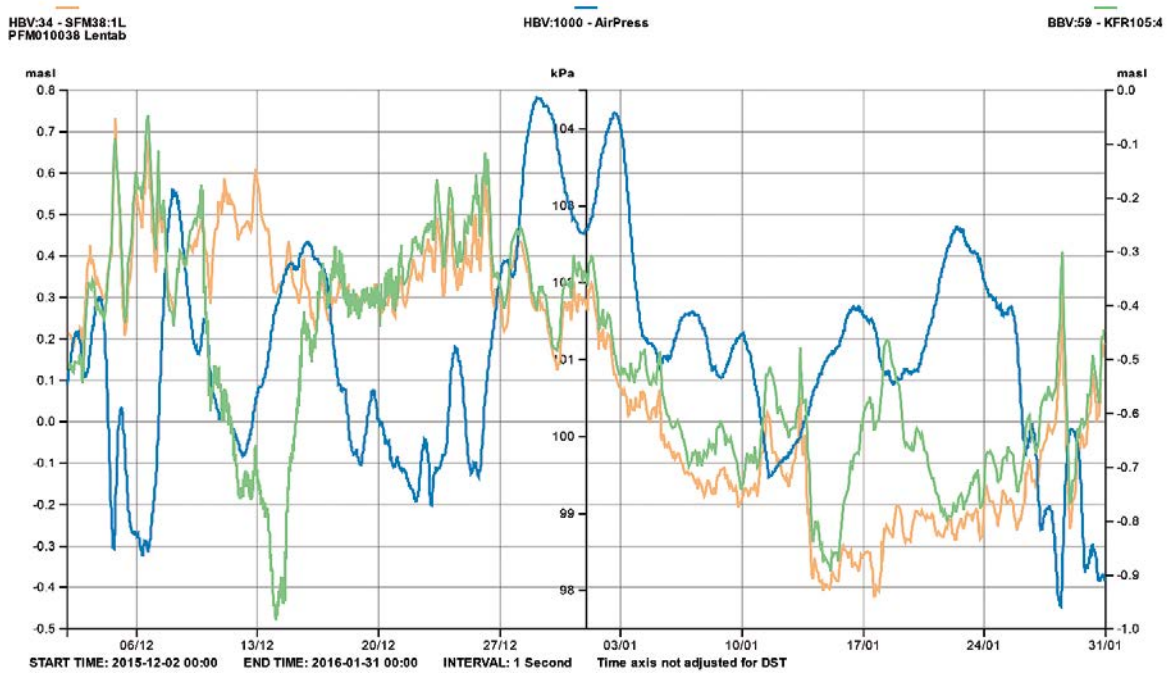


Figure A1-11. Linear plot of observed head versus time in the observation borehole KFR105:4 during the interference pumping tests in KFR27: 47.0–57.0 m. Pumping period occurred between 2015-12-09 and 2015-12-14.

A1.1.2 Low confidence responses in observation sections for test in KFR27: 47.0–57.0 m

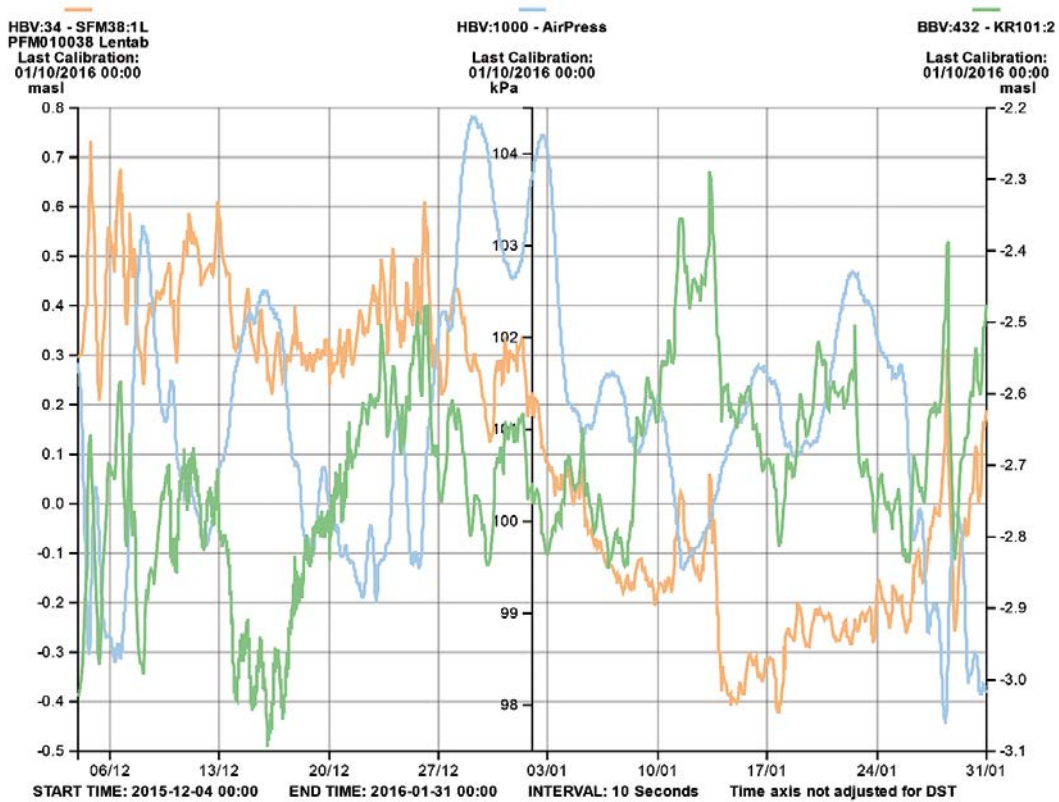


Figure A1-12. Linear plot of observed head versus time in the observation borehole KFR101:2 during the interference pumping tests in KFR27: 47.0–57.0 m. Pumping period occurred between 2015-12-09 and 2015-12-14.

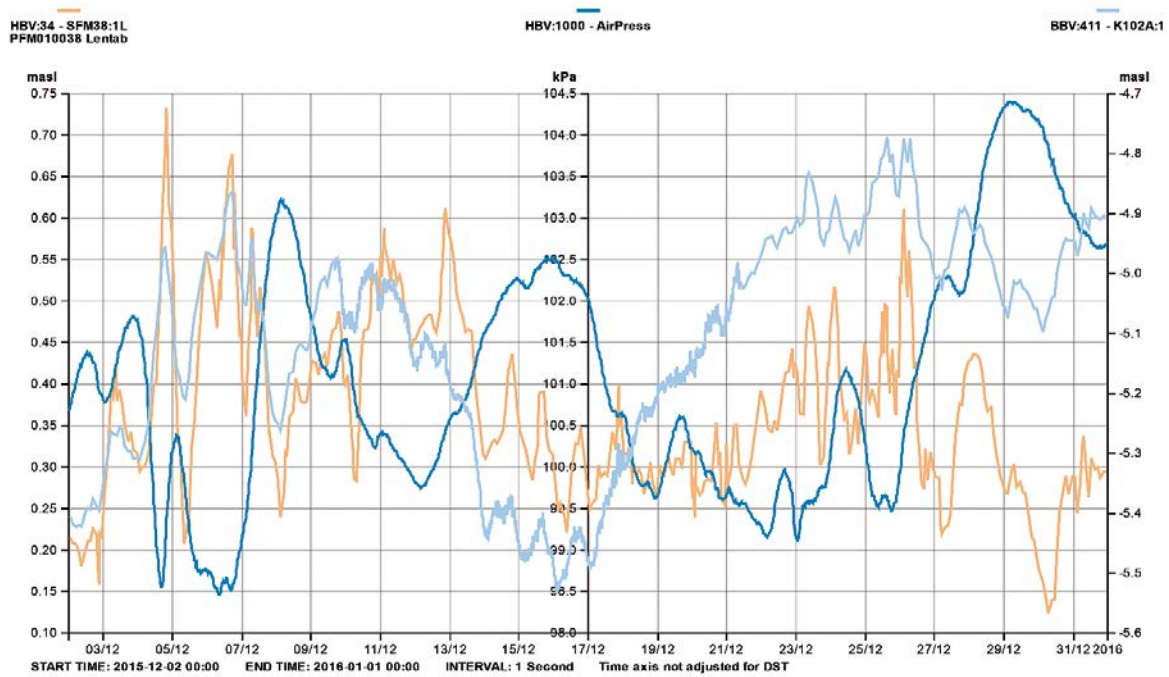


Figure A1-13. Linear plot of observed head versus time in the observation borehole KFR102A:1 during the interference pumping tests in KFR27: 47.0–57.0 m. Pumping period occurred between 2015-12-09 and 2015-12-14.

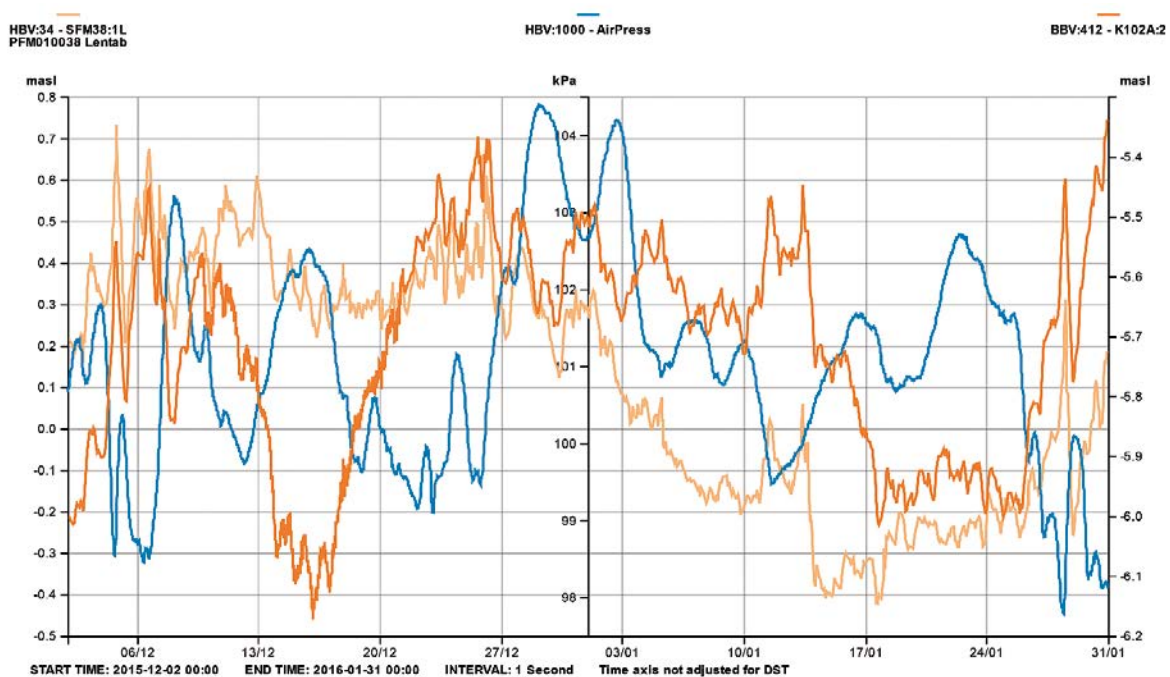


Figure A1-14. Linear plot of observed head versus time in the observation borehole KFR102A:2 during the interference pumping tests in KFR27: 47.0–57.0 m. Pumping period occurred between 2015-12-09 and 2015-12-14

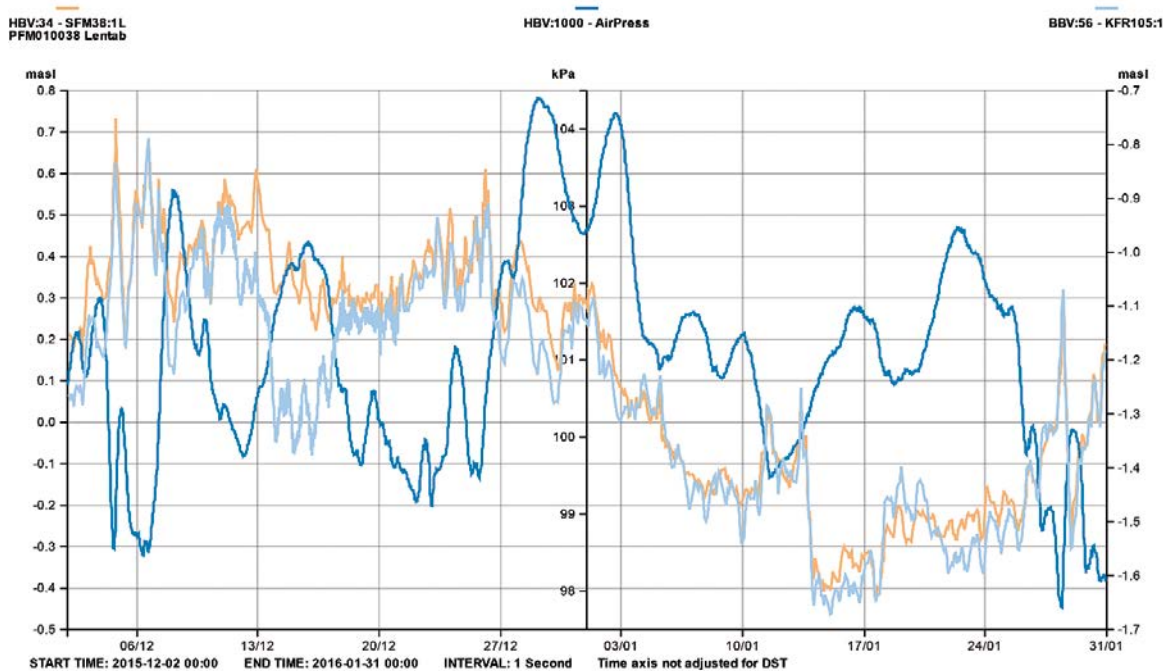


Figure A1-15. Linear plot of observed head versus time in the observation borehole KFR105:1 during the interference pumping tests in KFR27: 47.0–57.0 m. Pumping period occurred between 2015-12-09 and 2015-12-14.

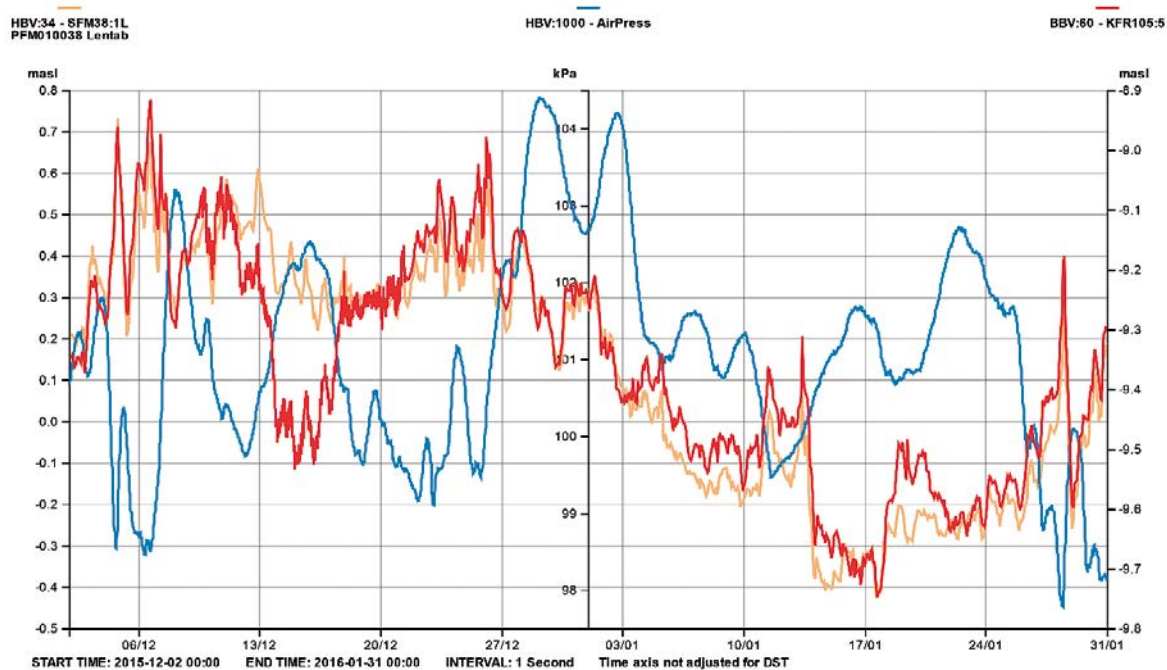


Figure A1-16. Linear plot of observed head versus time in the observation borehole KFR105:5 during the interference pumping tests in KFR27: 47.0–57.0 m. Pumping period occurred between 2015-12-09 and 2015-12-14.

A1.2 Interference test in KFR27: 189.4–94.4 m

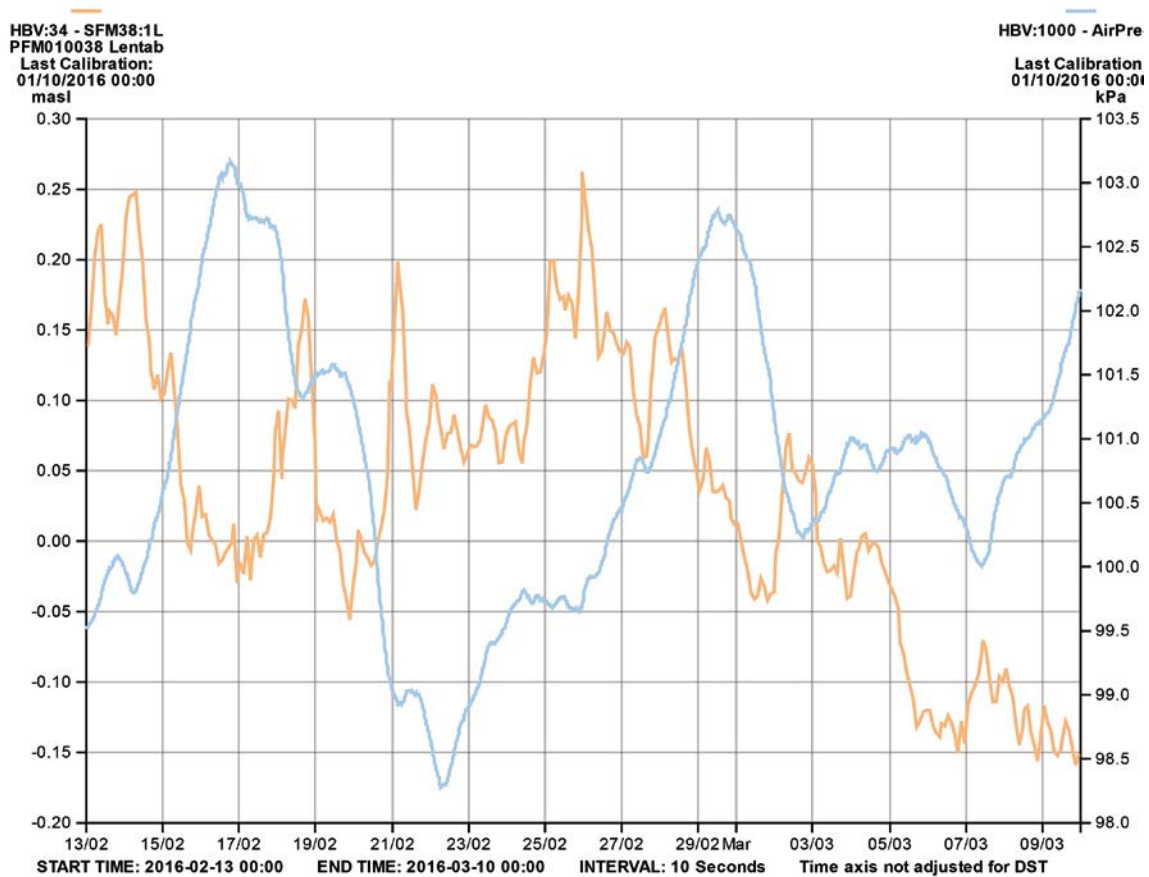


Figure A1-17. Registered air pressure (blue line) and sea water level (orange line) at SFR during the interference test period in KFR27: 189.4–194.4 m, with data from circa ten days before and ten days after. Each parameter has its own Y-scale. Pumping period occurred between 2016-02-23 and 2016-02-26.

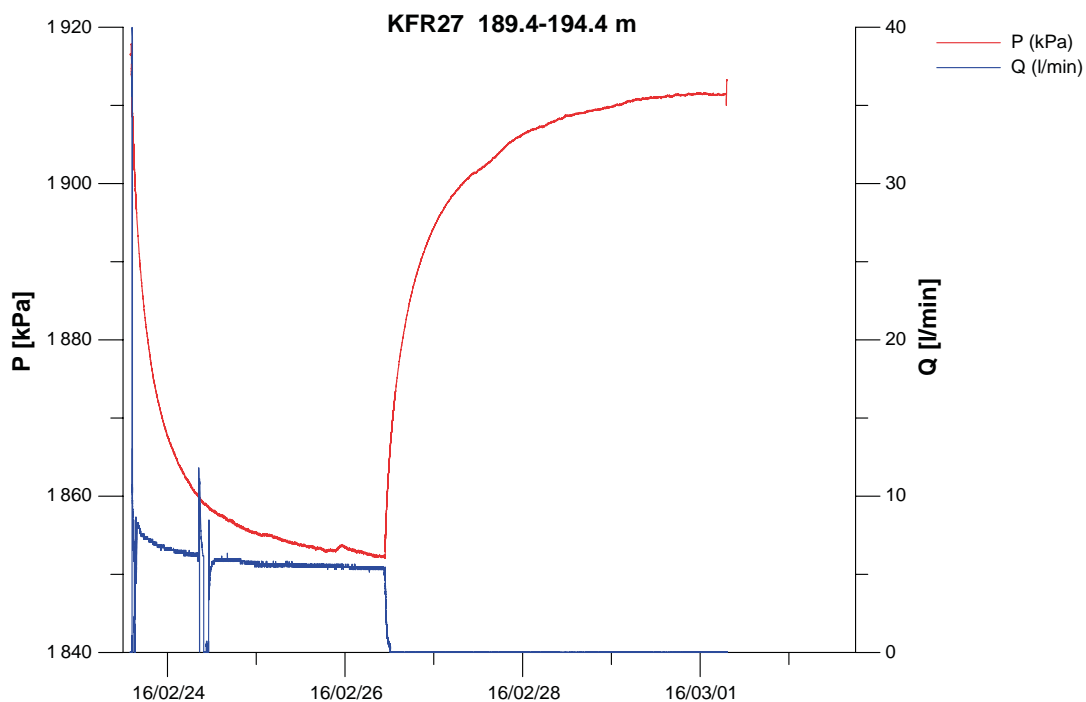


Figure A1-18. Linear plot of observed pressure and pumped flow versus time in the pumping borehole KFR27: 189.4–194.4 m during the interference pumping test.

A1.2.1 Responses in observation sections for test in KFR27: 189.4–194.4 m

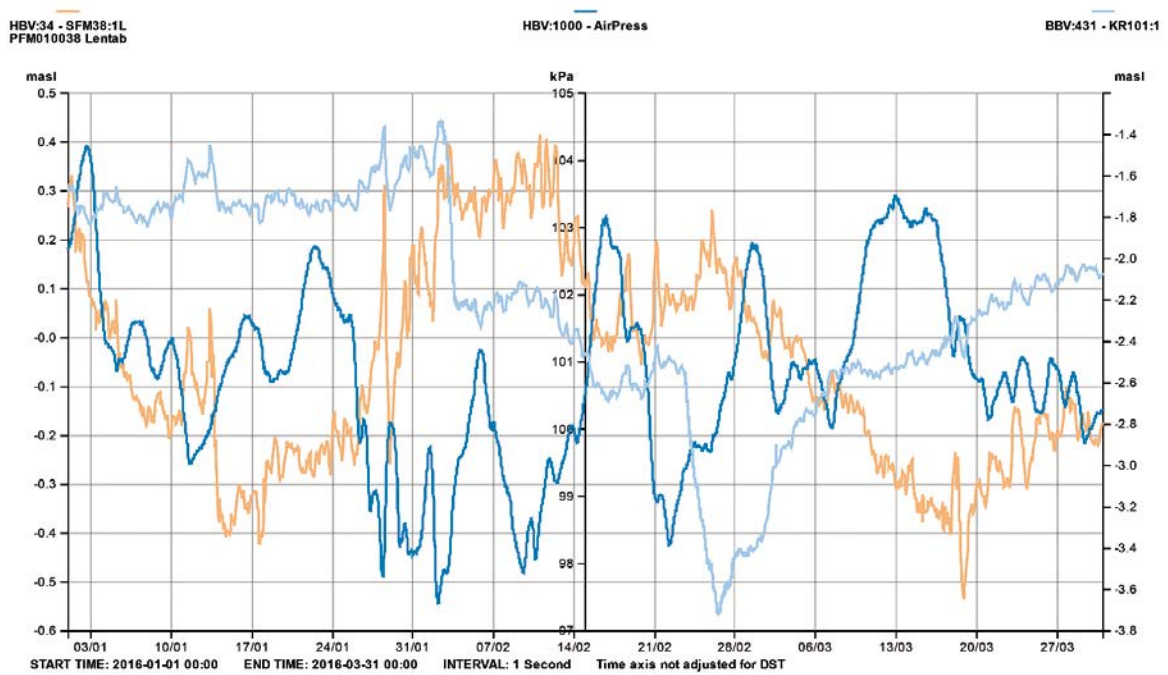


Figure A1-19. Linear plot of observed head versus time in the observation borehole KFR101:1 during the interference pumping tests in KFR27: 189.4–194.4 m. Pumping period occurred between 2016-02-23 and 2016-02-26.

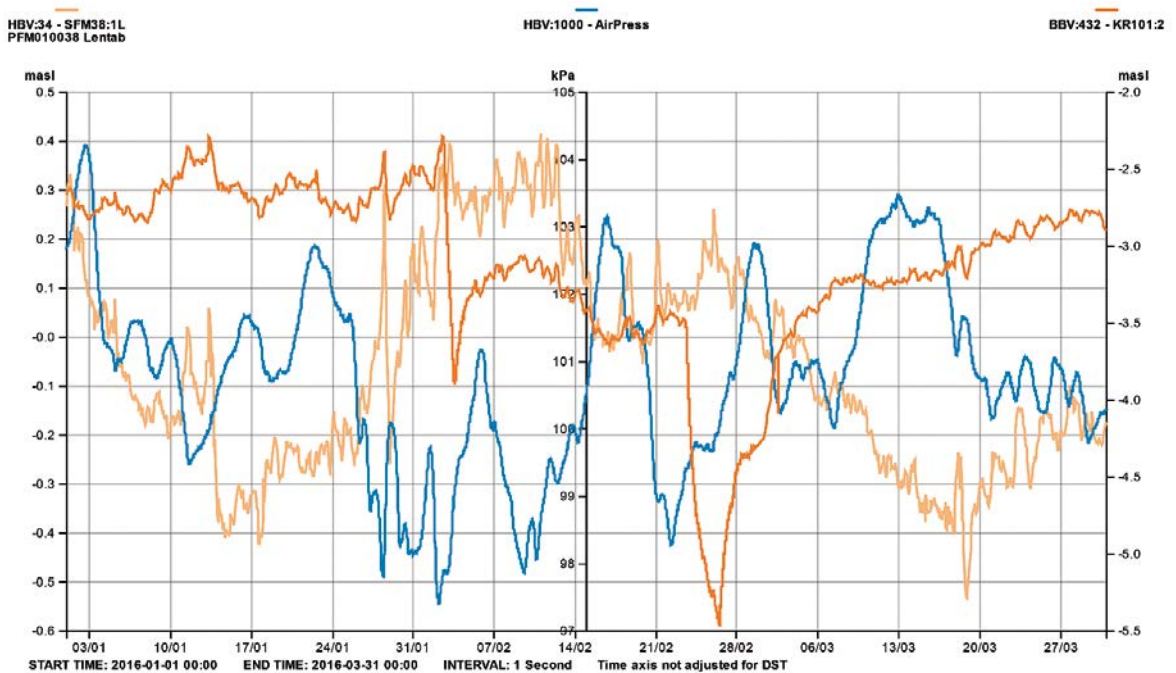


Figure A1-20. Linear plot of observed head versus time in the observation borehole KFR101:2 during the interference pumping tests in KFR27: 189.4–194.4 m. Pumping period occurred between 2016-02-23 and 2016-02-26.

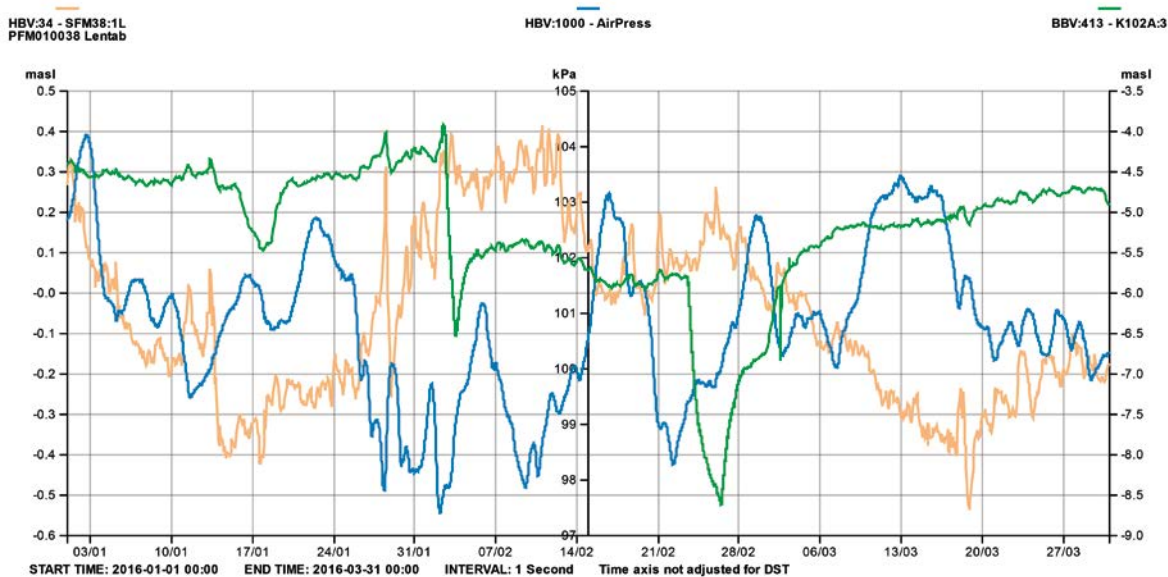


Figure A1-21. Linear plot of observed head versus time in the observation borehole KFR102A:3 during the interference pumping tests in KFR27: 189.4–194.4 m. Pumping period occurred between 2016-02-23 and 2016-02-26.

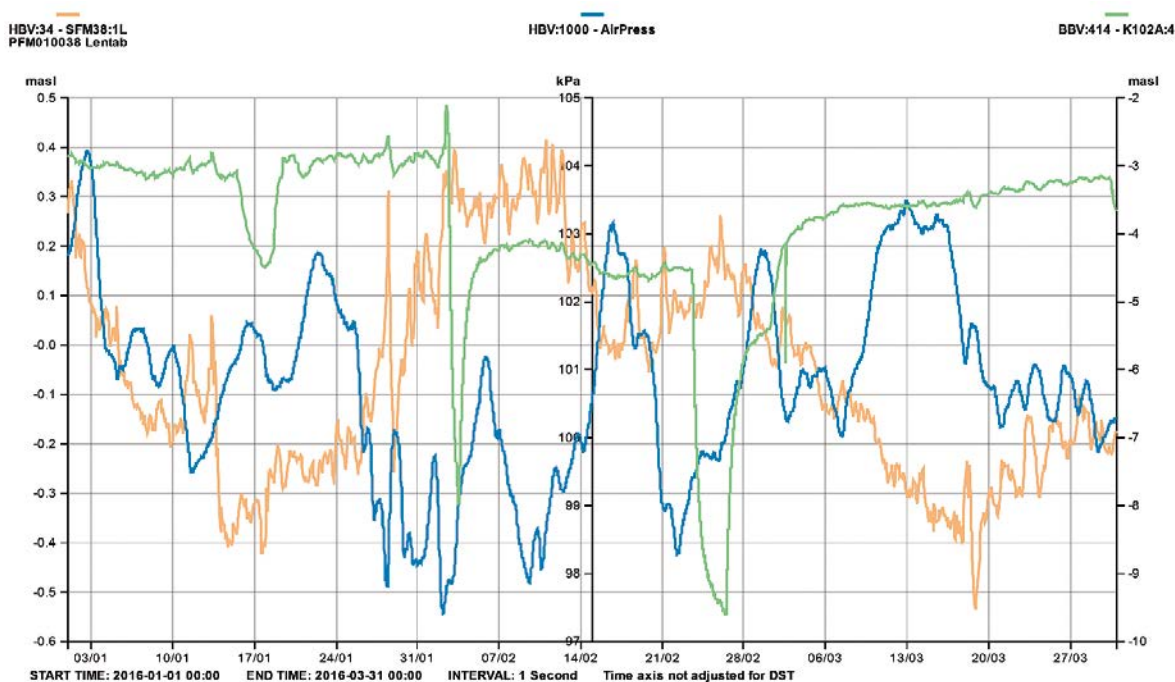


Figure A1-22. Linear plot of observed head versus time in the observation borehole KFR102A:4 during the interference pumping tests in KFR27: 189.4–194.4 m. Pumping period occurred between 2016-02-23 and 2016-02-26.

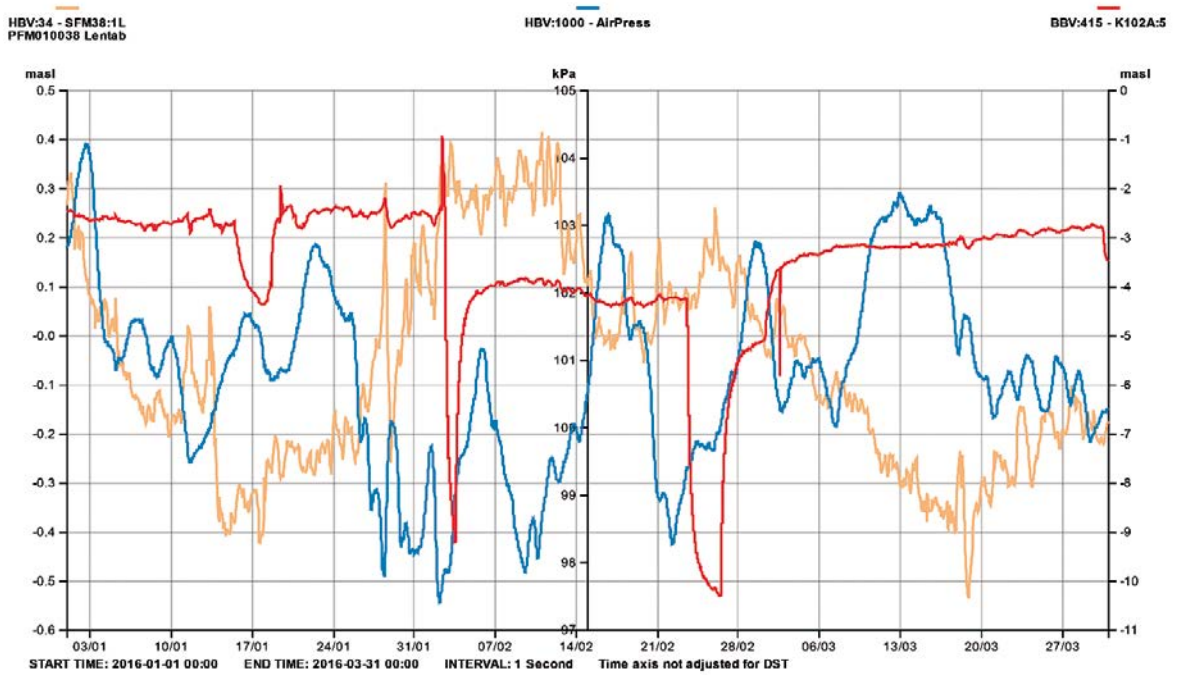


Figure A1-23. Linear plot of observed head versus time in the observation borehole KFR102A:5 during the interference pumping tests in KFR27: 189.4–194.4 m. Pumping period occurred between 2016-02-23 and 2016-02-26.

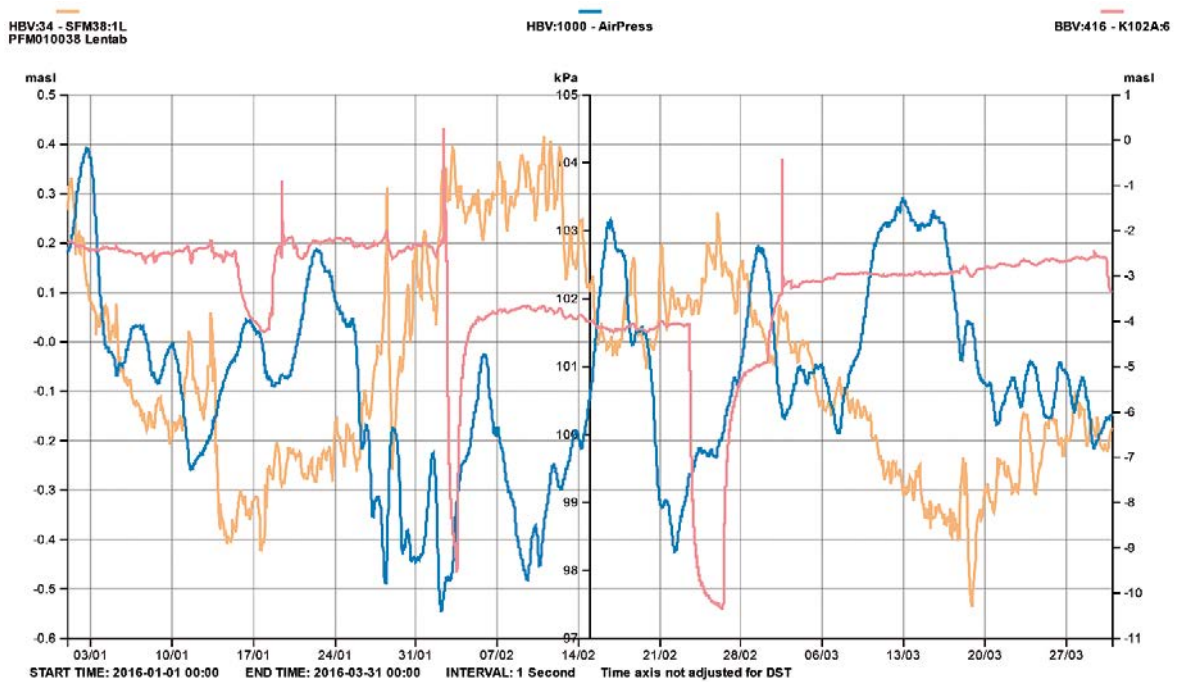


Figure A1-24. Linear plot of observed head versus time in the observation borehole KFR102A:6 during the interference pumping tests in KFR27: 189.4–194.4 m. Pumping period occurred between 2016-02-23 and 2016-02-26.

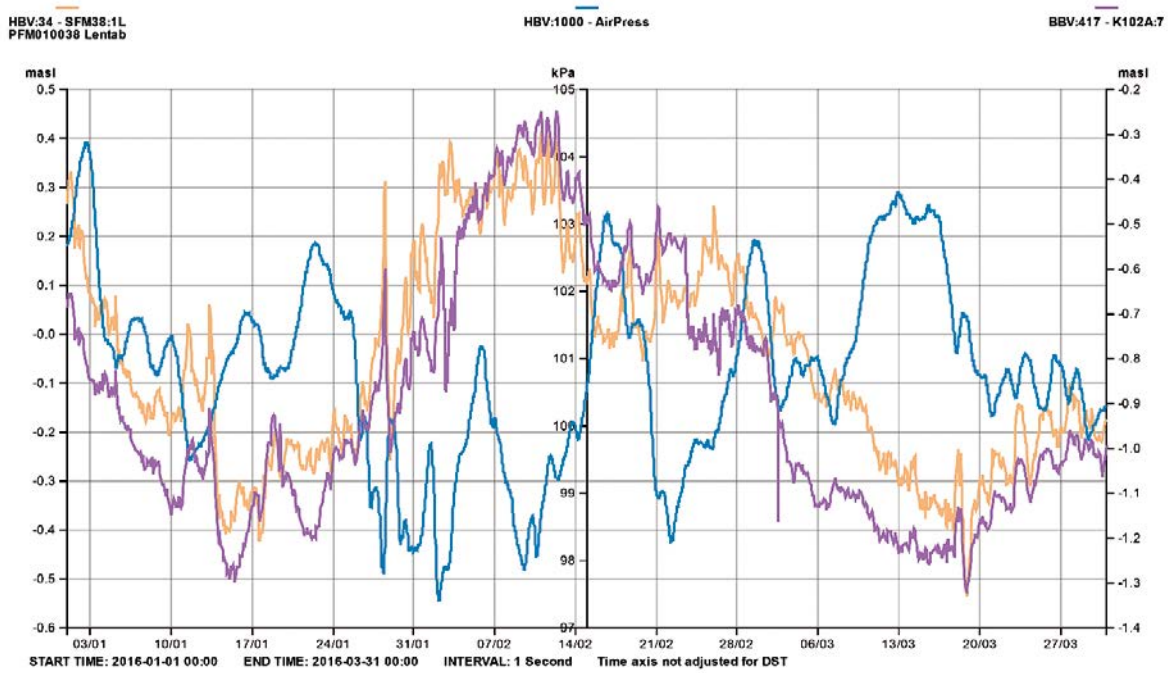


Figure A1-25. Linear plot of observed head versus time in the observation borehole KFR102A:7 during the interference pumping tests in KFR27: 189.4–194.4 m. Pumping period occurred between 2016-02-23 and 2016-02-26.

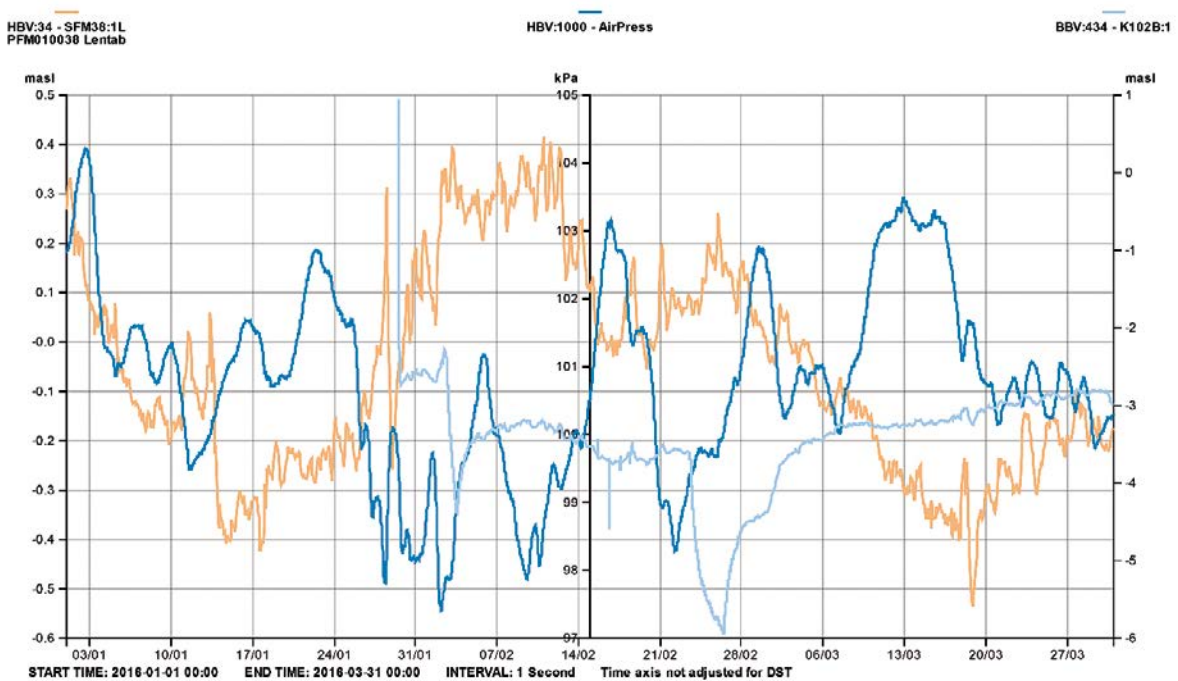


Figure A1-26. Linear plot of observed head versus time in the observation borehole KFR102B:1 during the interference pumping tests in KFR27: 189.4–194.4 m. Pumping period occurred between 2016-02-23 and 2016-02-26.

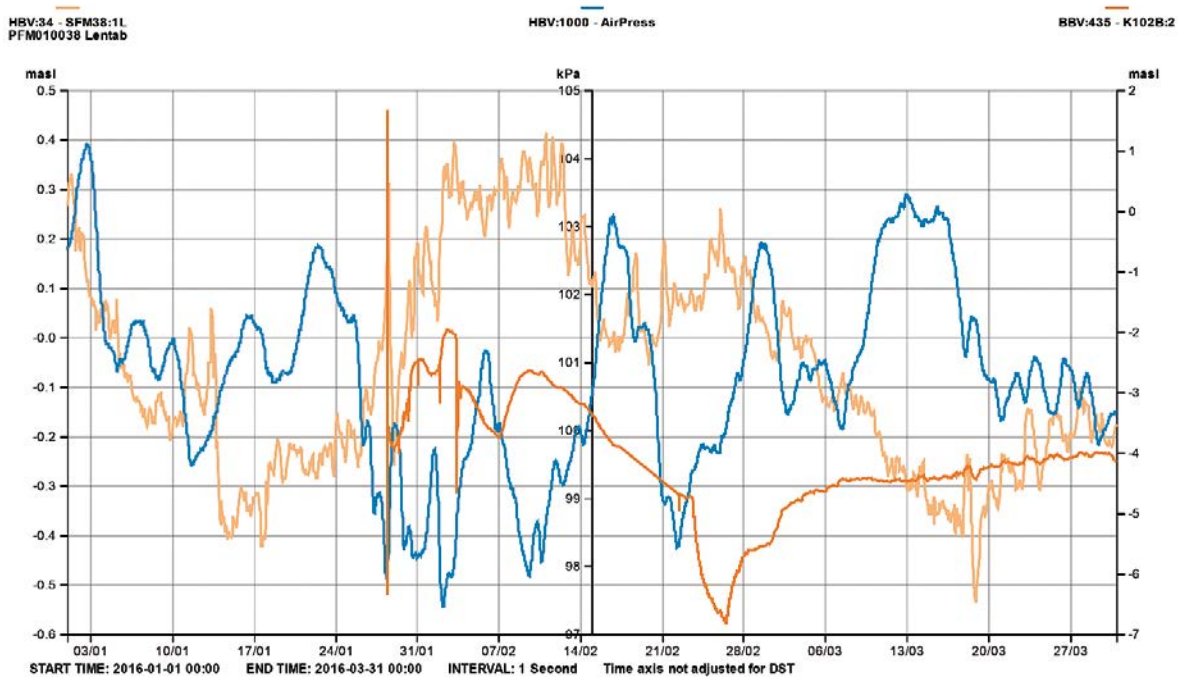


Figure A1-27. Linear plot of observed head versus time in the observation borehole KFR102B:2 during the interference pumping tests in KFR27: 189.4–194.4 m. Pumping period occurred between 2016-02-23 and 2016-02-26.

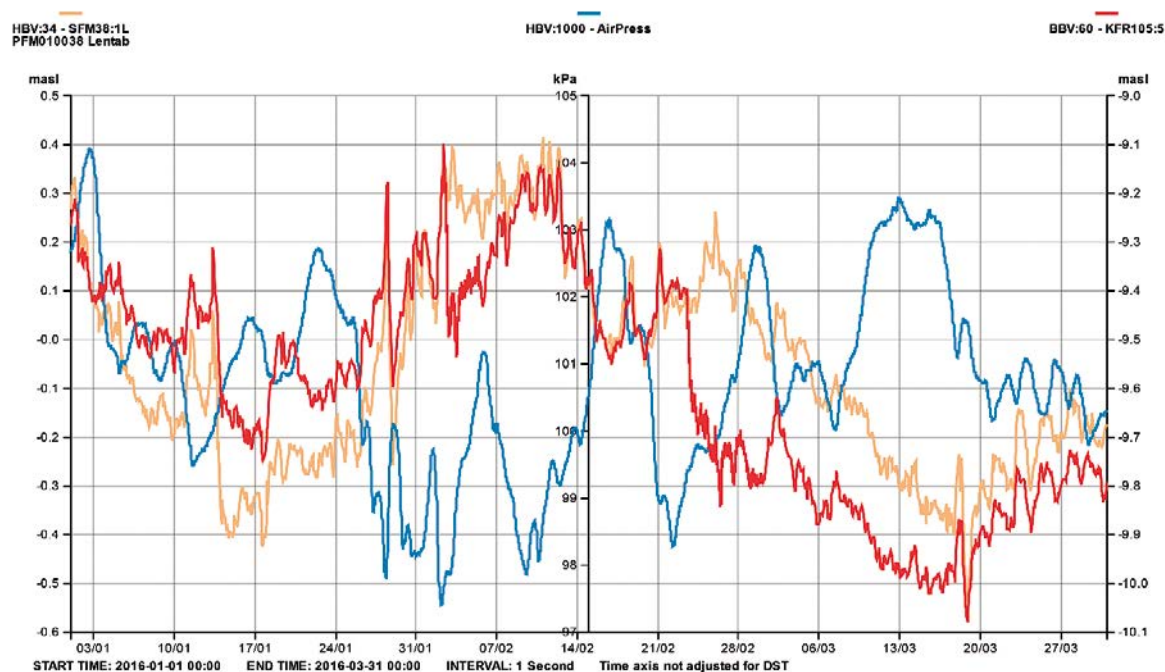


Figure A1-28. Linear plot of observed head versus time in the observation borehole KFR105:5 during the interference pumping tests in KFR27: 189.4–194.4 m. Pumping period occurred between 2016-02-23 and 2016-02-26.

A1.2.2 Low confidence responses in observation sections for test in KFR27: 189.4–194.4 m

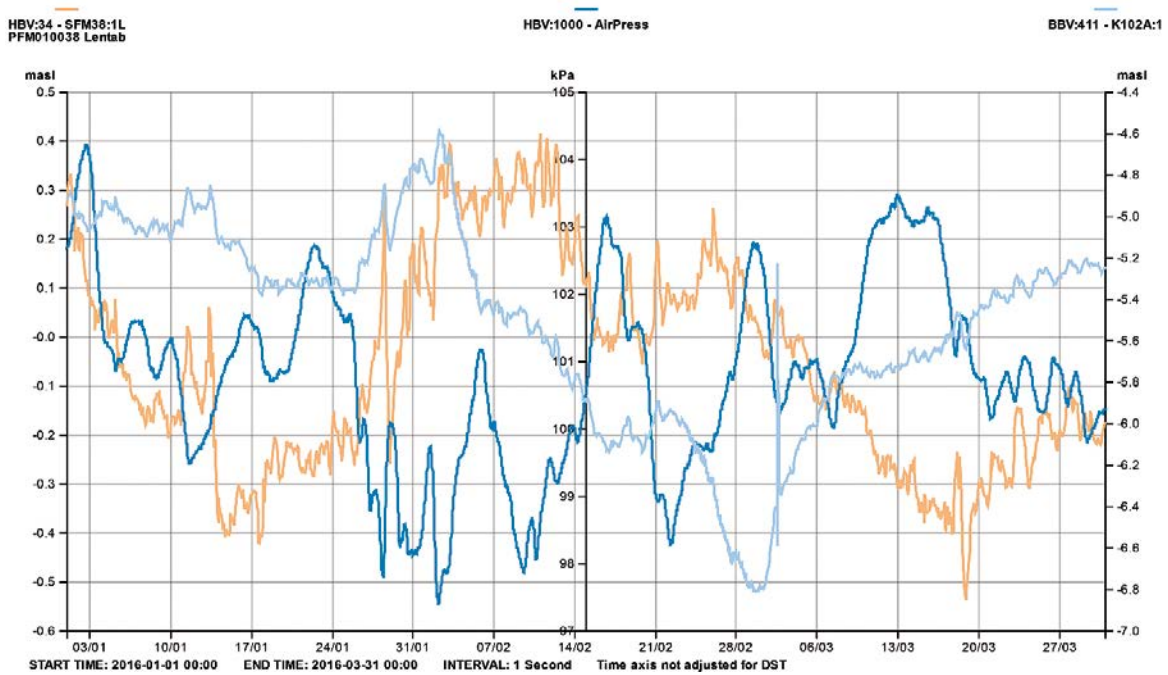


Figure A1-29. Linear plot of observed head versus time in the observation borehole KFR102A:1 during the interference pumping tests in KFR27: 189.4–194.4 m. Pumping period occurred between 2016-02-23 and 2016-02-26.

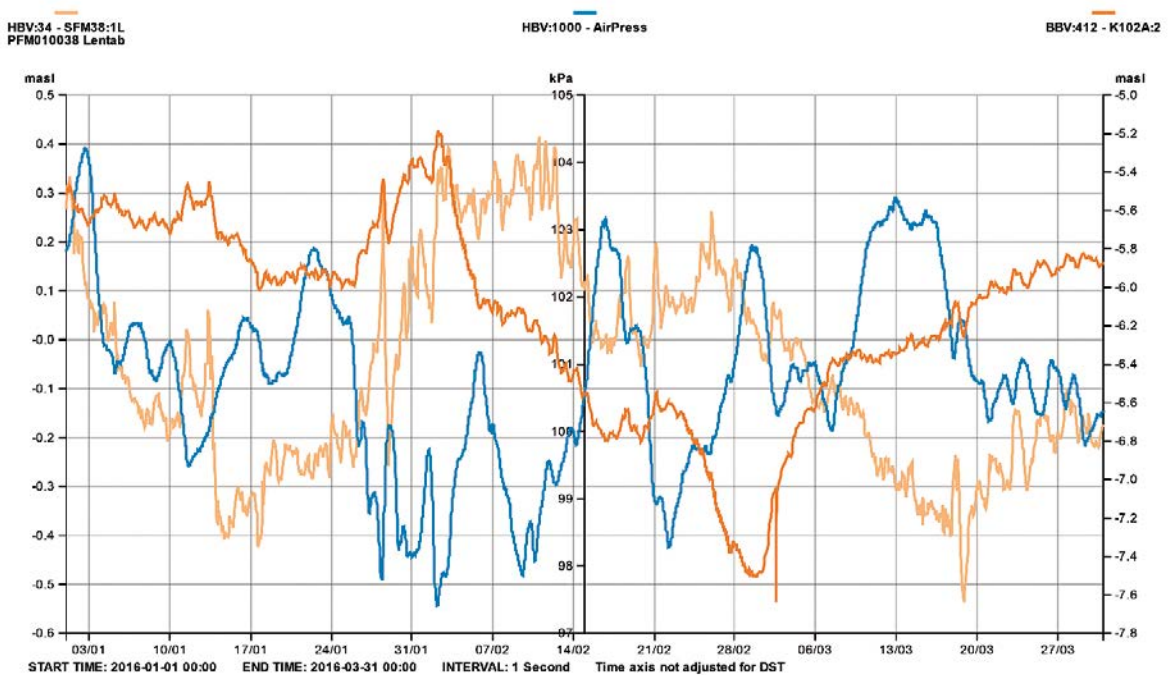


Figure A1-30. Linear plot of observed head versus time in the observation borehole KFR102B:2 during the interference pumping tests in KFR27: 189.4–194.4 m. Pumping period occurred between 2016-02-23 and 2016-02-26.

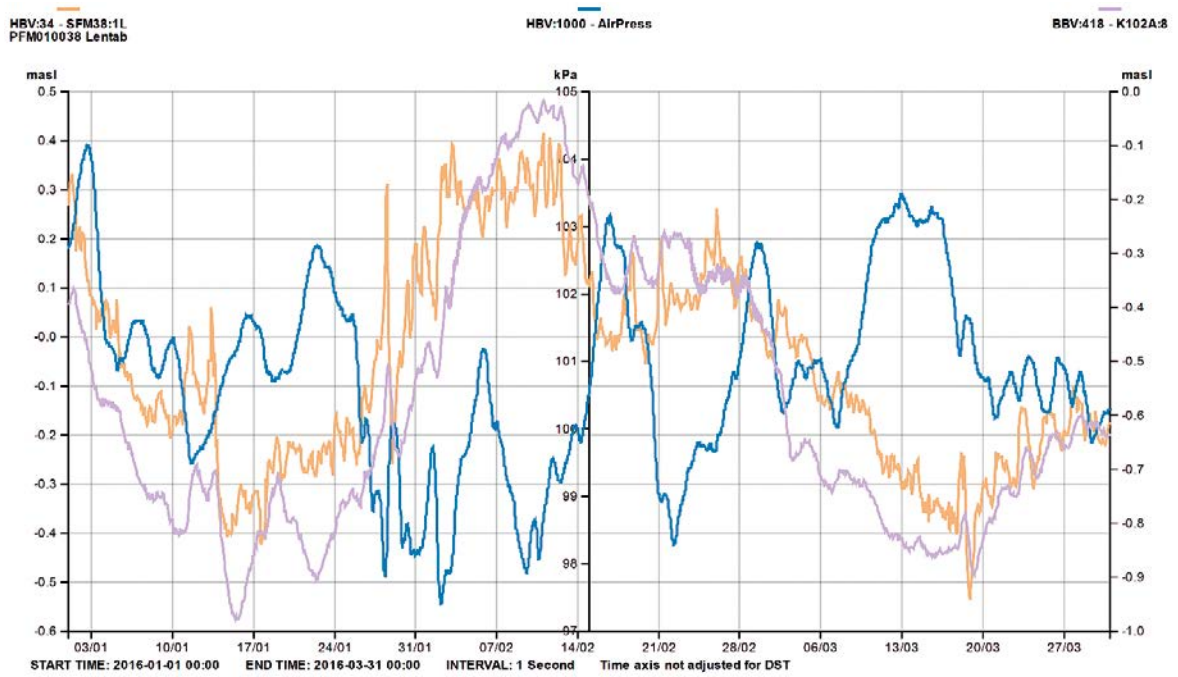


Figure A1-31. Linear plot of observed head versus time in the observation borehole KFR102B:8 during the interference pumping tests in KFR27: 189.4–194.4 m. Pumping period occurred between 2016-02-23 and 2016-02-26.

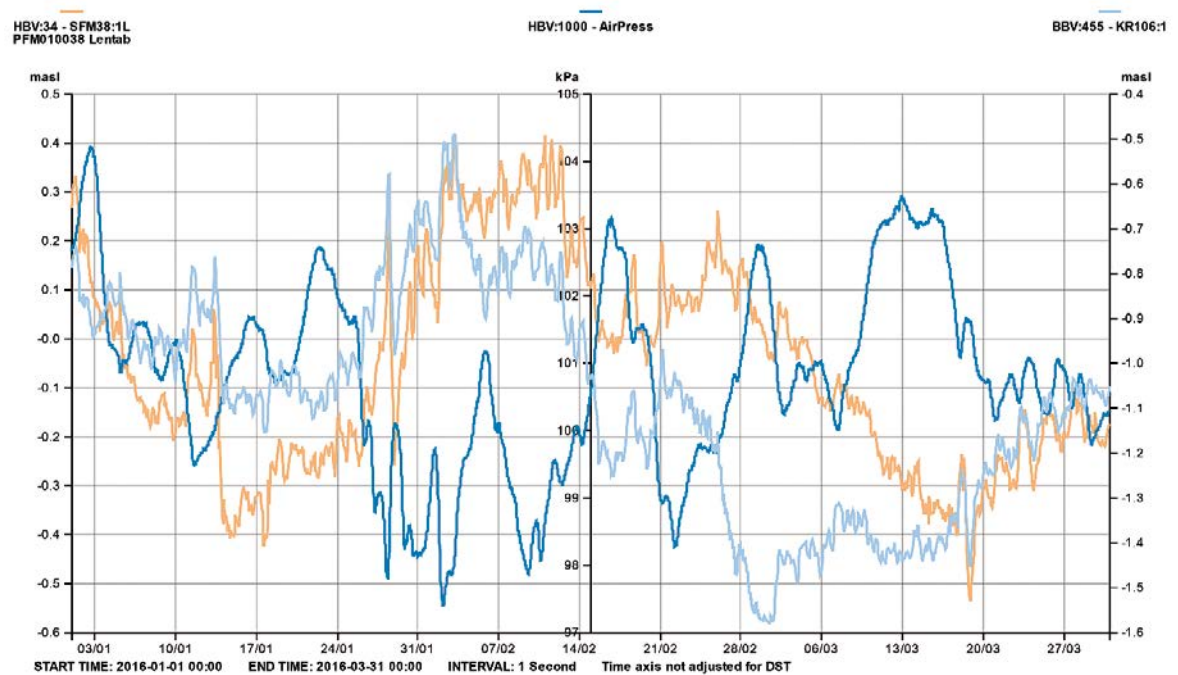


Figure A1-32. Linear plot of observed head versus time in the observation borehole KFR106:1 during the interference pumping tests in KFR27: 189.4–194.4 m. Pumping period occurred between 2016-02-23 and 2016-02-26.

A1.3 Interference test in KFR103: 83.5–93.5 m

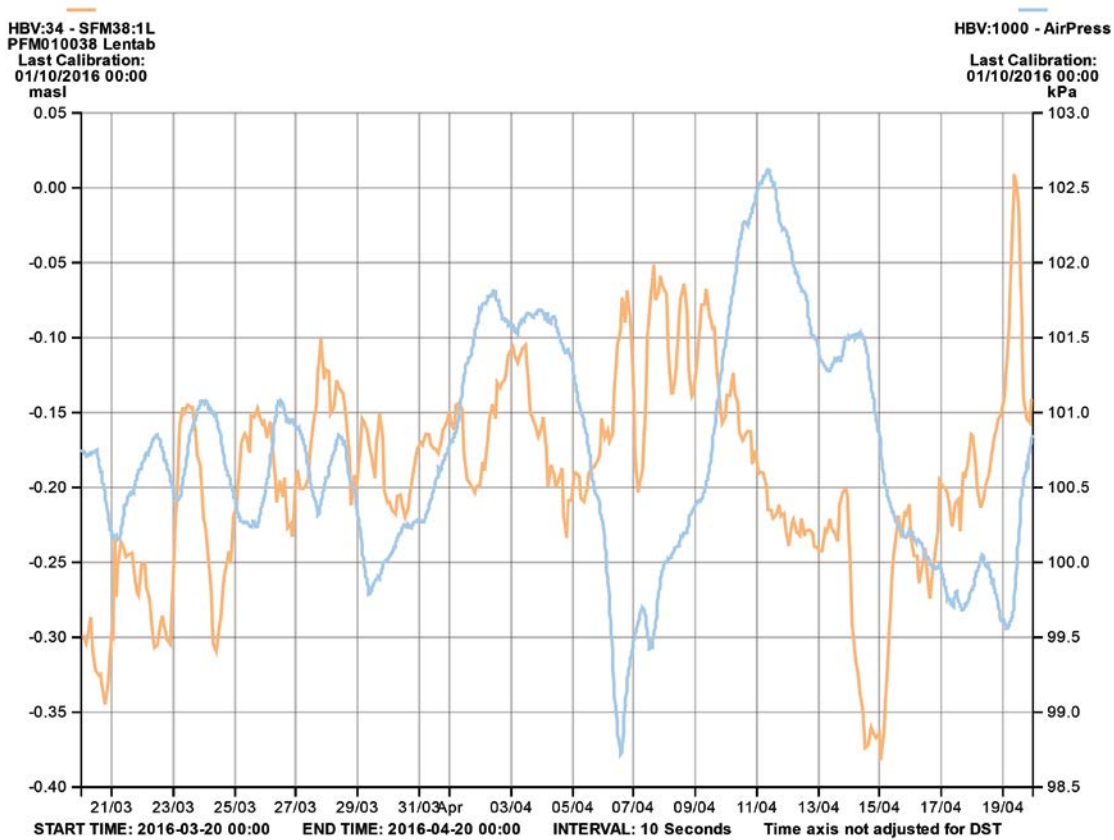


Figure A1-33. Registered air pressure (blue line) and sea water level (orange line) at SFR during the interference test period in KFR103: 83.5–93.5 m, with data from circa ten days before and ten days after. Each parameter has its own Y-scale. Pumping period occurred between 2016-04-01 and 2016-04-04.

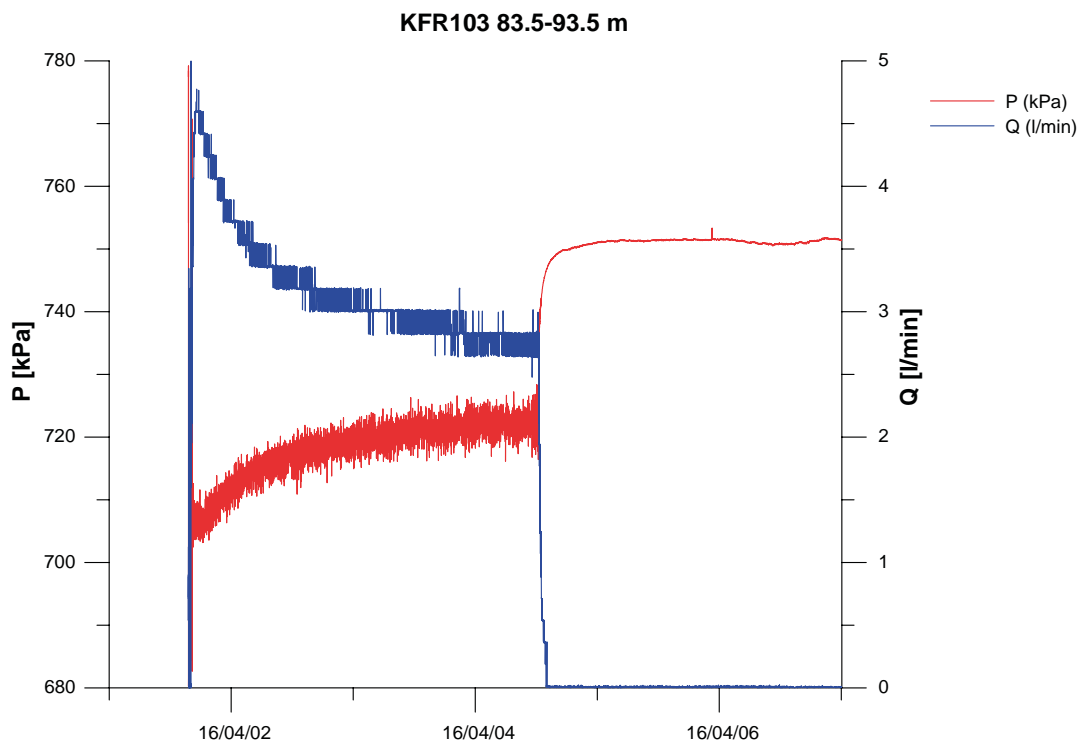


Figure A1-34. Linear plot of observed pressure and pumped flow versus time in the pumping borehole KFR103: 83.5–93.5 m during the interference pumping test.

A1.3.1 Responses in observation sections for test in KFR103: 83.5–93.5 m

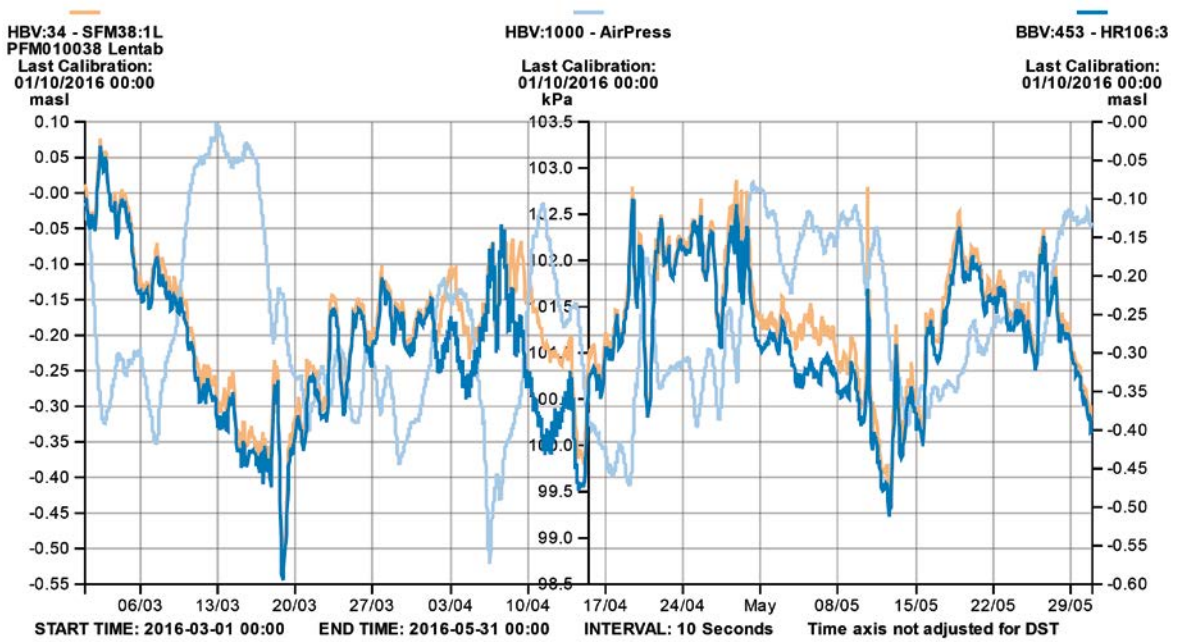


Figure A1-35. Linear plot of observed head versus time in the observation borehole HFR106:3 during the interference pumping tests in KFR103: 83.5–93.5 m. Pumping period occurred between 2016-04-01 and 2016-04-04.

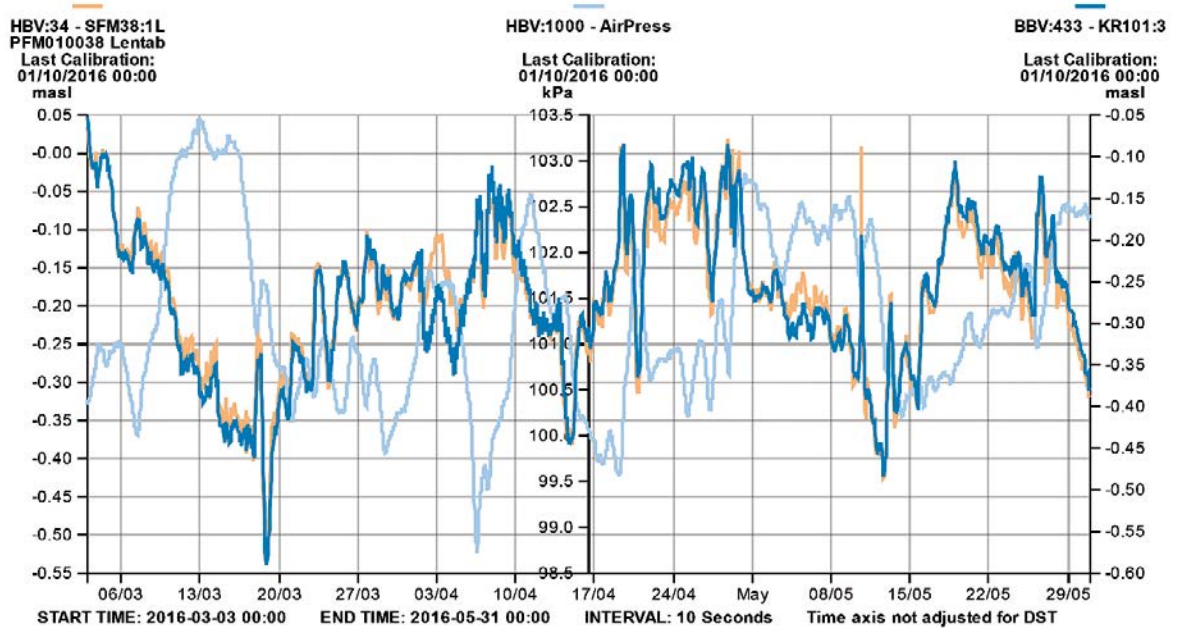


Figure A1-36. Linear plot of observed head versus time in the observation borehole KFR101:3 during the interference pumping tests in KFR103: 83.5–93.5 m. Pumping period occurred between 2016-04-01 and 2016-04-04.

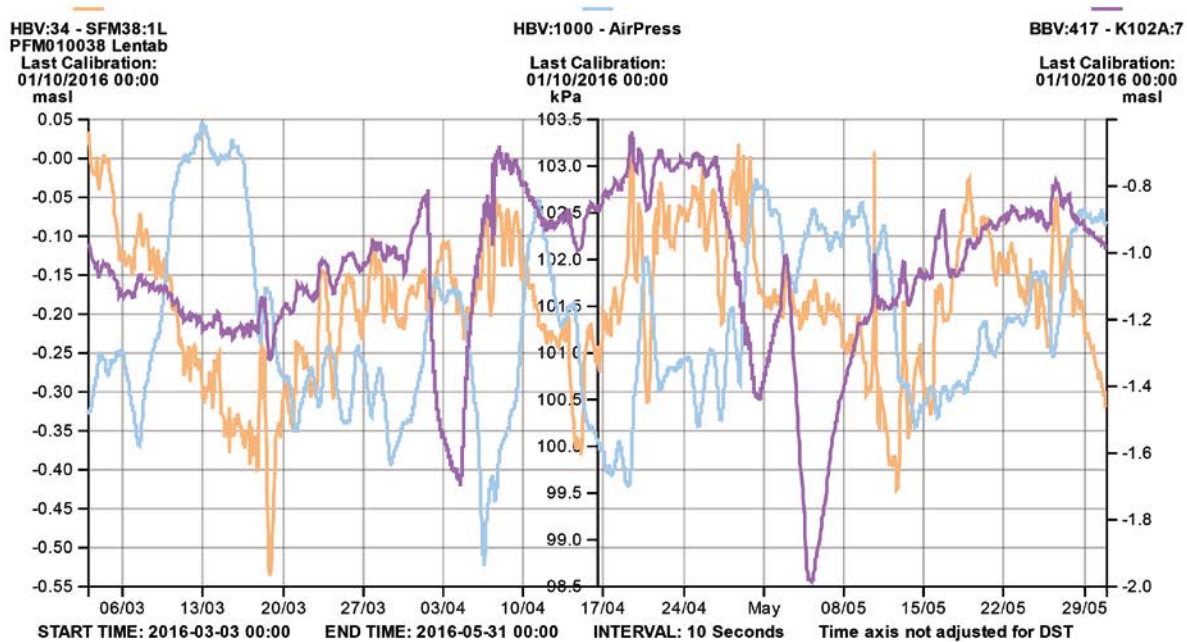


Figure A1-37. Linear plot of observed head versus time in the observation borehole KFR102A:7 during the interference pumping tests in KFR103: 83.5–93.5 m. Pumping period occurred between 2016-04-01 and 2016-04-04.

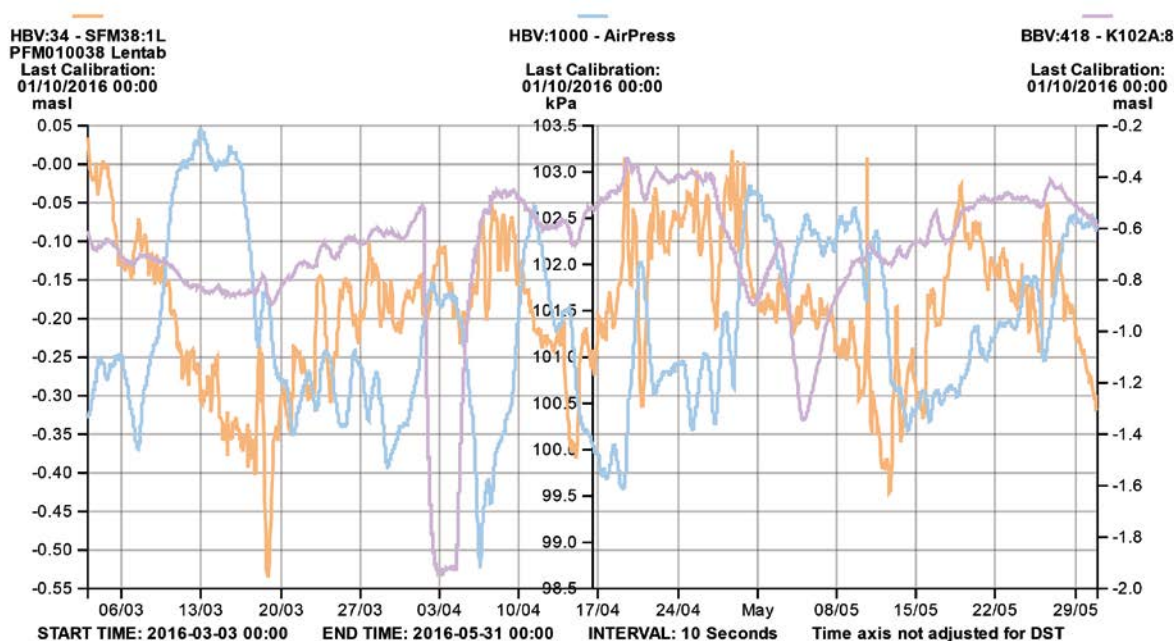


Figure A1-38. Linear plot of observed head versus time in the observation borehole KFR102A:8 during the interference pumping tests in KFR103: 83.5–93.5 m. Pumping period occurred between 2016-04-01 and 2016-04-04.

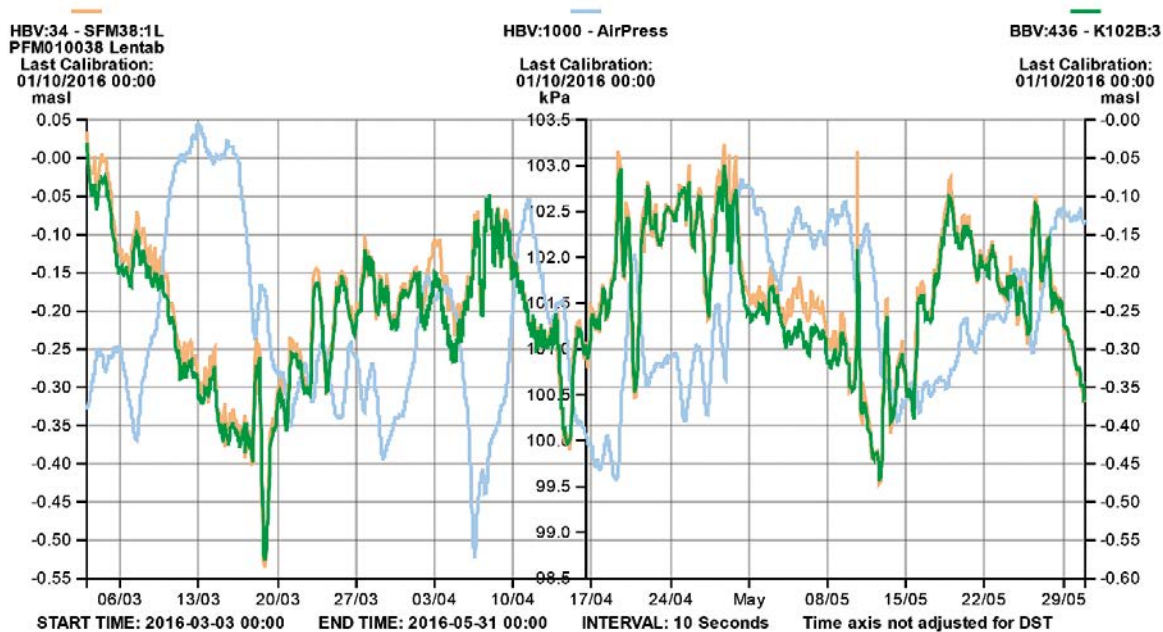


Figure A1-39. Linear plot of observed head versus time in the observation borehole KFR102B:3 during the interference pumping tests in KFR103: 83.5–93.5 m. Pumping period occurred between 2016-04-01 and 2016-04-04.

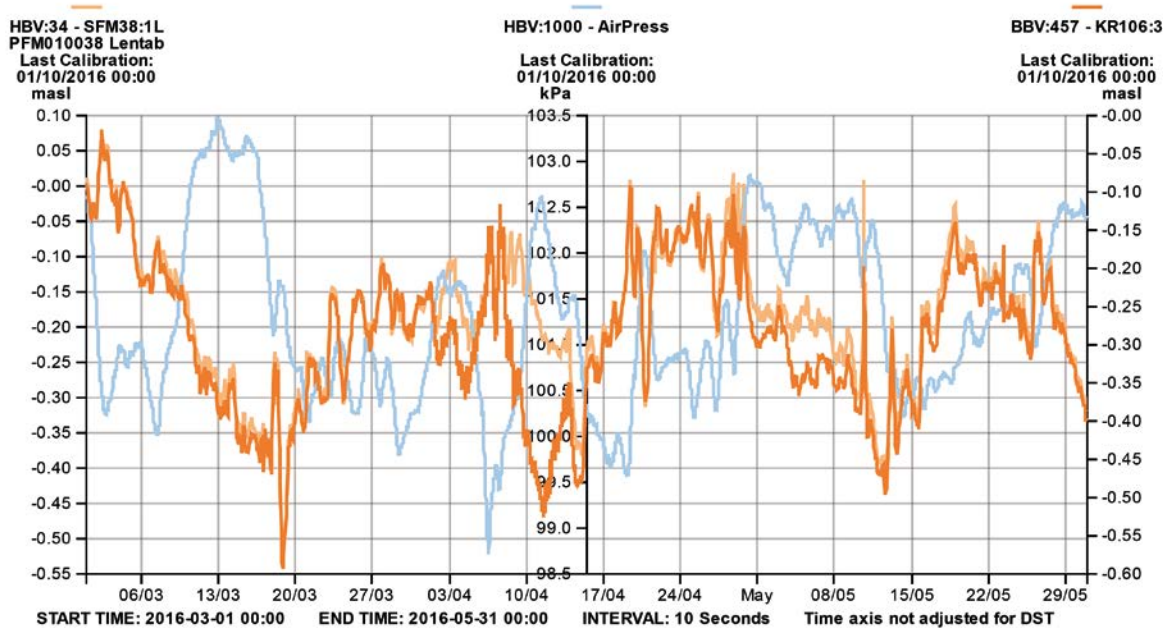


Figure A1-40. Linear plot of observed head versus time in the observation borehole KFR106:3 during the interference pumping tests in KFR103: 83.5–93.5 m. Pumping period occurred between 2016-04-01 and 2016-04-04.

A1.3.2 Low confidence responses in observation sections for test in KFR103: 83.5–93.5 m

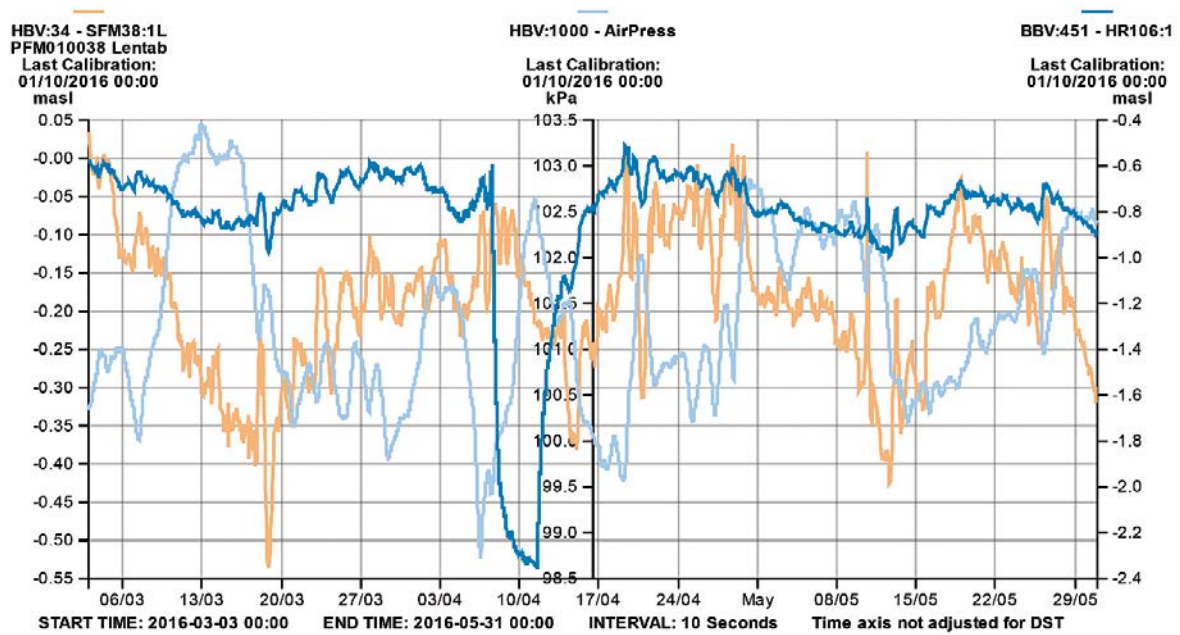


Figure A1-41. Linear plot of observed head versus time in the observation borehole HFR106:1 during the interference pumping tests in KFR103: 83.5–93.5 m. Pumping period occurred between 2016-04-01 and 2016-04-04.

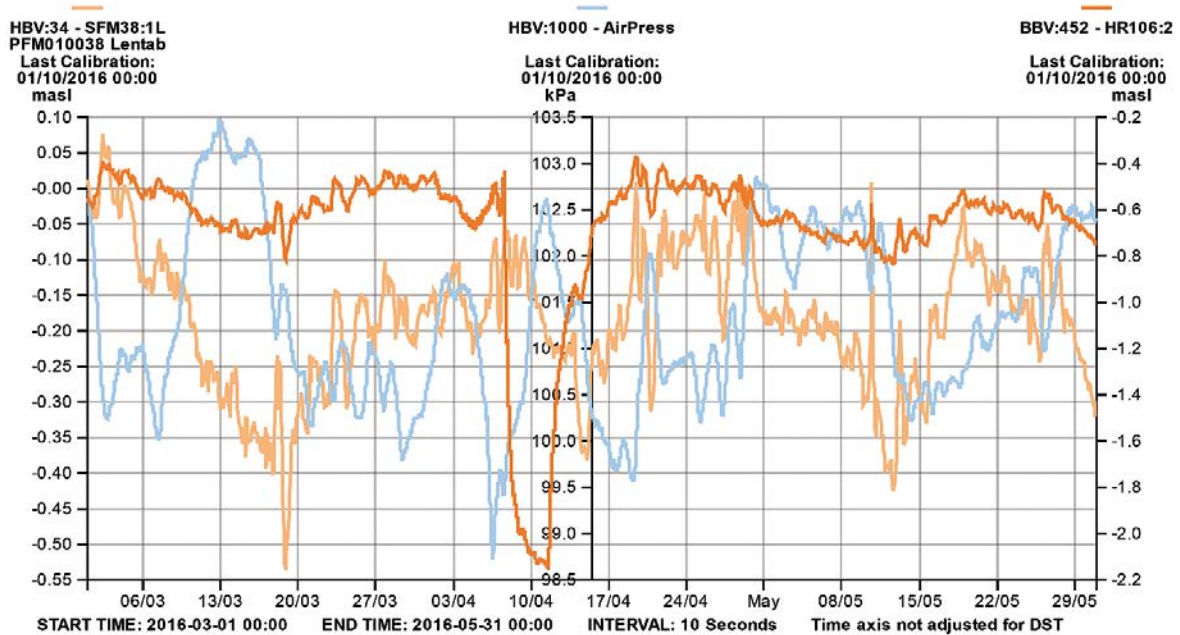


Figure A1-42. Linear plot of observed head versus time in the observation borehole HFR106:2 during the interference pumping tests in KFR103: 83.5–93.5 m. Pumping period occurred between 2016-04-01 and 2016-04-04.

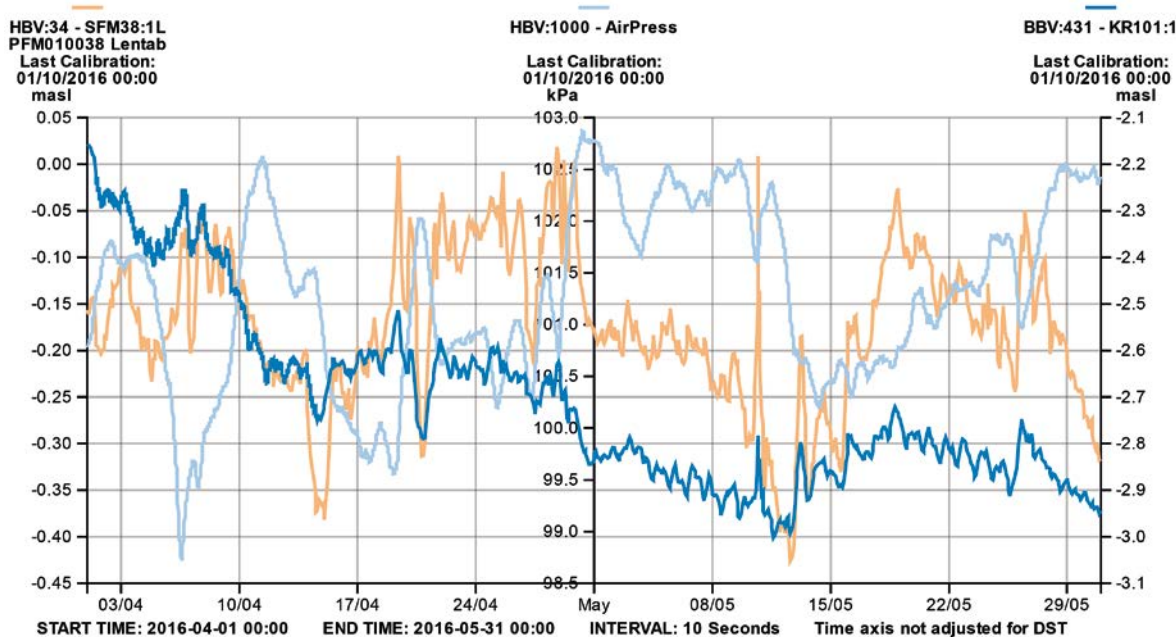


Figure A1-43. Linear plot of observed head versus time in the observation borehole KFR101:1 during the interference pumping tests in KFR103: 83.5–93.5 m. Pumping period occurred between 2016-04-01 and 2016-04-04.

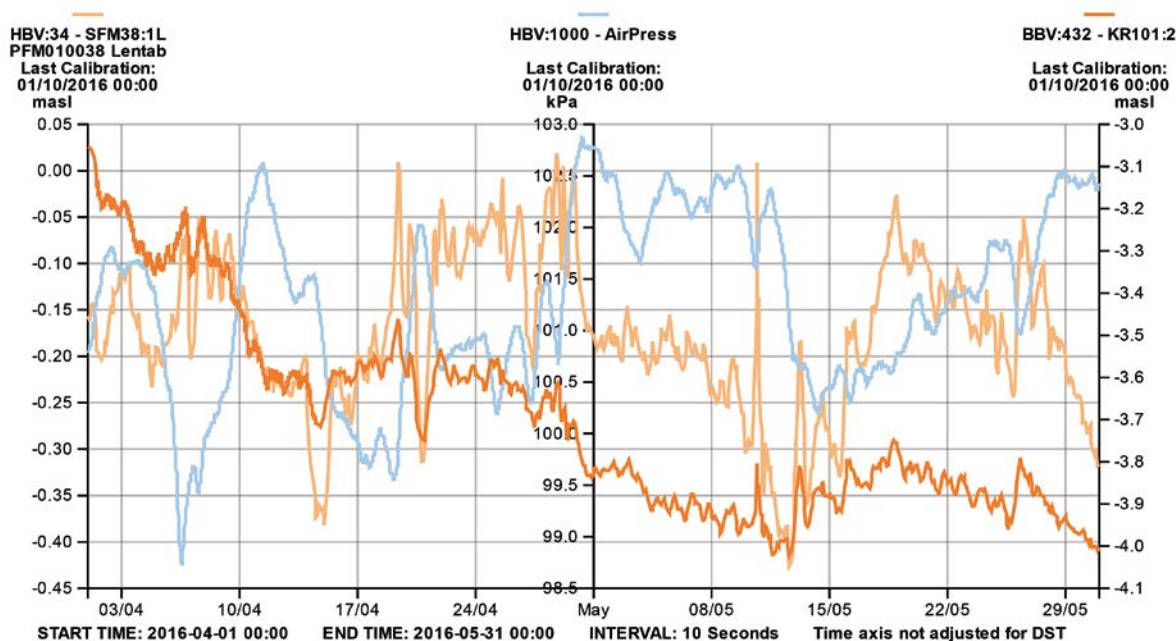


Figure A1-44. Linear plot of observed head versus time in the observation borehole KFR101:2 during the interference pumping tests in KFR103: 83.5–93.5 m. Pumping period occurred between 2016-04-01 and 2016-04-04.

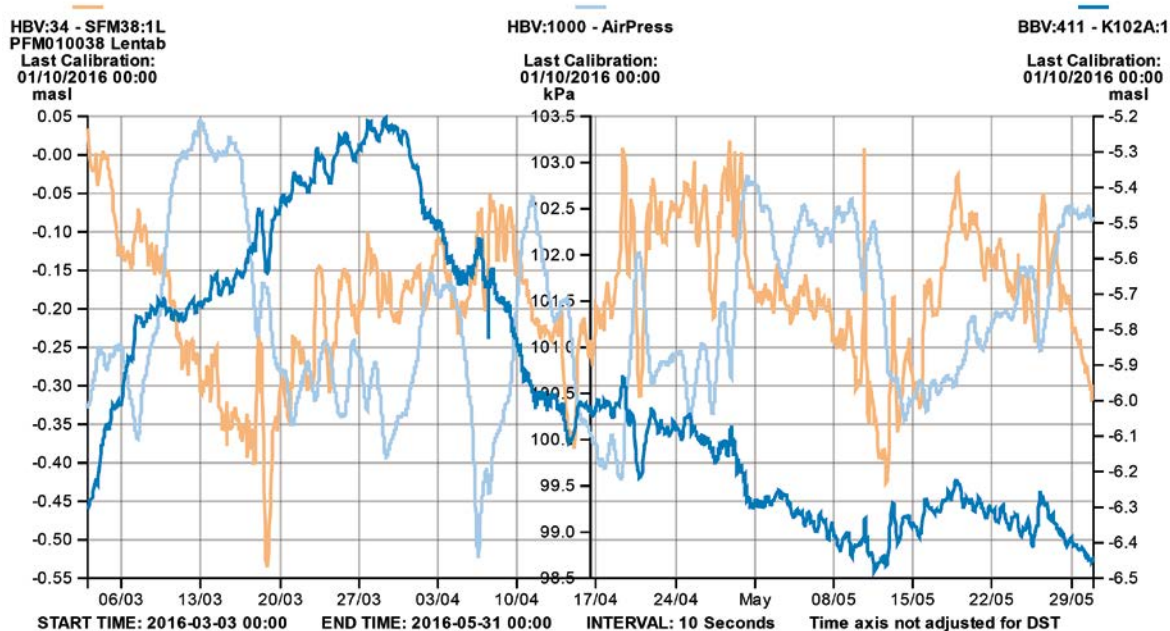


Figure A1-45. Linear plot of observed head versus time in the observation borehole KFR102A:1 during the interference pumping tests in KFR103: 83.5–93.5 m. Pumping period occurred between 2016-04-01 and 2016-04-04.

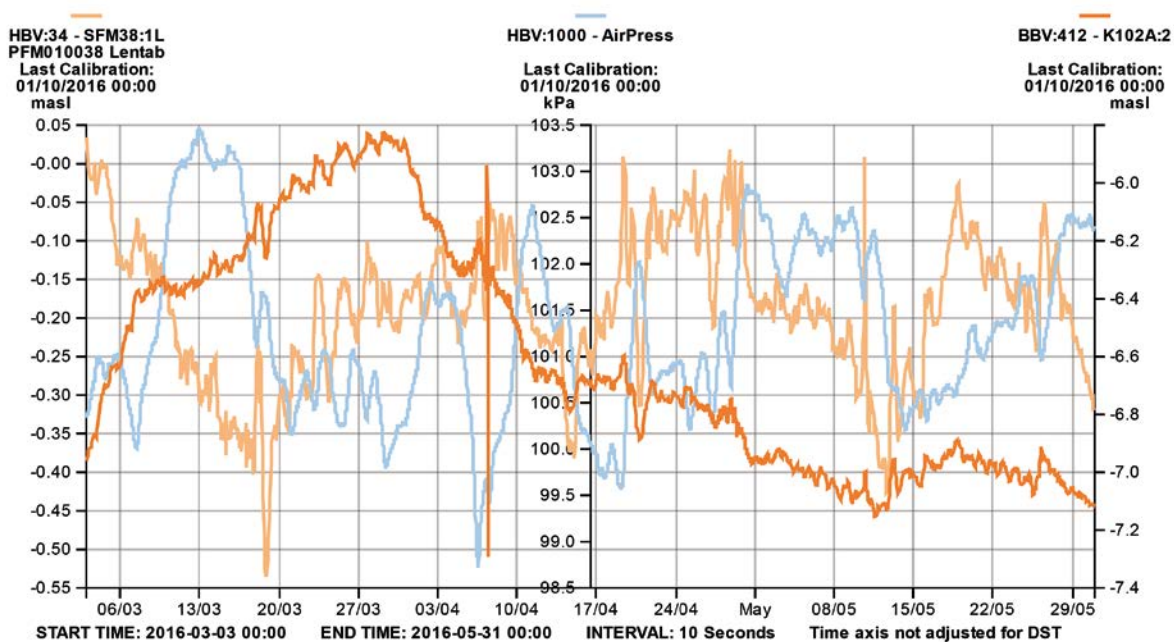


Figure A1-46. Linear plot of observed head versus time in the observation borehole KFR102A:2 during the interference pumping tests in KFR103: 83.5–93.5 m. Pumping period occurred between 2016-04-01 and 2016-04-04.

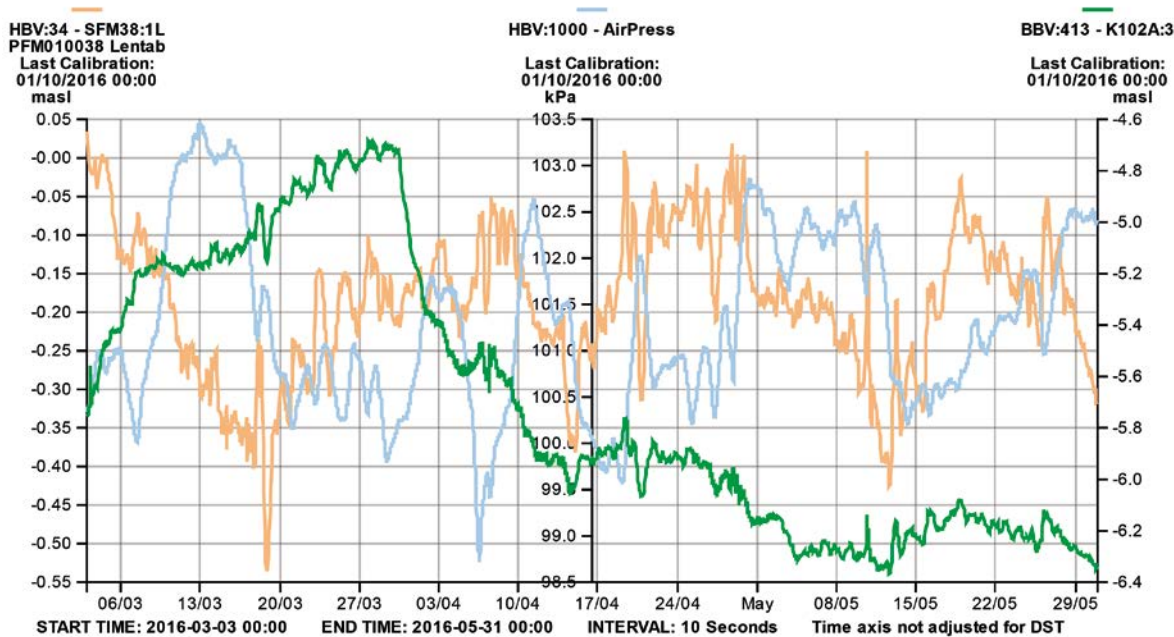


Figure A1-47. Linear plot of observed head versus time in the observation borehole KFR102A:3 during the interference pumping tests in KFR103: 83.5–93.5 m. Pumping period occurred between 2016-04-01 and 2016-04-04.

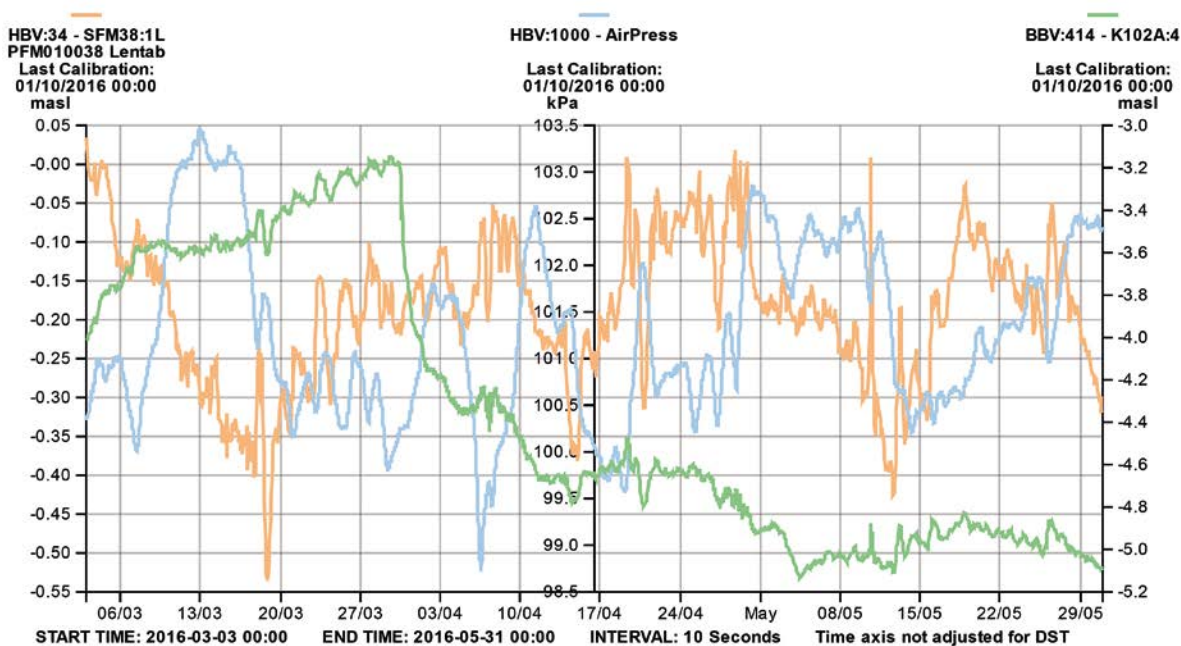


Figure A1-48. Linear plot of observed head versus time in the observation borehole KFR102A:4 during the interference pumping tests in KFR103: 83.5–93.5 m. Pumping period occurred between 2016-04-01 and 2016-04-04.

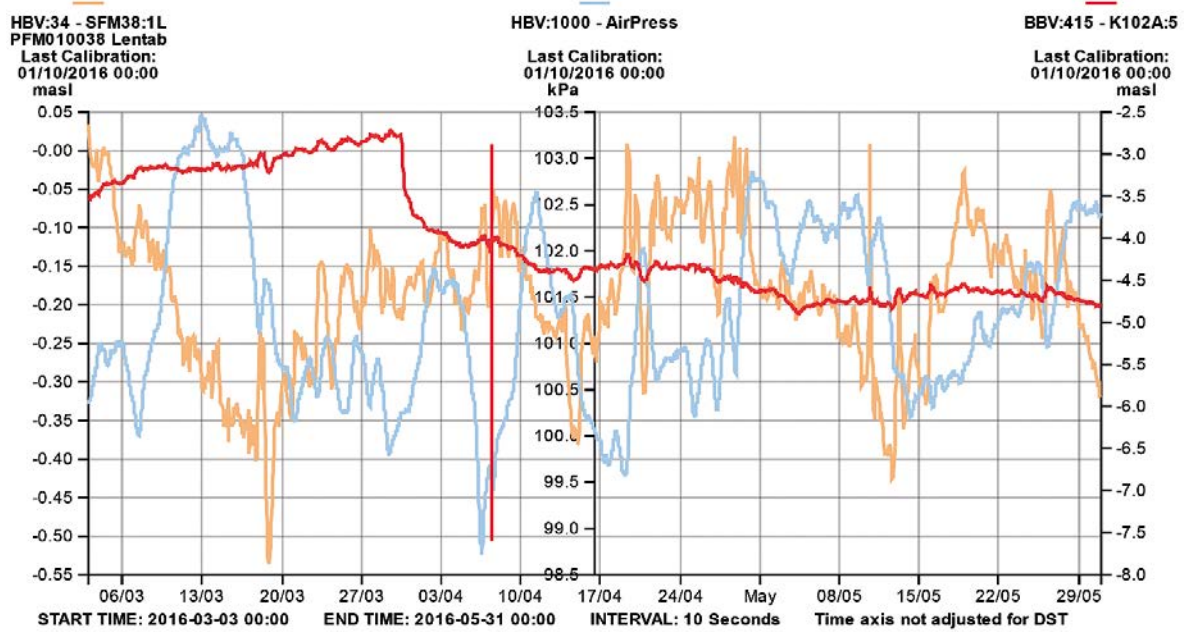


Figure A1-49. Linear plot of observed head versus time in the observation borehole KFR102A:5 during the interference pumping tests in KFR103: 83.5–93.5 m. Pumping period occurred between 2016-04-01 and 2016-04-04.

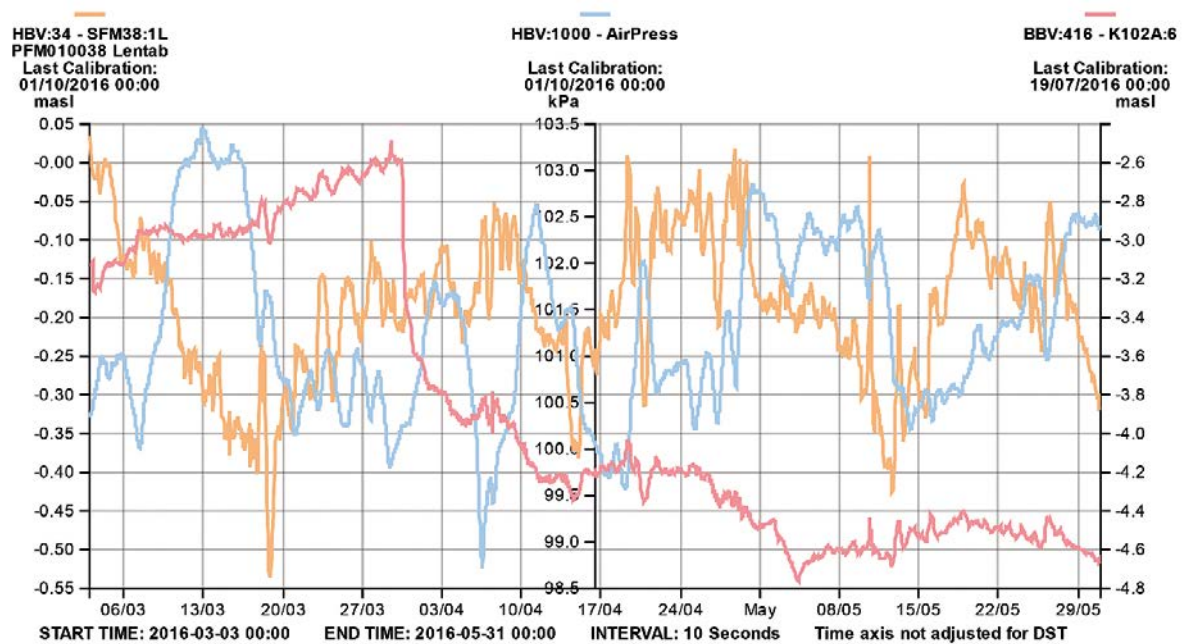


Figure A1-50. Linear plot of observed head versus time in the observation borehole KFR102A:6 during the interference pumping tests in KFR103: 83.5–93.5 m. Pumping period occurred between 2016-04-01 and 2016-04-04.

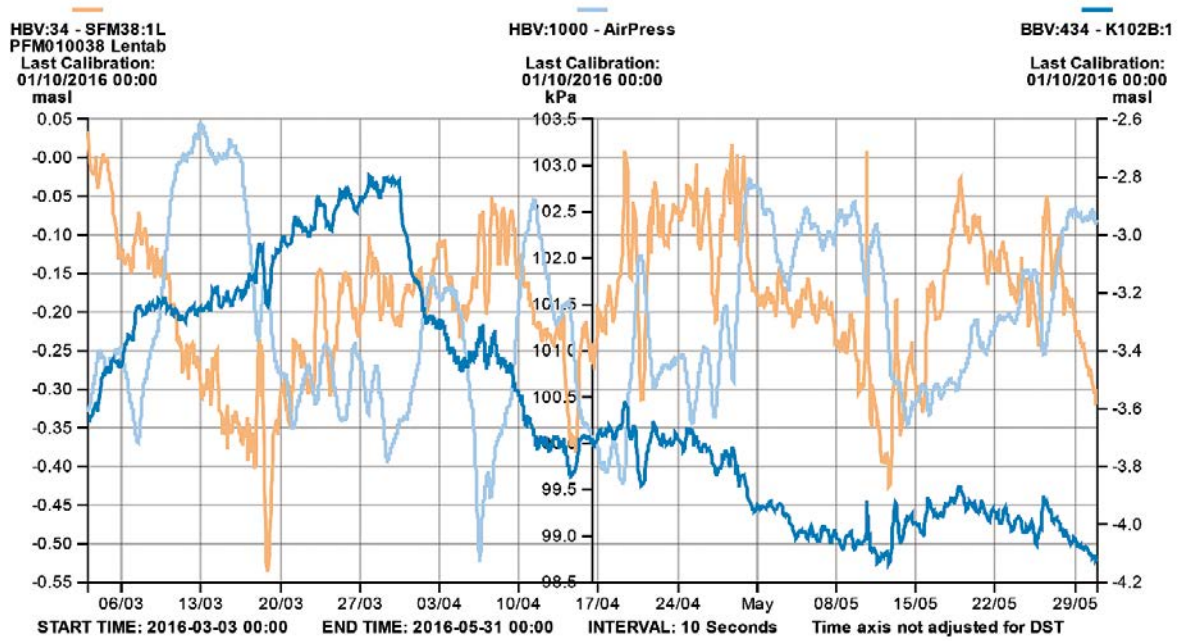


Figure A1-51. Linear plot of observed head versus time in the observation borehole KFR102B:1 during the interference pumping tests in KFR103: 83.5–93.5 m. Pumping period occurred between 2016-04-01 and 2016-04-04.

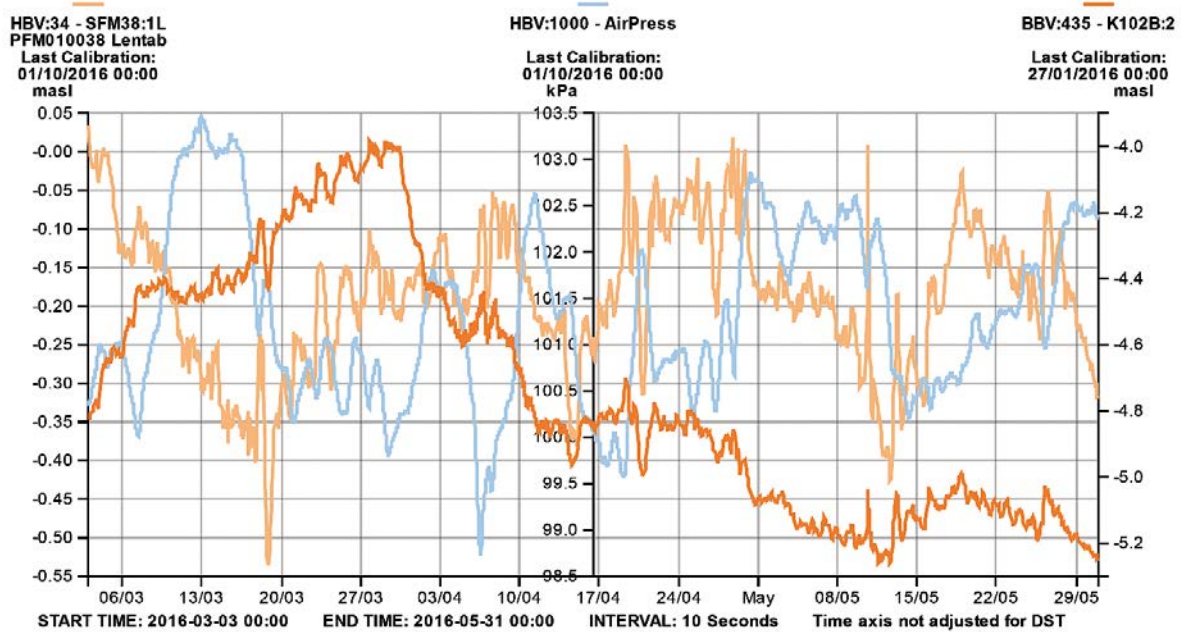


Figure A1-52. Linear plot of observed head versus time in the observation borehole KFR102B:2 during the interference pumping tests in KFR103: 83.5–93.5 m. Pumping period occurred between 2016-04-01 and 2016-04-04.

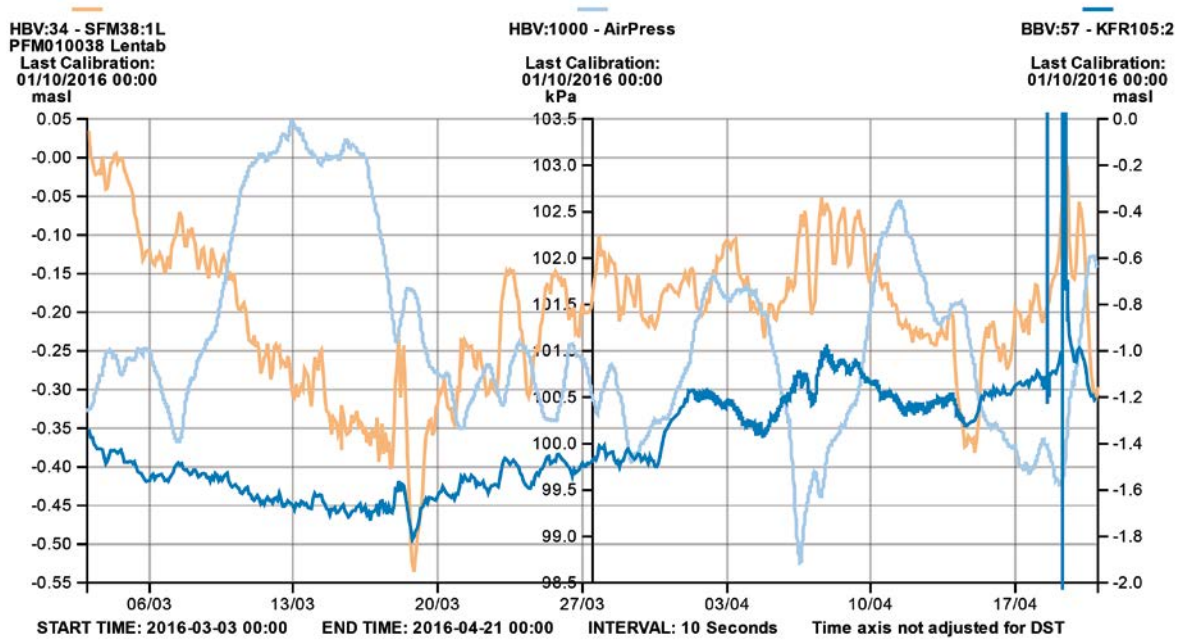


Figure A1-53. Linear plot of observed head versus time in the observation borehole KFR105:2 during the interference pumping tests in KFR103: 83.5–93.5 m. Pumping period occurred between 2016-04-01 and 2016-04-04.

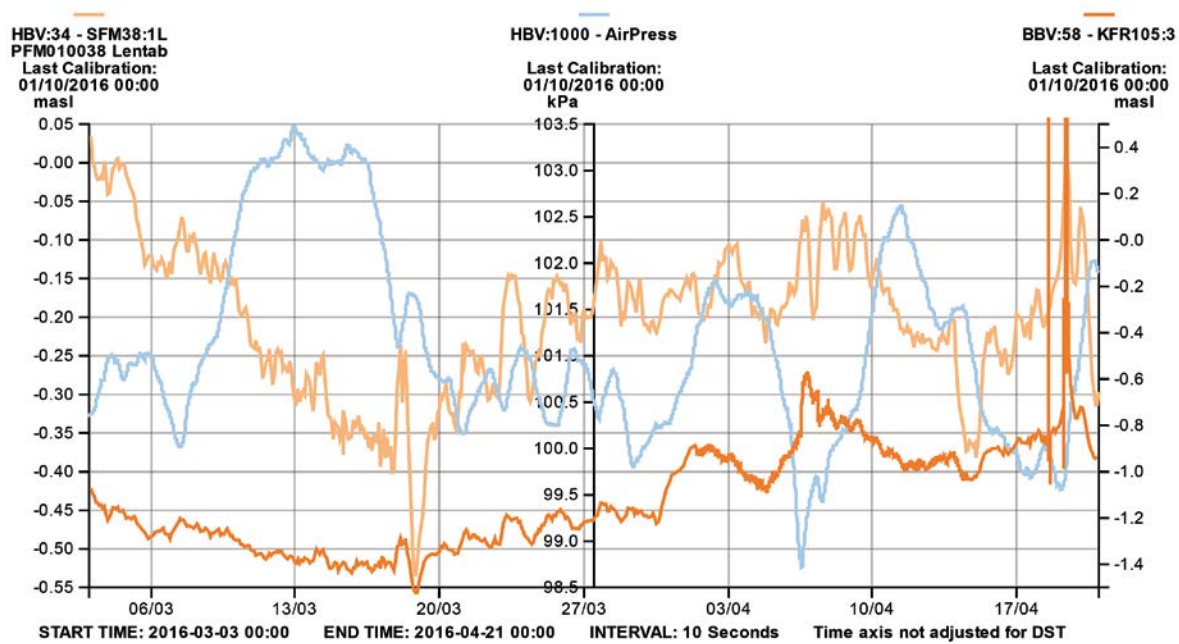


Figure A1-54. Linear plot of observed head versus time in the observation borehole KFR105:3 during the interference pumping tests in KFR103: 83.5–93.5 m. Pumping period occurred between 2016-04-01 and 2016-04-04.

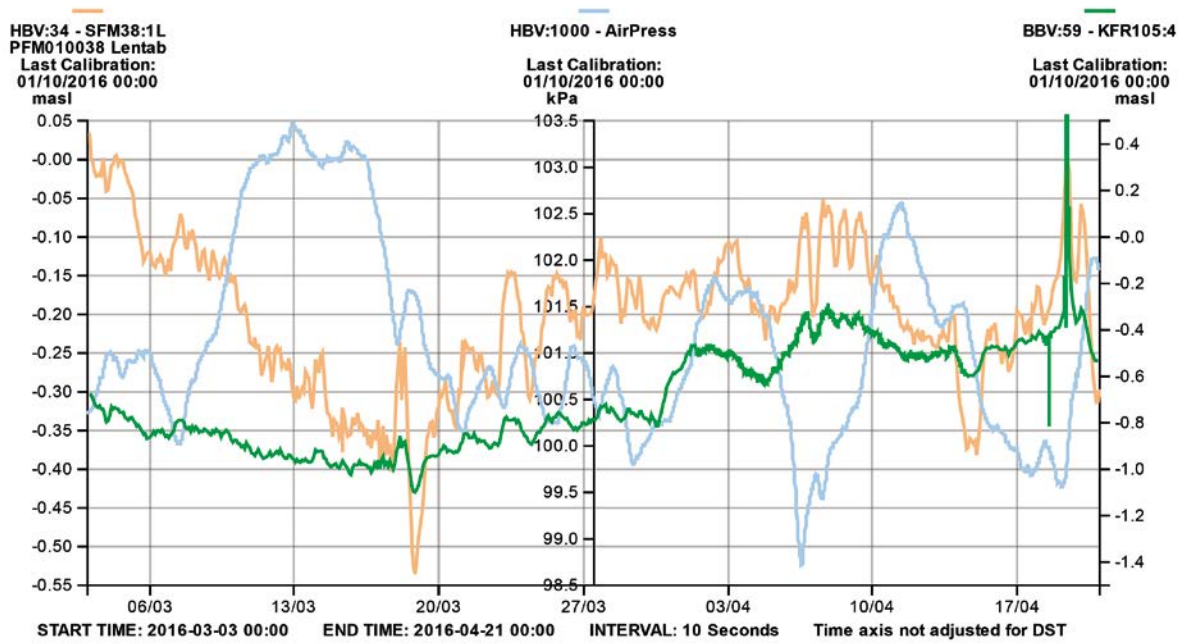


Figure AI-55. Linear plot of observed head versus time in the observation borehole KFR105:4 during the interference pumping tests in KFR103: 83.5–93.5 m. Pumping period occurred between 2016-04-01 and 2016-04-04.

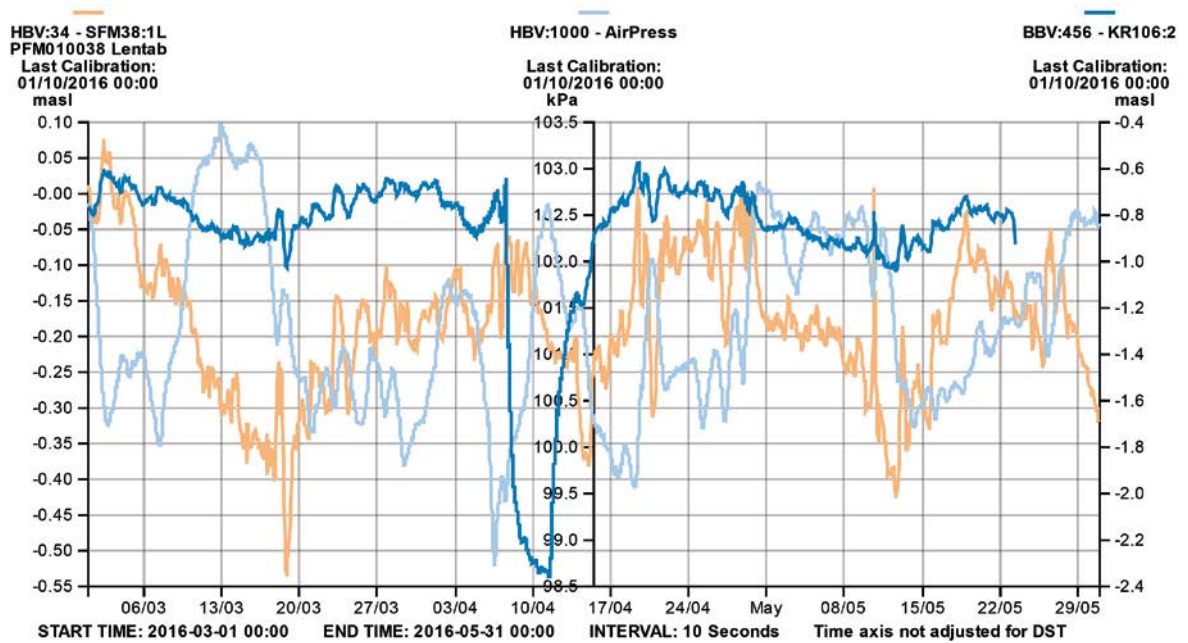


Figure AI-56. Linear plot of observed head versus time in the observation borehole KFR106:2 during the interference pumping tests in KFR103: 83.5–93.5 m. Pumping period occurred between 2016-04-01 and 2016-04-04.

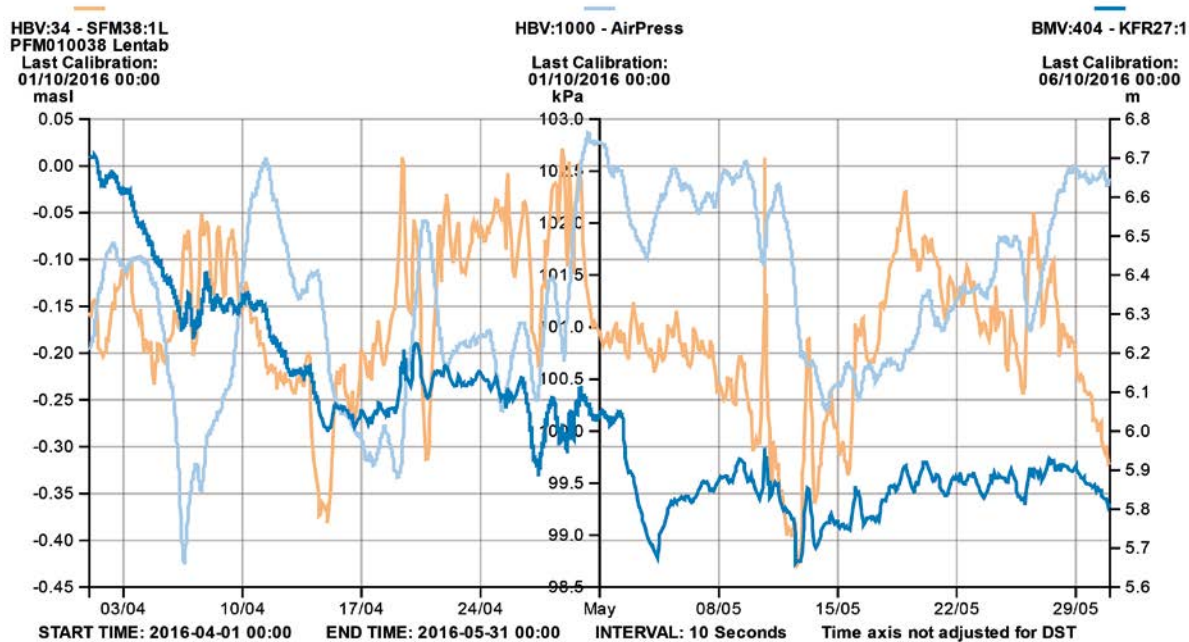


Figure A1-57. Linear plot of observed head versus time in the observation borehole KFR27:1 during the interference pumping tests in KFR103: 83.5–93.5 m. Pumping period occurred between 2016-04-01 and 2016-04-04.

A1.4 Interference test in KFR103: 177.0–187.0 m

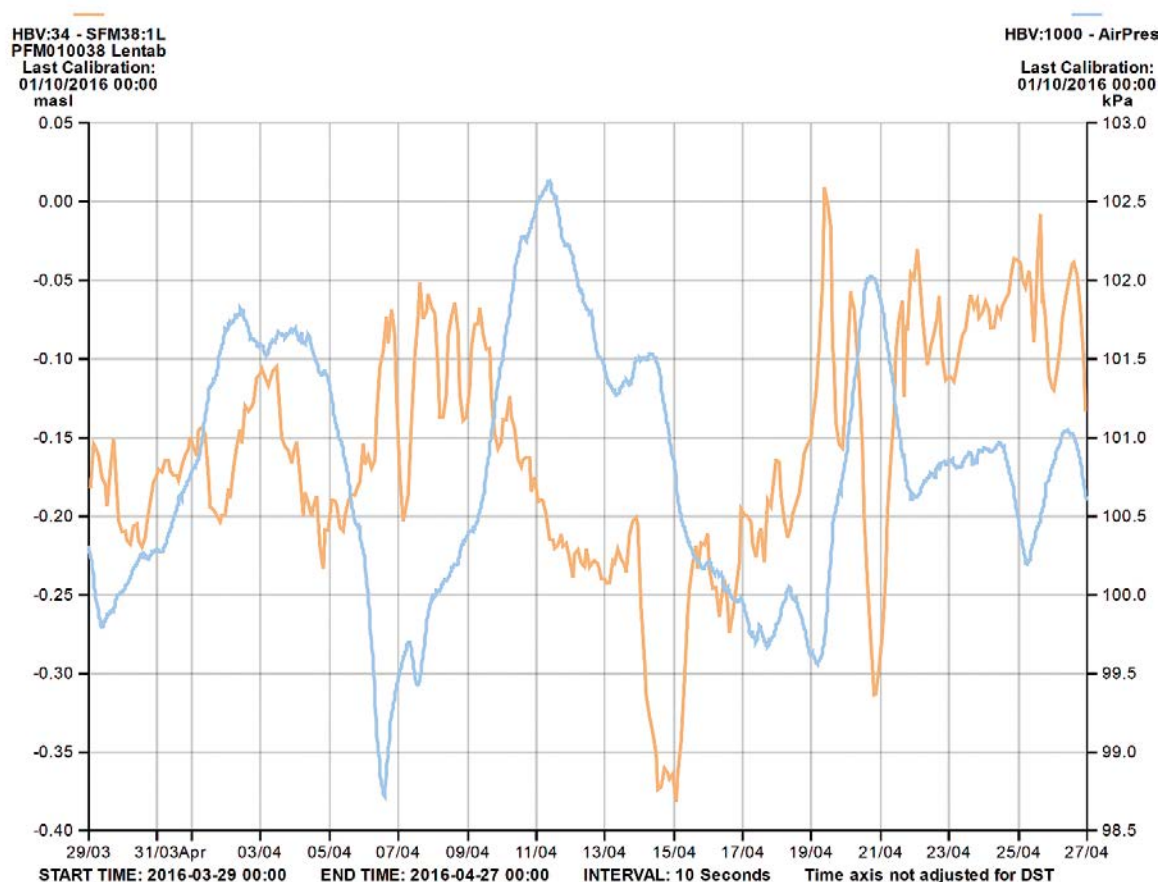


Figure A1-58. Registered air pressure (blue line) and sea water level (orange line) at SFR during the interference test period in KFR103: 177–187 m, with data from circa ten days before and ten days after. Each parameter has its own Y-scale. Pumping period occurred between 2016-04-07 and 2016-04-11.

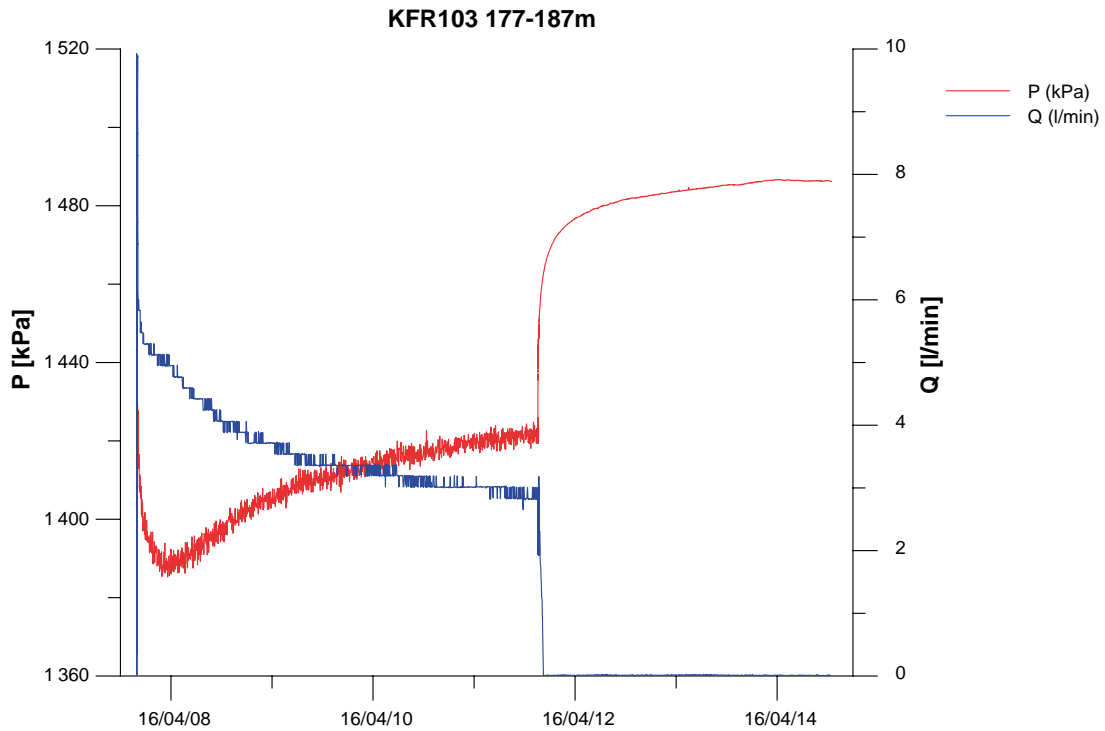


Figure A1-59. Linear plot of observed pressure and pumped flow versus time in the pumping borehole KFR103 177.0–187.0 m during the interference pumping test.

A1.4.1 Responses in observation sections for test in KFR103: 177.0–187.0 m

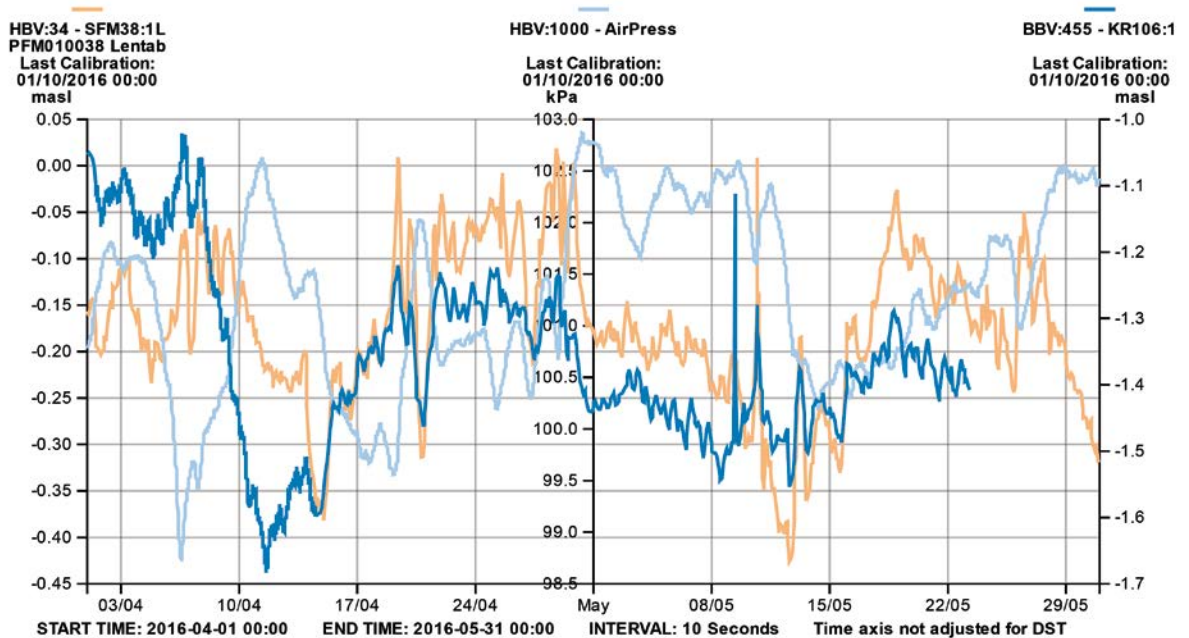


Figure A1-60. Linear plot of observed head versus time in the observation borehole HFR106:1 during the interference pumping tests in KFR103: 177.0–187.0 m. Pumping period occurred between 2016-04-07 and 2016-04-11.

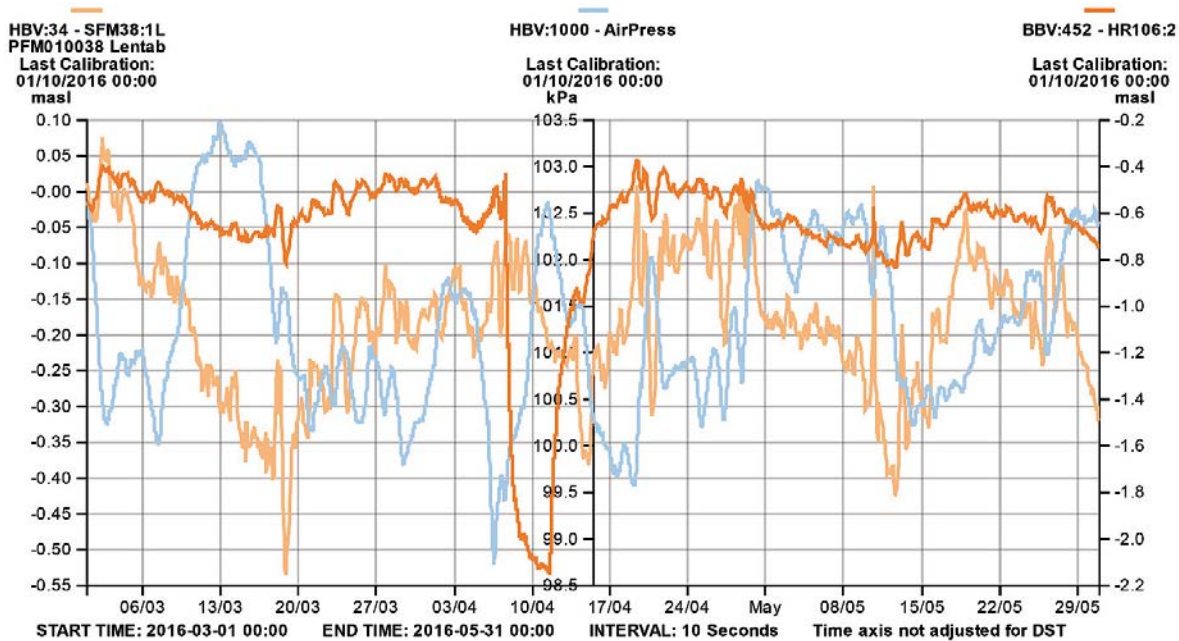


Figure A1-61. Linear plot of observed head versus time in the observation borehole HFR106:2 during the interference pumping tests in KFR103: 177.0–187.0 m. Pumping period occurred between 2016-04-07 and 2016-04-11.

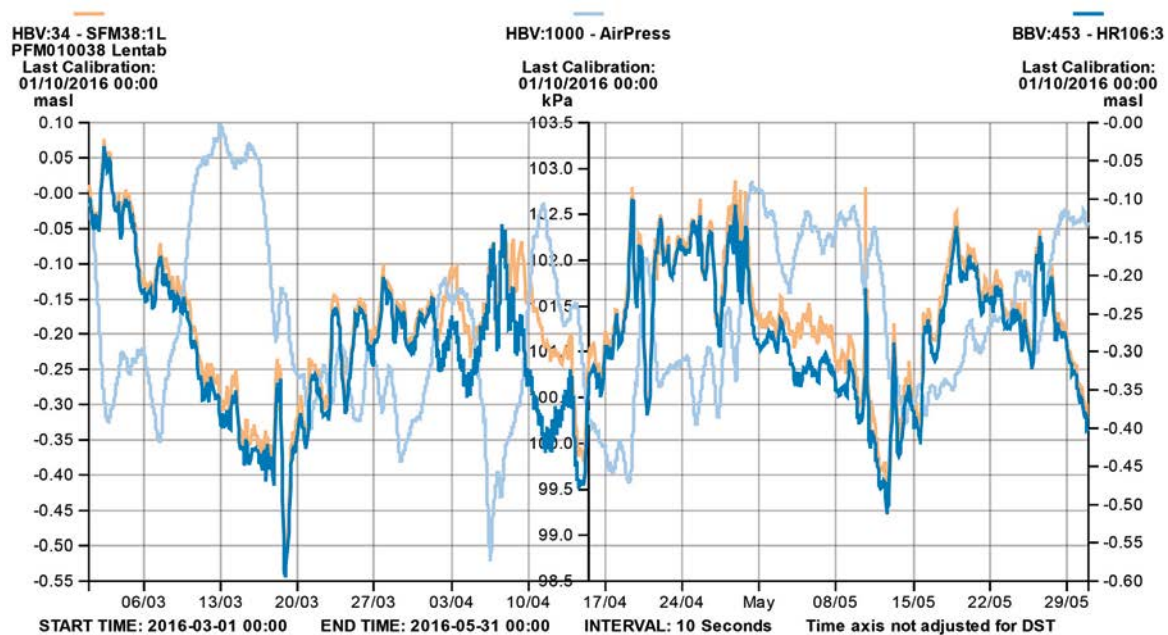


Figure A1-62. Linear plot of observed head versus time in the observation borehole HFR106:3 during the interference pumping tests in KFR103: 177.0–187.0 m. Pumping period occurred between 2016-04-07 and 2016-04-11.

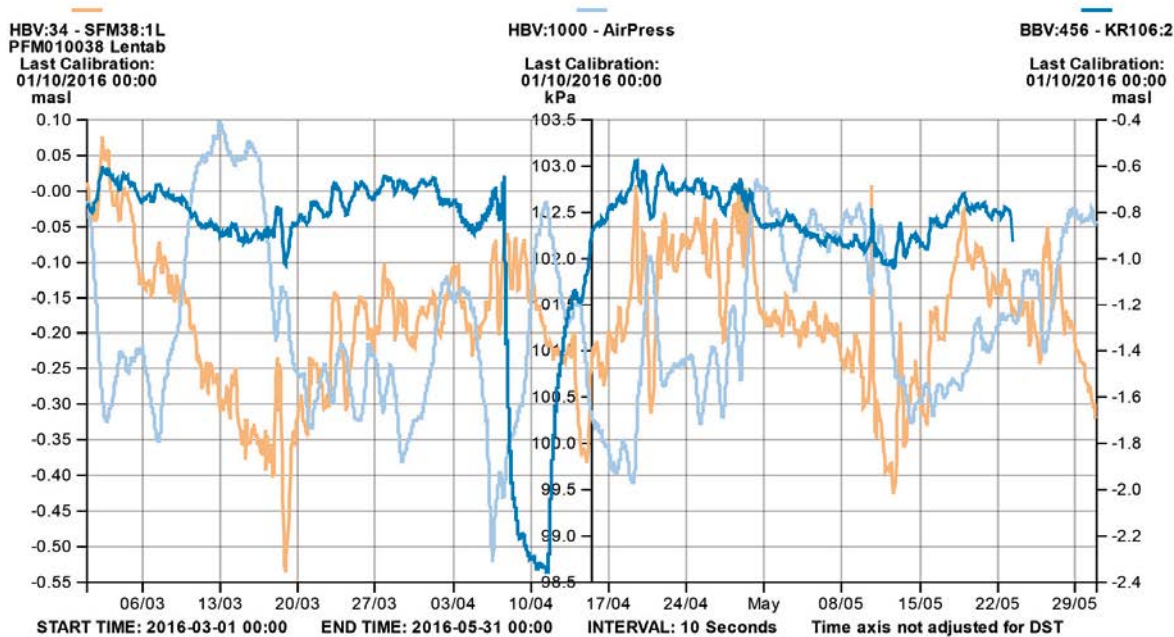


Figure A1-63. Linear plot of observed head versus time in the observation borehole KFR106:2 during the interference pumping tests in KFR103: 177.0–187.0 m. Pumping period occurred between 2016-04-07 and 2016-04-11.

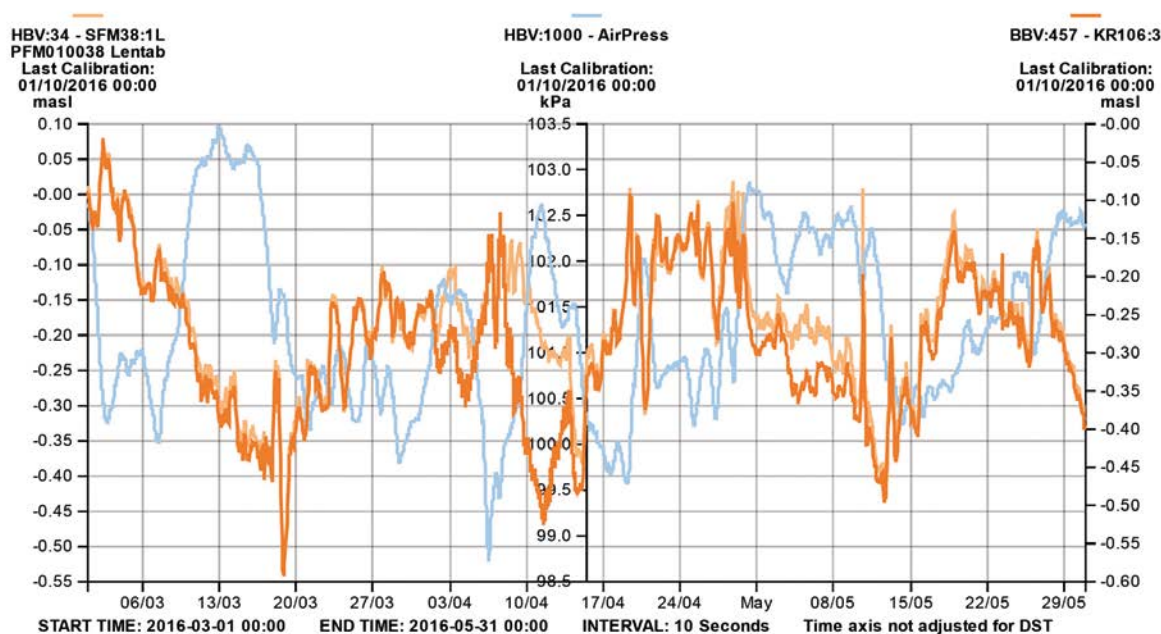


Figure A1-64. Linear plot of observed head versus time in the observation borehole KFR106:3 during the interference pumping tests in KFR103: 177.0–187.0 m. Pumping period occurred between 2016-04-07 and 2016-04-11.

**A1.4.2 Low confidence responses in observation sections for test in KFR103:
177.0–187.0 m**

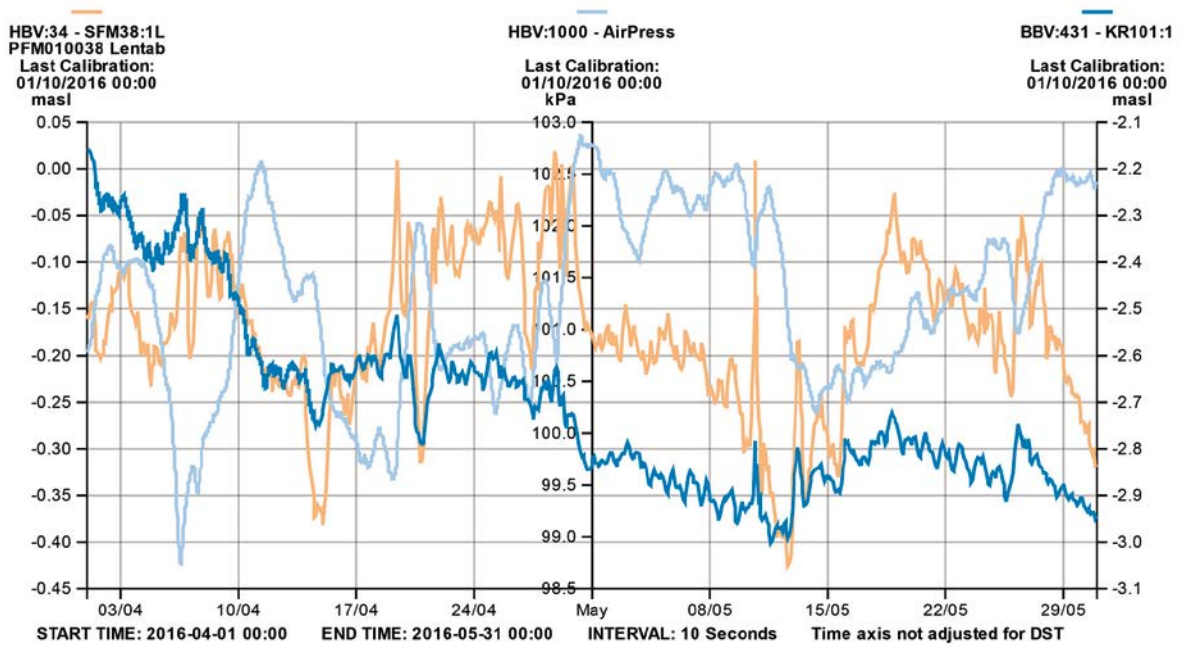


Figure A1-65. Linear plot of observed head versus time in the observation borehole KFR101:1 during the interference pumping tests in KFR103: 177.0–187.0 m. Pumping period occurred between 2016-04-07 and 2016-04-11.

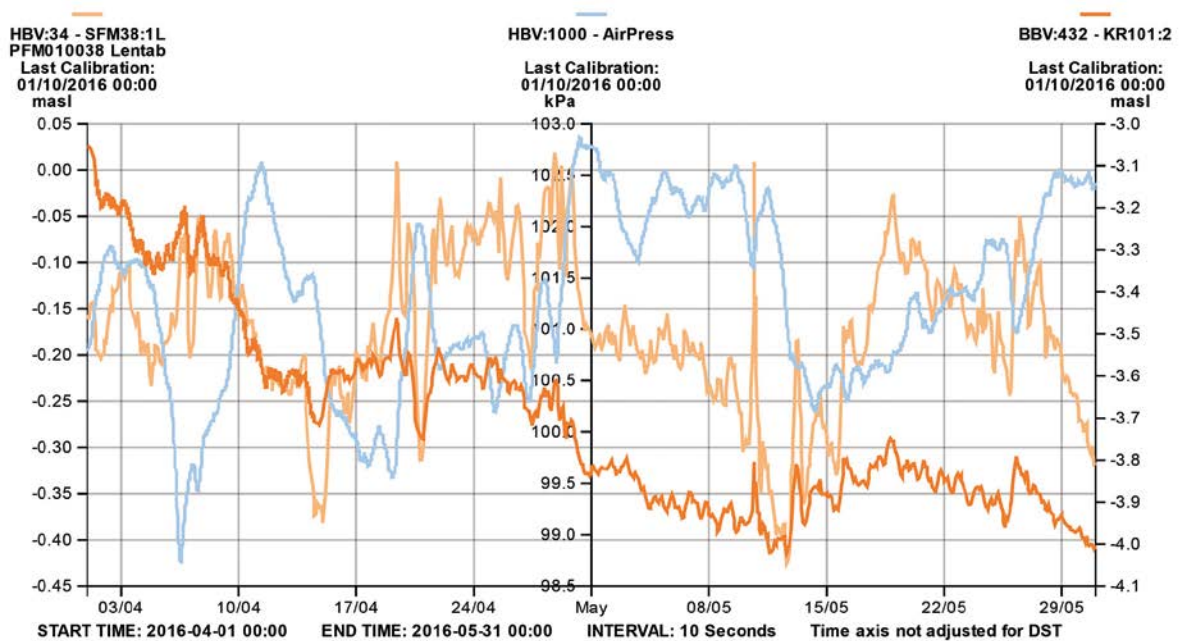


Figure A1-66. Linear plot of observed head versus time in the observation borehole KFR101:2 during the interference pumping tests in KFR103: 177.0–187.0 m. Pumping period occurred between 2016-04-07 and 2016-04-11.

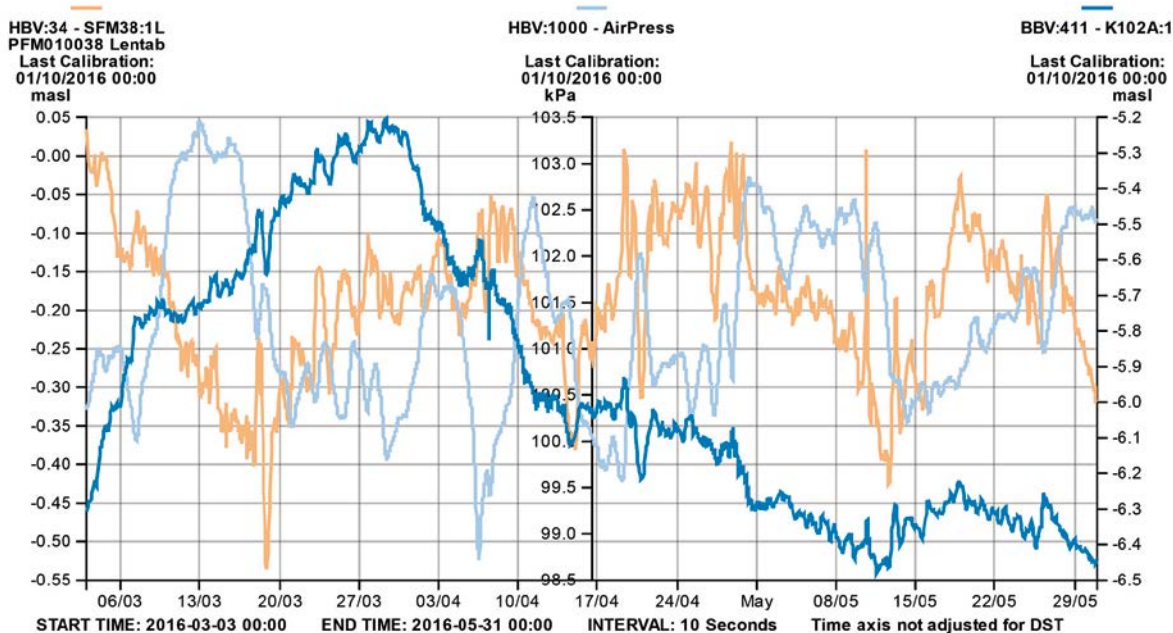


Figure A1-67. Linear plot of observed head versus time in the observation borehole KFR102A:1 during the interference pumping tests in KFR103: 177.0–187.0 m. Pumping period occurred between 2016-04-07 and 2016-04-11.

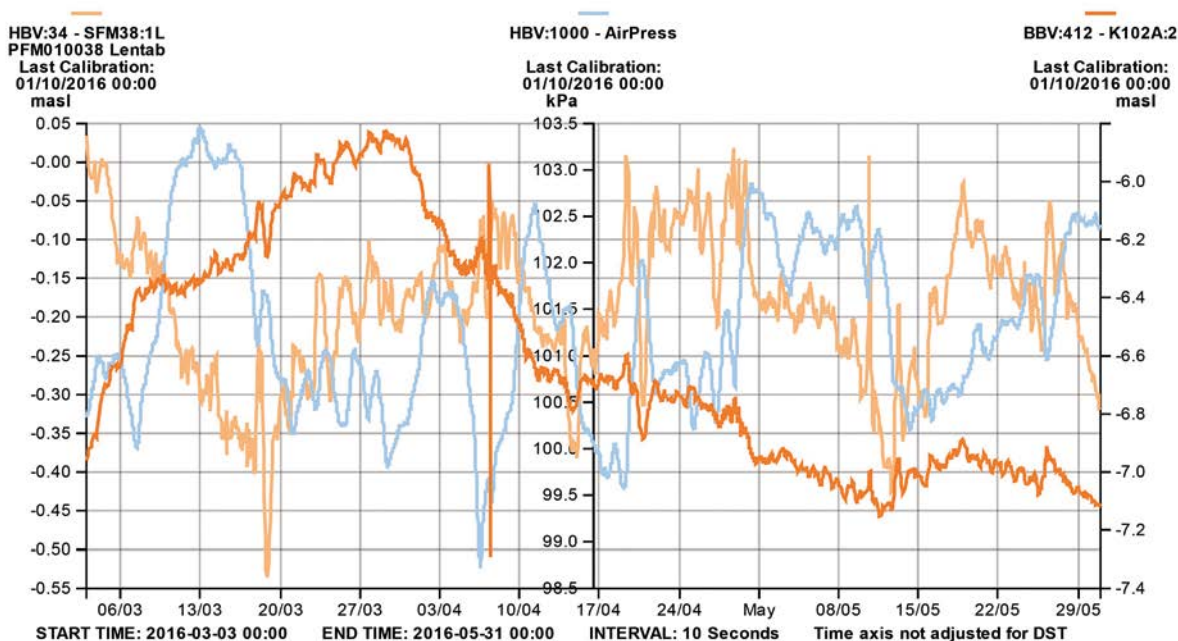


Figure A1-68. Linear plot of observed head versus time in the observation borehole KFR102A:2 during the interference pumping tests in KFR103: 177.0–187.0 m. Pumping period occurred between 2016-04-07 and 2016-04-11.

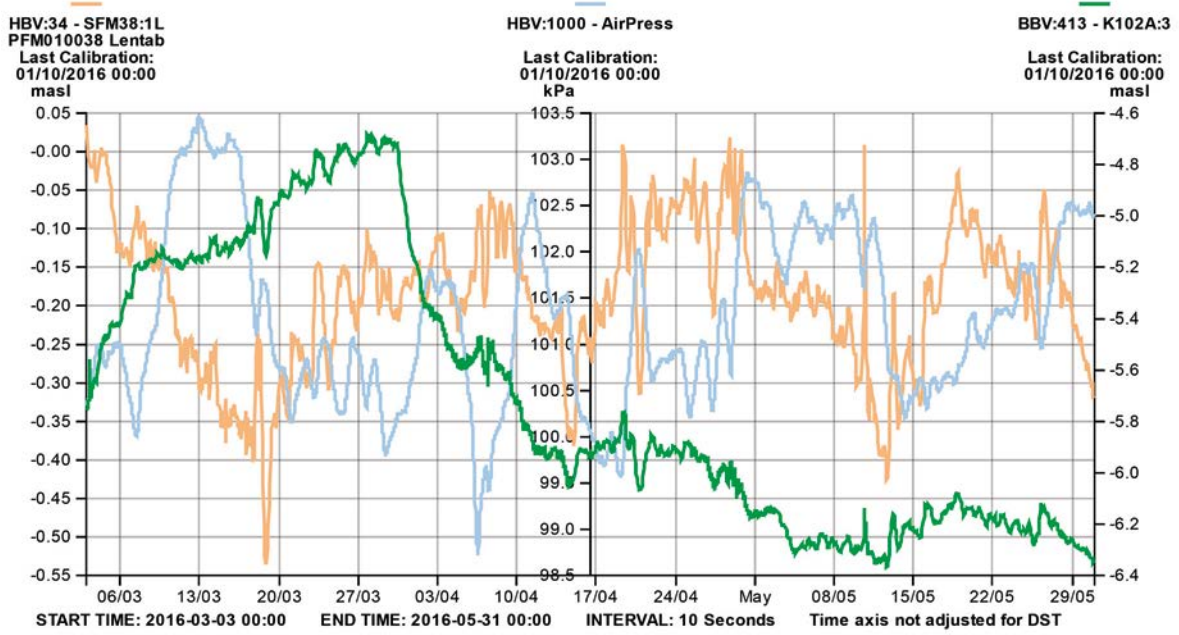


Figure A1-69. Linear plot of observed head versus time in the observation borehole KFR102A:3 during the interference pumping tests in KFR103: 177.0–187.0 m. Pumping period occurred between 2016-04-07 and 2016-04-11.

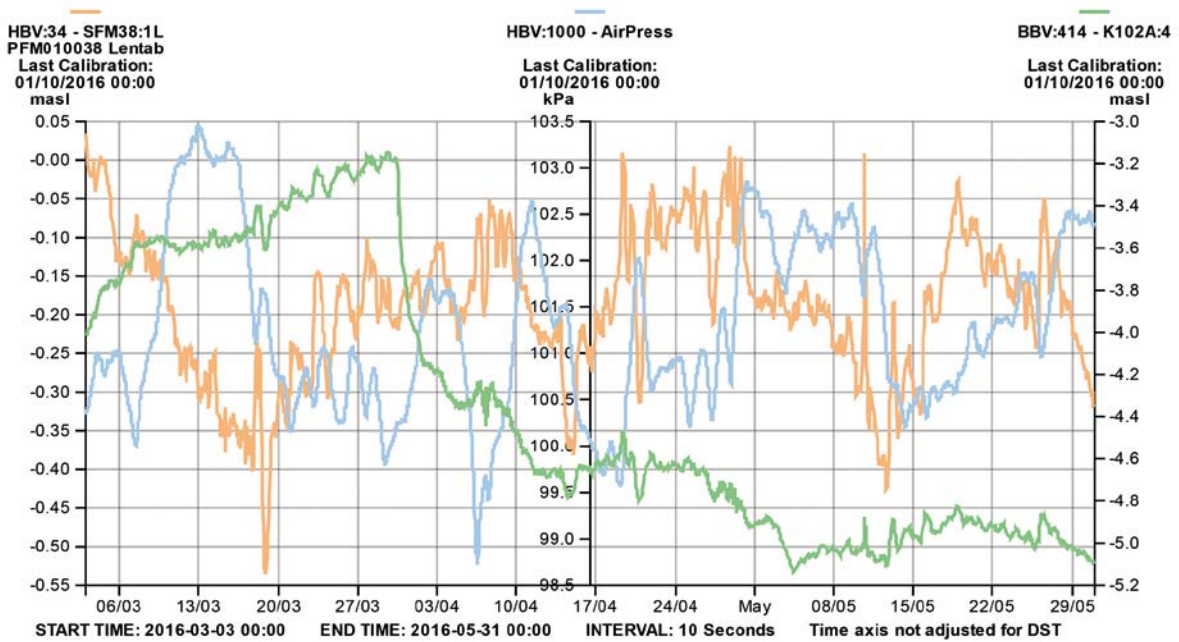


Figure A1-70. Linear plot of observed head versus time in the observation borehole KFR102A:4 during the interference pumping tests in KFR103: 177.0–187.0 m. Pumping period occurred between 2016-04-07 and 2016-04-11.

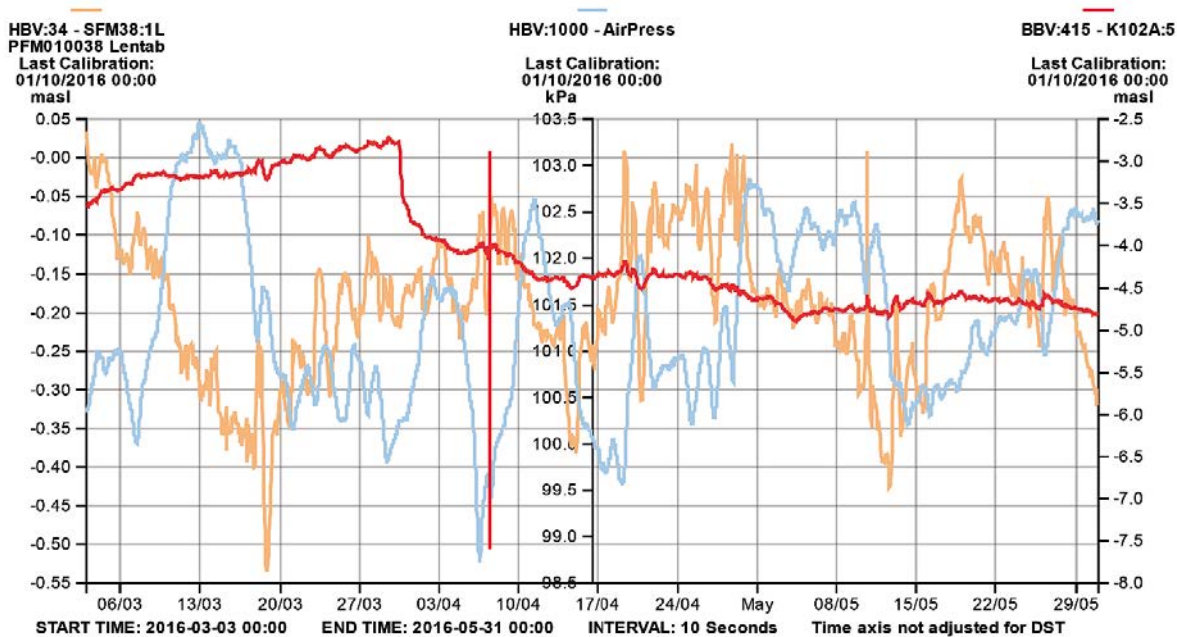


Figure A1-71. Linear plot of observed head versus time in the observation borehole KFR102A:5 during the interference pumping tests in KFR103: 177.0–187.0 m. Pumping period occurred between 2016-04-07 and 2016-04-11.

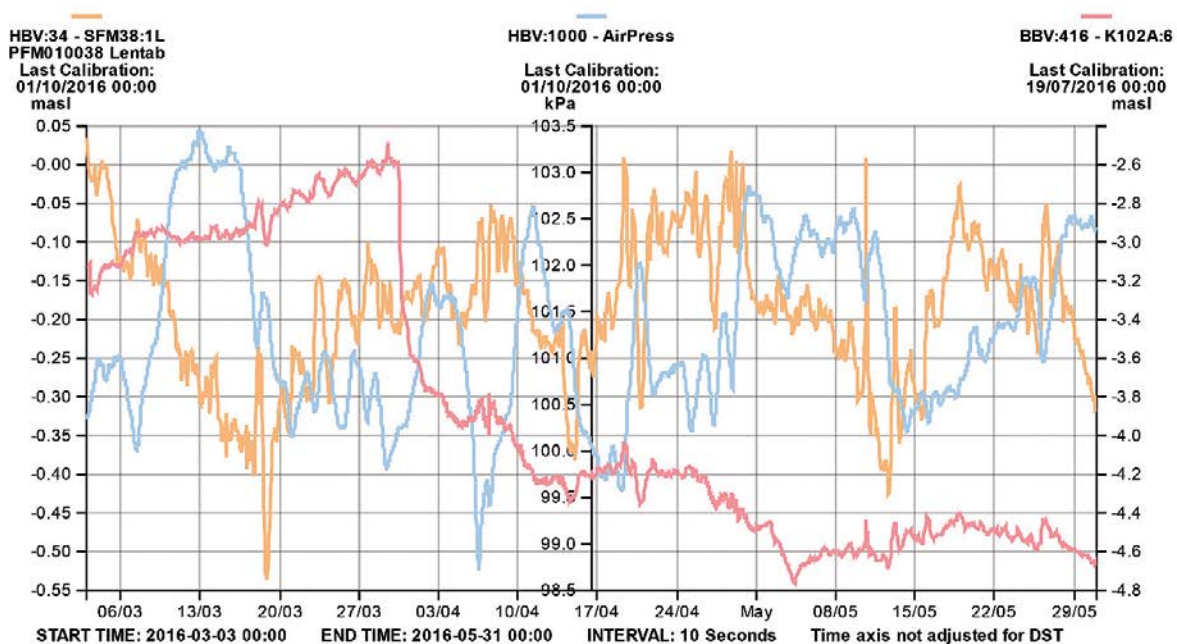


Figure A1-72. Linear plot of observed head versus time in the observation borehole KFR102A:6 during the interference pumping tests in KFR103: 177.0–187.0 m. Pumping period occurred between 2016-04-07 and 2016-04-11.

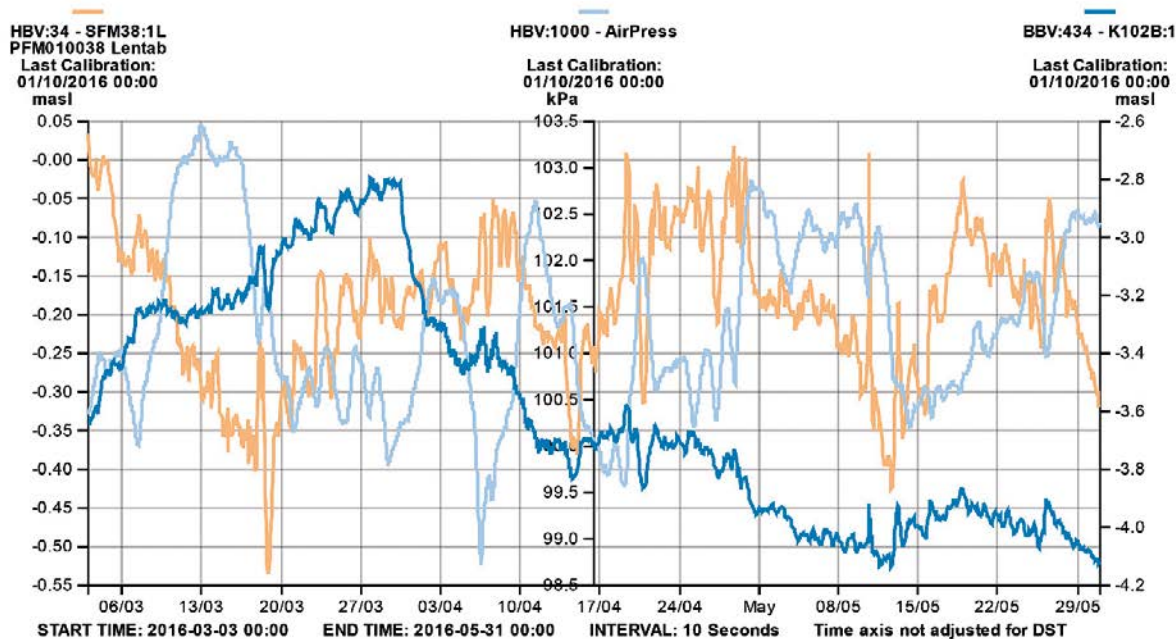


Figure A1-73. Linear plot of observed head versus time in the observation borehole KFR102B:1 during the interference pumping tests in KFR103: 177.0–187.0 m. Pumping period occurred between 2016-04-07 and 2016-04-11.

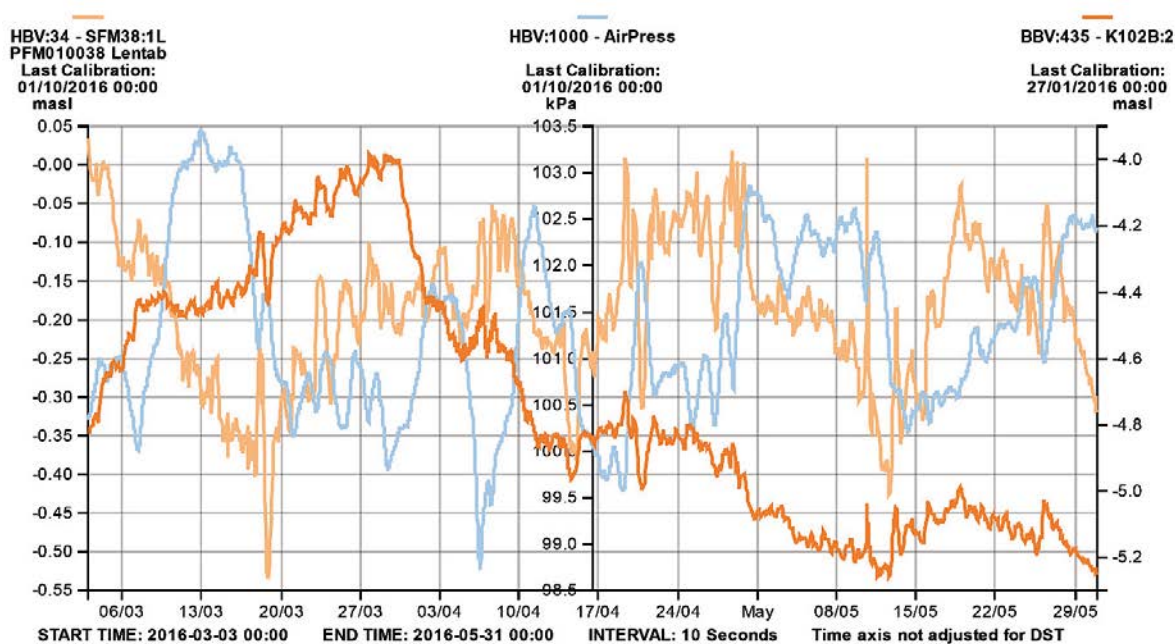


Figure A1-74. Linear plot of observed head versus time in the observation borehole KFR102B:2 during the interference pumping tests in KFR103: 177.0–187.0 m. Pumping period occurred between 2016-04-07 and 2016-04-11.

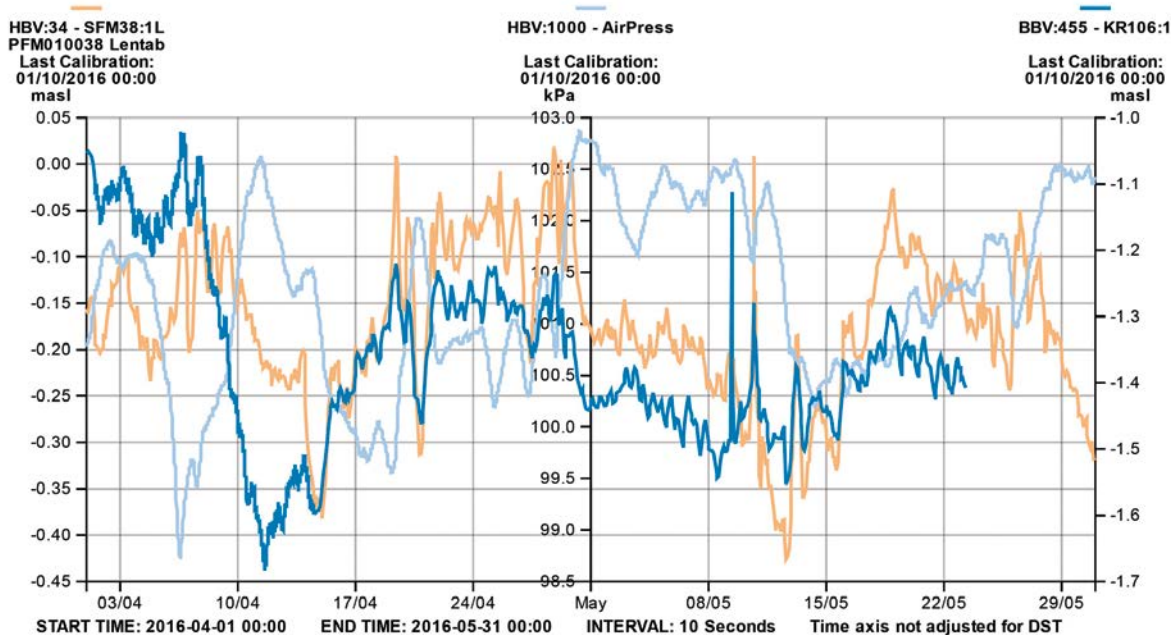


Figure A1-75. Linear plot of observed head versus time in the observation borehole KFR106:1 during the interference pumping tests in KFR103: 177.0–187.0 m. Pumping period occurred between 2016-04-07 and 2016-04-11. After 2016-05-23 there is no data for KFR106:1.

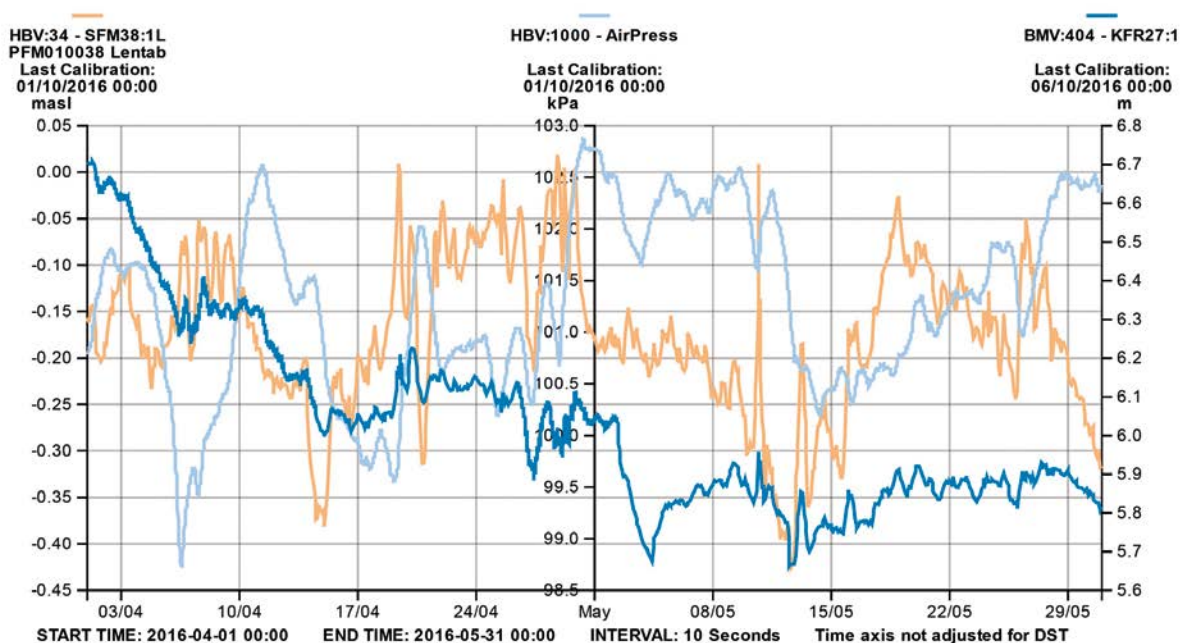


Figure A1-76. Linear plot of observed head versus time in the observation borehole KFR27:1 during the interference pumping tests in KFR103: 177.0–187.0 m. Pumping period occurred between 2016-04-07 and 2016-04-11.

A1.1 Interference test in KFR105: 120.0–137.0 m

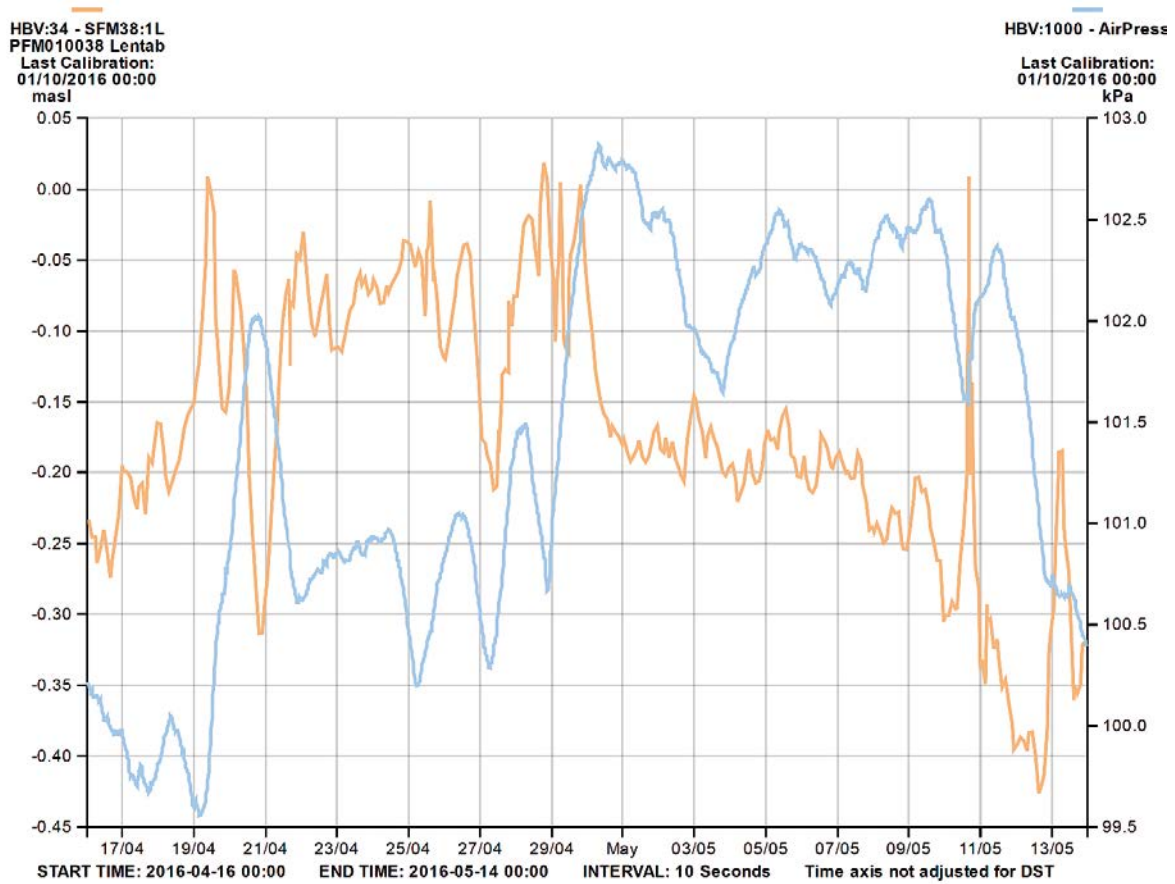


Figure A1-77. Registered air pressure (blue line) and sea water level (orange line) at SFR during the interference test period in KFR105:120–137 m, with data from circa ten days before and ten days after. Each parameter has its own Y-scale. Pumping period occurred between 2016-04-26 and 2016-04-29.

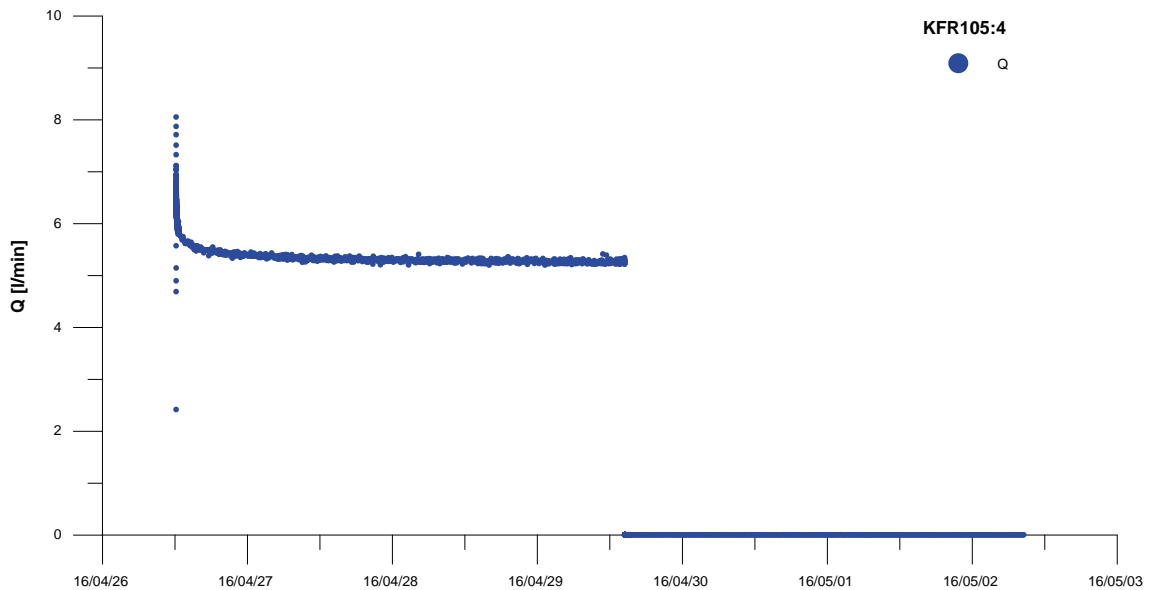


Figure A1-78. Linear plot of observed pumped flow versus time in the pumping borehole KFR105: 120–137 m during the interference pumping test.

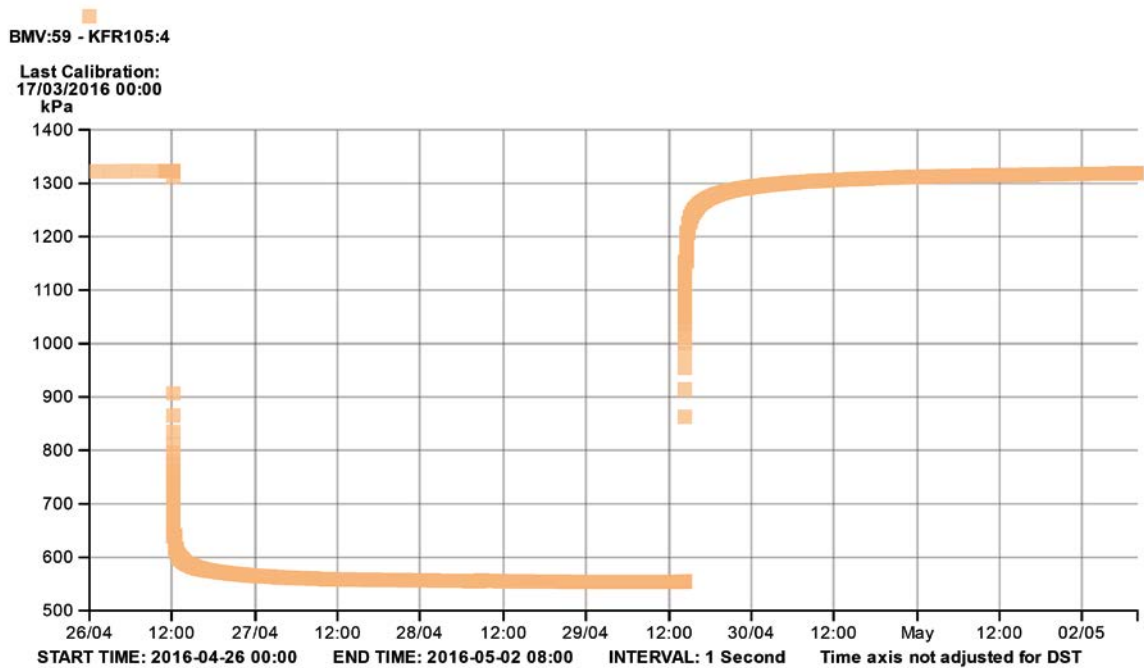


Figure A1-79. Linear plot of observed pressure versus time in the pumping borehole KFR105: 120–137 m during the interference pumping test.

A1.4.3 Responses in observation sections for test in KFR105: 120.0–137.0 m

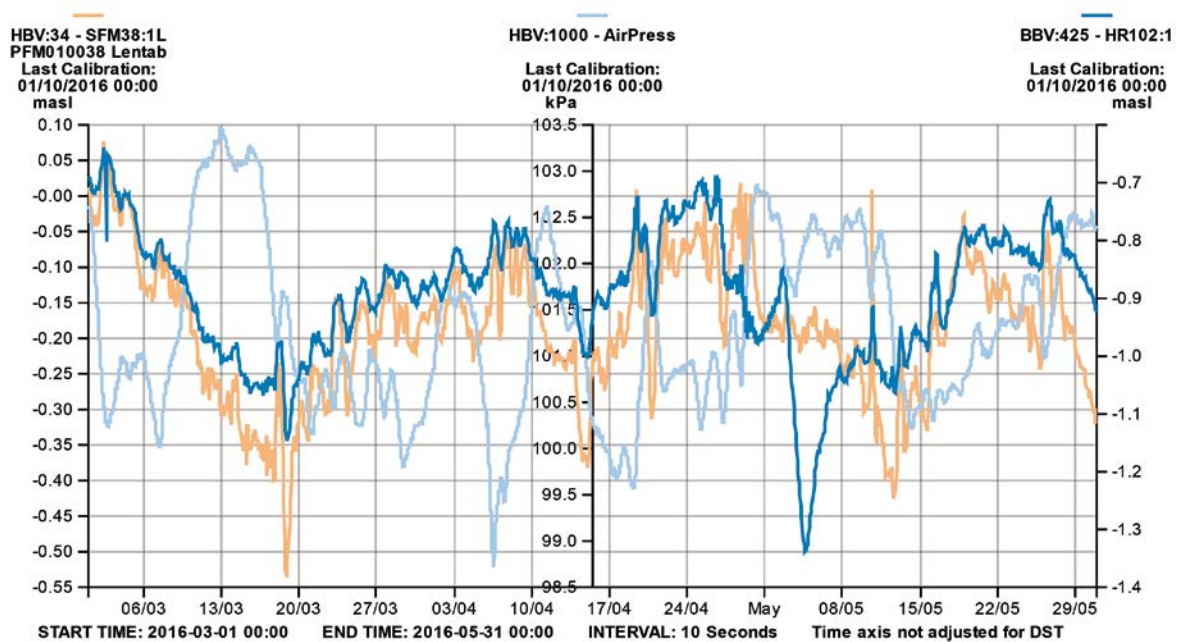


Figure A1-80. Linear plot of observed head versus time in the observation borehole HFR102:1 during the interference pumping tests in KFR105: 129.0–137.0 m. Pumping period occurred between 2016-04-26 and 2016-04-29.

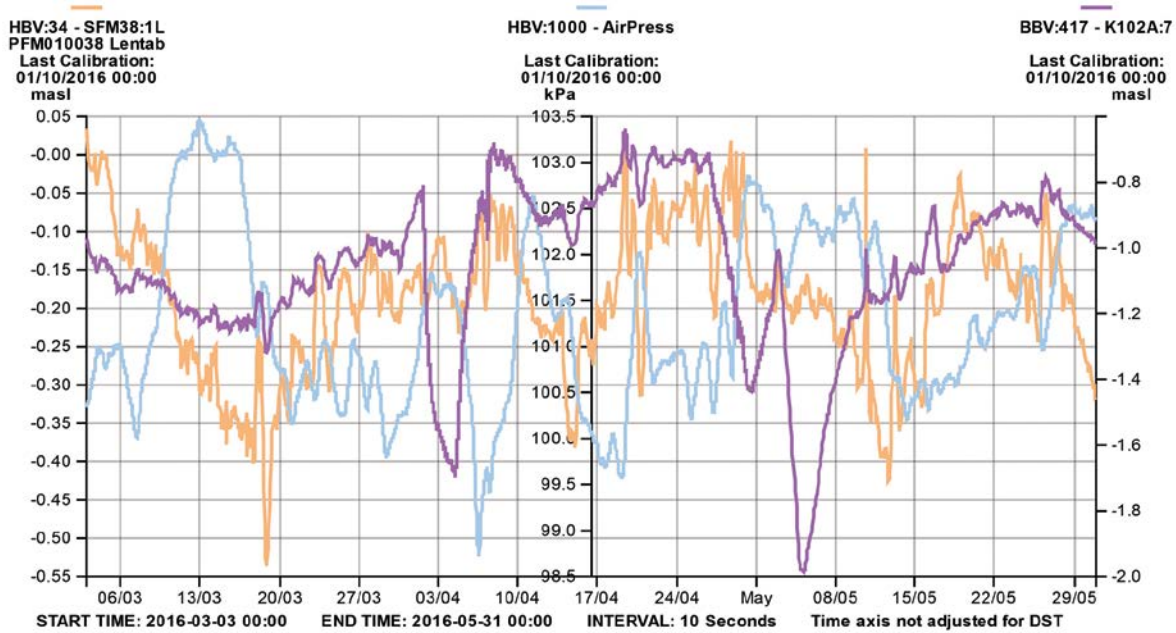


Figure AI-81. Linear plot of observed head versus time in the observation borehole KFR102A:7 during the interference pumping tests in KFR105: 129.0–137.0 m. Pumping period occurred between 2016-04-26 and 2016-04-29.

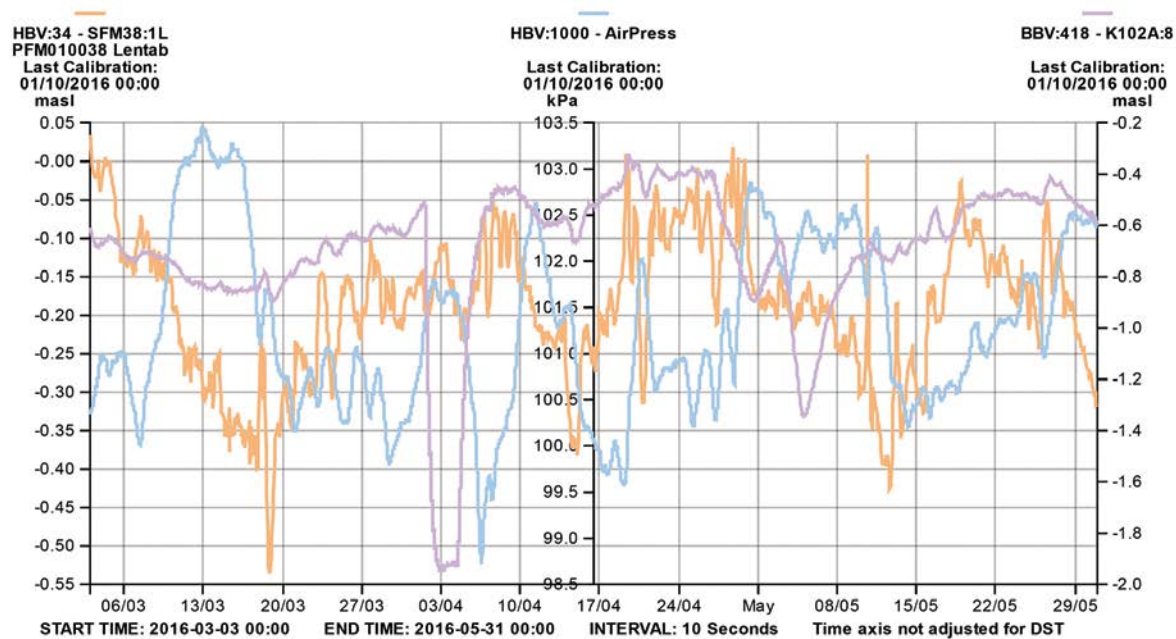


Figure AI-82. Linear plot of observed head versus time in the observation borehole KFR102A:8 during the interference pumping tests in KFR105: 129.0–137.0 m. Pumping period occurred between 2016-04-26 and 2016-04-29.

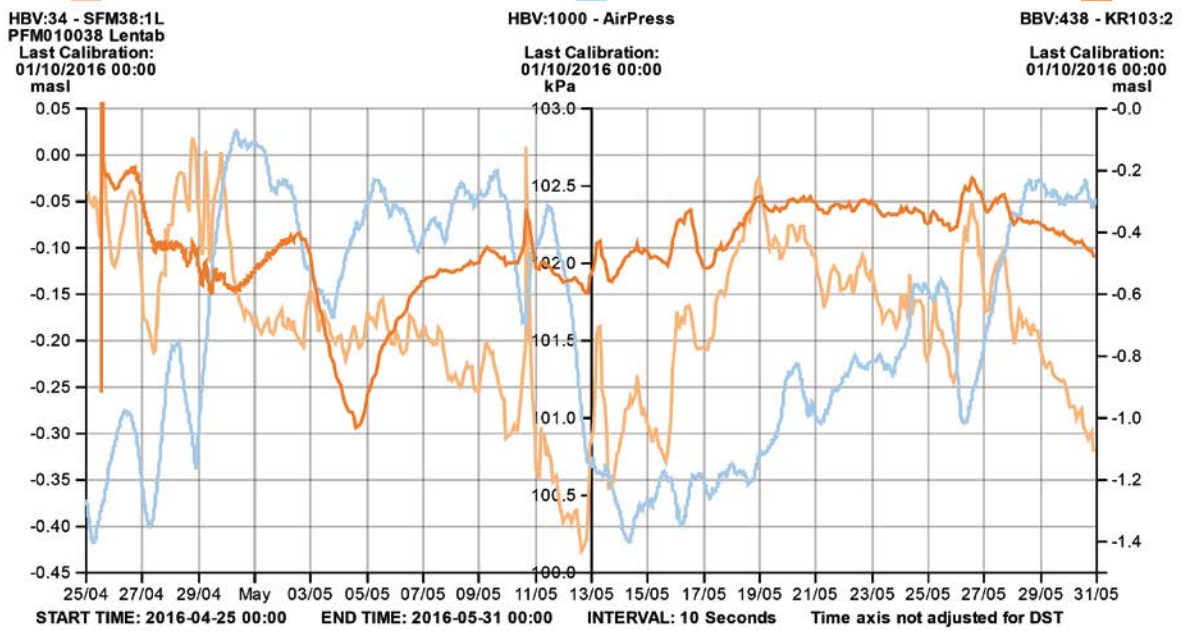


Figure A1-83. Linear plot of observed head versus time in the observation borehole KFR103:2 during the interference pumping tests in KFR105: 129.0–137.0 m. Pumping period occurred between 2016-04-26 and 2016-04-29.

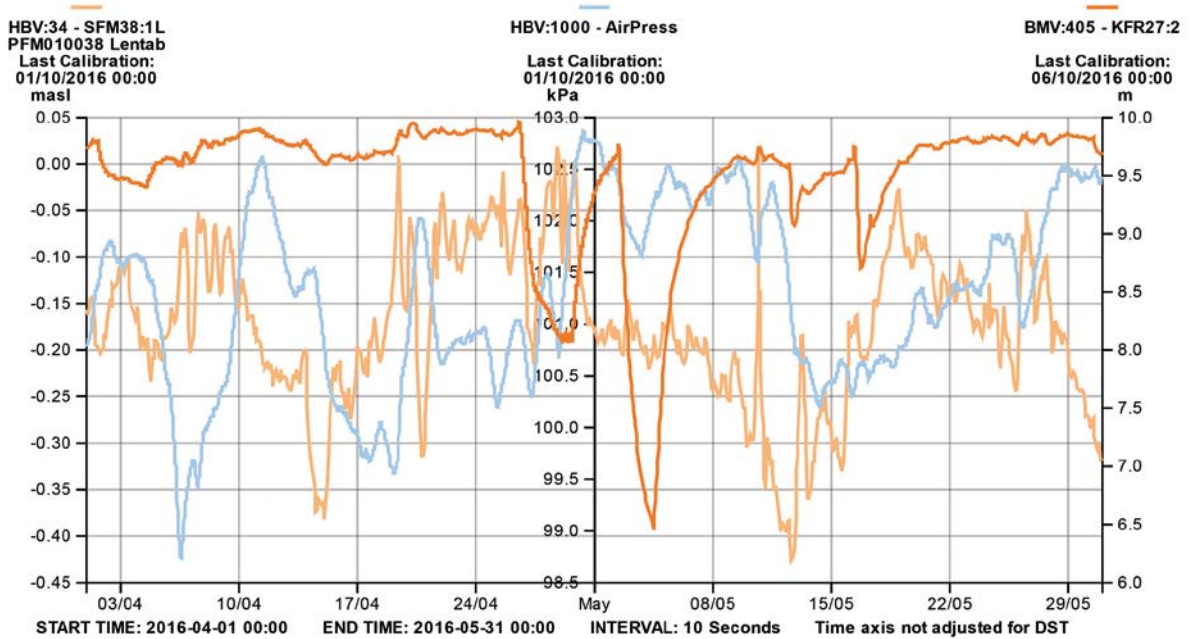


Figure A1-84. Linear plot of observed head versus time in the observation borehole KFR27:2 during the interference pumping tests in KFR105: 129.0–137.0 m. Pumping period occurred between 2016-04-26 and 2016-04-29.

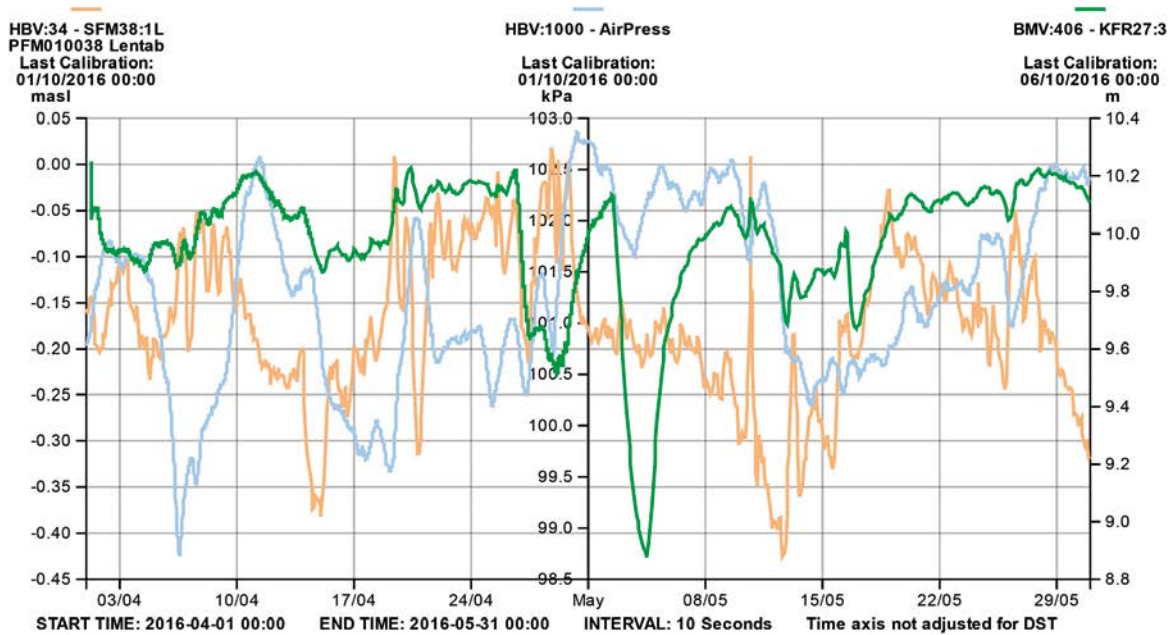


Figure A1-85. Linear plot of observed head versus time in the observation borehole KFR27:3 during the interference pumping tests in KFR105: 129.0–137.0 m. Pumping period occurred between 2016-04-26 and 2016-04-29.

A1.4.4 Low confidence responses in observation sections for test in KFR105: 120.0–137.0 m

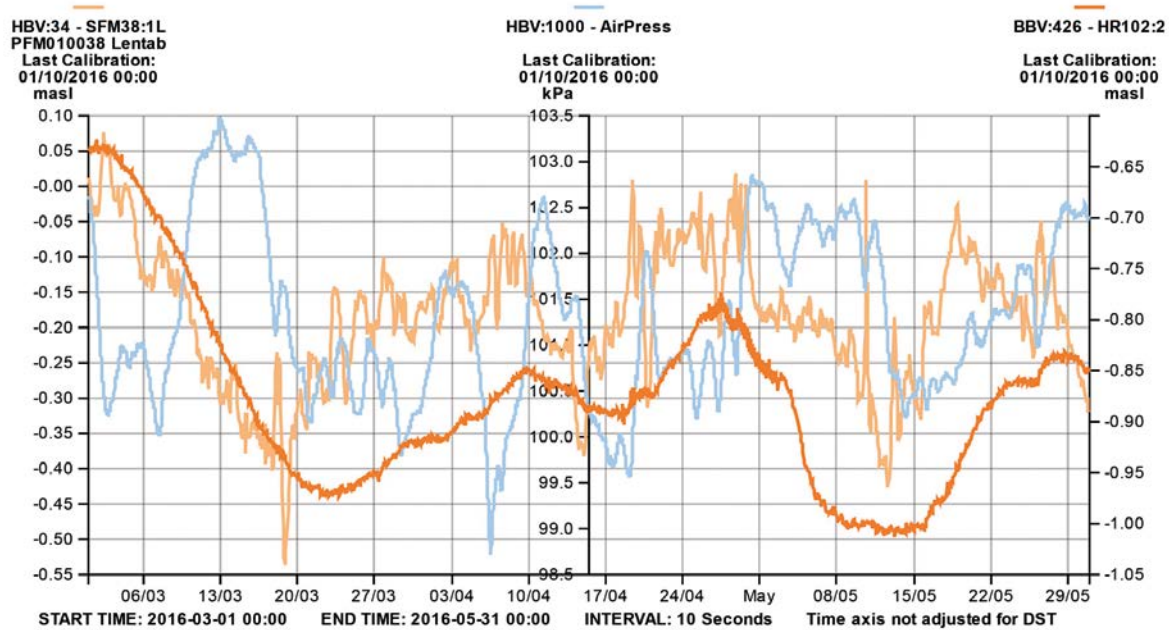


Figure A1-86. Linear plot of observed head versus time in the observation borehole HFR102:2 during the interference pumping tests in KFR105: 129.0–137.0 m. Pumping period occurred between 2016-04-26 and 2016-04-29.

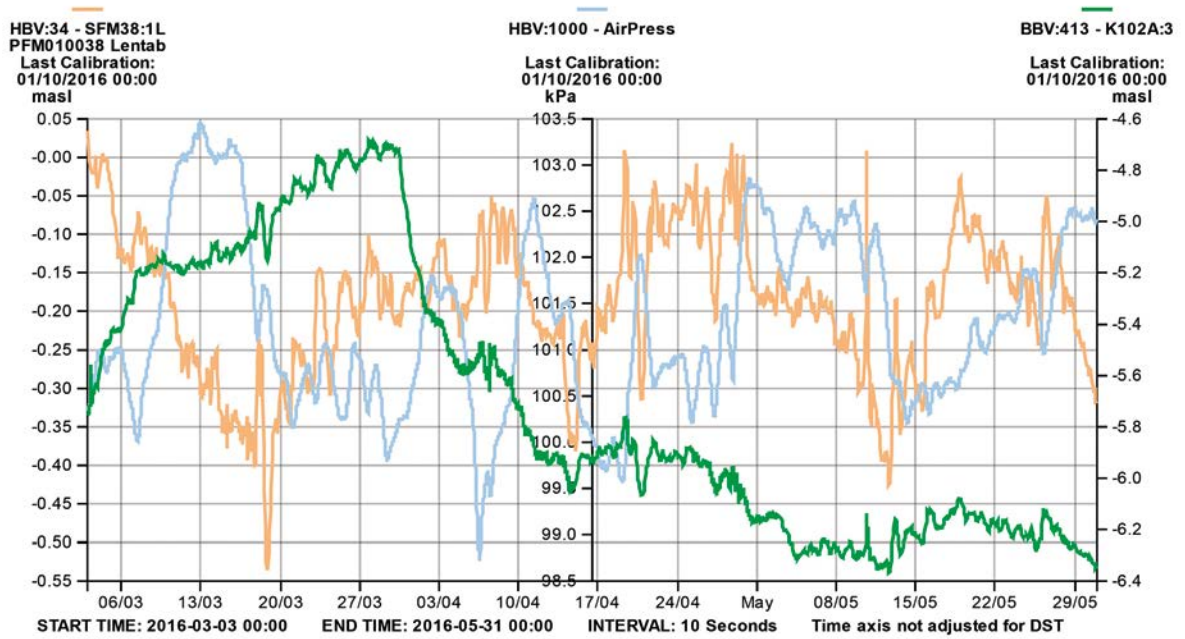


Figure A1-87. Linear plot of observed head versus time in the observation borehole KFR102A:3 during the interference pumping tests in KFR105: 129.0–137.0 m. Pumping period occurred between 2016-04-26 and 2016-04-29.

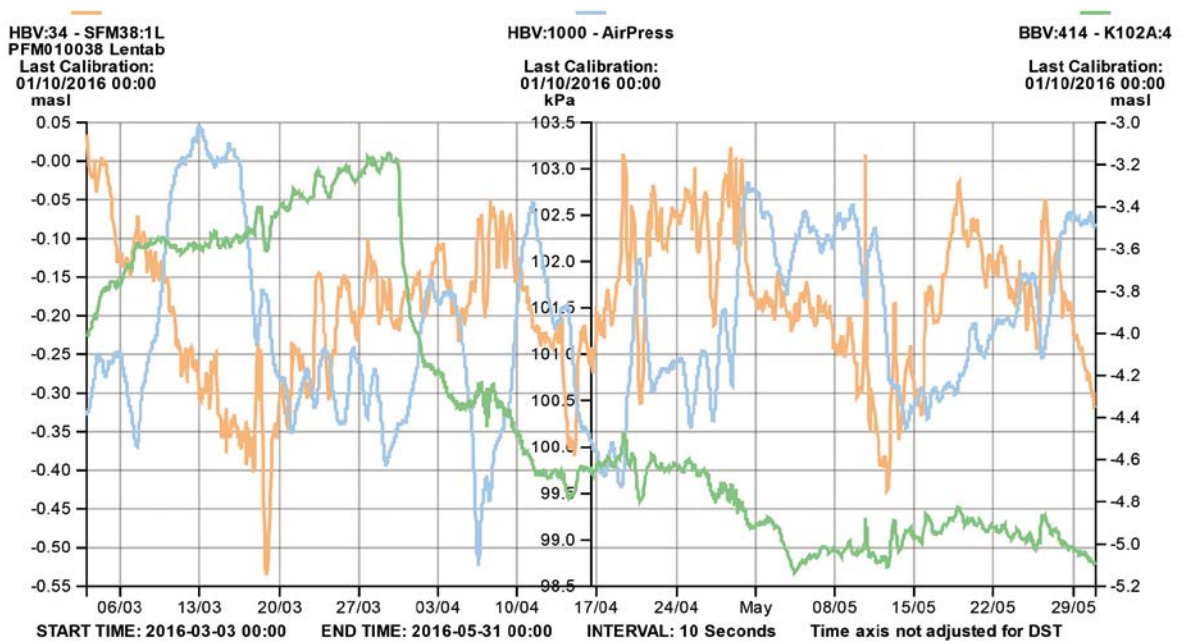


Figure A1-88. Linear plot of observed head versus time in the observation borehole KFR102A:4 during the interference pumping tests in KFR105: 129.0–137.0 m. Pumping period occurred between 2016-04-26 and 2016-04-29.

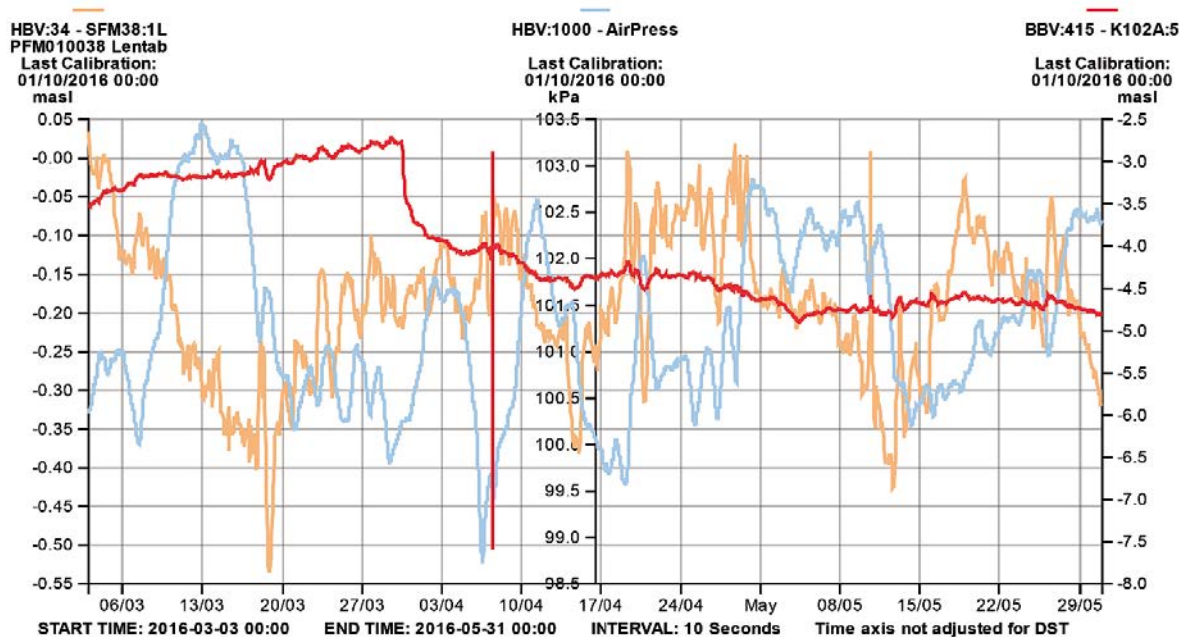


Figure A1-89. Linear plot of observed head versus time in the observation borehole KFR102A:5 during the interference pumping tests in KFR105: 129.0–137.0 m. Pumping period occurred between 2016-04-26 and 2016-04-29.

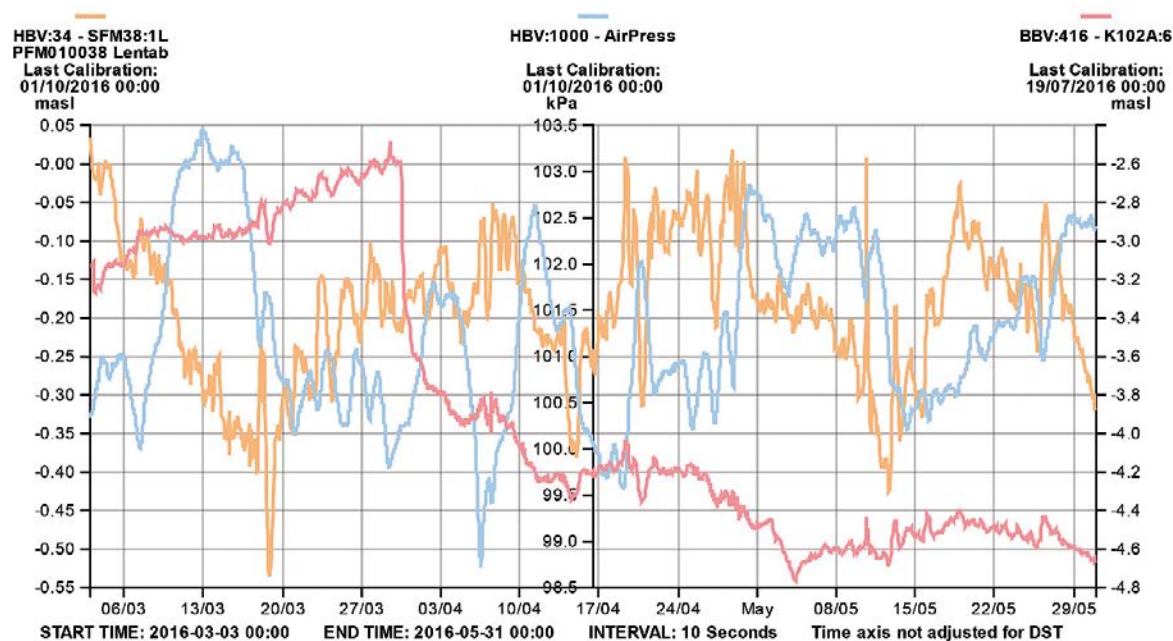


Figure A1-90. Linear plot of observed head versus time in the observation borehole KFR102A:6 during the interference pumping tests in KFR105: 129.0–137.0 m. Pumping period occurred between 2016-04-26 and 2016-04-29.

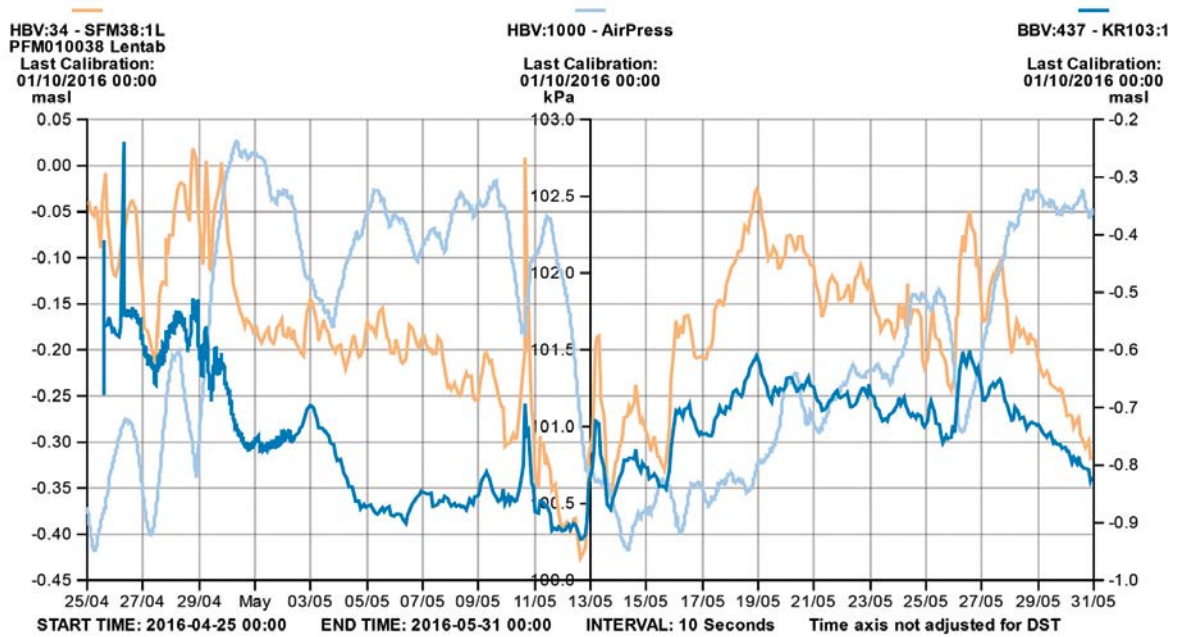


Figure A1-91. Linear plot of observed head versus time in the observation borehole KFR103:1 during the interference pumping tests in KFR105: 129.0–137.0 m. Pumping period occurred between 2016-04-26 and 2016-04-29.

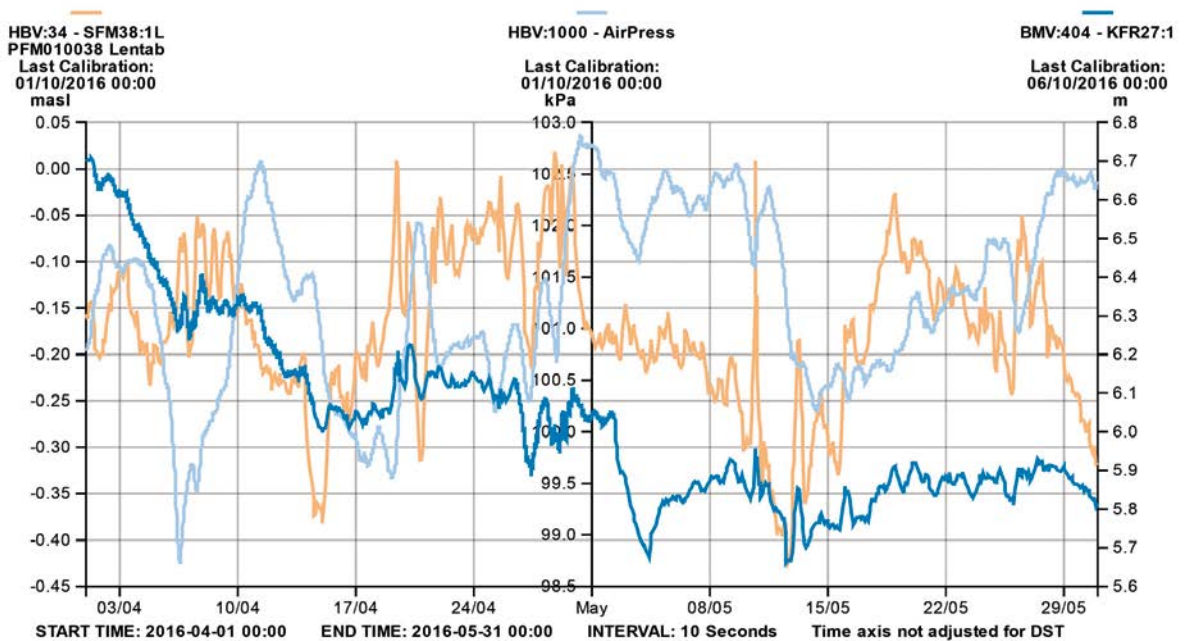


Figure A1-92. Linear plot of observed head versus time in the observation borehole KFR27:1 during the interference pumping tests in KFR105: 129.0–137.0 m. Pumping period occurred between 2016-04-26 and 2016-04-29.

Hydraulic interference test diagrams

Nomenclature:

T = transmissivity (m²/s)

S = storativity (-)

K_z/K_r = ratio of hydraulic conductivities in the vertical and radial direction (set to 1)

Sw = skin factor

r(w) = borehole radius (m)

b = thickness of formation (m)

A2.1 Interference test in KFR27: 47.00–57.00m

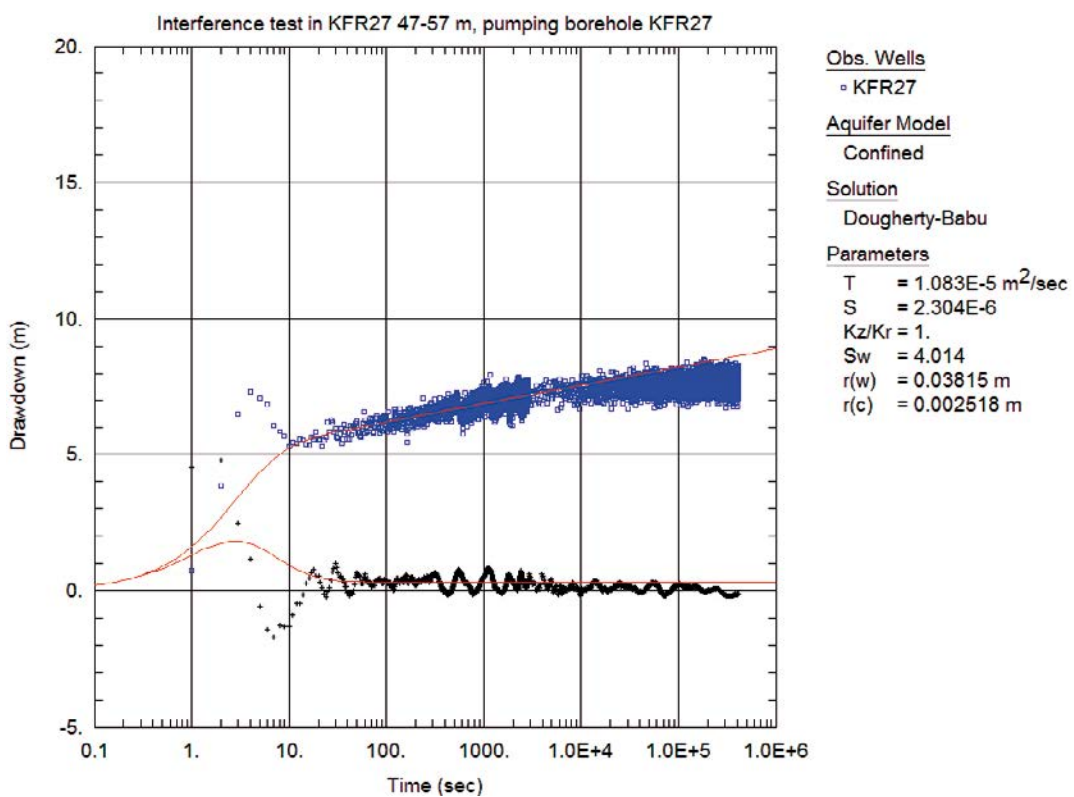


Figure A2-1a. Lin-log plot of drawdown (□) and drawdown derivative, $ds/d(\ln t)$ (+), versus time in the pumping borehole section during the interference test in KFR27: 47.00–57.00 m and simulated corresponding curves (solid lines). The evaluation is made on the early part.

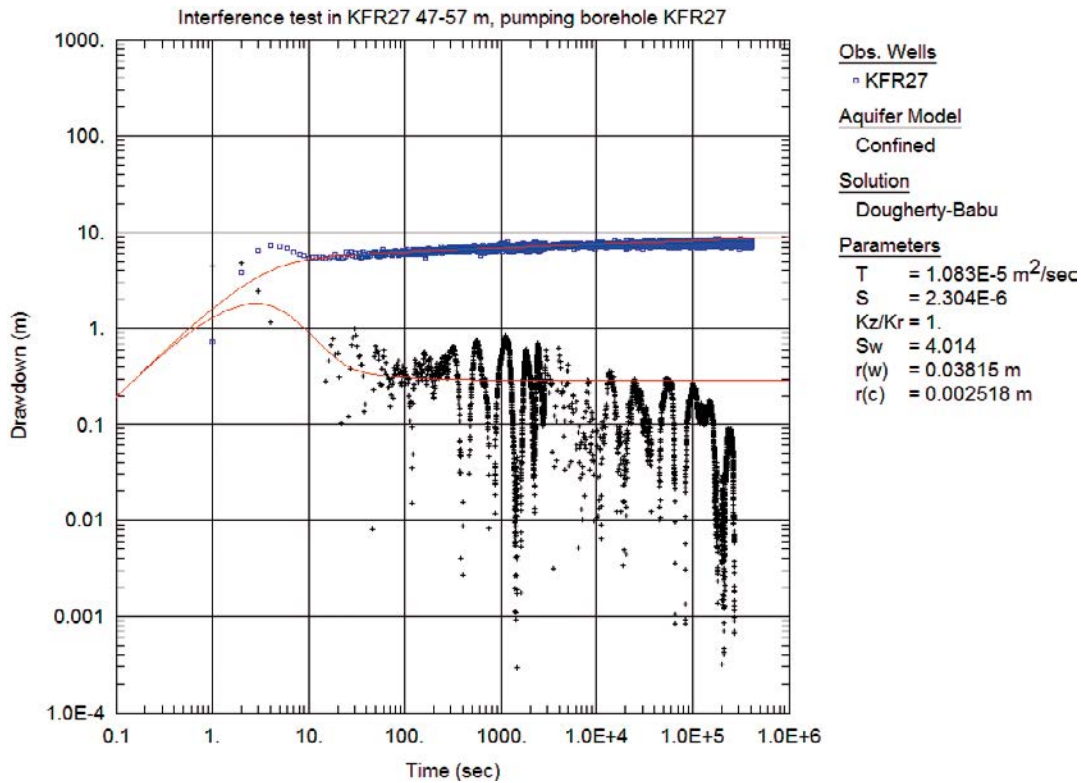


Figure A2-1b. Same as above but log-log plot.

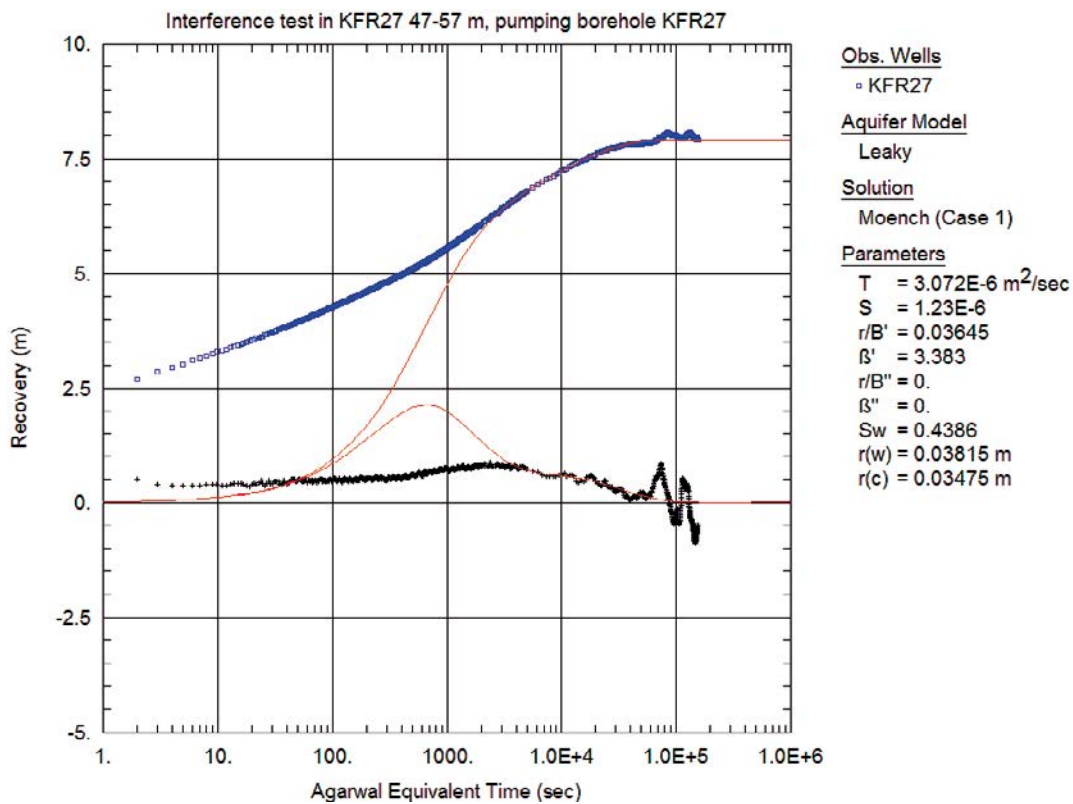


Figure A2-2a. Lin-log plot of recovery (◻) and derivative, $ds/d(\ln t)$ (+), versus equivalent time in the pumping borehole section during the interference test in KFR27: 47.00–57.00 m and simulated corresponding curves (solid lines). The evaluation is made on the last part.

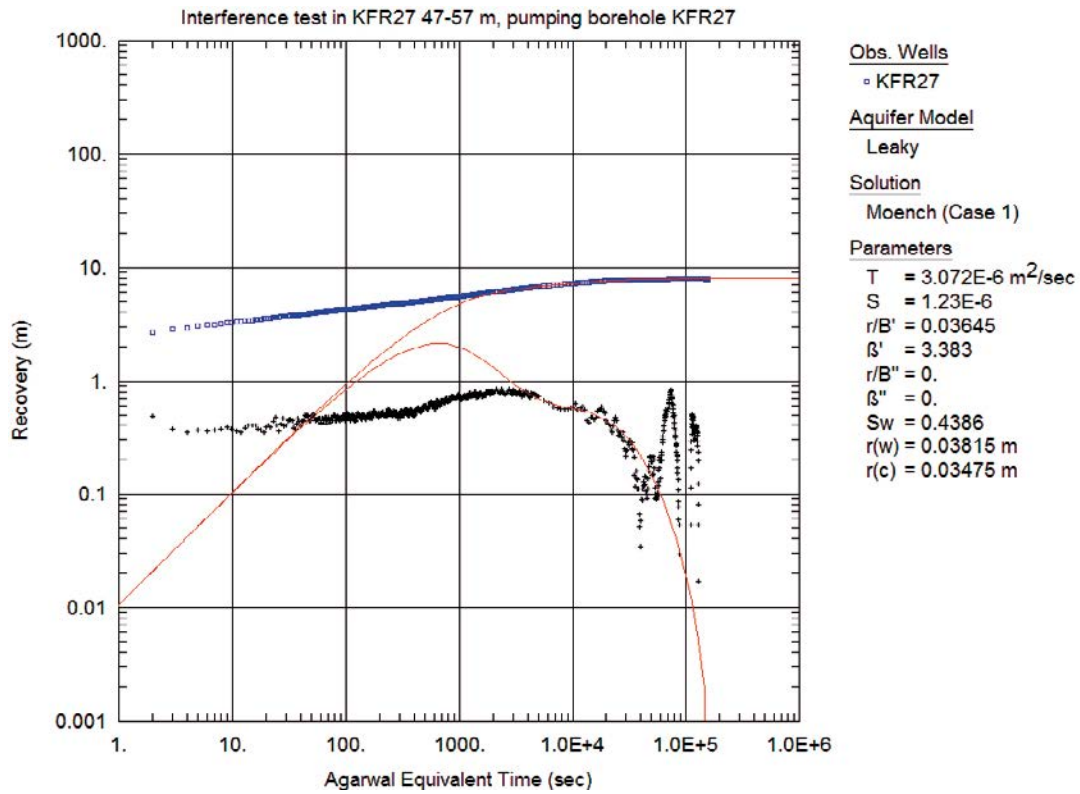


Figure A2-2b. Same as above but log-log plot.

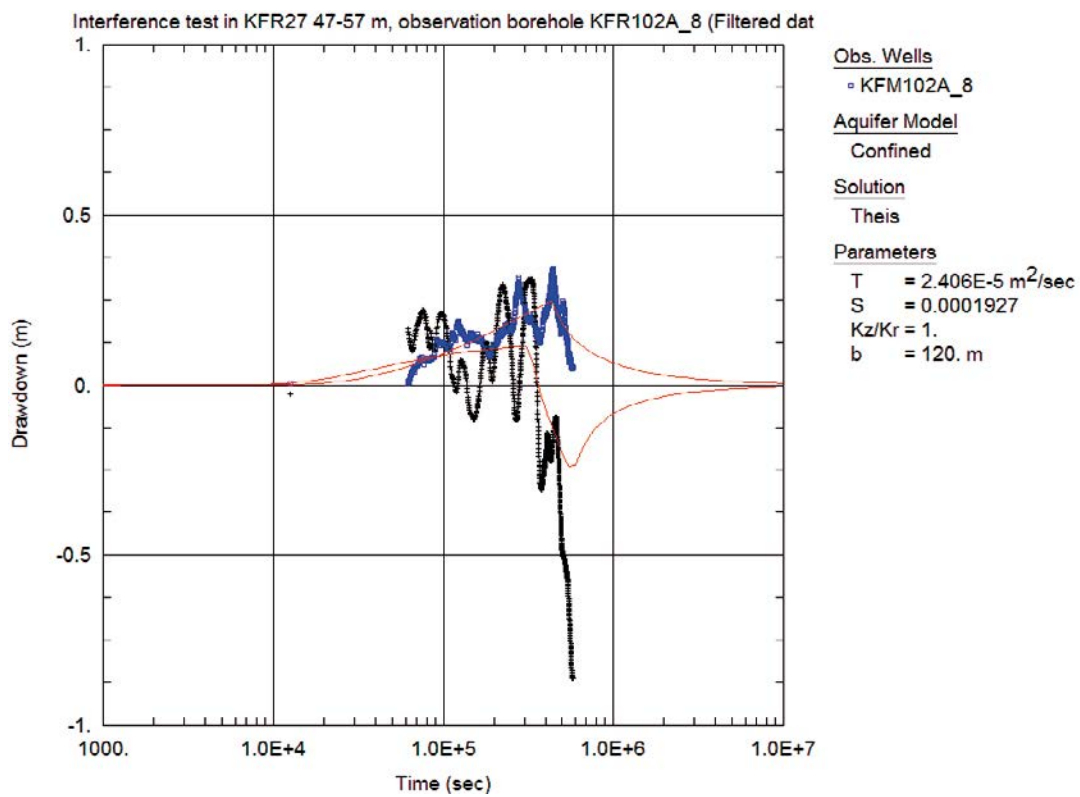


Figure A2-3a. Lin-log plot of drawdown (°) and derivative, $ds/d(\ln t)$ (+), versus time in the observation borehole section KFR102A:8 during the interference test in KFR27: 47.00–57.00 m and simulated corresponding curves (solid lines). The evaluation is made on the last part.

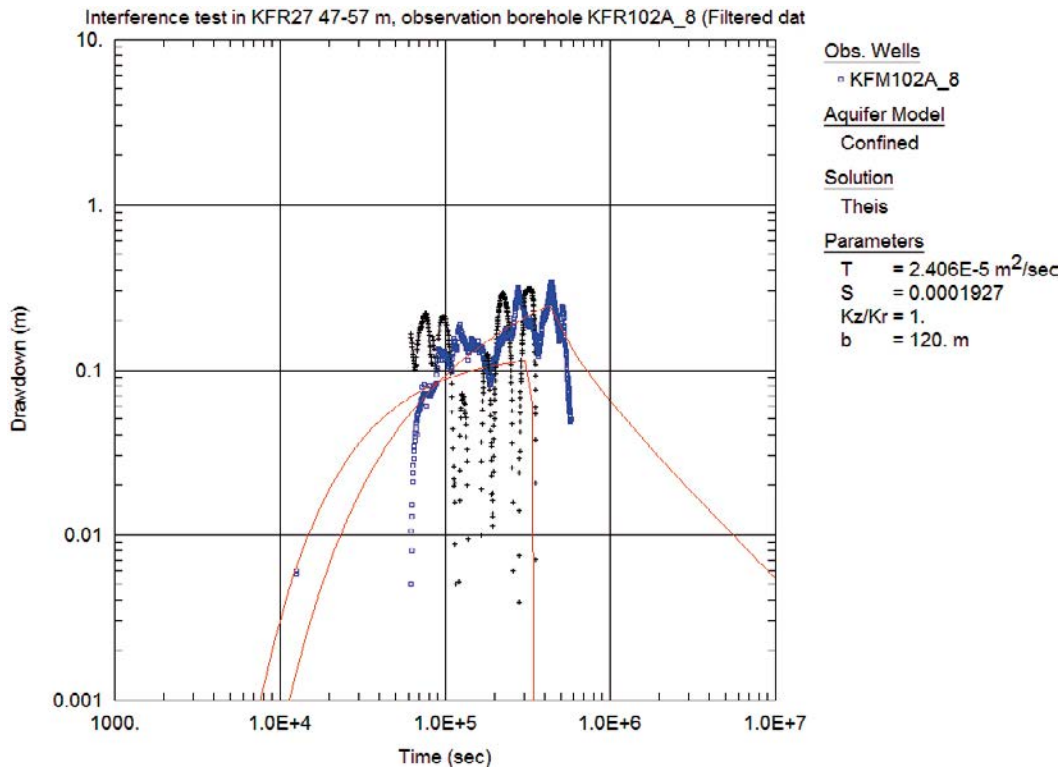


Figure A2-3b. Same as above but log-log plot.

A2.2 Interference test in KFR27: 189.40–194.40 m

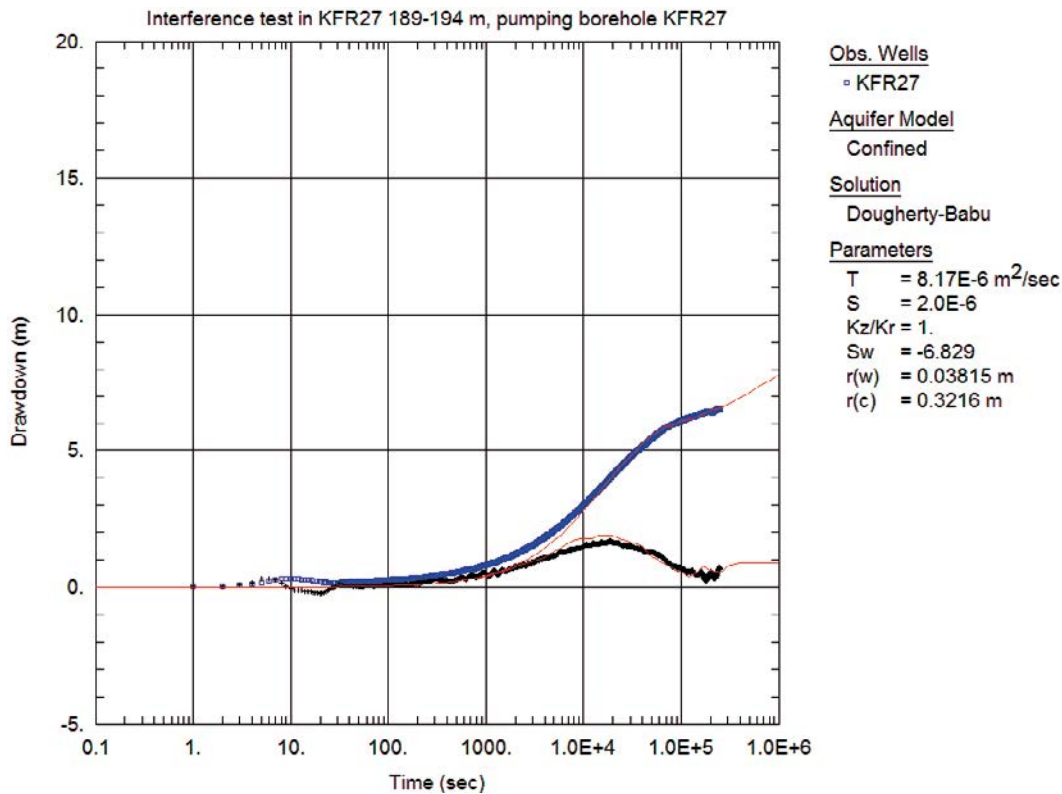


Figure A2-4a. Lin-log plot of drawdown (◻) and drawdown derivative, $ds/d(\ln t)$ (+), versus time in the pumping borehole section during the interference test in KFR27: 189.40–194.40 m and simulated corresponding curves (solid lines). The evaluation is made on the last part.

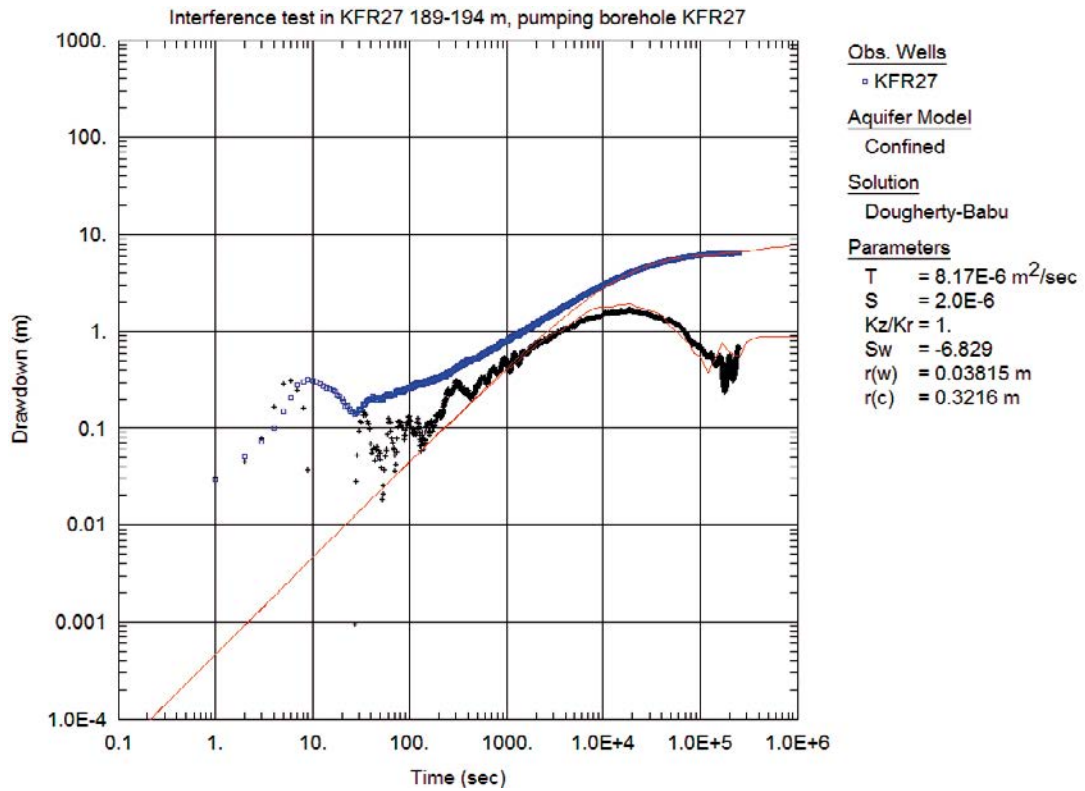


Figure A2-4b. Same as above but log-log plot.

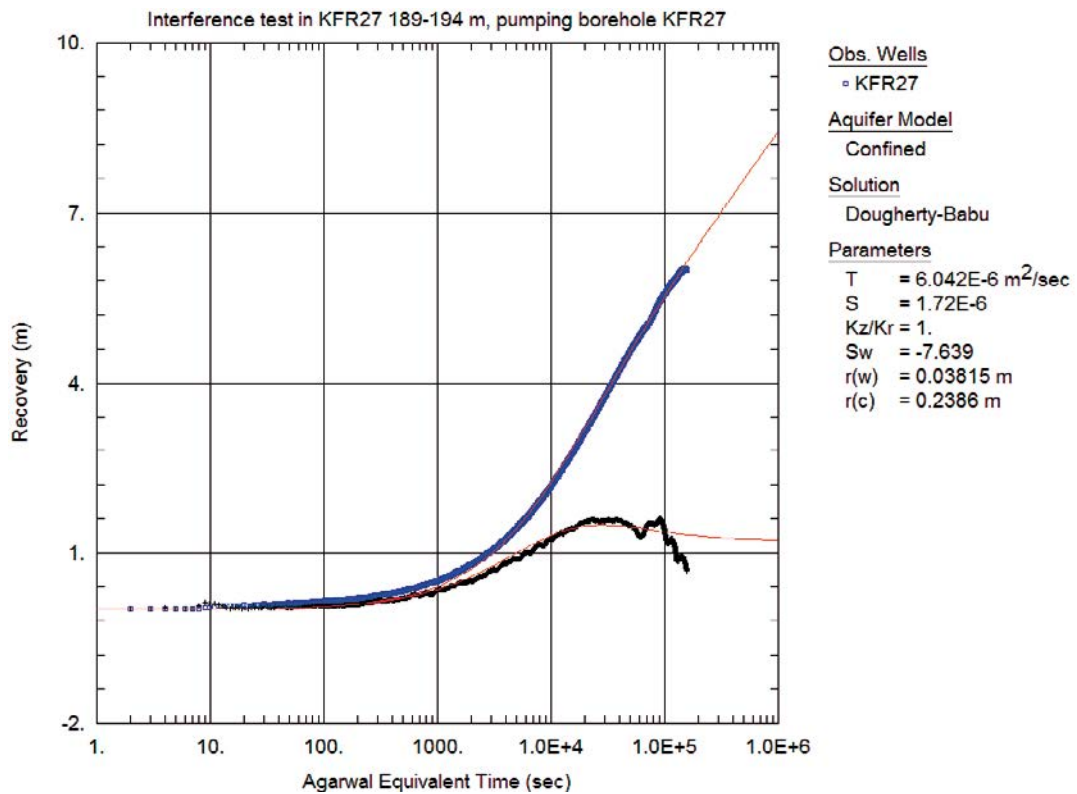


Figure A2-5a. Lin-log plot of recovery (□) and derivative, $ds/d(\ln t)$ (+), versus equivalent time in the pumping borehole section during the interference test in KFR27: 189.40–194.40 m and simulated corresponding curves (solid lines). The evaluation is made on the entire curve.

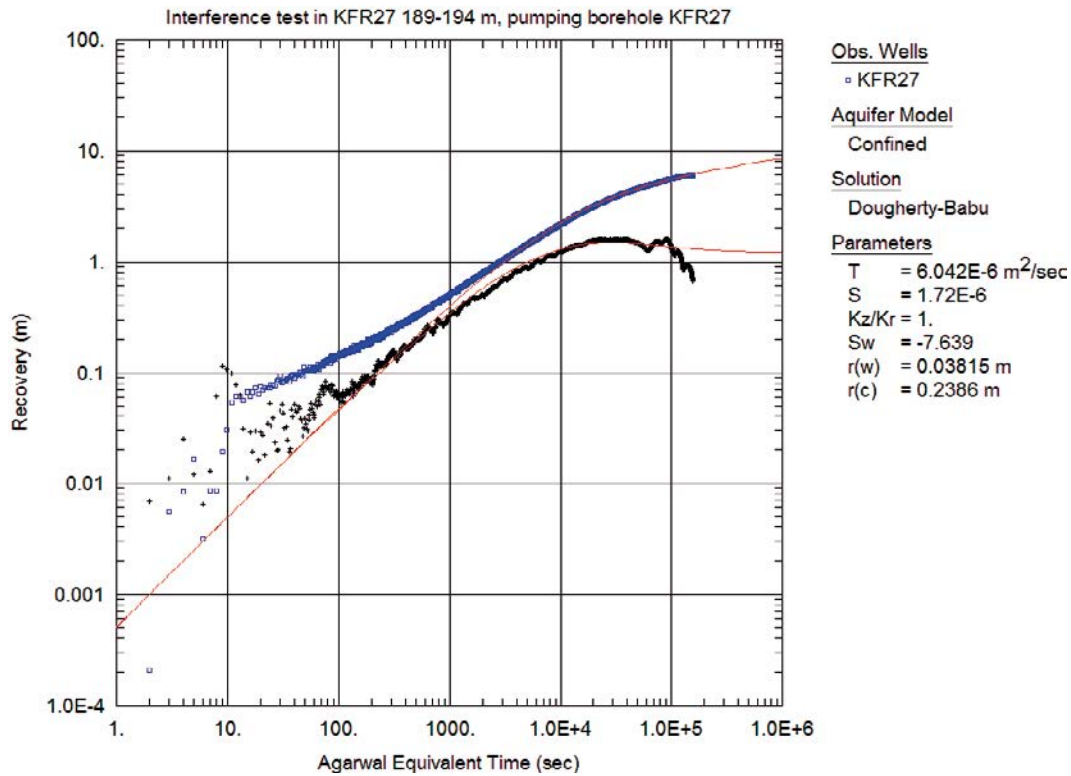


Figure A2-5b. Same as above but log-log plot.

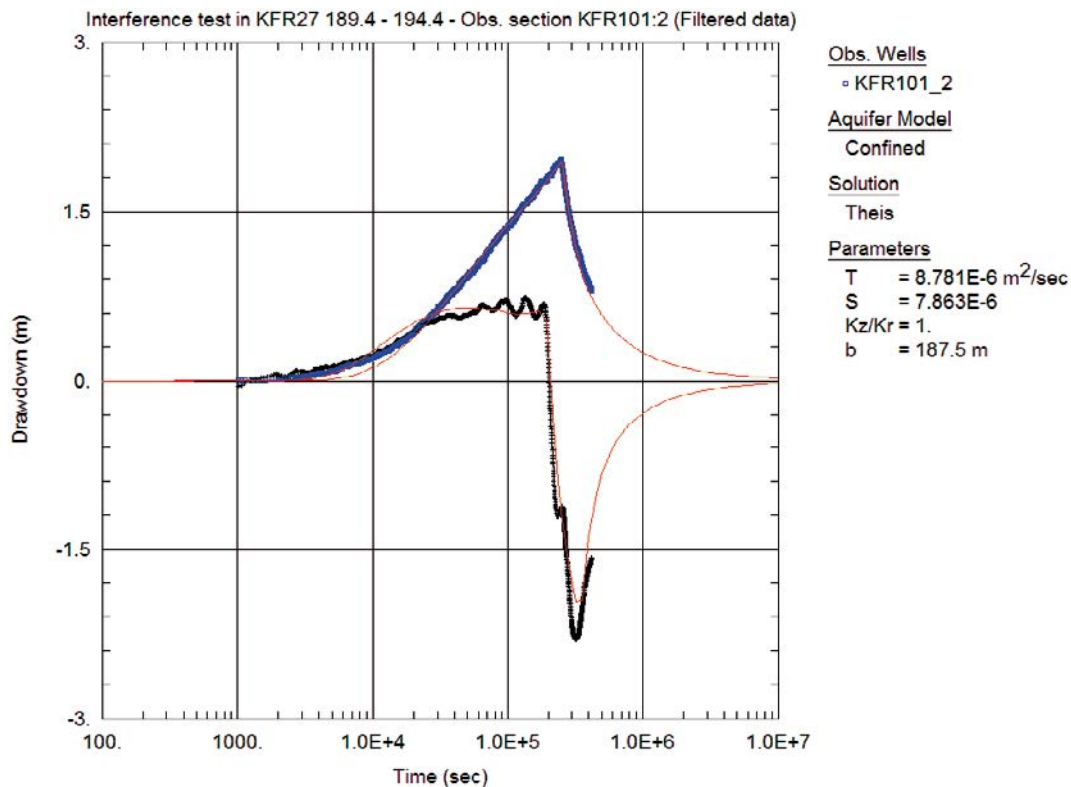


Figure A2-6a. Lin-log plot of drawdown (○) and derivative, $ds/d(\ln t)$ (+), versus time in the observation borehole section KFR101:2 during the interference test in KFR27: 189.40–194.40 m and simulated corresponding curves (solid lines). The evaluation is made on the entire curve.

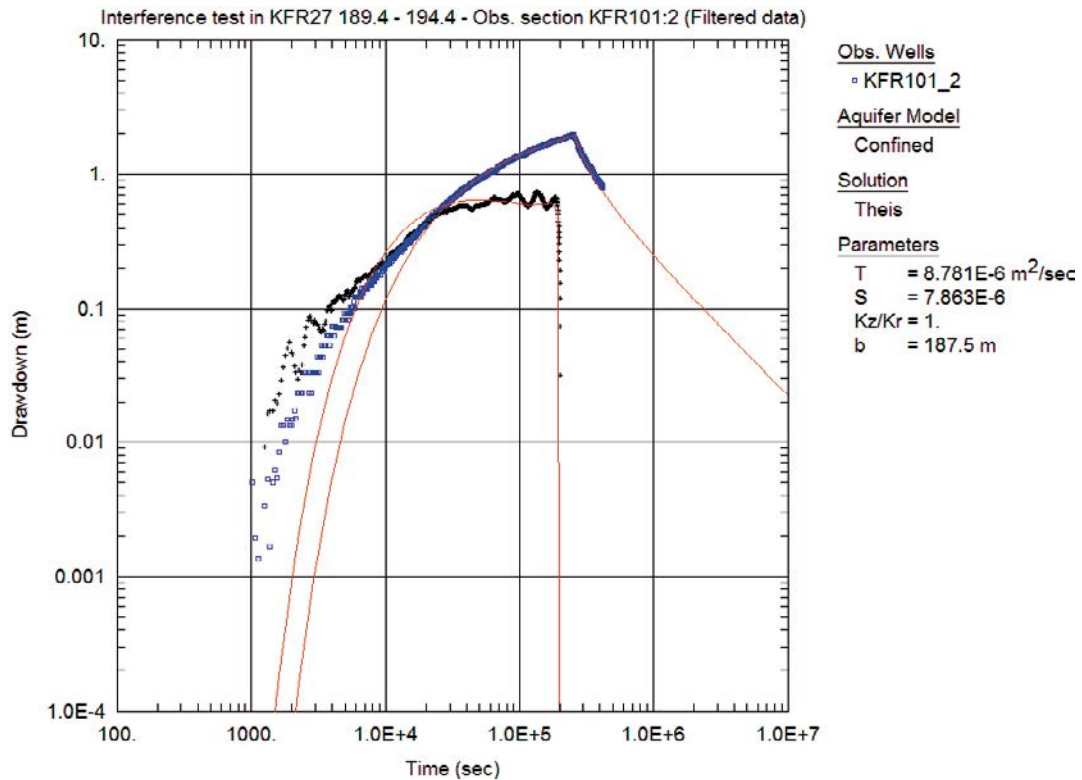


Figure A2-6b. Same as above but log-log plot.

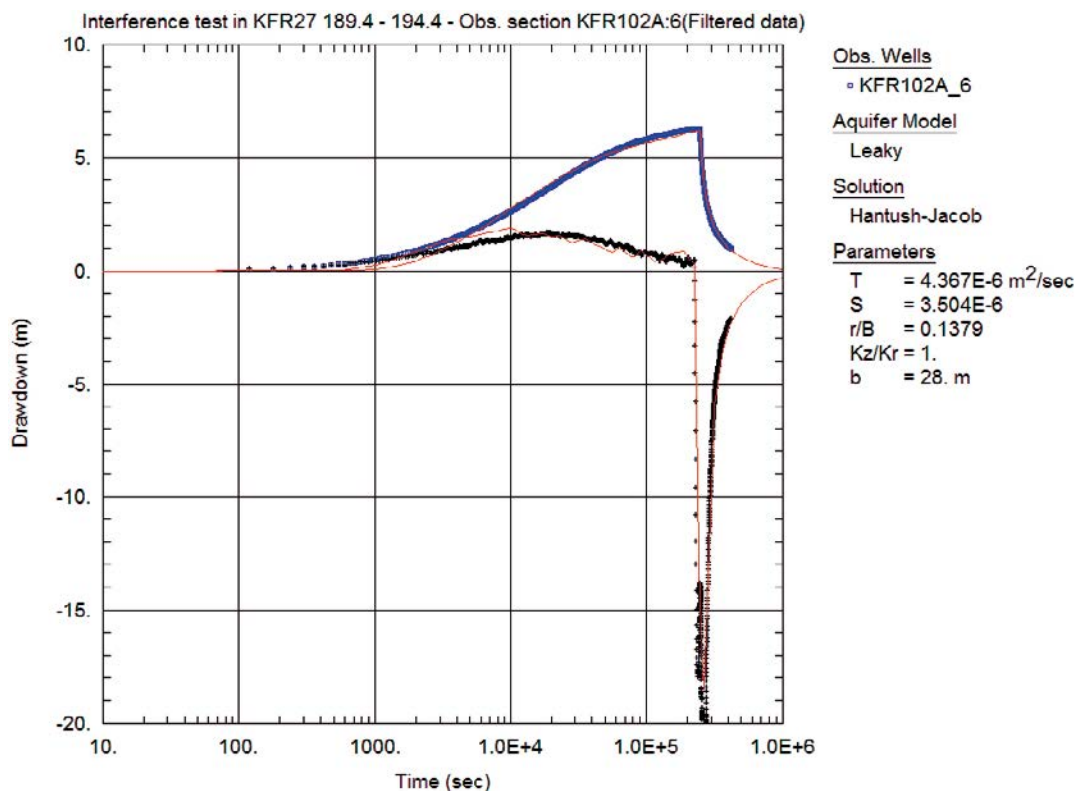


Figure A2-7a. Lin-log plot of drawdown (□) and derivative, $ds/d(\ln t)$ (+), versus time in the observation borehole section KFR102A:6 during the interference test in KFR27: 189.40–194.40 m and simulated corresponding curves (solid lines). The evaluation is made on the entire curve.

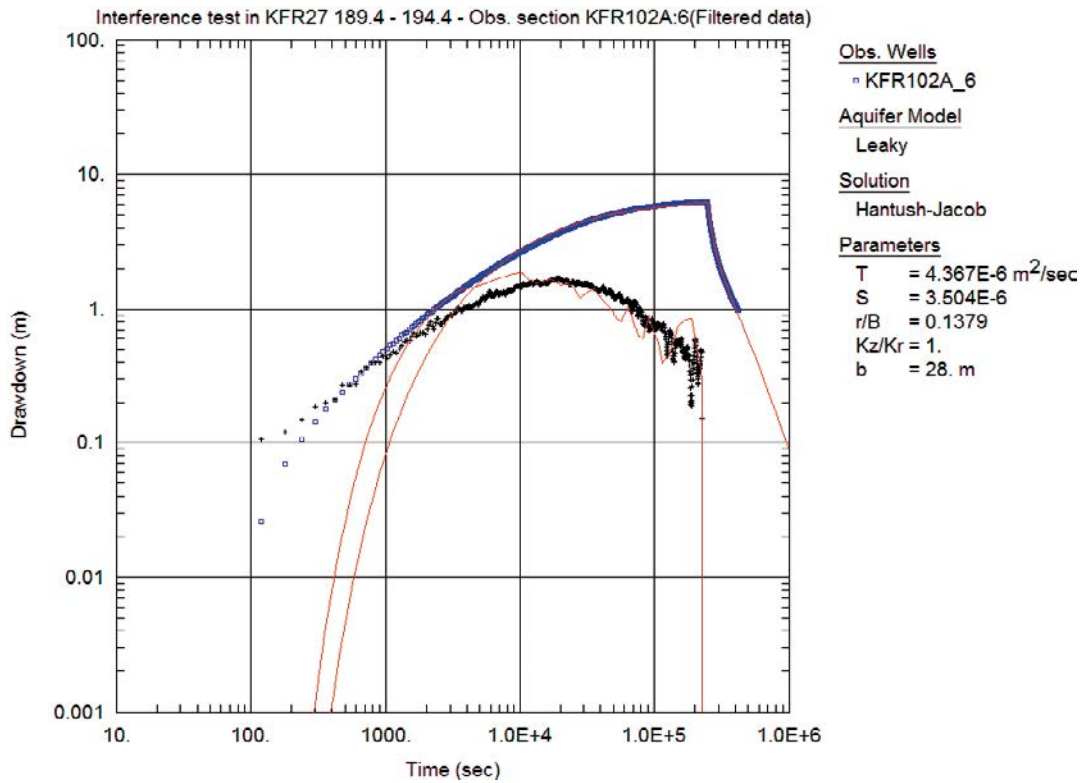


Figure A2-7b. Same as above but log-log plot.

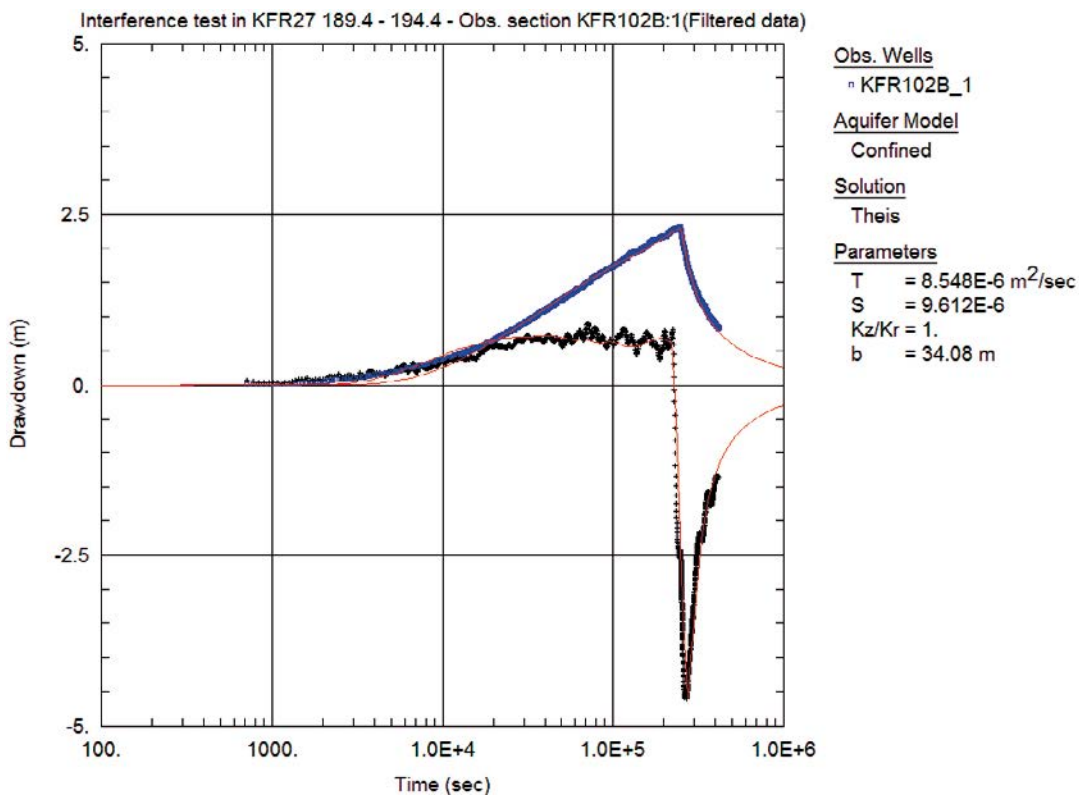


Figure A2-8a. Lin-log plot of drawdown (°) and derivative, $ds/d(\ln t)$ (+), versus time in the observation borehole section KFR102B:1 during the interference test in KFR27: 189.40–194.40 m and simulated corresponding curves (solid lines). The evaluation is made on the entire curve.

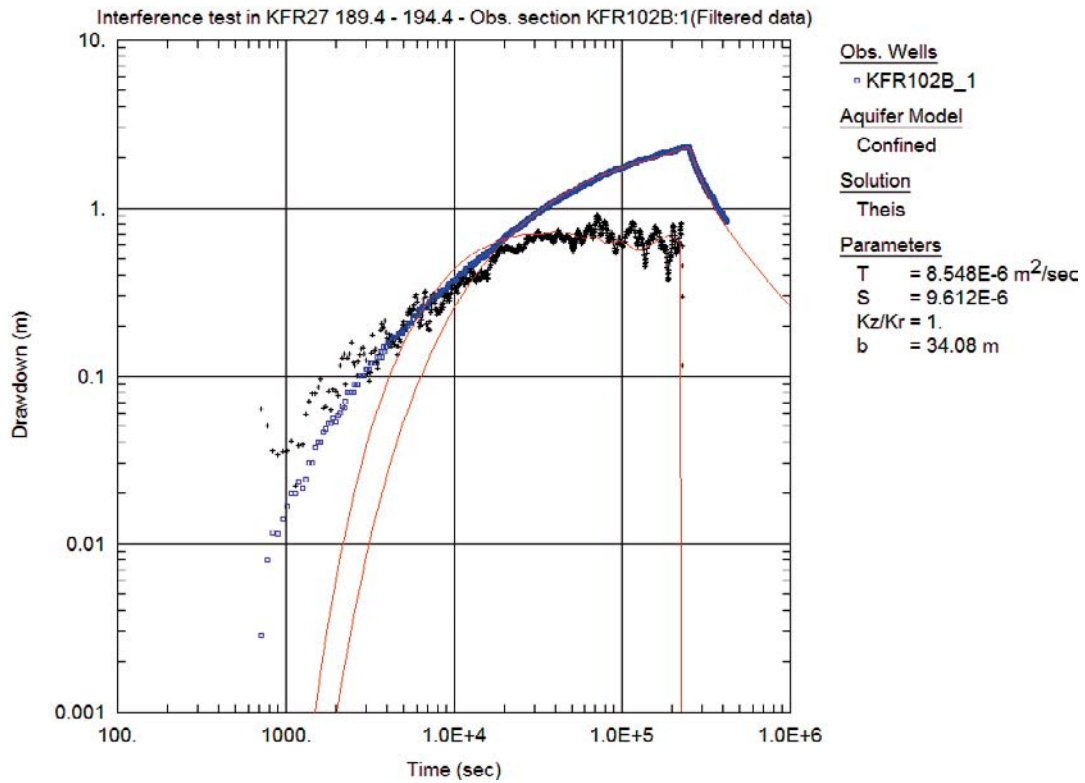


Figure A2-8b. Same as above but log-log plot.

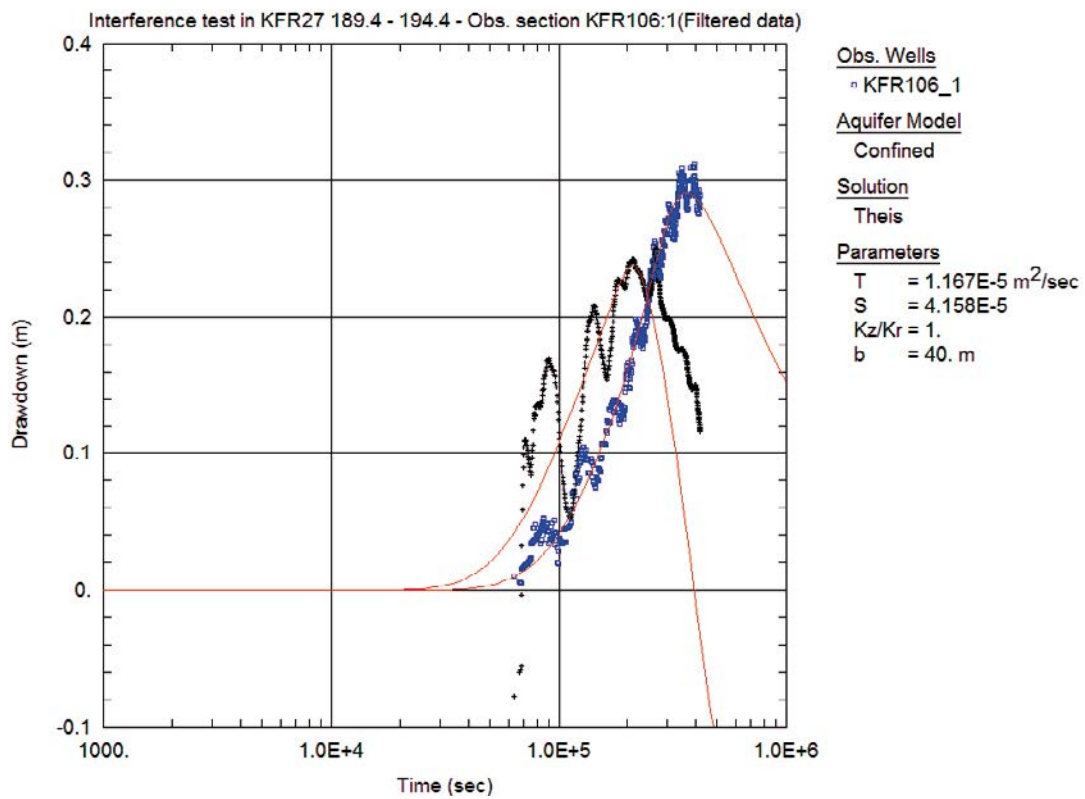


Figure A2-9a. Lin-log plot of drawdown (◻) and derivative, $ds/d(\ln t)$ (+), versus time in the observation borehole section KFR106:1 during the interference test in KFR27: 189.40–194.40 m and simulated corresponding curves (solid lines). The evaluation is made on the entire curve.

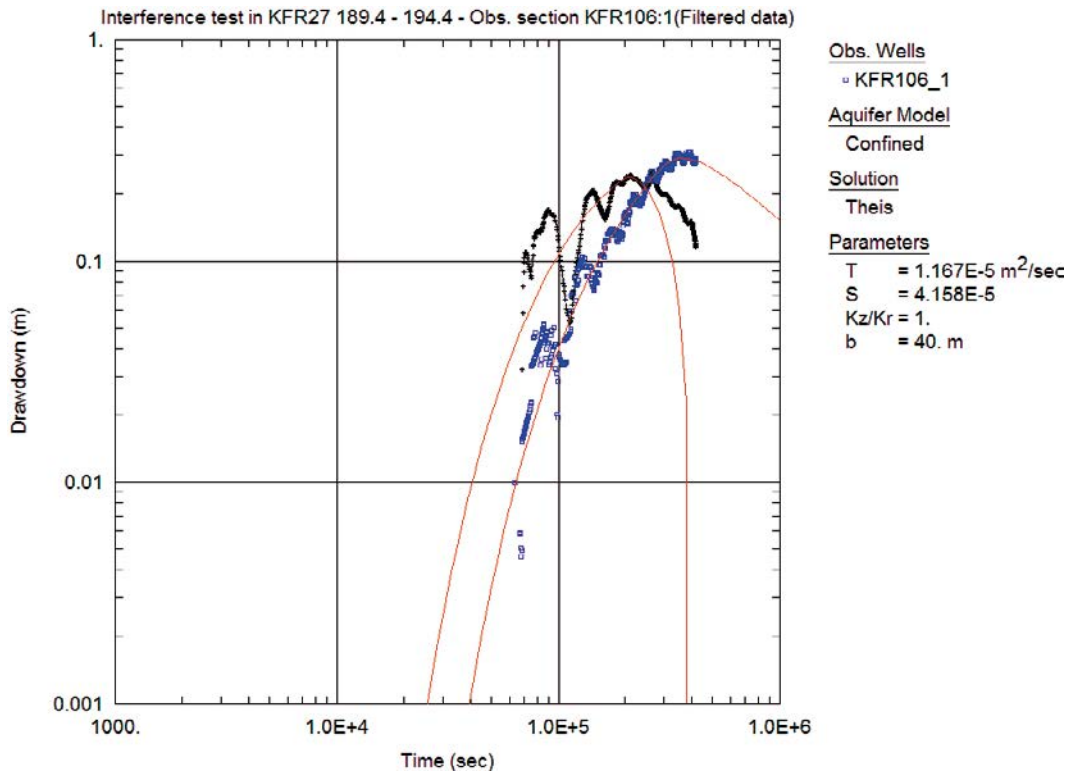


Figure A2-9b. Same as above but log-log plot.

A2.3 Interference test in KFR103: 83.50–93.50m

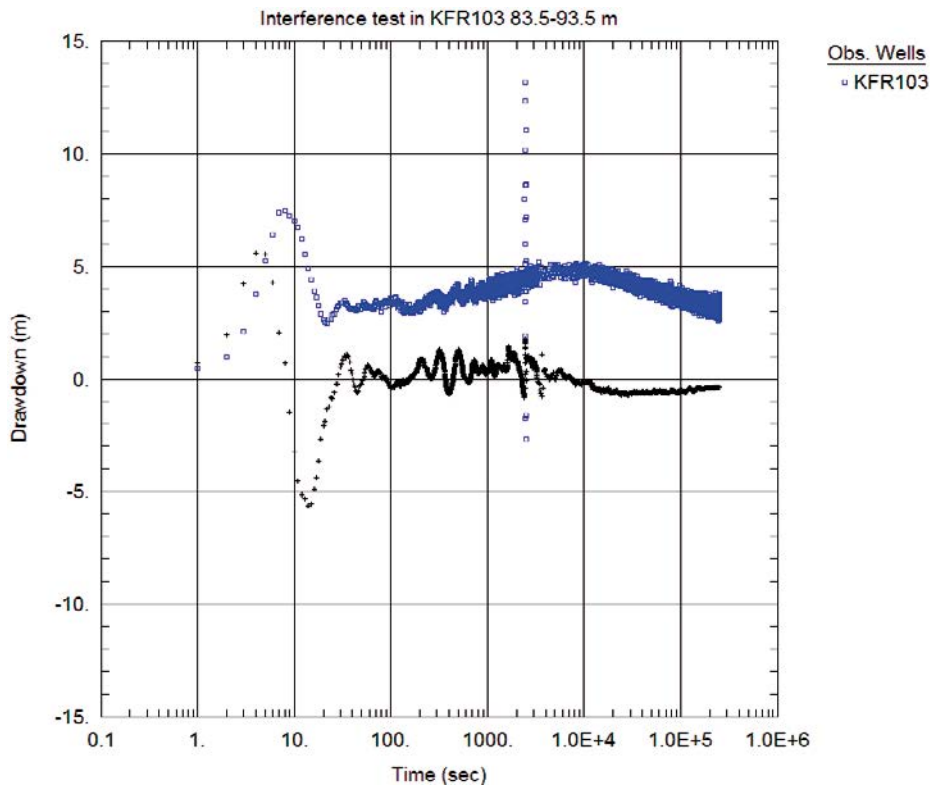


Figure A2-10a. Lin-log plot of drawdown (□) and drawdown derivative, $ds/d(\ln t)$ (+), versus time in the pumping borehole section during the interference test in KFR103: 83.50–93.50 m. No unambiguous evaluation possible.

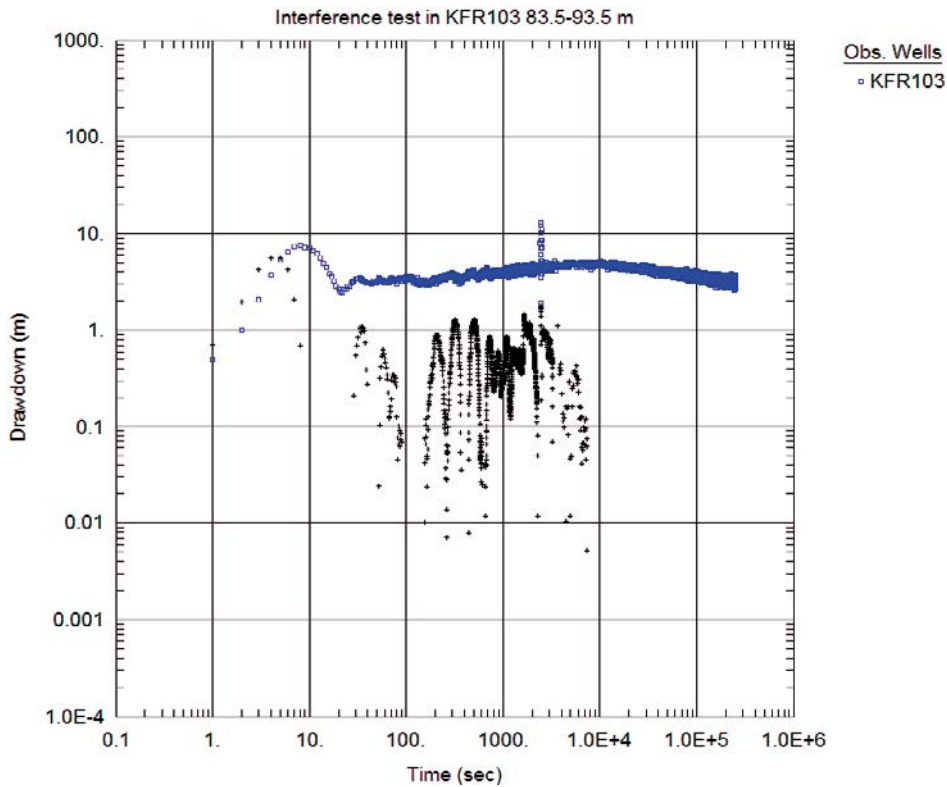


Figure A2-10b. Same as above but log-log plot.

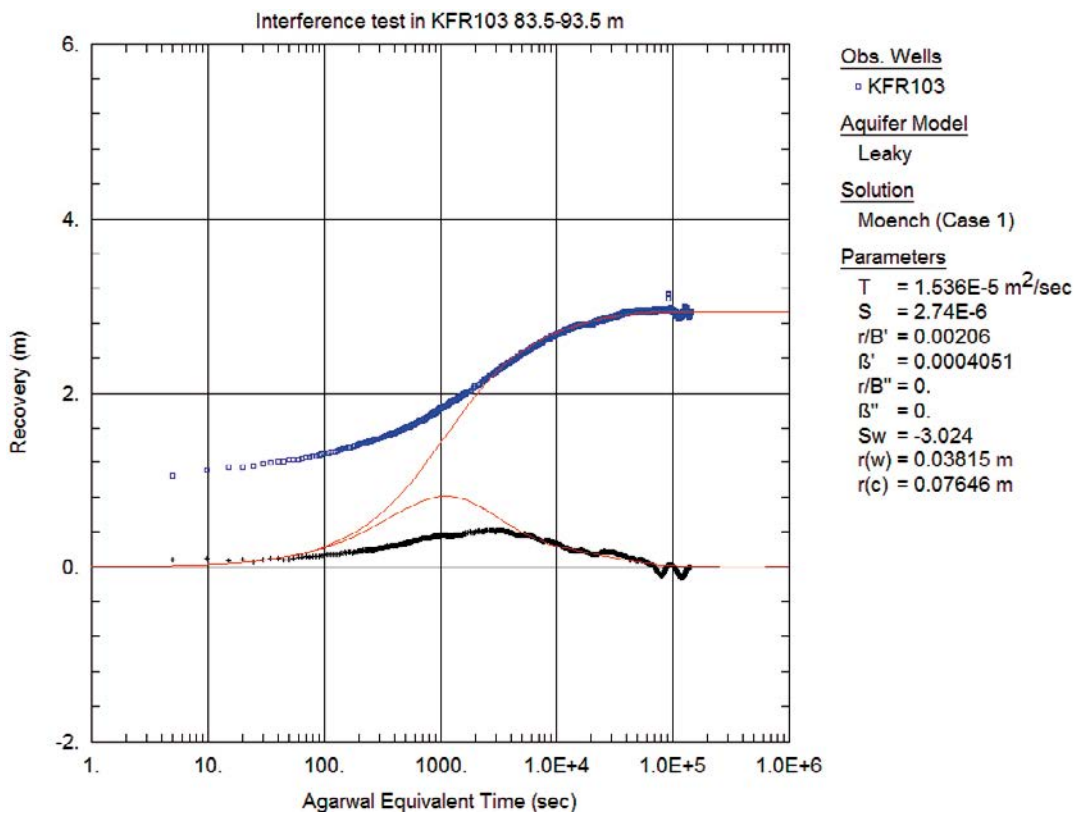


Figure A2-11a. Lin-log plot of recovery (\square) and derivative, $ds/d(\ln t)$ ($+$), versus equivalent time in the pumping borehole section during the interference test in KFR103: 83.50–93.50 m and simulated corresponding curves (solid lines). The evaluation is made on the last part.

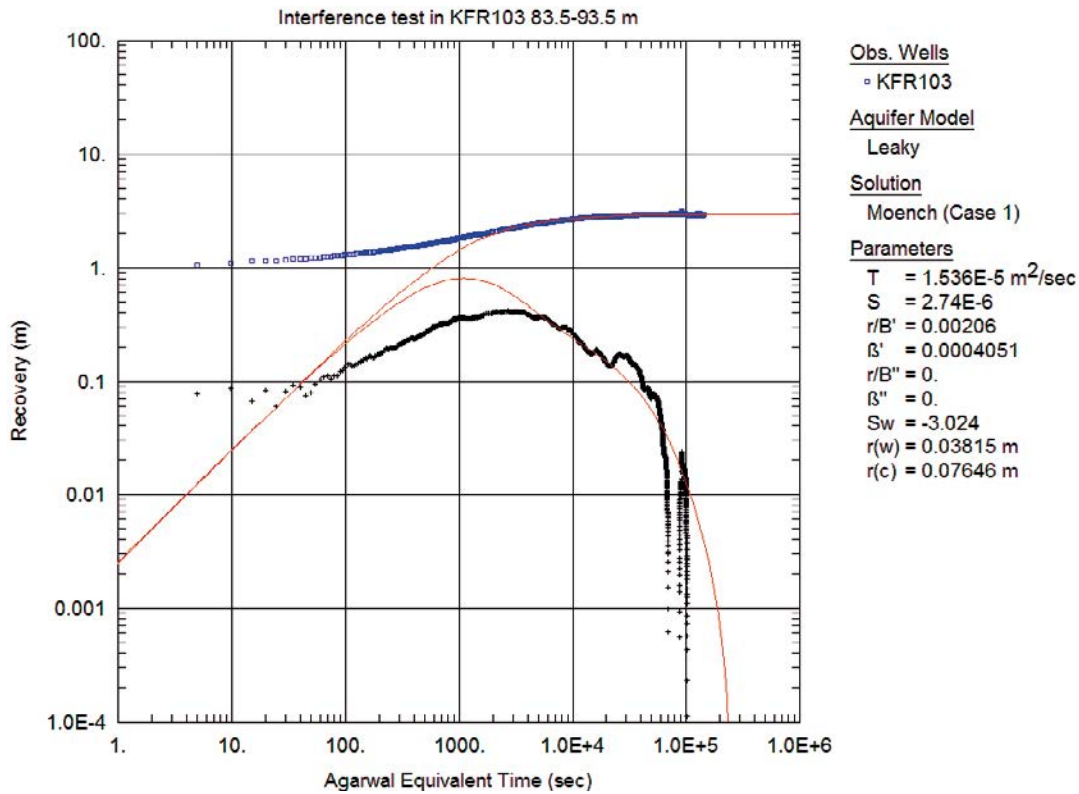


Figure A2-11b. Same as above but log-log plot.

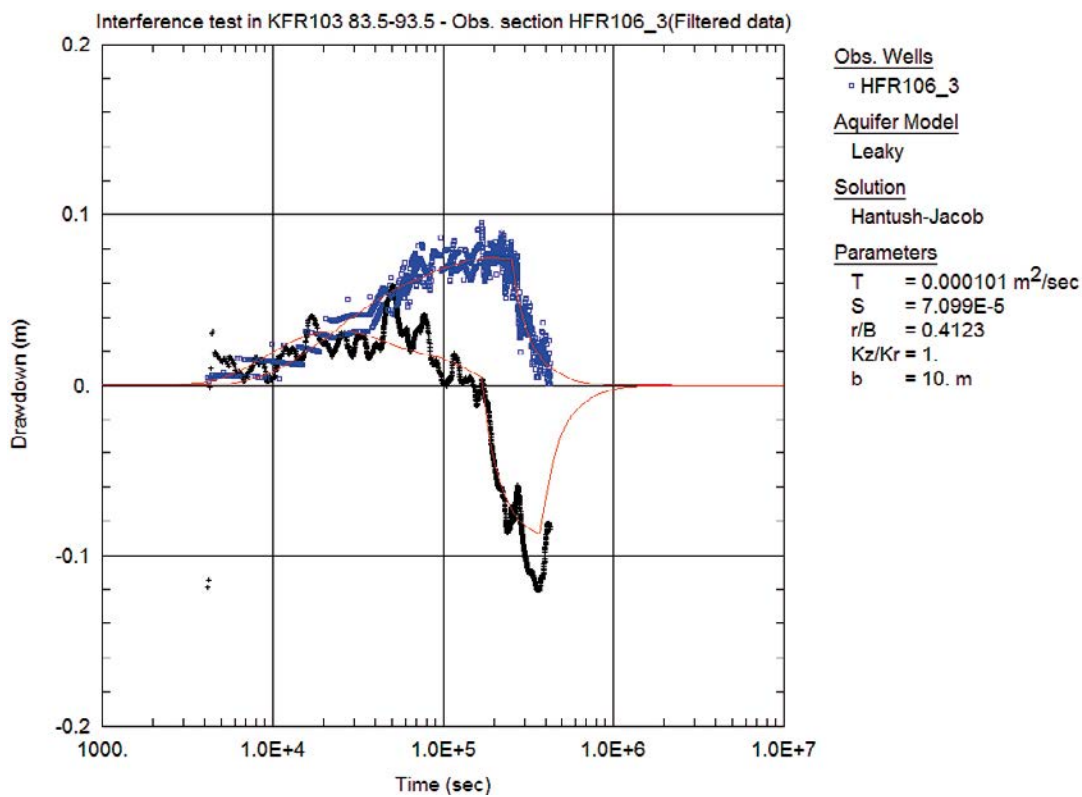


Figure A2-12a. Lin-log plot of drawdown (◻) and derivative, $ds/d(\ln t)$ (+), versus time in the observation borehole section HFR106:3 during the interference test in KFR103: 83.50–93.50 m and simulated corresponding curves (solid lines). The evaluation is made on the entire curve.

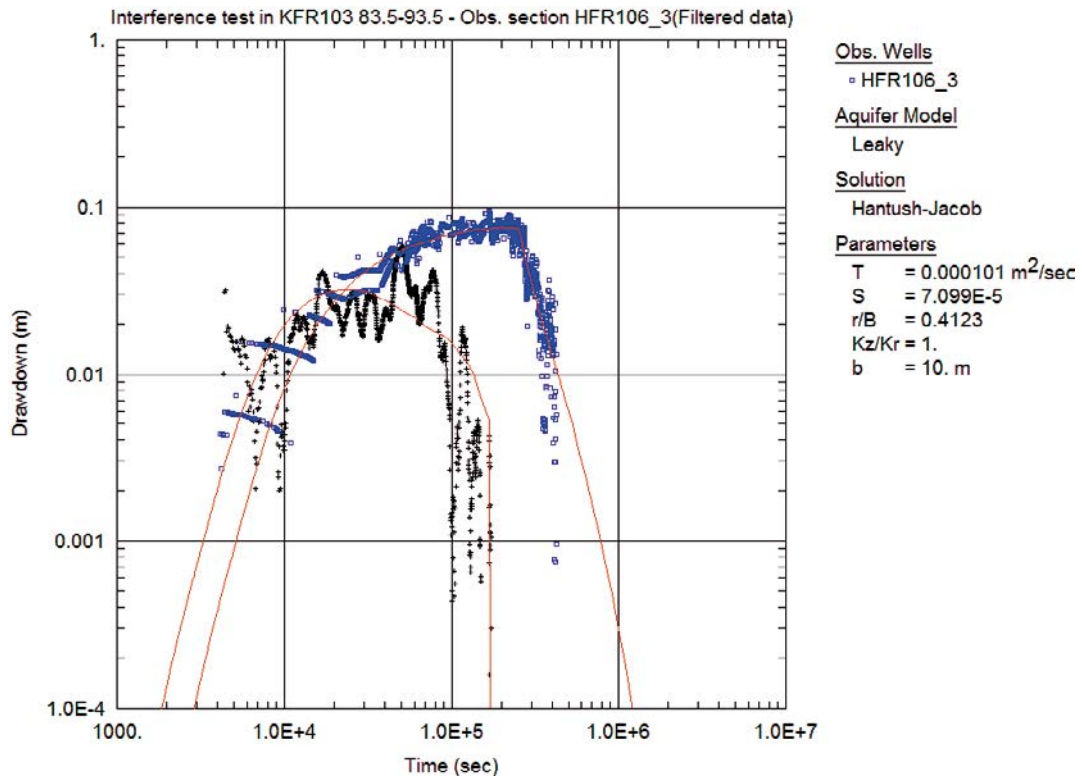


Figure A2-12b. Same as above but log-log plot

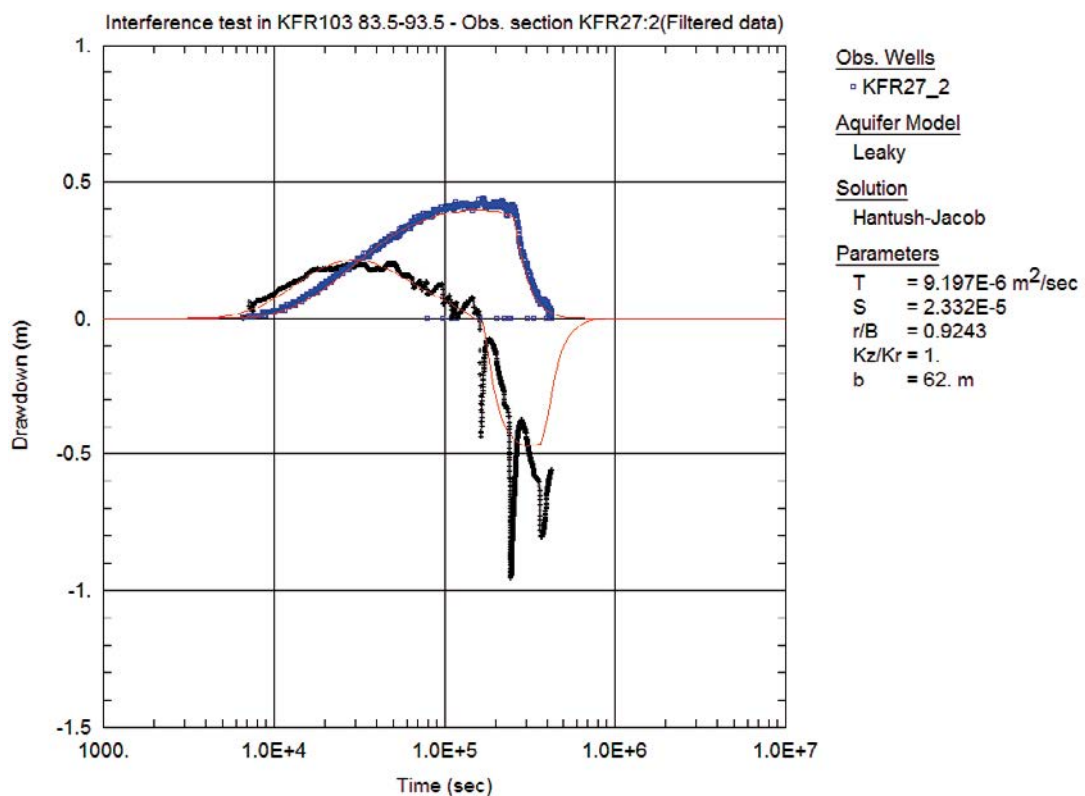


Figure A2-13a. Lin-log plot of drawdown (◻) and derivative, $ds/d(\ln t)$ (+), versus time in the observation borehole section KFR27:2 during the interference test in KFR103: 83.50–93.50 m and simulated corresponding curves (solid lines). The evaluation is made on the entire curve.

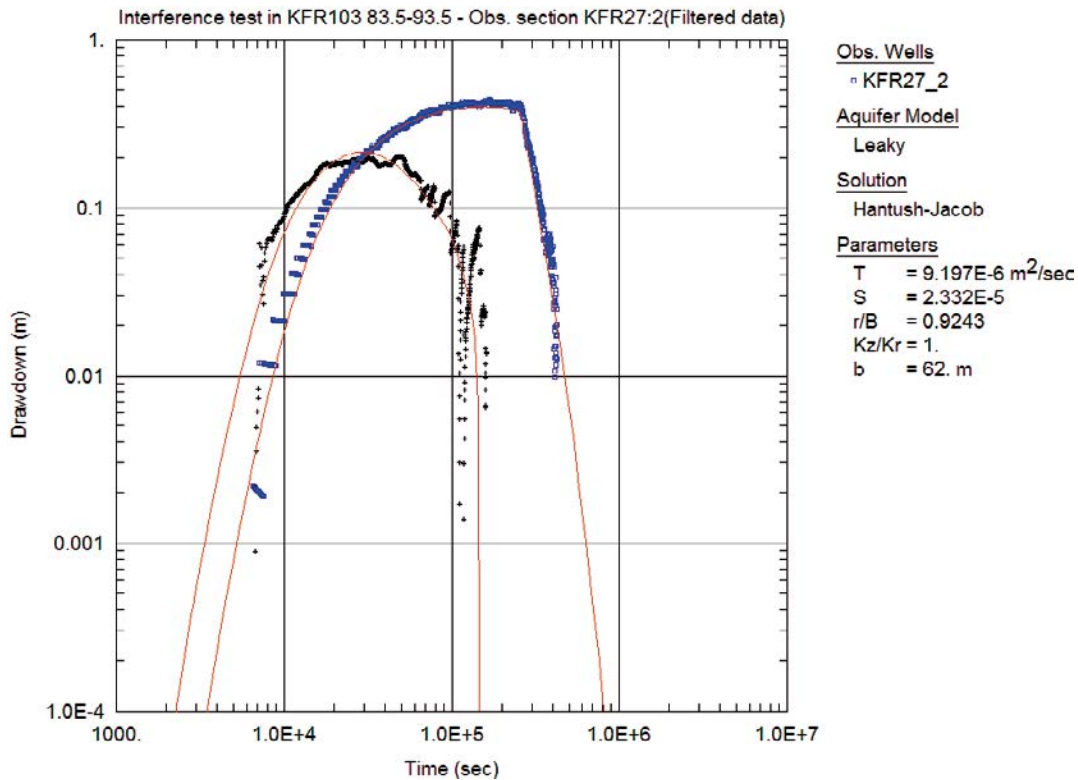


Figure A2-13b. Same as above but log-log plot.

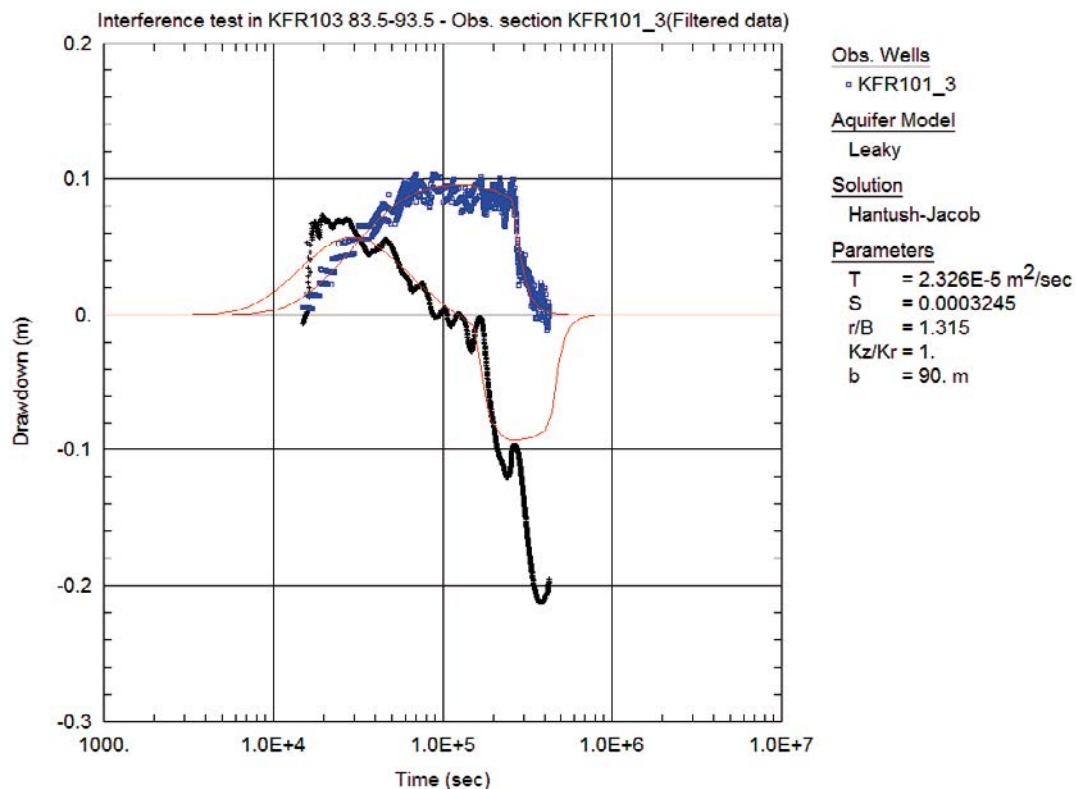


Figure A2-14a. Lin-log plot of drawdown (◻) and derivative, $ds/d(\ln t)$ (+), versus time in the observation borehole section KFR101:3 during the interference test in KFR103: 83.50–93.50 m and simulated corresponding curves (solid lines). The evaluation is made on the entire curve.

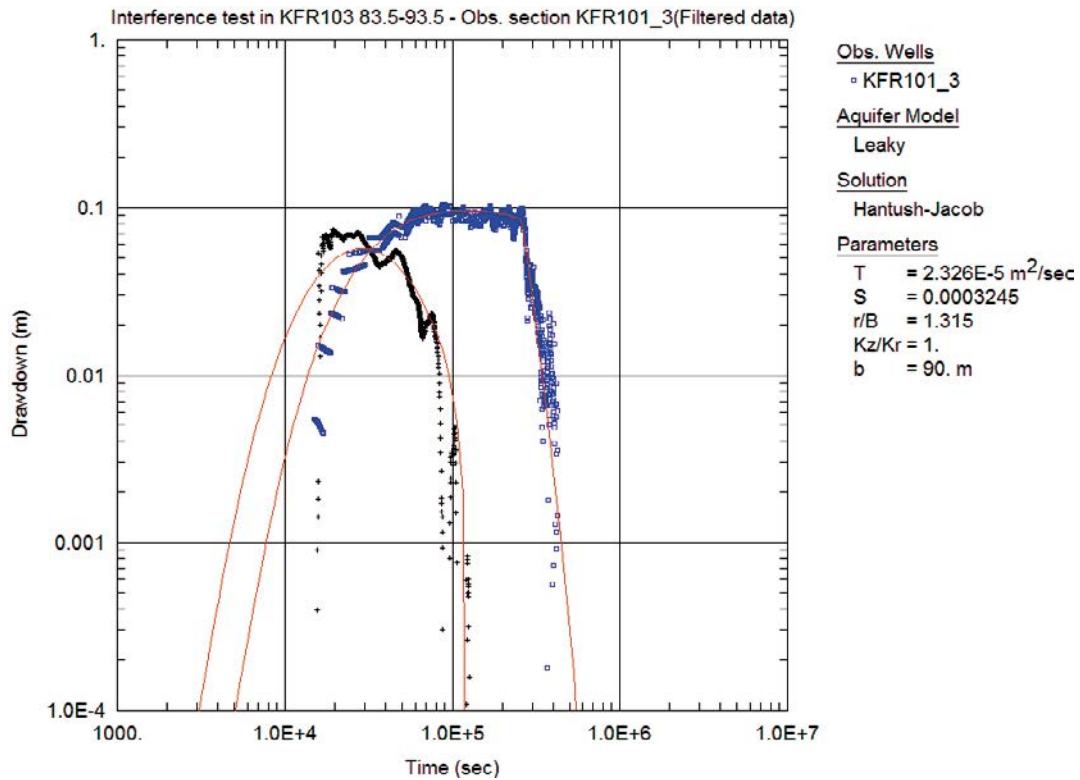


Figure A2-14b. Same as above but log-log plot.

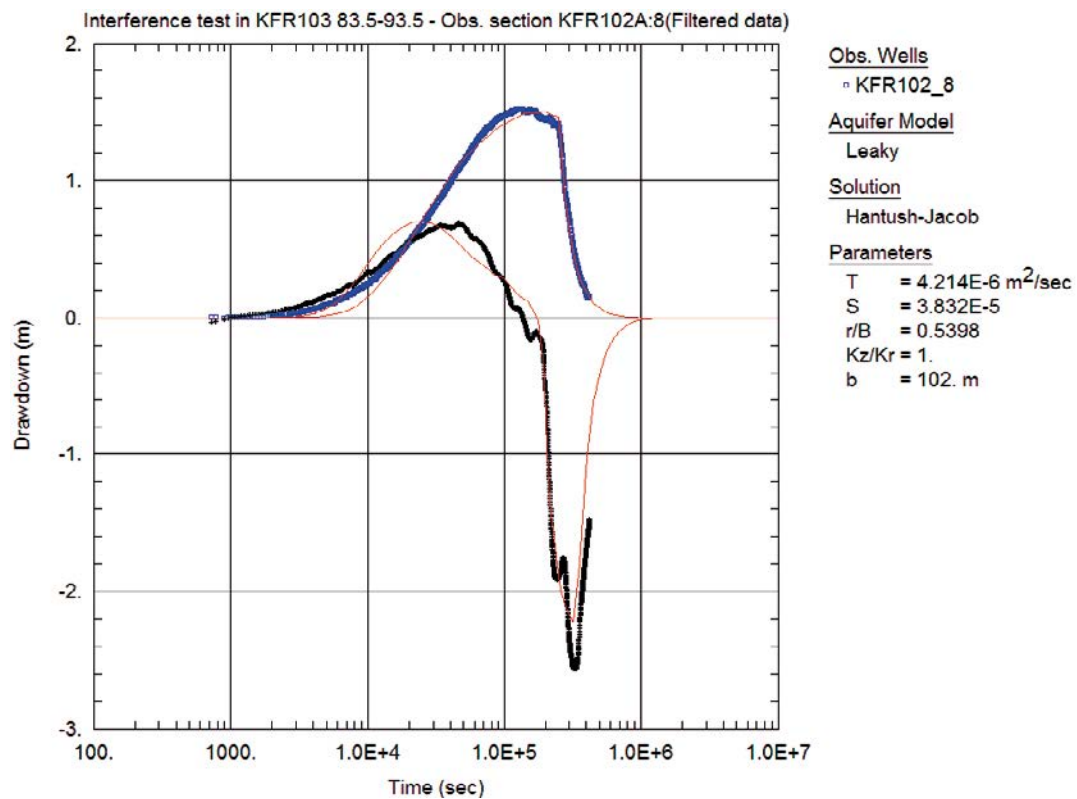


Figure A2-15a. Lin-log plot of drawdown (◻) and derivative, $ds/d(\ln t)$ (+), versus time in the observation borehole section KFR102A:8 during the interference test in KFR103: 83.50–93.50 m and simulated corresponding curves (solid lines). The evaluation is made on the first part.

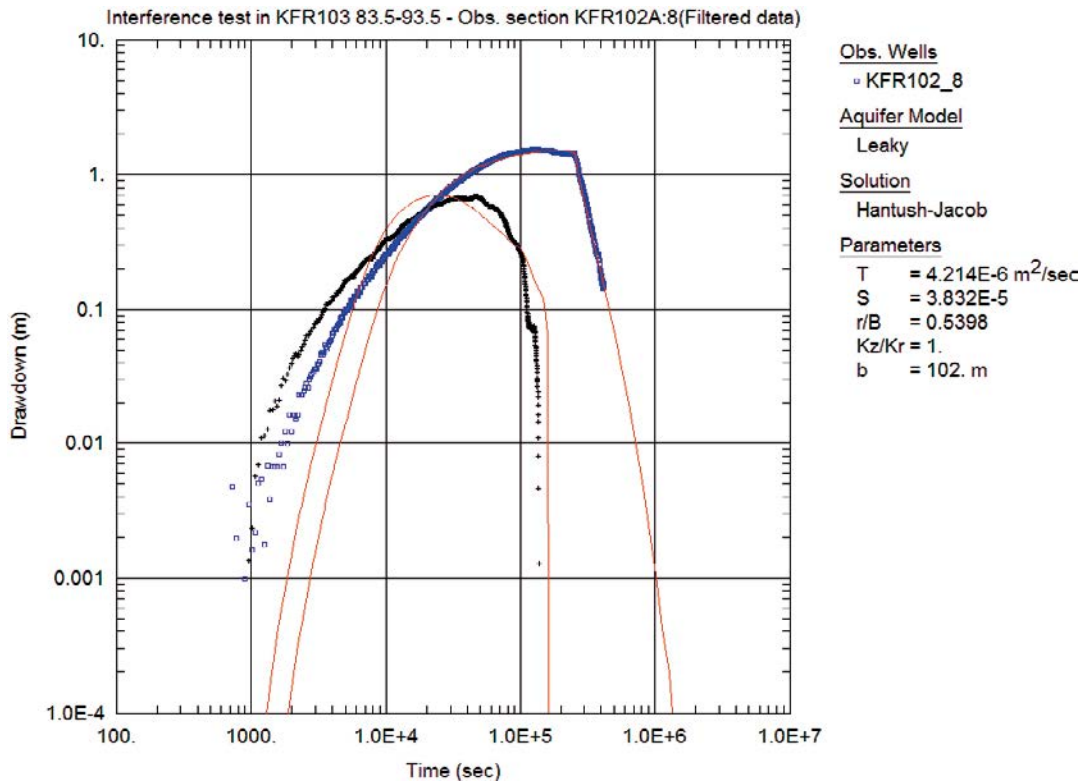


Figure A2-15b. Same as above but log-log plot.

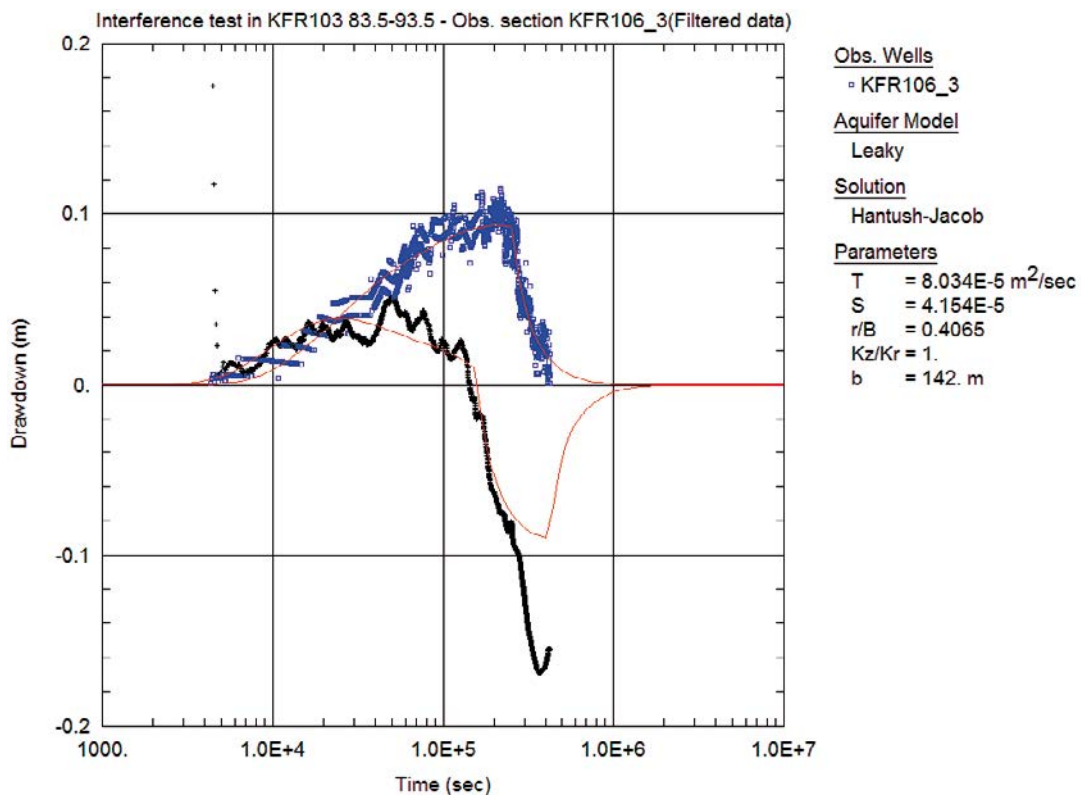


Figure A2-16a. Lin-log plot of drawdown (□) and derivative, $ds/d(\ln t)$ (+), versus time in the observation borehole section KFR106:3 during the interference test in KFR103: 83.50–93.50 m and simulated corresponding curves (solid lines). The evaluation is made on the entire curve.

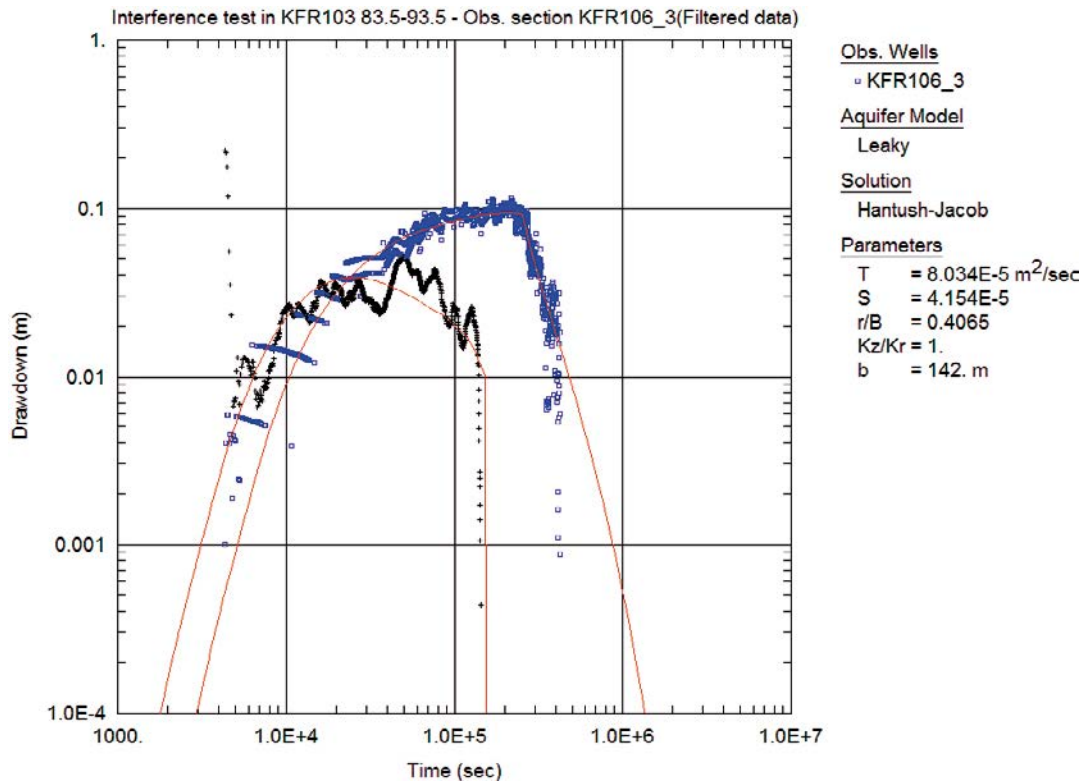


Figure A2-16b. Same as above but log-log plot.

A2.4 Interference test in KFR103: 177.00–187.00 m

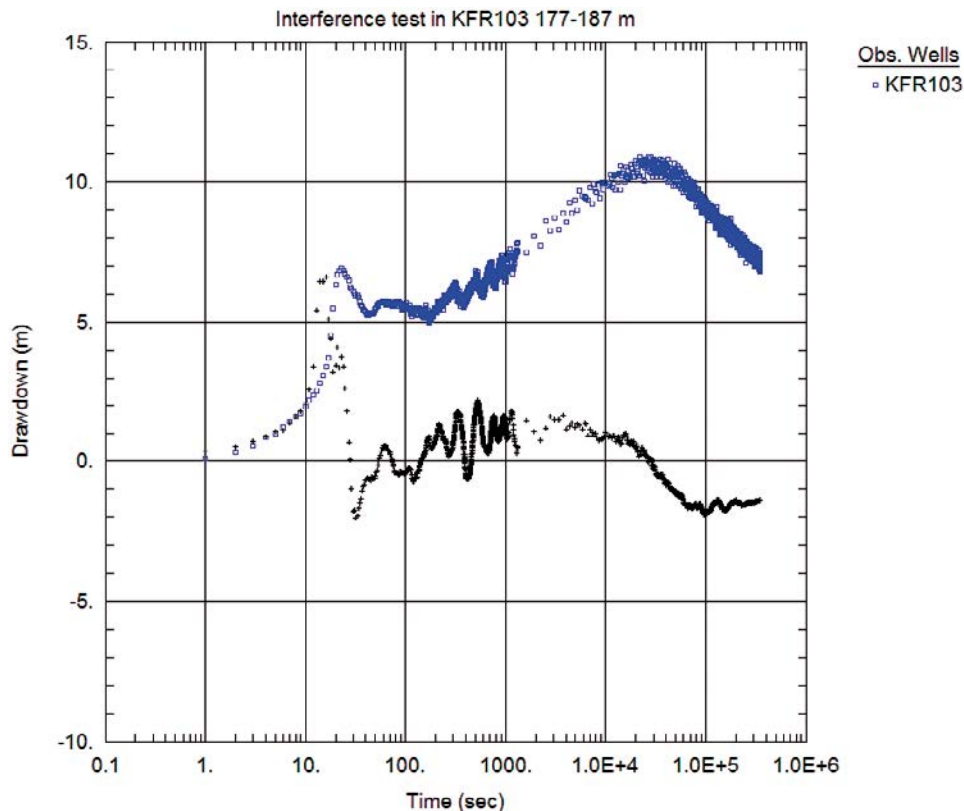


Figure A2-17a. Lin-log plot of drawdown (◻) and drawdown derivative, $ds/d(\ln t)$ (+), versus time in the pumping borehole section during the interference test in KFR103: 177.00–187.00 m. No unambiguous evaluation possible.

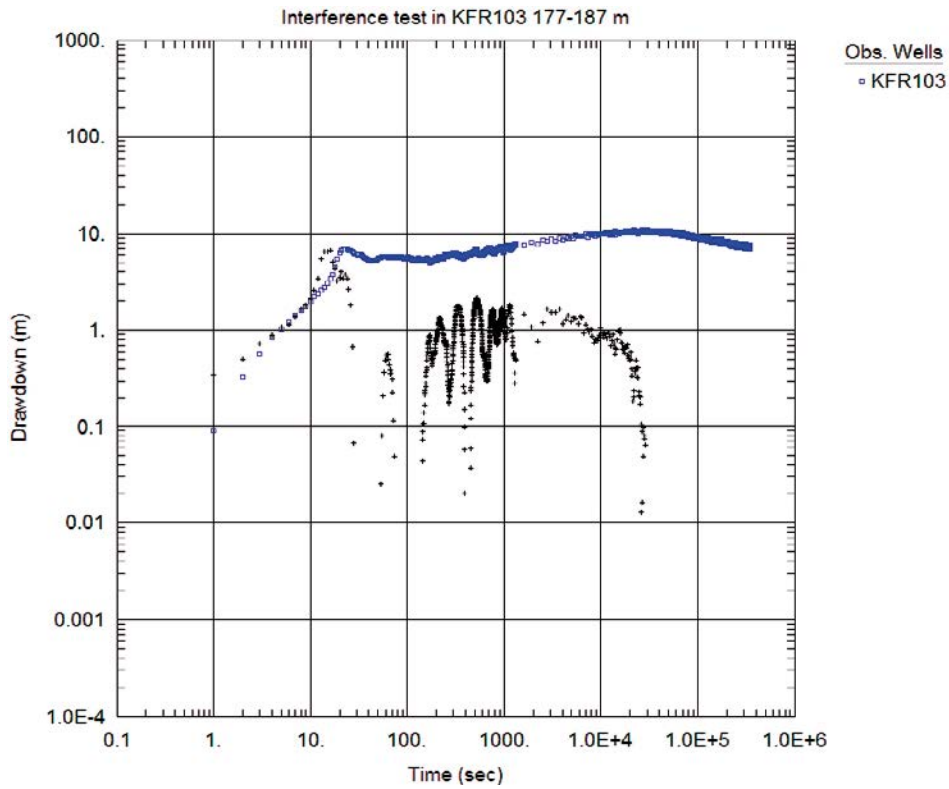


Figure A2-17b. Same as above but log-log plot.

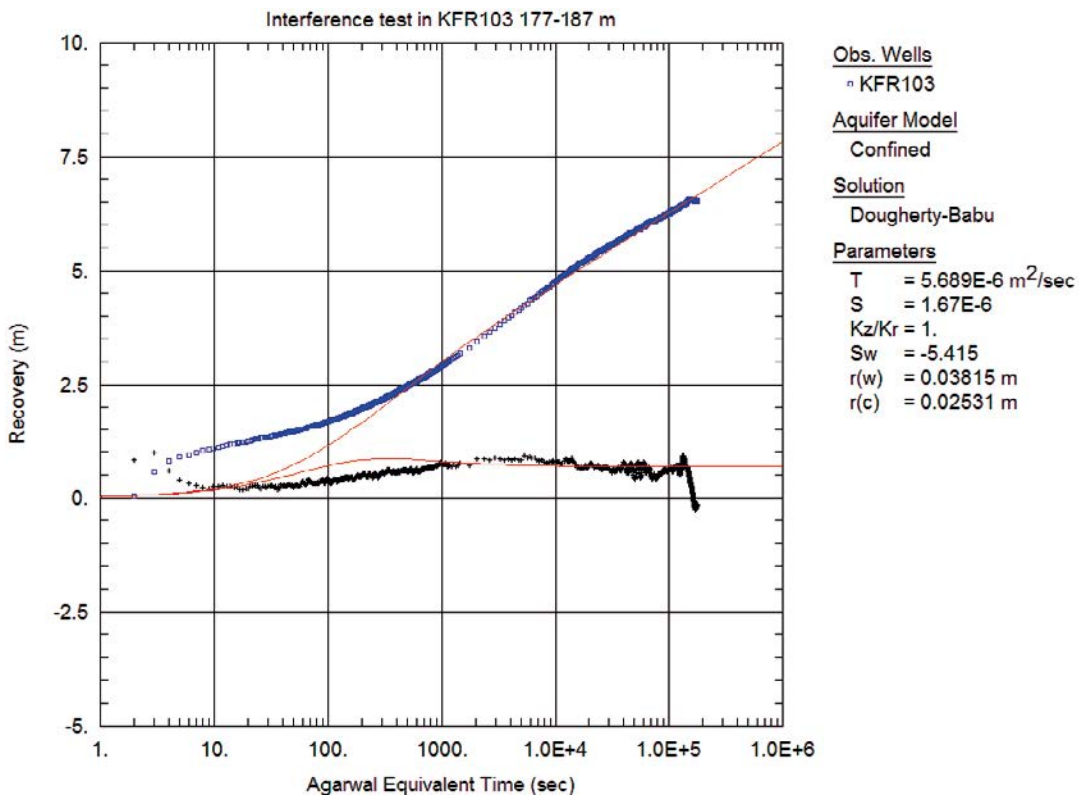


Figure A2-18a. Lin-log plot of recovery (\square) and derivative, $ds/d(\ln t)$ (+), versus equivalent time in the pumping borehole section during the interference test in KFR103: 177.00–187.00 m and simulated corresponding curves (solid lines). The evaluation is made on the last part.

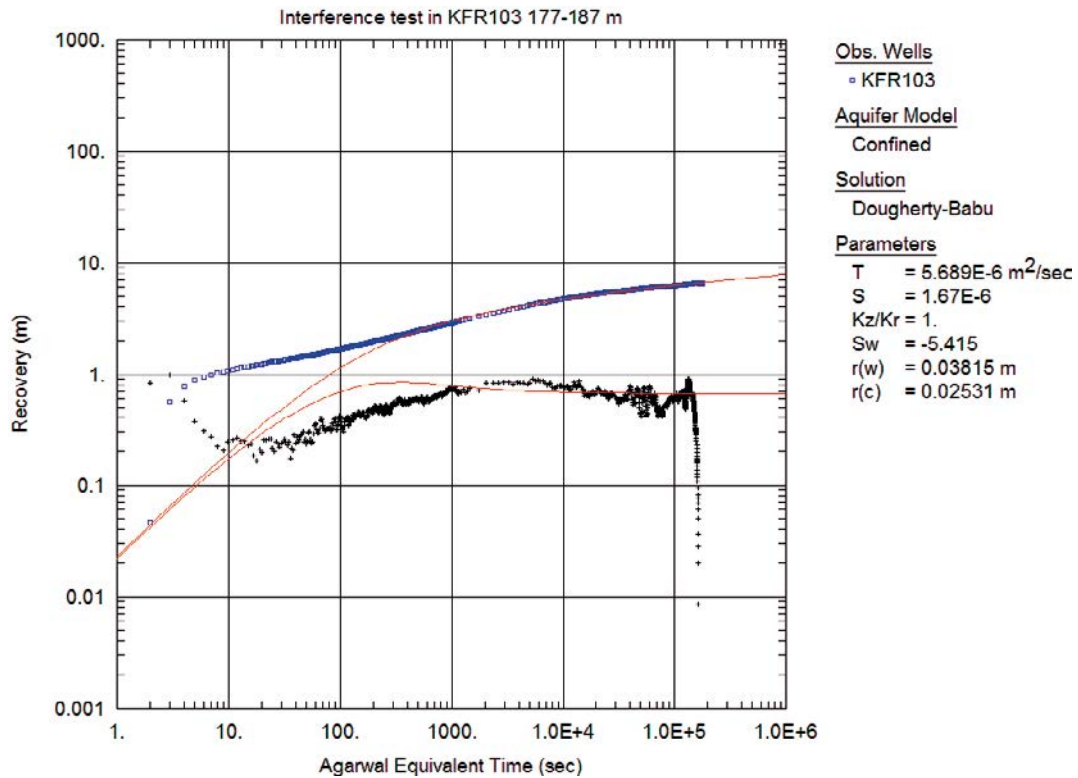


Figure A2-18b. Same as above but log-log plot.

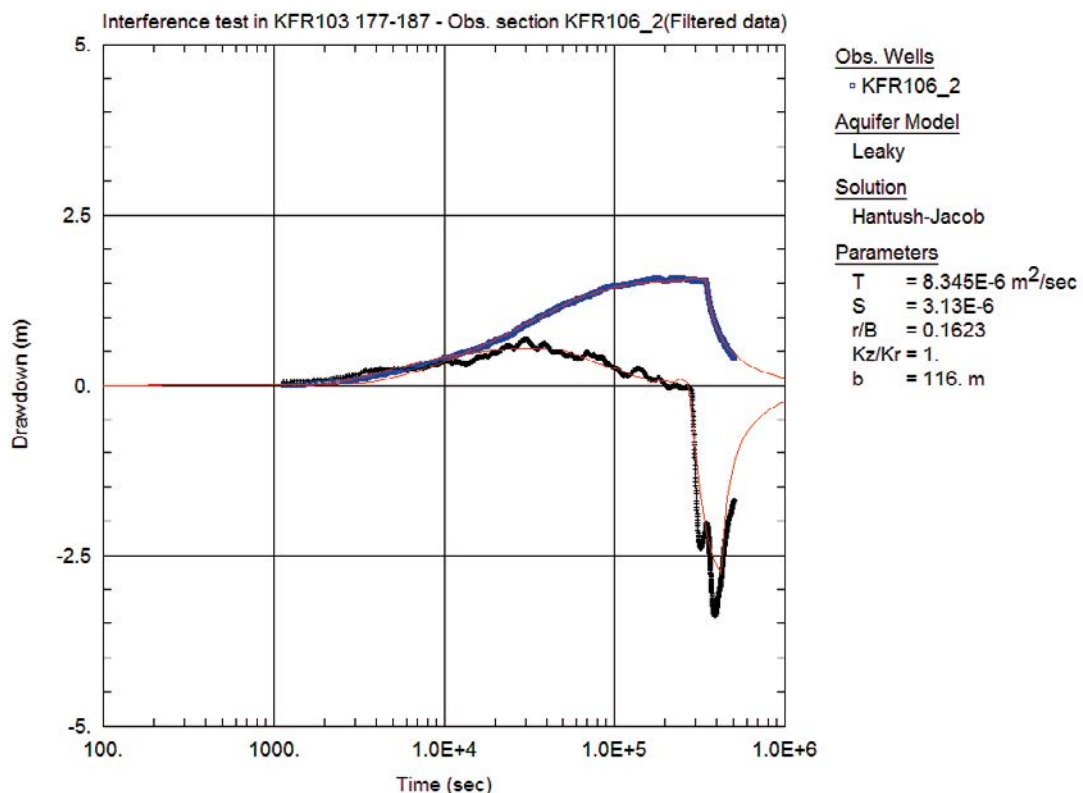


Figure A2-19a. Lin-log plot of drawdown (◻) and derivative, $ds/d(\ln t)$ (+), versus time in the observation borehole section KFR106:2 during the interference test in KFR103: 177.00–187.00 m and simulated corresponding curves (solid lines). The evaluation is made on the entire curve.

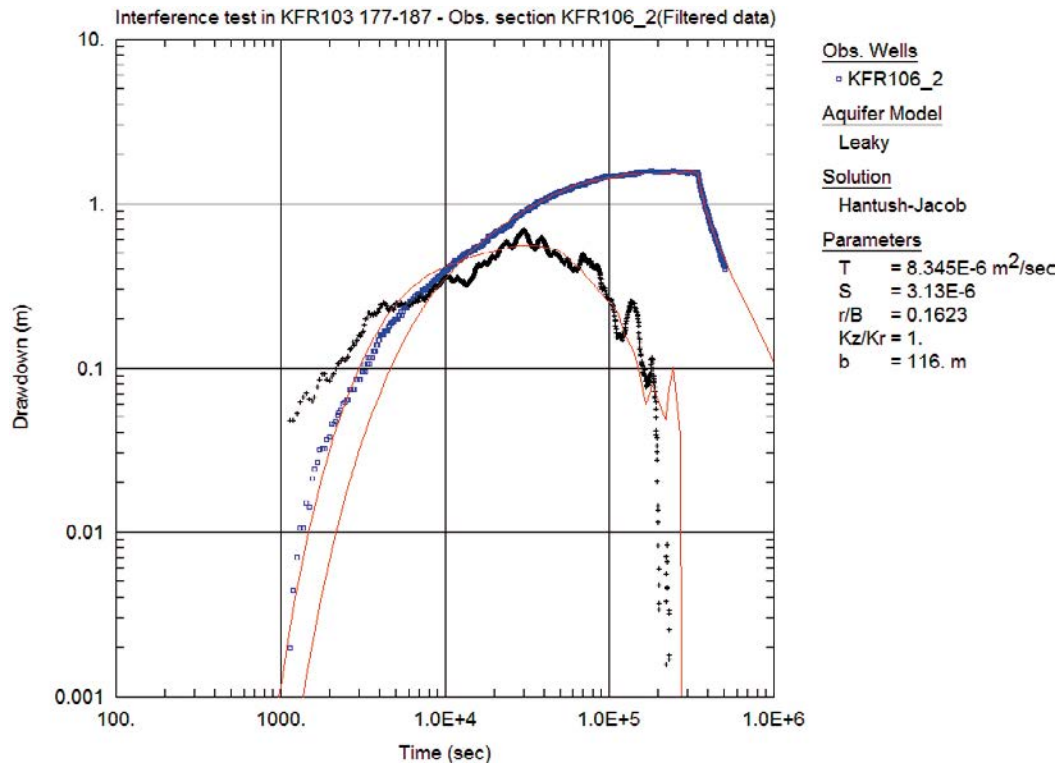


Figure A2-19b. Same as above but log-log plot.

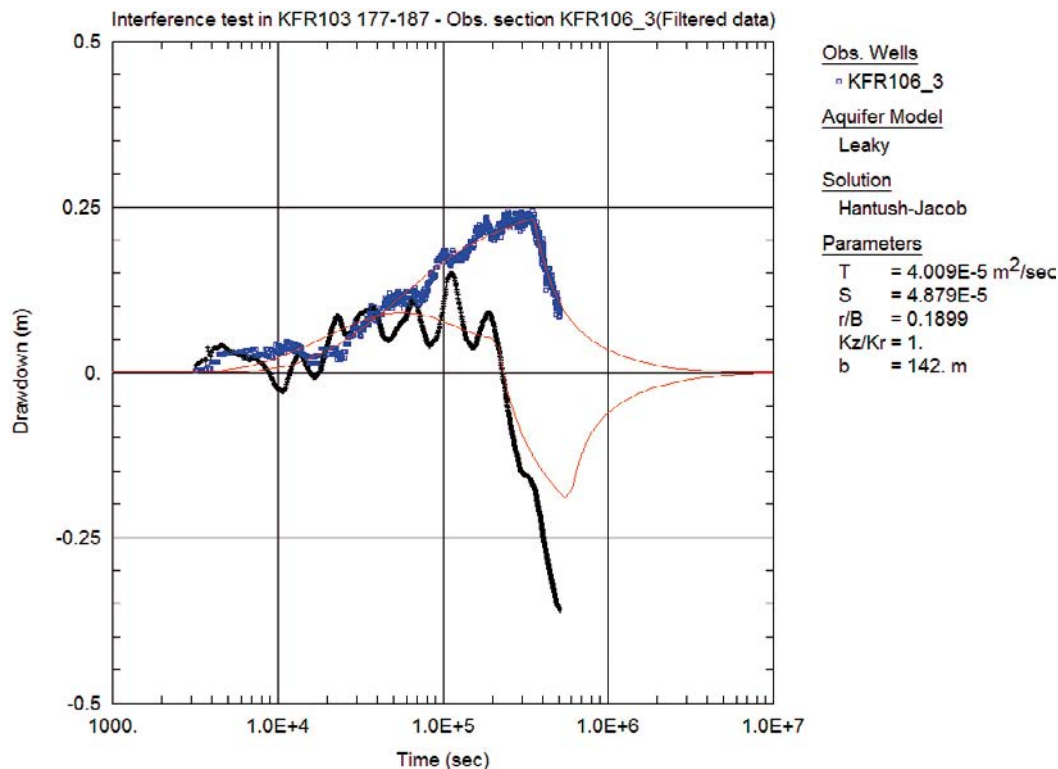


Figure A2-20a. Lin-log plot of drawdown (°) and derivative, $ds/d(\ln t)$ (+), versus time in the observation borehole section KFR106:3 during the interference test in KFR103: 177.00–187.00 m and simulated corresponding curves (solid lines). The evaluation is made on the entire curve.

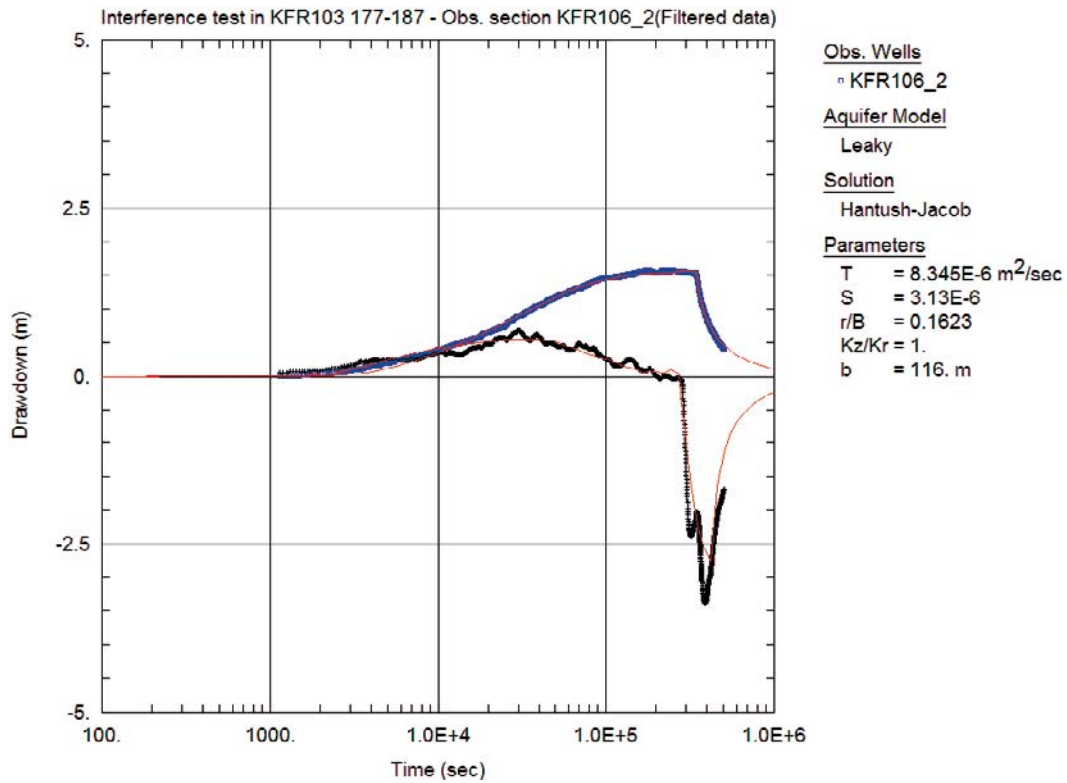


Figure A2-20b. Same as above but log-log plot.

A2.5 Interference test in KR105: 120.00–137.00 m

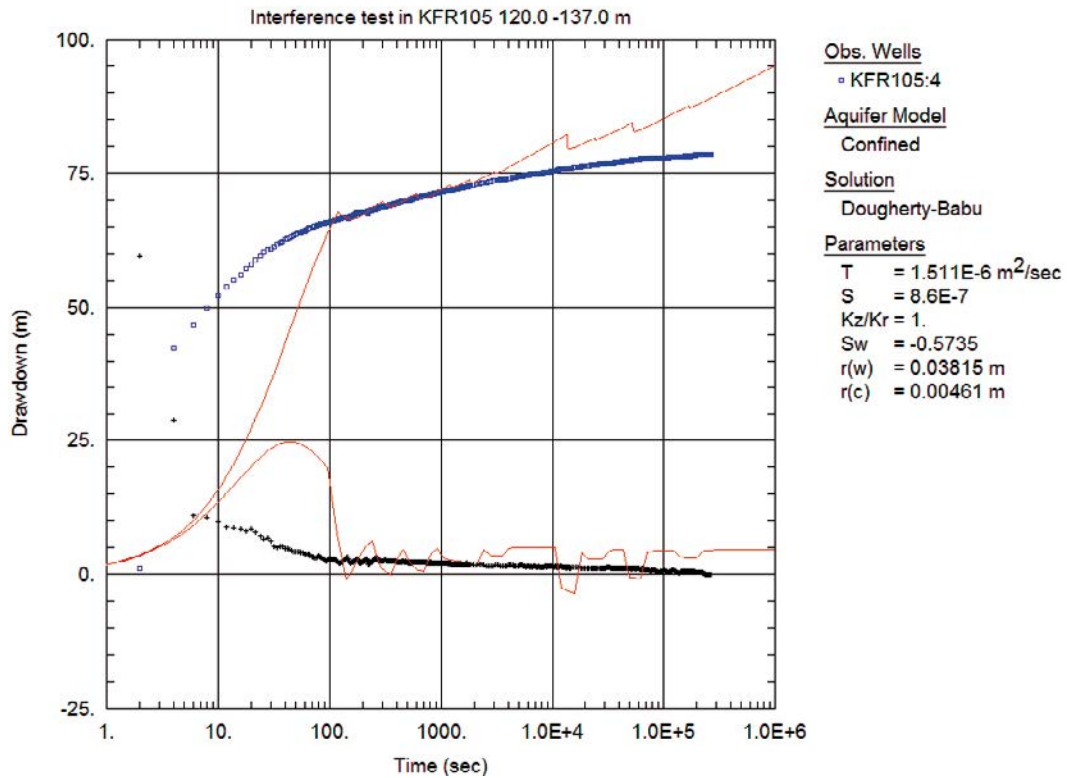


Figure A2-21a. Lin-log plot of drawdown (○) and drawdown derivative, $ds/d(\ln t)$ (+), versus time in the pumping borehole section during the interference test in KFR105: 120.00–137.00 m and simulated corresponding curves (solid lines). The evaluation is made on the first part.

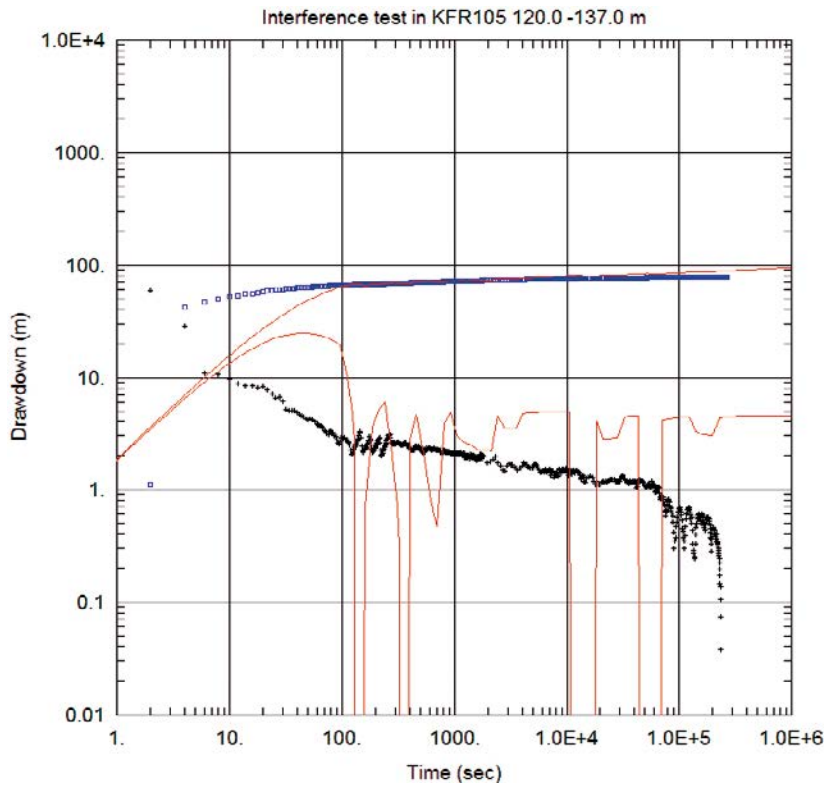


Figure A2-21b. Same as above but log-log plot.

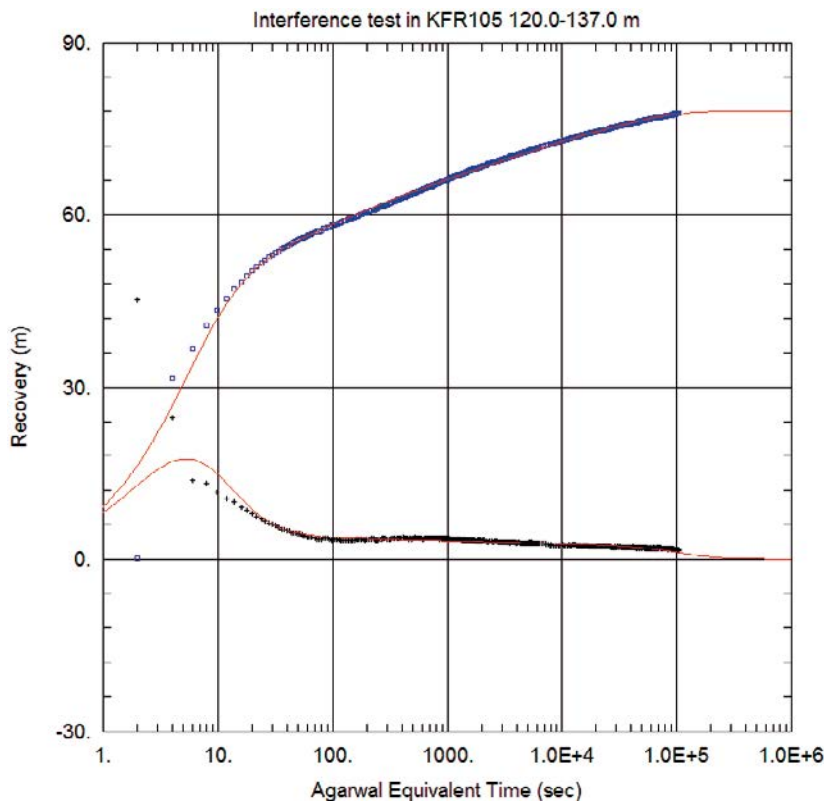


Figure A2-22a. Lin-log plot of recovery (°) and derivative, $ds/d(\ln t)$ (+), versus equivalent time in the pumping borehole section during the interference test in KFR105: 120.00–137.00 m and simulated corresponding curves (solid lines). The evaluation is made on the entire curve.

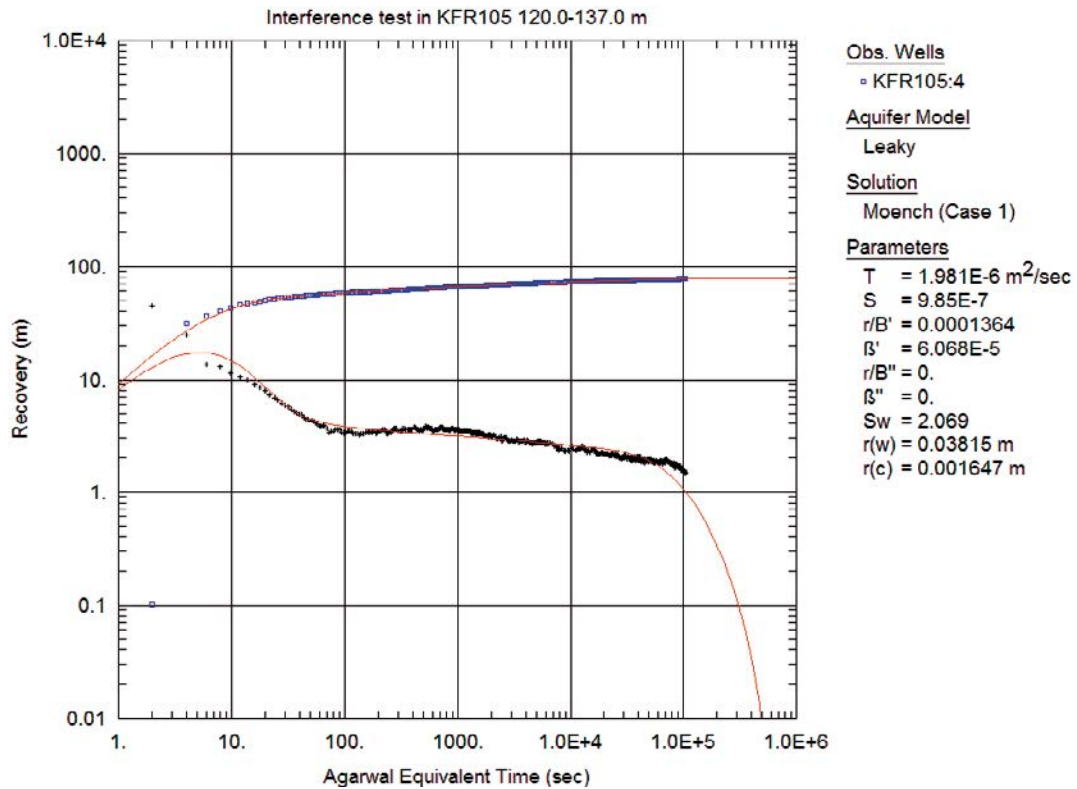


Figure A2-22b. Same as above but log-log plot.

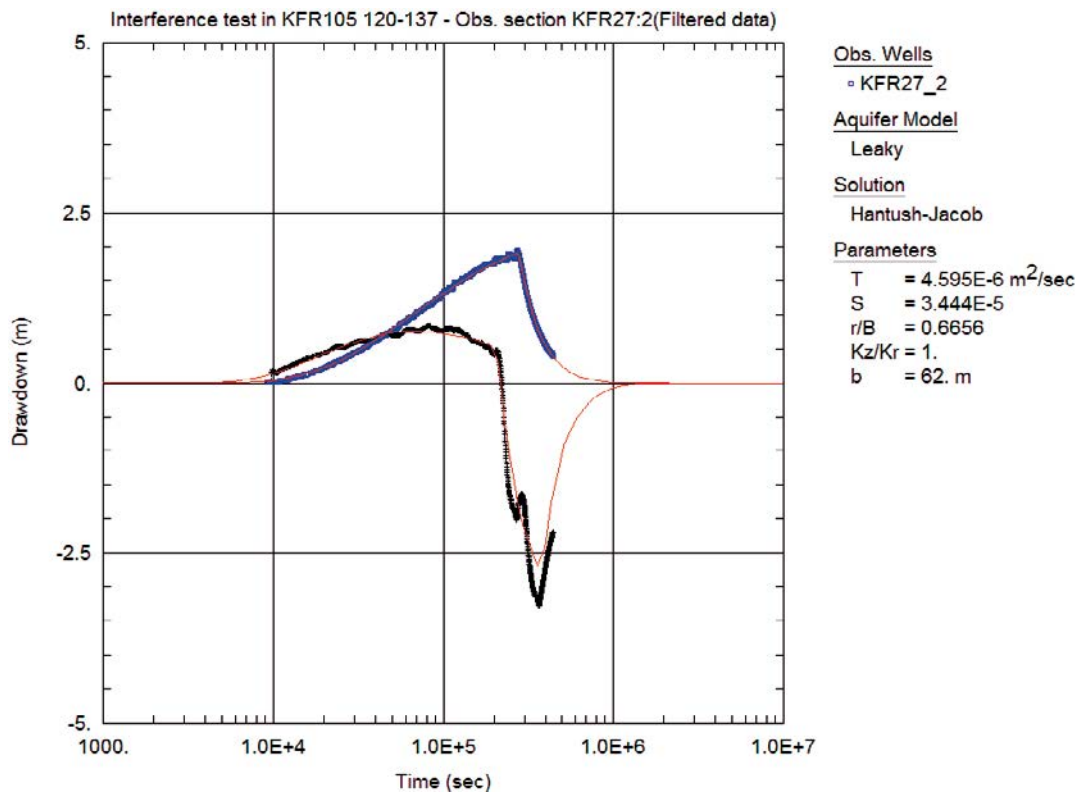


Figure A2-23a. Lin-log plot of drawdown (°) and derivative, $ds/d(\ln t)$ (+), versus time in the observation borehole section KFR27:2 during the interference test in KFR105: 120.00–137.00 m and simulated corresponding curves (solid lines). The evaluation is made on the entire curve.

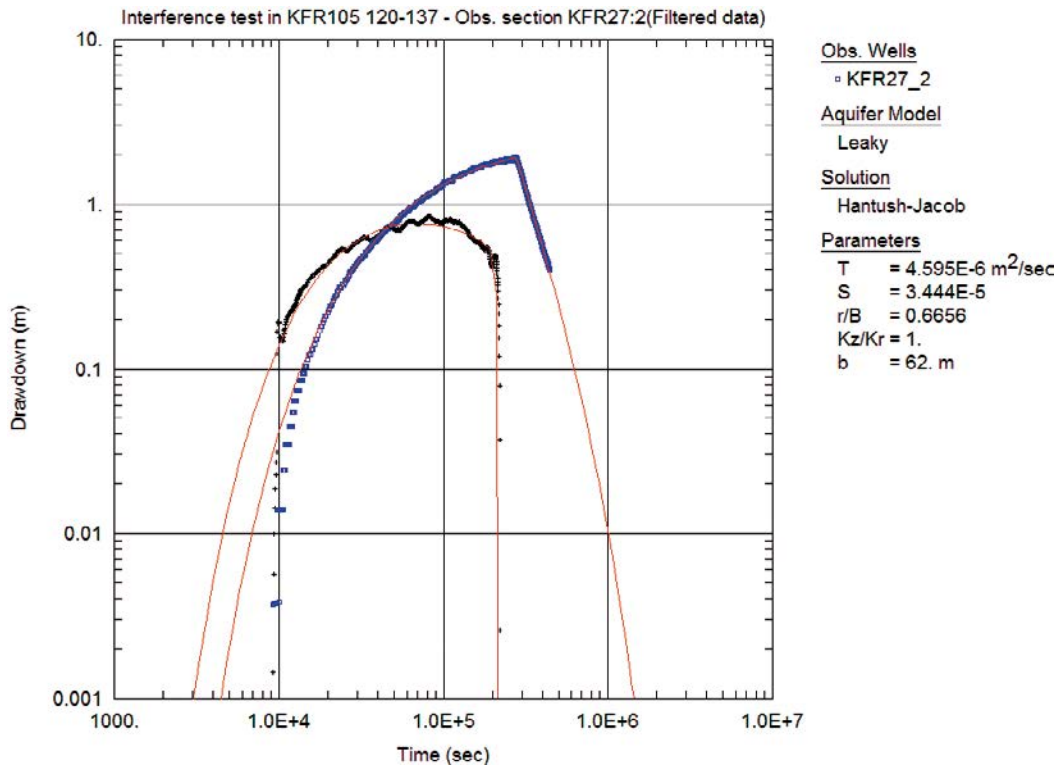


Figure A2-23b. Same as above but log-log plot.

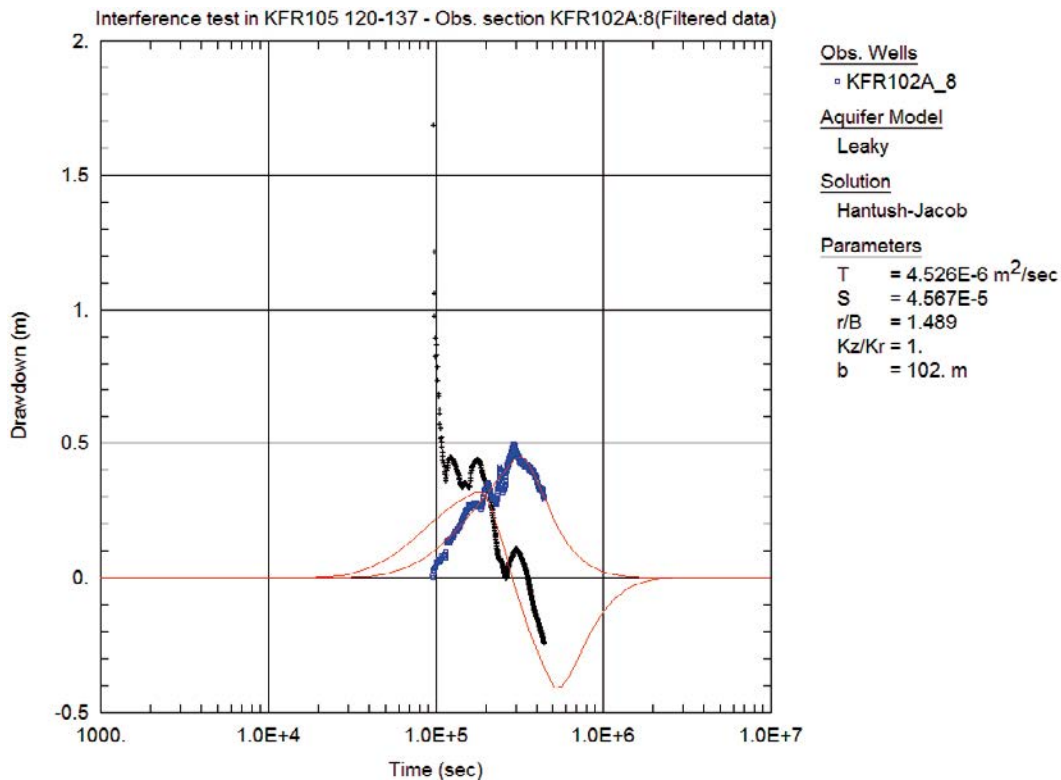


Figure A2-24a. Lin-log plot of drawdown (◦) and derivative, $ds/d(\ln t)$ (+), versus time in the observation borehole section KFR102A:8 during the interference test in KFR105: 120.00–137.00 m and simulated corresponding curves (solid lines). The evaluation is made on the entire curve.

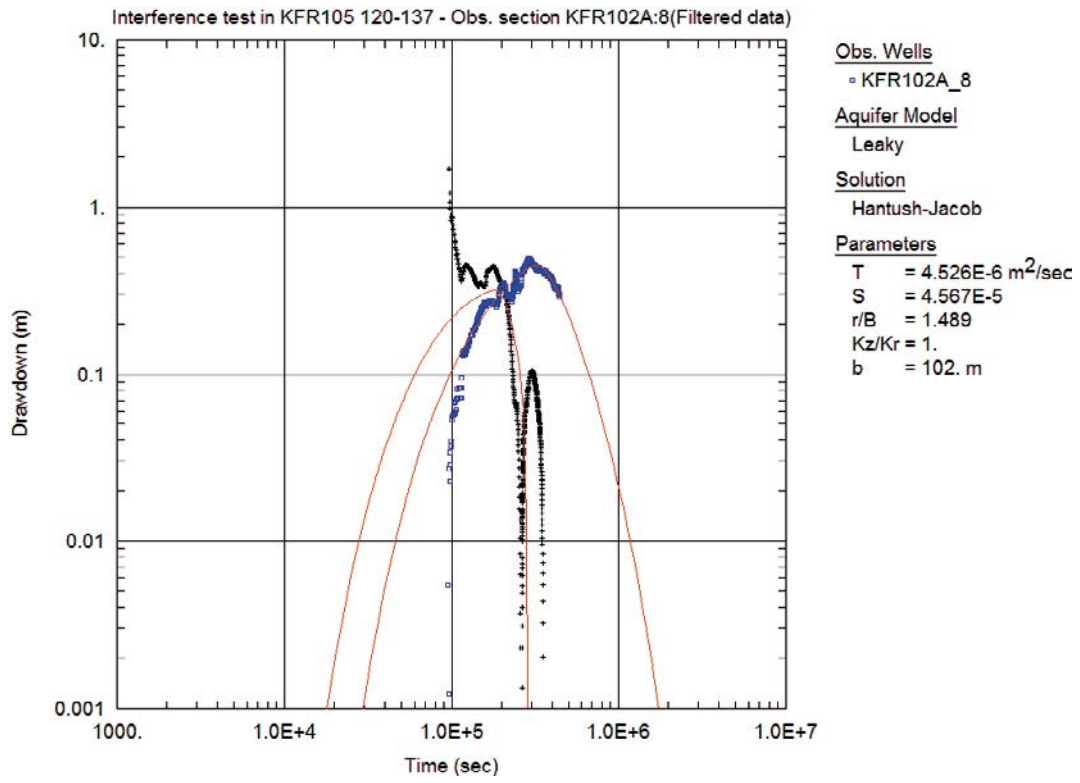


Figure A2-24b. Same as above but log-log plot.

Observation borehole sections

Table A3-1. Observation borehole sections during the two interference tests in borehole KFR27.

Observation borehole ID	Secup (mbl TOC)	Elevation Secup (m RHB70)	Seclow (mbl TOC)	Elevation Seclow (m RHB70)
HFM34:2	22.00	-16.35	90.00	-74.3
HFM34:3	0.00	2.45	21.00	-15.5
HFM35:1	182.00	-137.33	200.75	-150.4
HFM35:2	151.00	-115.43	181.00	-136.6
HFM35:3	34.00	-26.57	150.00	-114.7
HFM35:4	0.00	1.90	33.00	-25.8
HFR102:1	28.00	-21.44	55.04	-44.1
HFR102:2	0.00	2.32	27.00	-20.6
HFR105:1	134.00	-117.50	200.50	-178.0
HFR105:2	107.00	-92.88	133.00	-116.6
HFR105:3	61.00	-51.17	106.00	-92.0
HFR105:4	0.00	3.27	60.00	-50.3
HFR106:1	175.00	-140.72	190.40	-153.1
HFR106:2	47.00	-38.40	174.00	-139.9
HFR106:3	36.00	-29.27	46.00	-37.6
HFR106:4	0.00	1.27	35.00	-28.4
KFM11A:1	711.00	-602.55	851.21	-713.2
KFM11A:2	690.00	-585.75	710.00	-601.8
KFM11A:3	457.00	-394.69	689.00	-585.0
KFM11A:4	446.00	-385.40	456.00	-393.8
KFM11A:5	361.00	-313.06	445.00	-384.6
KFM11A:6	131.00	-112.97	360.00	-312.2
KFM11A:7	0.00	2.95	130.00	-112.1
KFR04:1	84.09	-158.41	100.50	-174.3
KFR04:2	44.09	-119.77	83.09	-157.4
KFR04:3	28.09	-104.32	43.09	-118.8
KFR04:4	5.09	-82.10	27.09	-103.4
KFR05:1	97.15	-168.45	131.00	-200.3
KFR05:2	80.15	-152.48	96.15	-167.5
KFR05:3	57.15	-130.87	79.15	-151.5
KFR05:4	12.15	-88.58	56.15	-129.9
KFR101:1	279.50	-217.76	341.76	-262.0
KFR101:2	91.00	-71.99	278.50	-217.0
KFR101:3	0.00	2.44	90.00	-71.2
KFR102A:1	444.00	-398.73	600.83	-537.3
KFR102A:2	423.00	-380.09	443.00	-397.9
KFR102A:3	255.00	-229.51	422.00	-379.2
KFR102A:4	220.00	-197.82	254.00	-228.6
KFR102A:5	214.00	-192.37	219.00	-196.9
KFR102A:6	185.00	-166.03	213.00	-191.5
KFR102A:7	103.00	-91.38	184.00	-165.1
KFR102A:8	0.00	2.66	102.00	-90.5
KFR102B:1	146.00	-115.57	180.08	-142.9
KFR102B:2	128.00	-101.10	145.00	-114.8
KFR102B:3	0.00	2.51	127.00	-100.3
KFR103:1	178.00	-140.93	200.50	-158.9
KFR103:2	79.00	-61.58	177.00	-140.1
KFR103:3	0.00	2.43	78.00	-60.8
KFR104:1	333.00	-260.61	454.57	-351.7

Observation borehole ID	Secup (mbi TOC)	Elevation Secup (m RHB70)	Seclow (mbi TOC)	Elevation Seclow (m RHB70)
KFR104:2	98.00	-76.90	332.00	-259.9
KFR104:3	0.00	2.83	97.00	-76.1
KFR105:1	265.00	-150.44	303.00	-156.1
KFR105:2	170.00	-135.40	264.00	-150.3
KFR105:3	138.00	-130.20	169.00	-135.2
KFR105:4	120.00	-127.22	137.00	-130.0
KFR105:5	4.00	-107.53	119.00	-127.1
KFR106:1	260.00	-242.35	300.13	-279.8
KFR106:2	143.00	-133.05	259.00	-241.4
KFR106:3	0.00	1.06	142.00	-132.1
KFR13:1	53.75	-177.09	76.60	-199.9
KFR13:2	33.75	-157.09	52.75	-176.1
KFR13:3	3.75	-127.09	32.75	-156.1
KFR55:1	48.53	-134.83	61.89	-137.4
KFR55:2	39.53	-133.12	47.53	-134.6
KFR55:3	21.53	-129.68	38.53	-132.9
KFR55:4	7.53	-127.01	20.53	-129.5
KFR07B:1	3.40	-136.53	7.60	-140.6
KFR07B:2	8.60	-141.55	21.10	-153.6
HFR101:1	0.00	2.63	209.30	-186.9

Table A3-2. Observation sections during the two interference tests in borehole KFR103.

Observation borehole ID	Secup (mbi TOC)	Elevation Secup (m RHB70)	Seclow (mbi TOC)	Elevation Seclow (m RHB70)
HFM34:2	22.00	-16.35	90.00	-74.3
HFM34:3	0.00	2.45	21.00	-15.5
HFM35:1	182.00	-137.33	200.75	-150.4
HFM35:2	151.00	-115.43	181.00	-136.6
HFM35:3	34.00	-26.57	150.00	-114.7
HFM35:4	0.00	1.90	33.00	-25.8
HFR105:1	134.00	-117.50	200.50	-178.0
HFR105:2	107.00	-92.88	133.00	-116.6
HFR105:3	61.00	-51.17	106.00	-92.0
HFR105:4	0.00	3.27	60.00	-50.3
HFR106:1	175.00	-140.72	190.40	-153.1
HFR106:2	47.00	-38.40	174.00	-139.9
HFR106:3	36.00	-29.27	46.00	-37.6
HFR106:4	0.00	1.27	35.00	-28.4
KFM11A:1	711.00	-602.55	851.21	-713.2
KFM11A:2	690.00	-585.75	710.00	-601.8
KFM11A:3	457.00	-394.69	689.00	-585.0
KFM11A:4	446.00	-385.40	456.00	-393.8
KFM11A:5	361.00	-313.06	445.00	-384.6
KFM11A:6	131.00	-112.97	360.00	-312.2
KFM11A:7	0.00	2.95	130.00	-112.1
KFR101:1	279.50	-217.76	341.76	-262.0
KFR101:2	91.00	-71.99	278.50	-217.0
KFR101:3	0.00	2.44	90.00	-71.2
KFR102A:1	444.00	-398.73	600.83	-537.3
KFR102A:2	423.00	-380.09	443.00	-397.9
KFR102A:3	255.00	-229.51	422.00	-379.2
KFR102A:4	220.00	-197.82	254.00	-228.6
KFR102A:5	214.00	-192.37	219.00	-196.9
KFR102A:6	185.00	-166.03	213.00	-191.5

Observation borehole ID	Secup (mbl TOC)	Elevation Secup (m RHB70)	Seclow (mbl TOC)	Elevation Seclow (m RHB70)
KFR102A:7	103.00	-91.38	184.00	-165.1
KFR102A:8	0.00	2.66	102.00	-90.5
KFR102B:1	146.00	-115.57	180.08	-142.9
KFR102B:2	128.00	-101.10	145.00	-114.8
KFR102B:3	0.00	2.51	127.00	-100.3
KFR104:1	333.00	-260.61	454.57	-351.7
KFR104:2	98.00	-76.90	332.00	-259.9
KFR104:3	0.00	2.83	97.00	-76.1
KFR105:1	265.00	-150.44	303.00	-156.1
KFR105:2	170.00	-135.40	264.00	-150.3
KFR105:3	138.00	-130.20	169.00	-135.2
KFR105:4	120.00	-127.22	137.00	-130.0
KFR105:5	4.00	-107.53	119.00	-127.1
KFR106:1	260.00	-242.35	300.13	-279.8
KFR106:2	143.00	-133.05	259.00	-241.4
KFR106:3	0.00	1.06	142.00	-132.1
KFR27:1	110.00	-107.12	501.64	-496.9
KFR27:2	47.00	-44.12	109.00	-106.1
KFR27:3	0.00	2.87	46.00	-43.1

Table A3-3. Observation sections during the interference test in borehole KFR105.

Observation borehole ID	Secup (mbl TOC)	Elevation Secup (m RHB70)	Seclow (mbl TOC)	Elevation Seclow (m RHB70)
KFR105:1	265.00	-150.44	303.00	-156.1
KFR105:2	170.00	-135.40	264.00	-150.3
KFR105:3	138.00	-130.20	169.00	-135.2
KFR105:5	4.00	-107.53	119.00	-127.1
HFM34:2	22.00	-16.35	90.00	-74.3
HFM34:3	0.00	2.45	21.00	-15.5
HFM35:1	182.00	-137.33	200.75	-150.4
HFM35:2	151.00	-115.43	181.00	-136.6
HFM35:3	34.00	-26.57	150.00	-114.7
HFM35:4	0.00	1.90	33.00	-25.8
HFR102:1	28.00	-21.44	55.04	-44.1
HFR102:2	0.00	2.32	27.00	-20.6
HFR105:1	134.00	-117.50	200.50	-178.0
HFR105:2	107.00	-92.88	133.00	-116.6
HFR105:3	61.00	-51.17	106.00	-92.0
HFR105:4	0.00	3.27	60.00	-50.3
KFM11A:1	711.00	-602.55	851.21	-713.2
KFM11A:2	690.00	-585.75	710.00	-601.8
KFM11A:3	457.00	-394.69	689.00	-585.0
KFM11A:4	446.00	-385.40	456.00	-393.8
KFM11A:5	361.00	-313.06	445.00	-384.6
KFM11A:6	131.00	-112.97	360.00	-312.2
KFM11A:7	0.00	2.95	130.00	-112.1
KFR102A:1	444.00	-398.73	600.83	-537.3
KFR102A:2	423.00	-380.09	443.00	-397.9
KFR102A:3	255.00	-229.51	422.00	-379.2
KFR102A:4	220.00	-197.82	254.00	-228.6
KFR102A:5	214.00	-192.37	219.00	-196.9
KFR102A:6	185.00	-166.03	213.00	-191.5
KFR102A:7	103.00	-91.38	184.00	-165.1
KFR102A:8	0.00	2.66	102.00	-90.5

Observation borehole ID	Secup (mbl TOC)	Elevation Secup (m RHB70)	Seclow (mbl TOC)	Elevation Seclow (m RHB70)
KFR103:1	178.00	-140.93	200.50	-158.9
KFR103:2	79.00	-61.58	177.00	-140.1
KFR103:3	0.00	2.43	78.00	-60.8
KFR104:1	333.00	-260.61	454.57	-351.7
KFR104:2	98.00	-76.90	332.00	-259.9
KFR104:3	0.00	2.83	97.00	-76.1
KFR27:1	110.00	-107.12	501.64	-496.9
KFR27:2	47.00	-44.12	109.00	-106.1
KFR27:3	0.00	2.87	46.00	-43.1
HFR101:1	0.00	2.63	209.30	-186.9

Filtered and non-filtered responses in observation sections

A4.1 Filtered responses for test in KFR27: 47–57 m

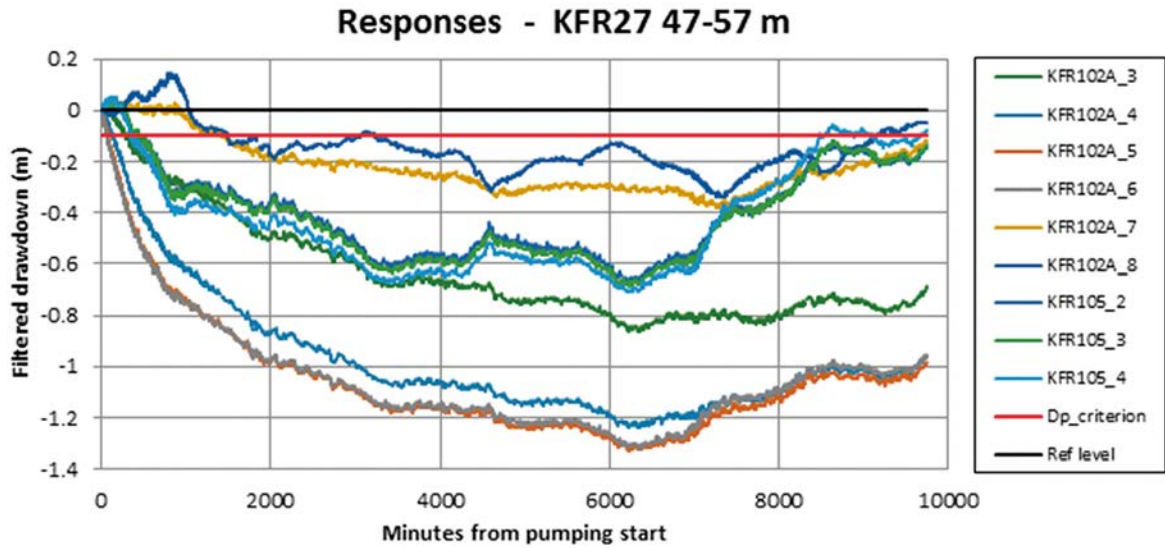


Figure A4-1. Filtered drawdown in observation sections showing a response at the test in KFR27: 47–57 m.

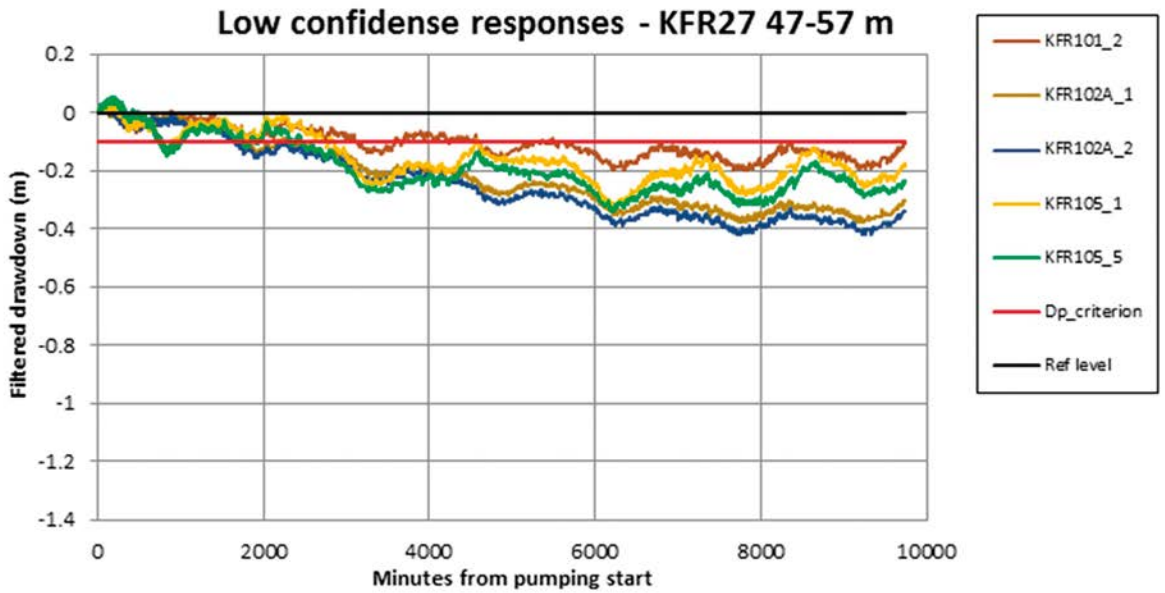


Figure A4-2. Filtered drawdown in observation sections showing a response with low confidence at the test in KFR27: 47–57 m.

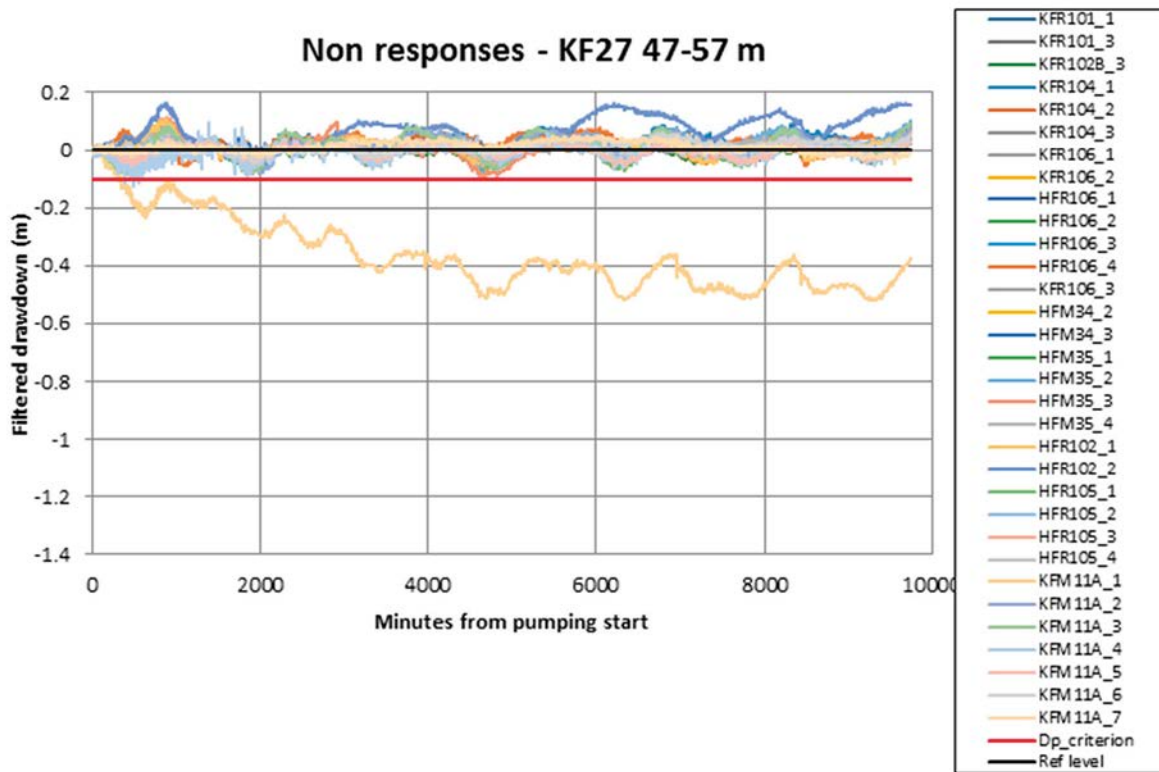


Figure A4-3. Filtered drawdown in observation sections not showing a response at the test in KFR27: 47–57 m.

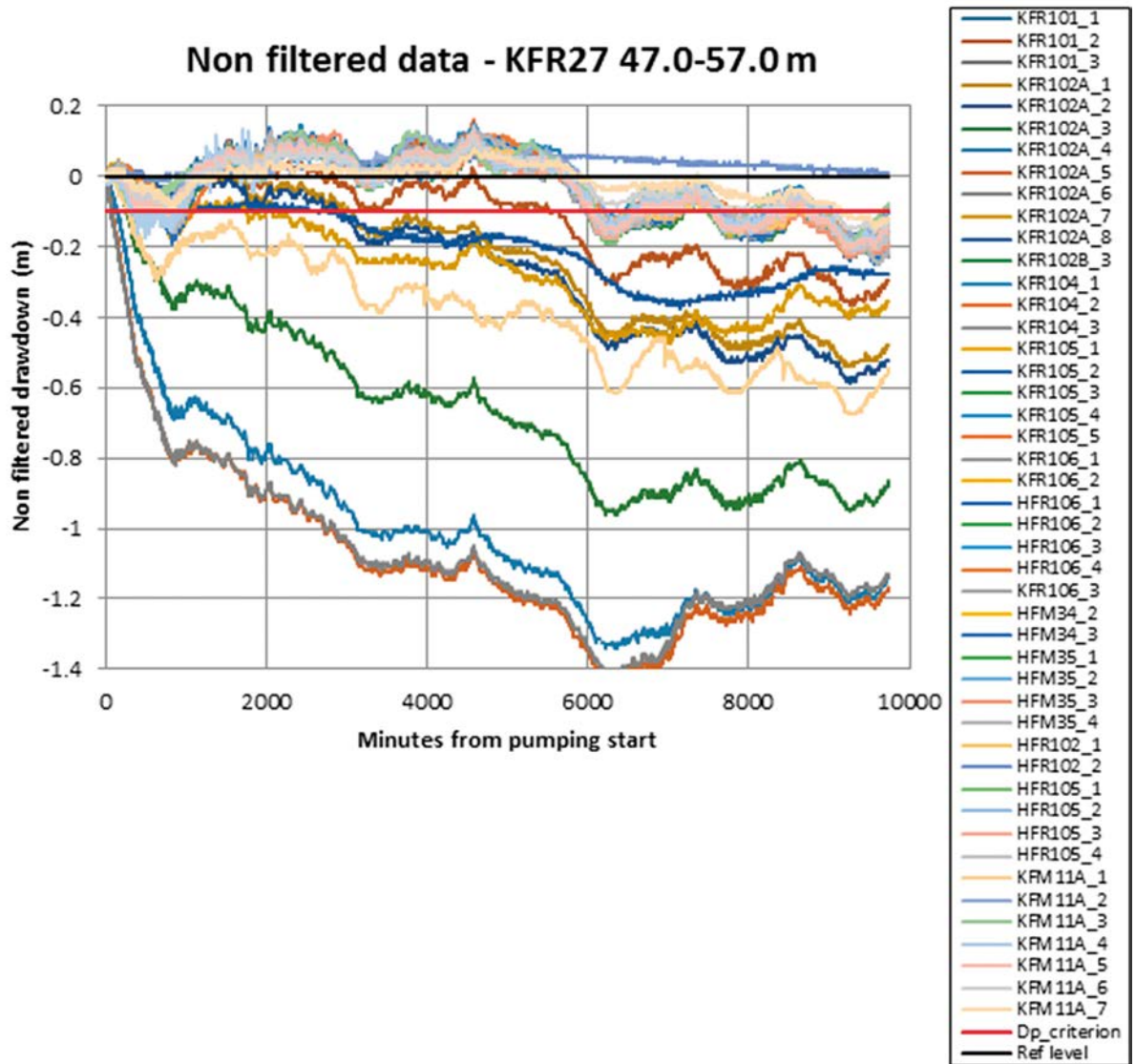


Figure A4-4. Non filtered data for all observation sections at the test in KFR27: 47–57 m.

A4.2 Filtered responses for test in KFR27: 189.4–194.4 m

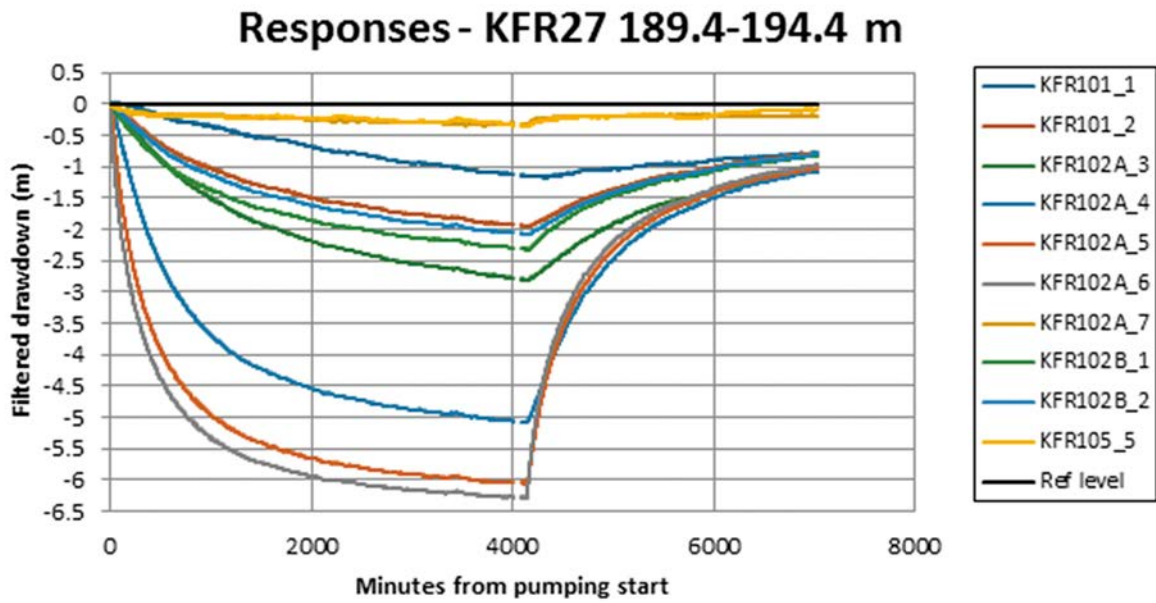


Figure A4-5. Filtered drawdown in observation sections showing a response at the test in KFR27: 189.4–194.4 m. Same figure in another scale in Figure A4-6.

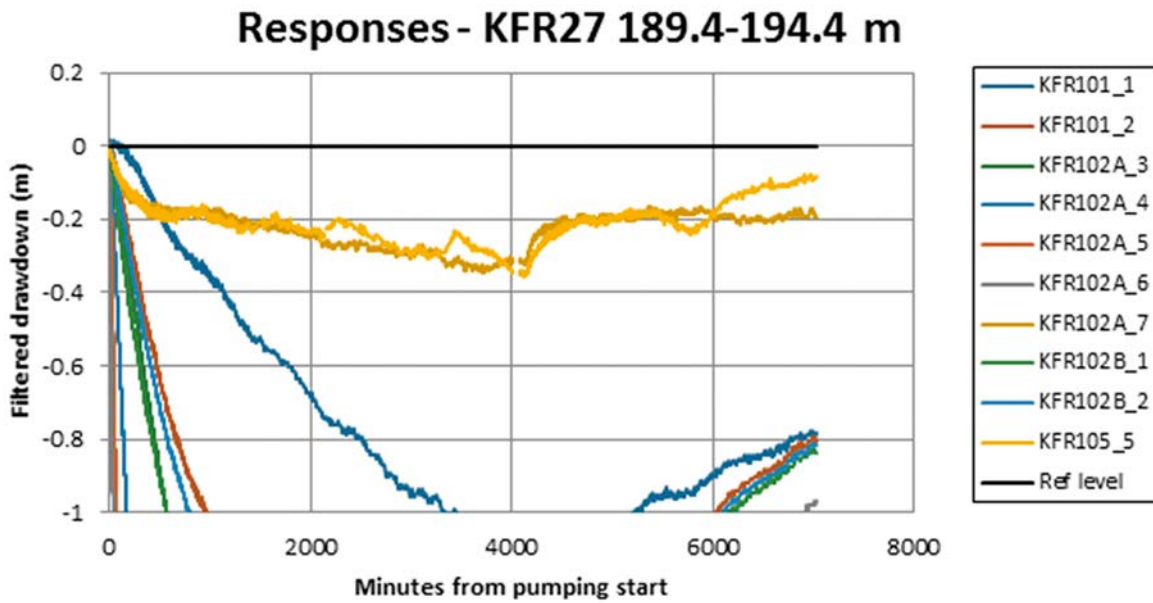


Figure A4-6. Filtered drawdown in observation sections showing a response at the test in KFR27: 189.4–194.4 m. Same figure in another scale in Figure A4-5.

Low confidence responses - KFR27 189.4-194.4 m

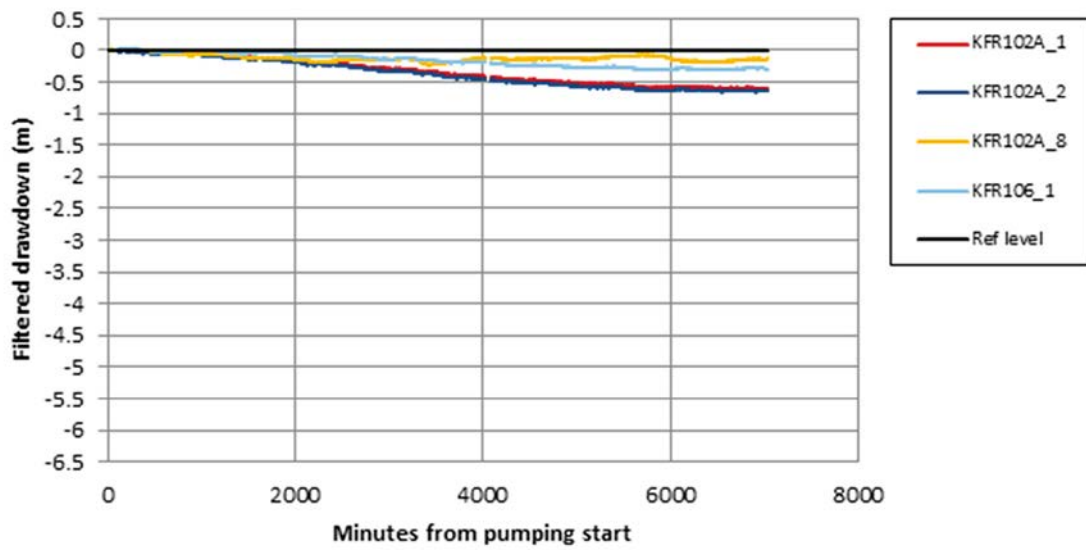


Figure A4-7. Filtered drawdown in observation sections showing a response with low confidence at the test in KFR27: 189.4–194.4 m. Same figure in another scale in Figure A4-8.

Low confidence responses - KFR27 189.4-194.4 m

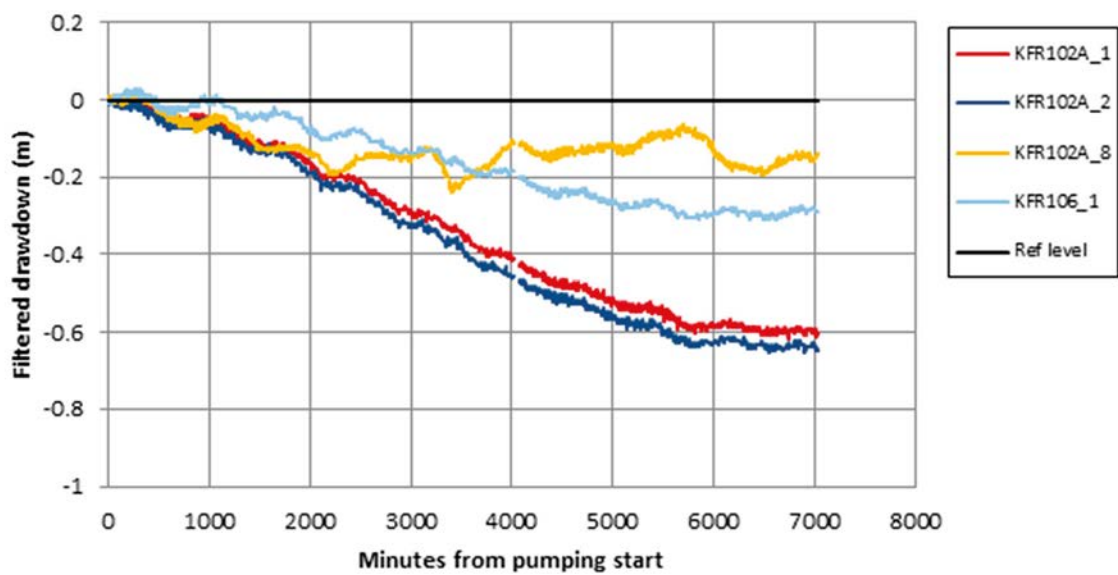


Figure A4-8. Filtered drawdown in observation sections showing a response with low confidence at the test in KFR27: 189.4–194.4 m. Same figure in another scale in Figure A4-7.

Non responses - KFR27 189.4-194.4 m

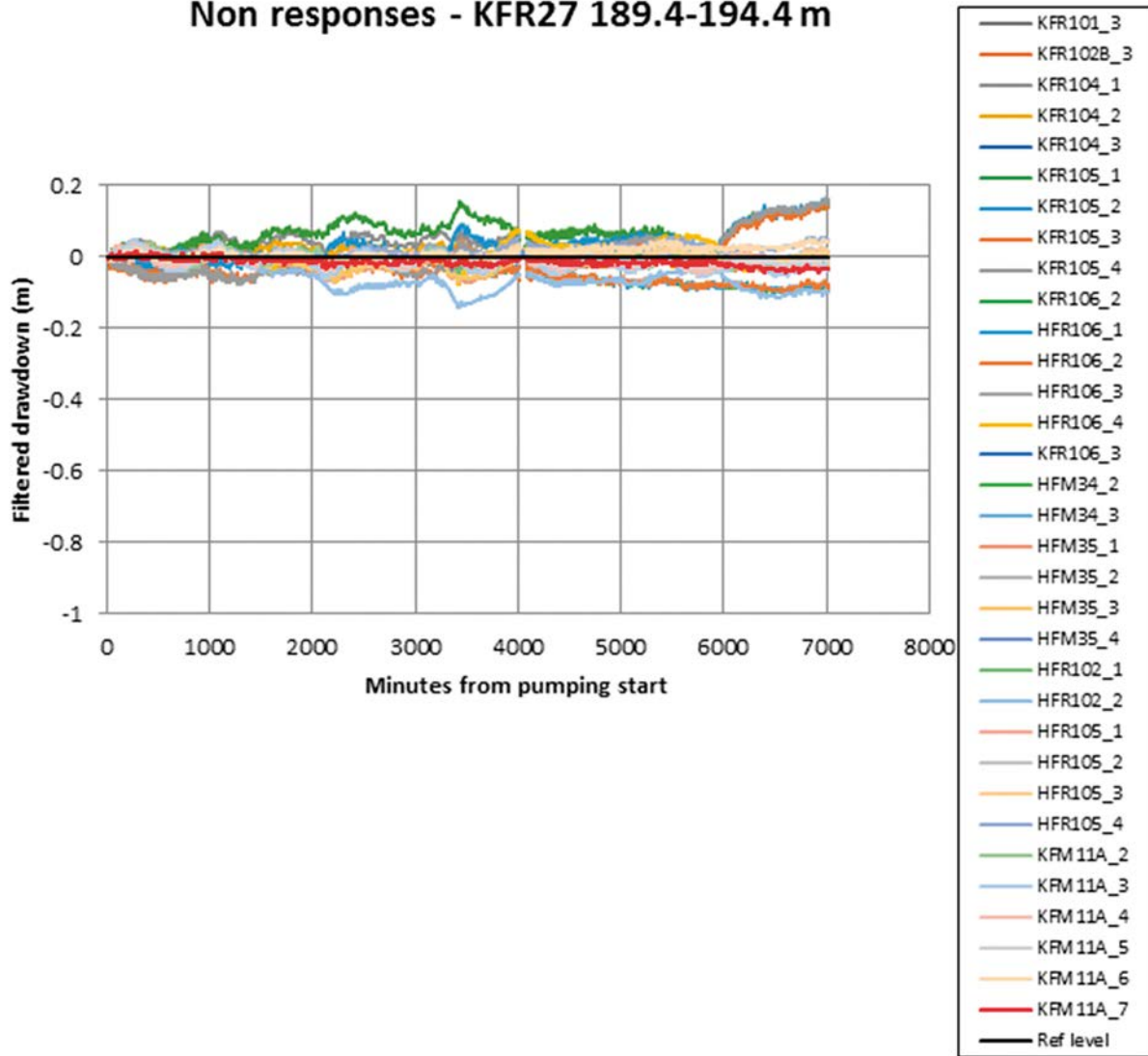


Figure A4-9. Filtered drawdown in observation sections not showing a response at the test in KFR27: 189.4–194.4 m.

Non filtered data - KFR27 189.4 - 194.4 m

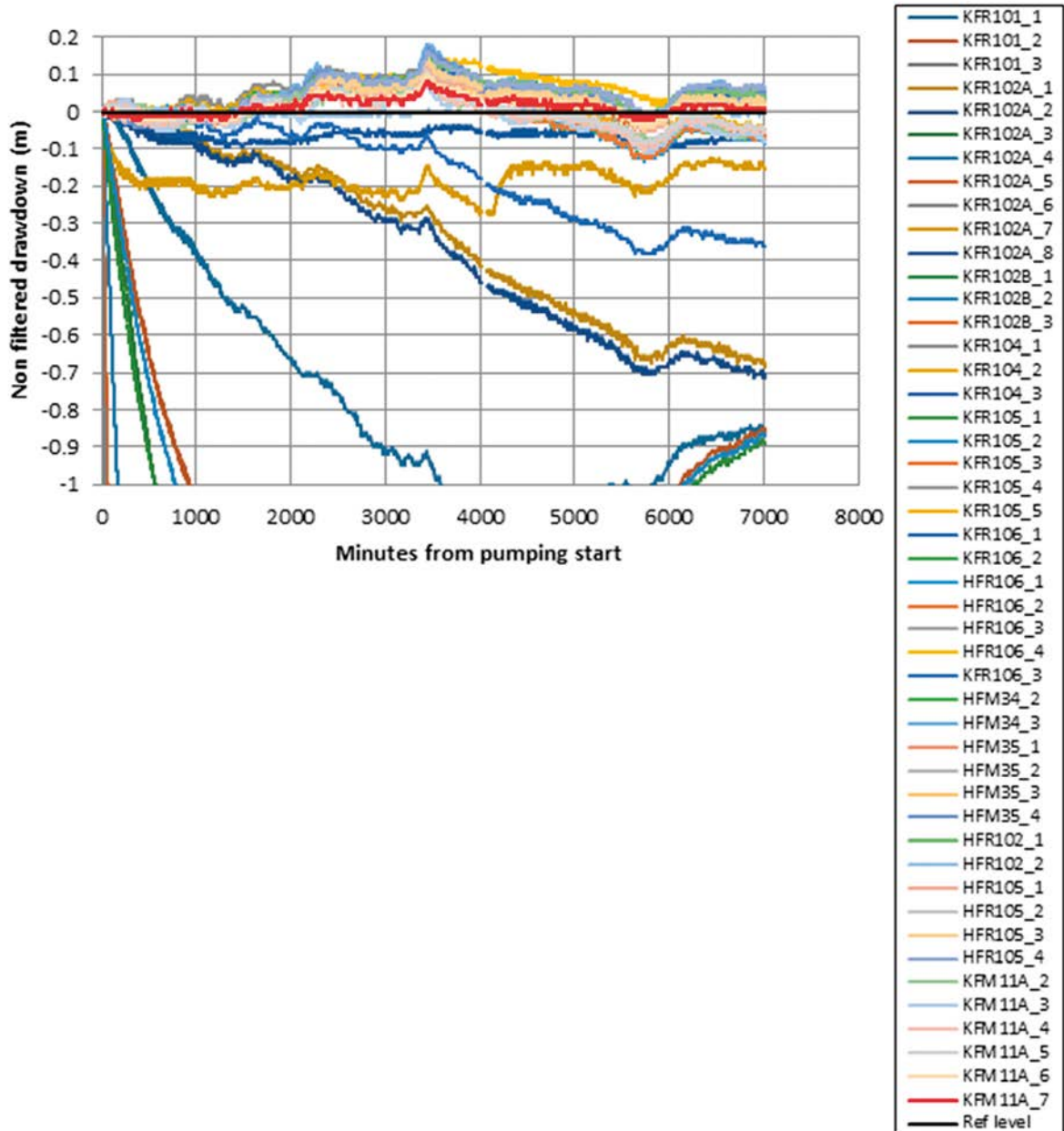


Figure A4-10. Non filtered data for all observation sections at the test in KFR27: 189.4–194.4 m.

A4.3 Filtered responses for test in KFR103: 83.5–93.5 m

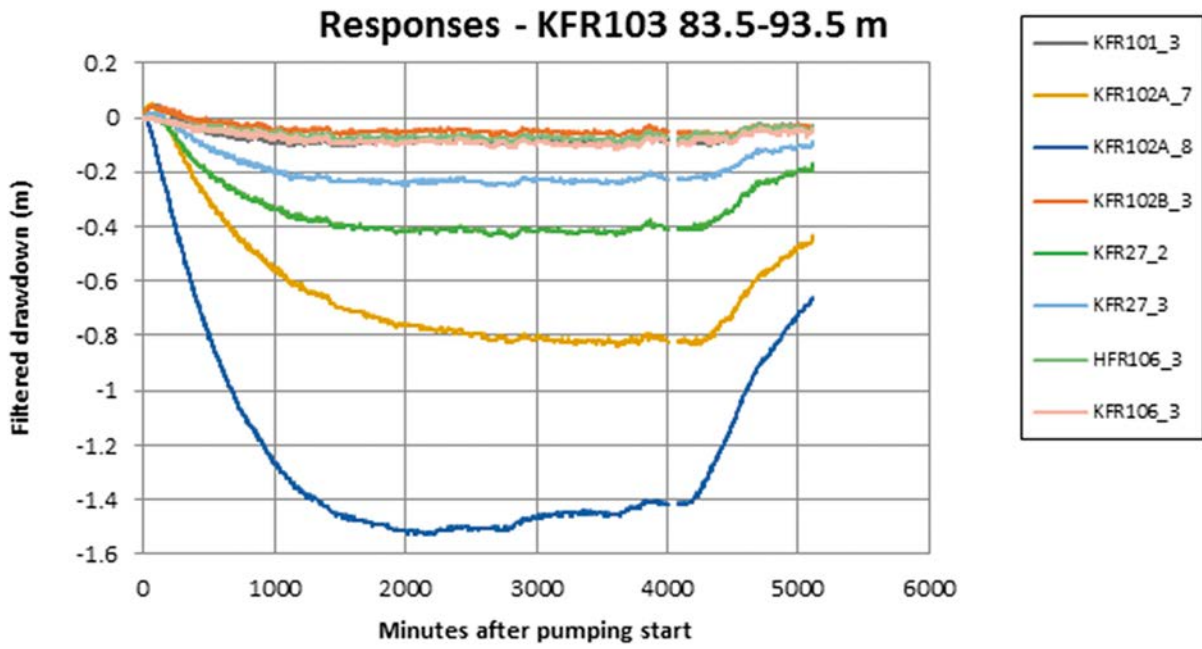


Figure A4-11. Filtered drawdown in observation sections showing a response at the test in KFR103: 83.5–93.5 m. Same figure in another scale in Figure A4-12.

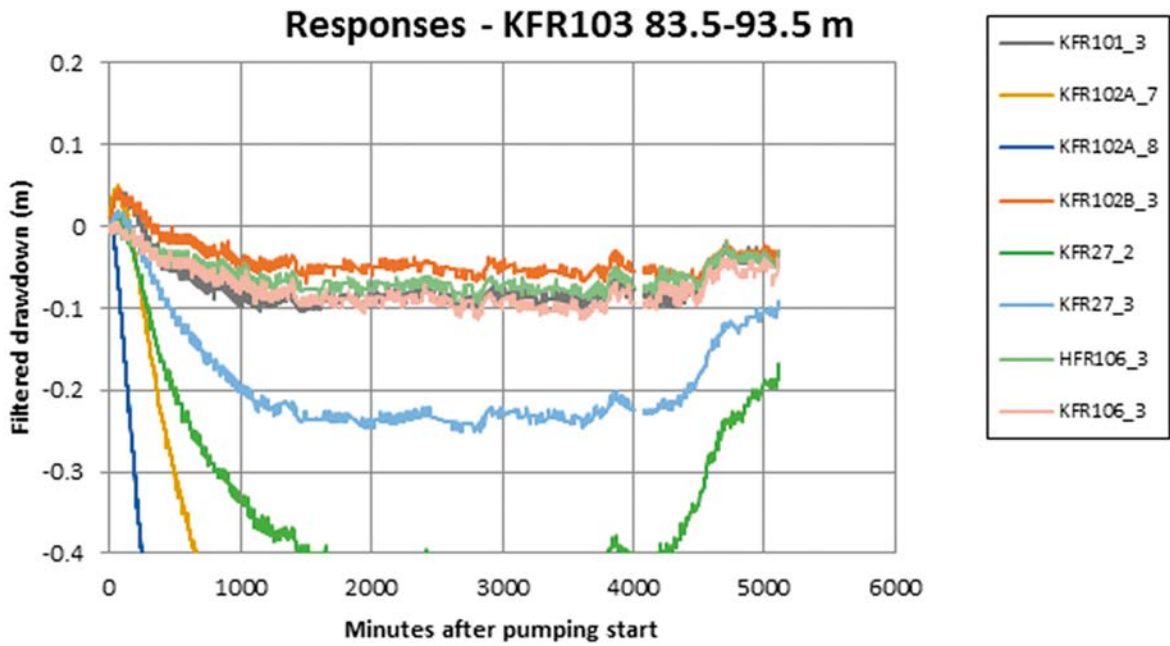


Figure A4-12. Filtered drawdown in observation sections showing a response at the test in KFR103: 83.5–93.5 m. Same figure in another scale in Figure A4-11.

Low confidence responses - KFR103 83.5-93.5 m

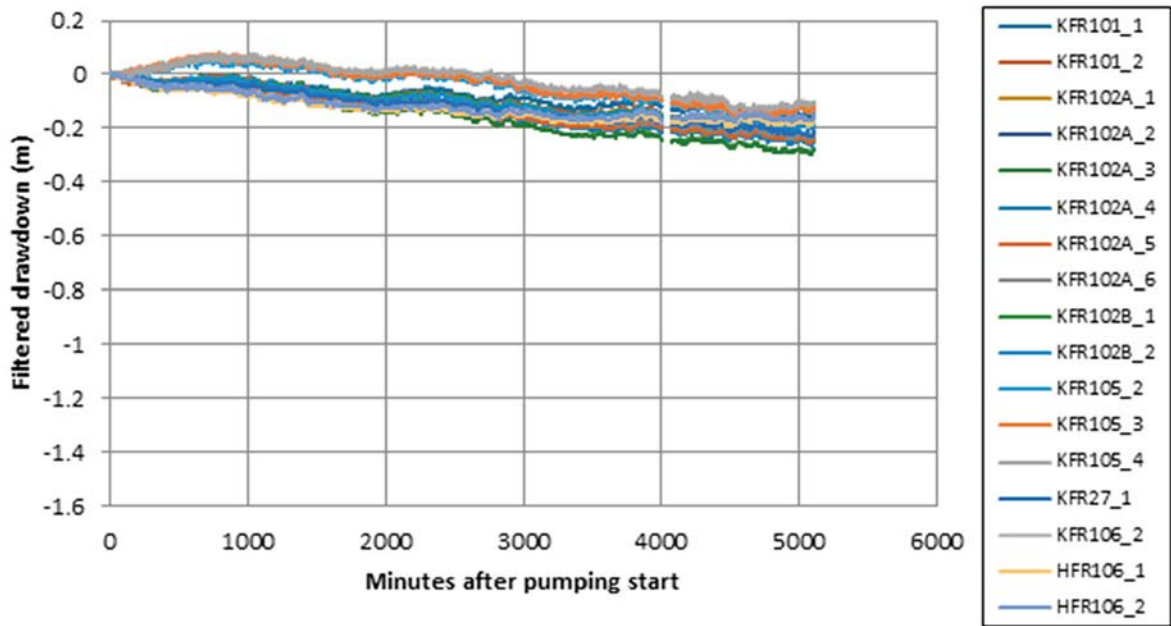


Figure A4-13. Filtered drawdown in observation sections showing a response with low confidence at the test in KFR103: 83.5–93.5 m. Same figure in another scale in Figure A4-14.

Low confidence responses - KFR103 83.5-93.5 m

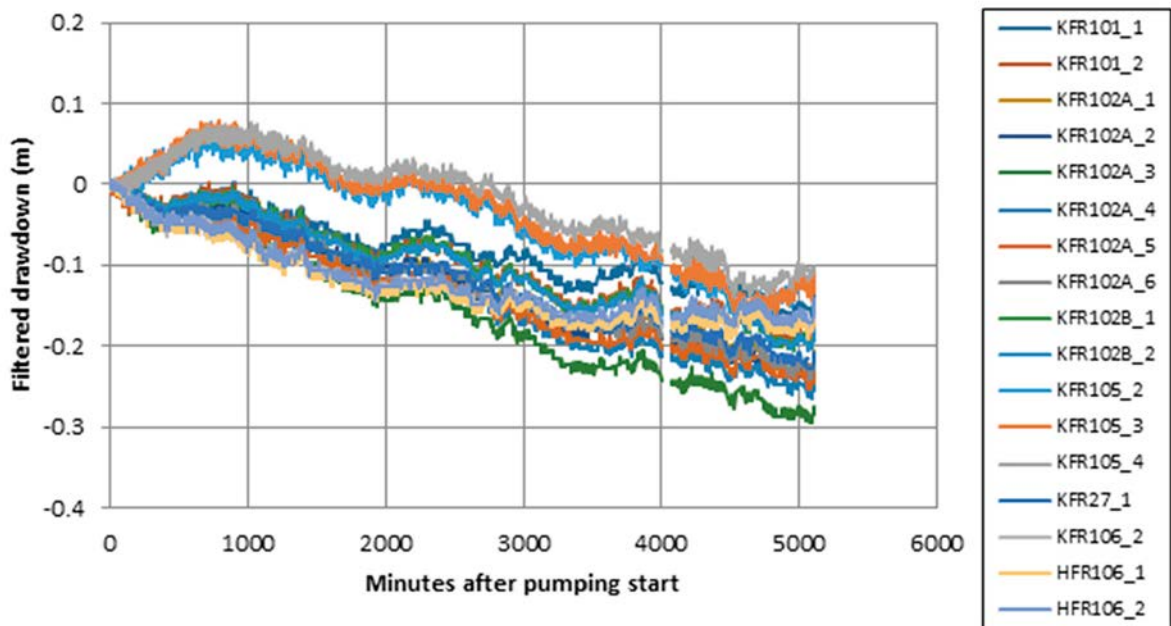


Figure A4-14. Filtered drawdown in observation sections showing a response with low confidence at the test in KFR103: 83.5–93.5 m. Same figure in another scale in Figure A4-13.

Non responses - KFR103 83.5-93.5 m

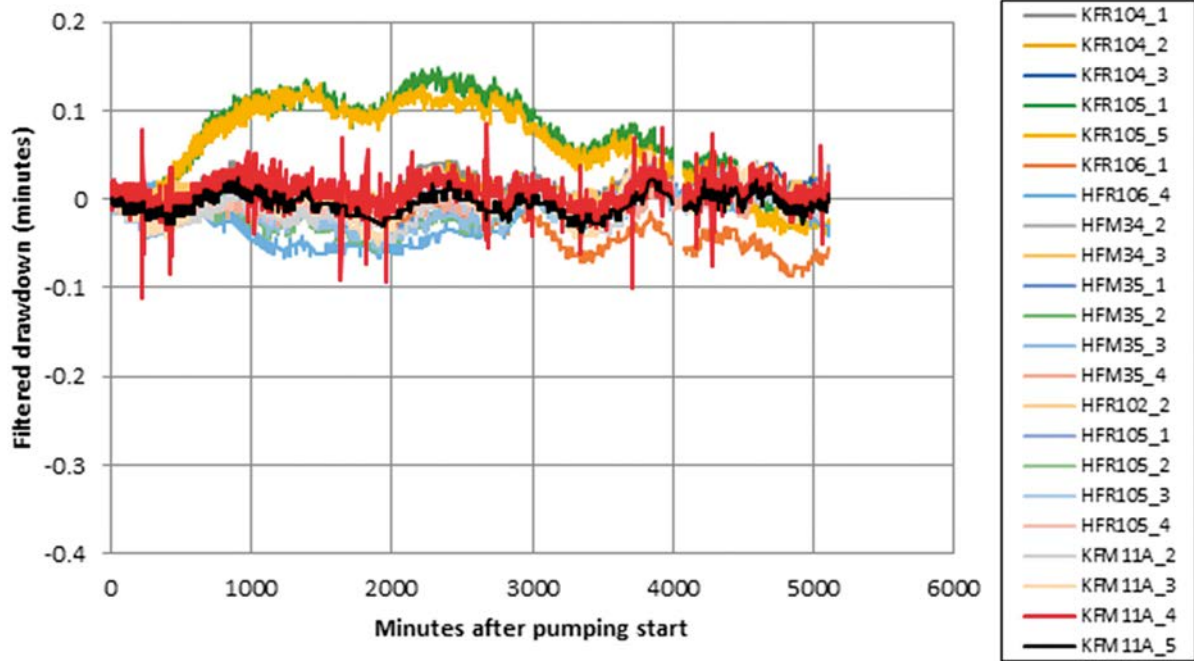


Figure A4-15. Filtered drawdown in observation sections not showing a response at the test in KFR103: 83.5–93.5 m.

Non filtered data - KFR103 83.5-93.5 m

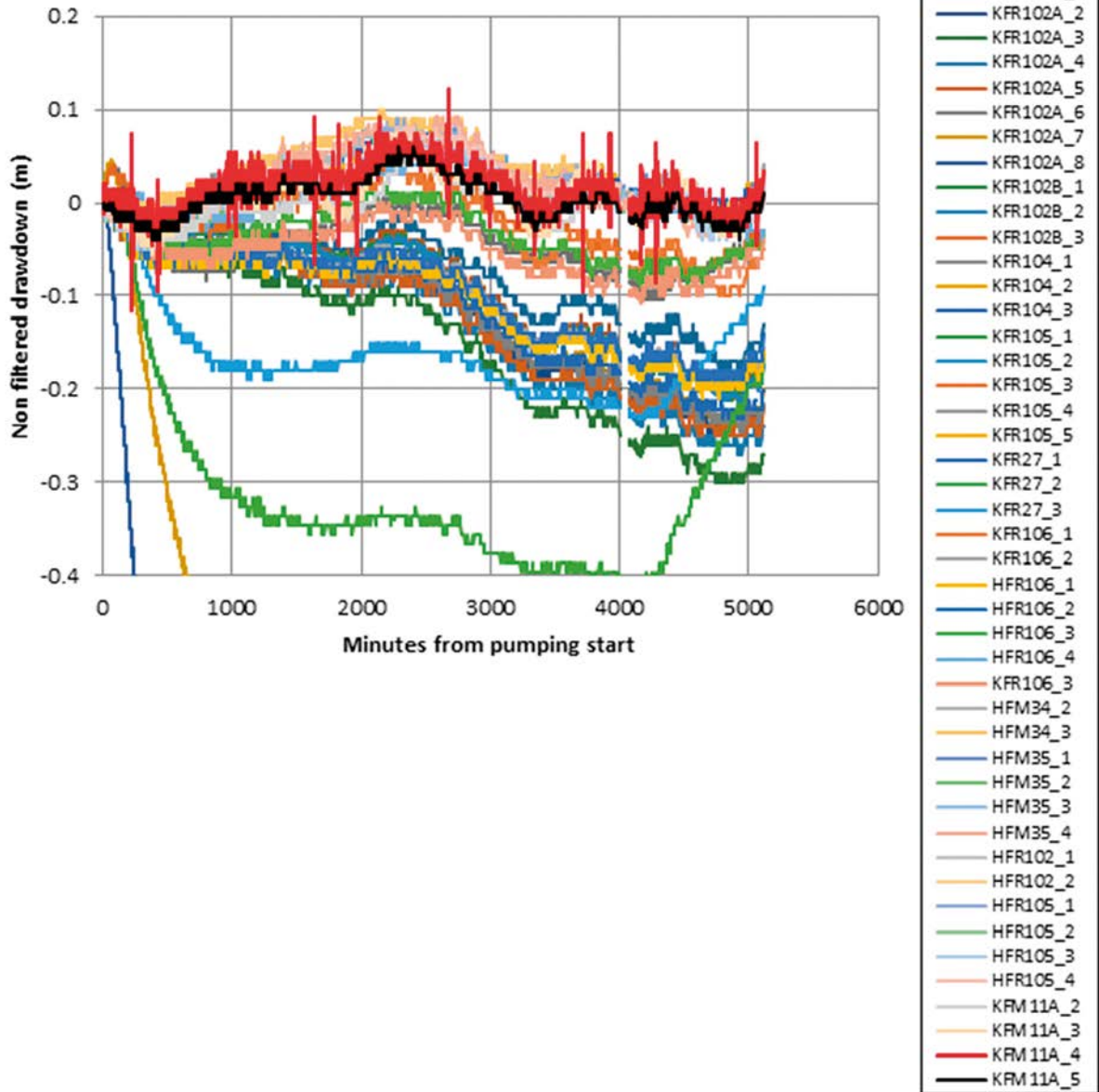


Figure A4-16. Non filtered data for all observation sections at the test in KFR103: 83.5–93.5 m.

A4.4 Filtered responses for test in KFR103: 177–187 m

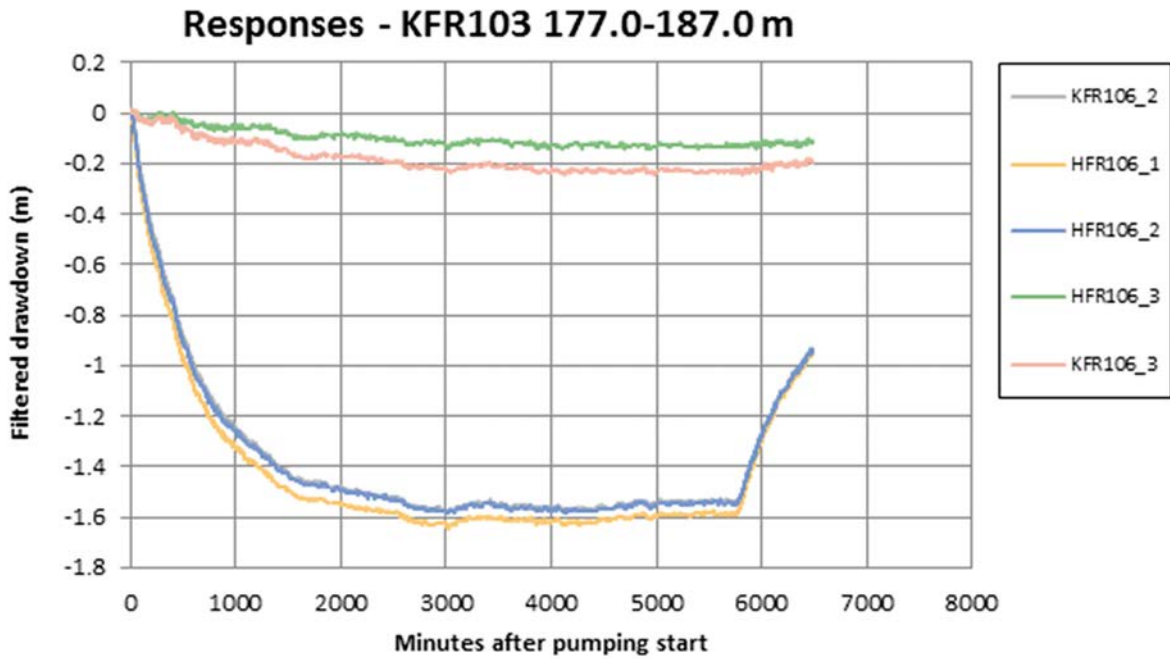


Figure A4-17. Filtered drawdown in observation sections showing a response at the test in KFR103: 177.0–187.0 m. Same figure in another scale in Figure A4-18.

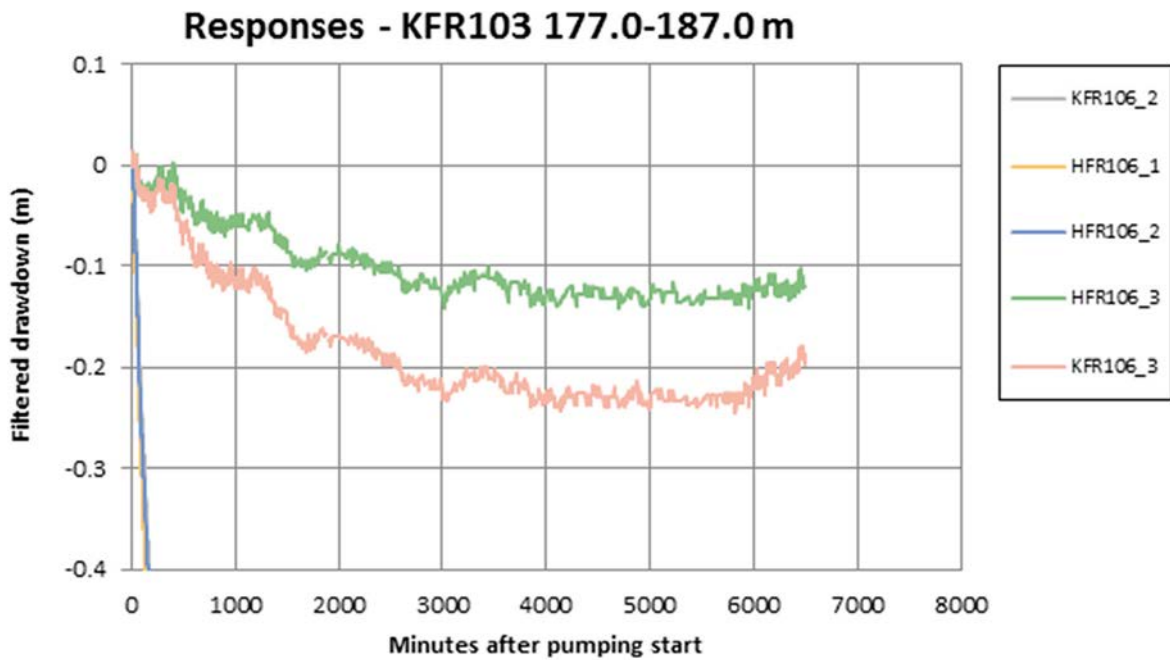


Figure A4-18. Filtered drawdown in observation sections showing a response at the test in KFR103: 177.0–187.0 m. Same figure in another scale in Figure A4-17.

Low confidence responses - KFR103 177.0-187.0 m

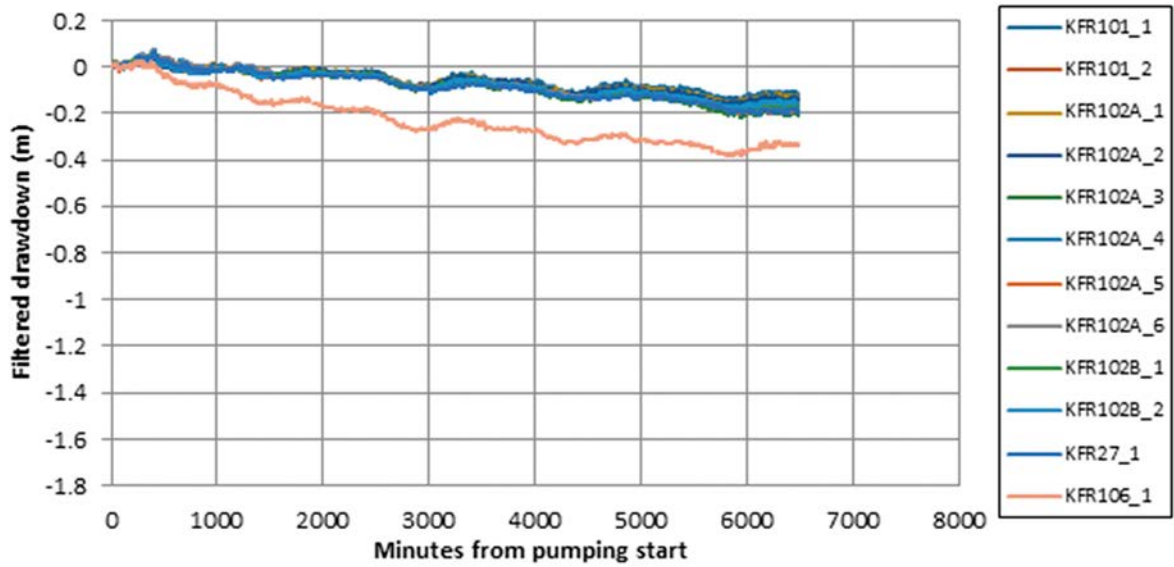


Figure A4-19. Filtered drawdown in observation sections showing a response with low confidence at the test in KFR103: 177.0–187.0 m. Same figure in another scale in Figure A4-20.

Low confidence responses - KFR103 177.0-187.0 m

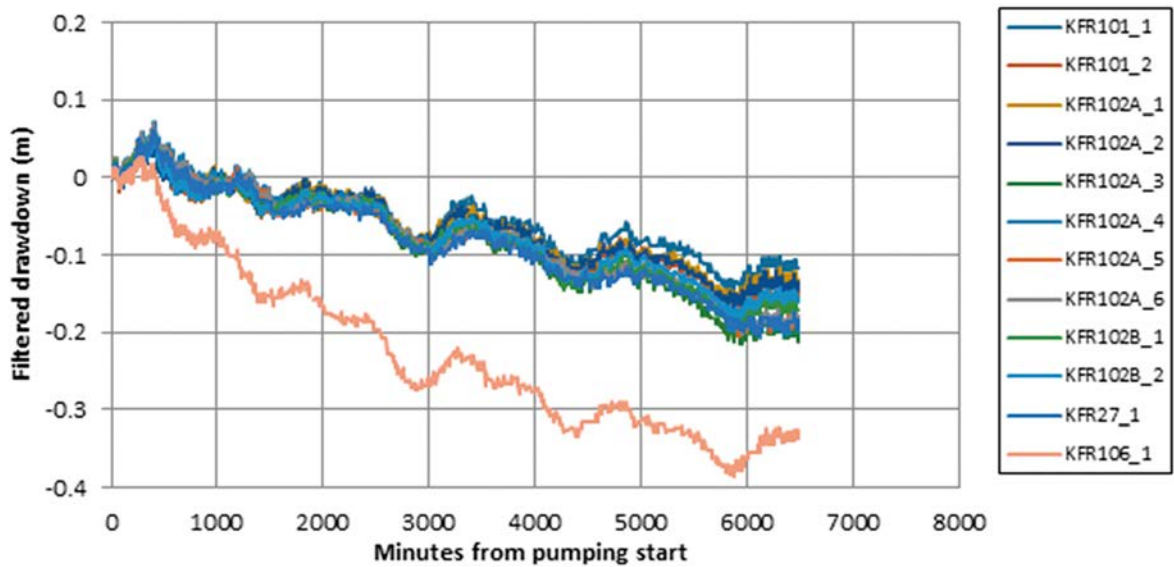


Figure A4-20. Filtered drawdown in observation sections showing a response with low confidence at the test in KFR103: 177.0–187.0 m. Same figure in another scale in Figure A4-19.

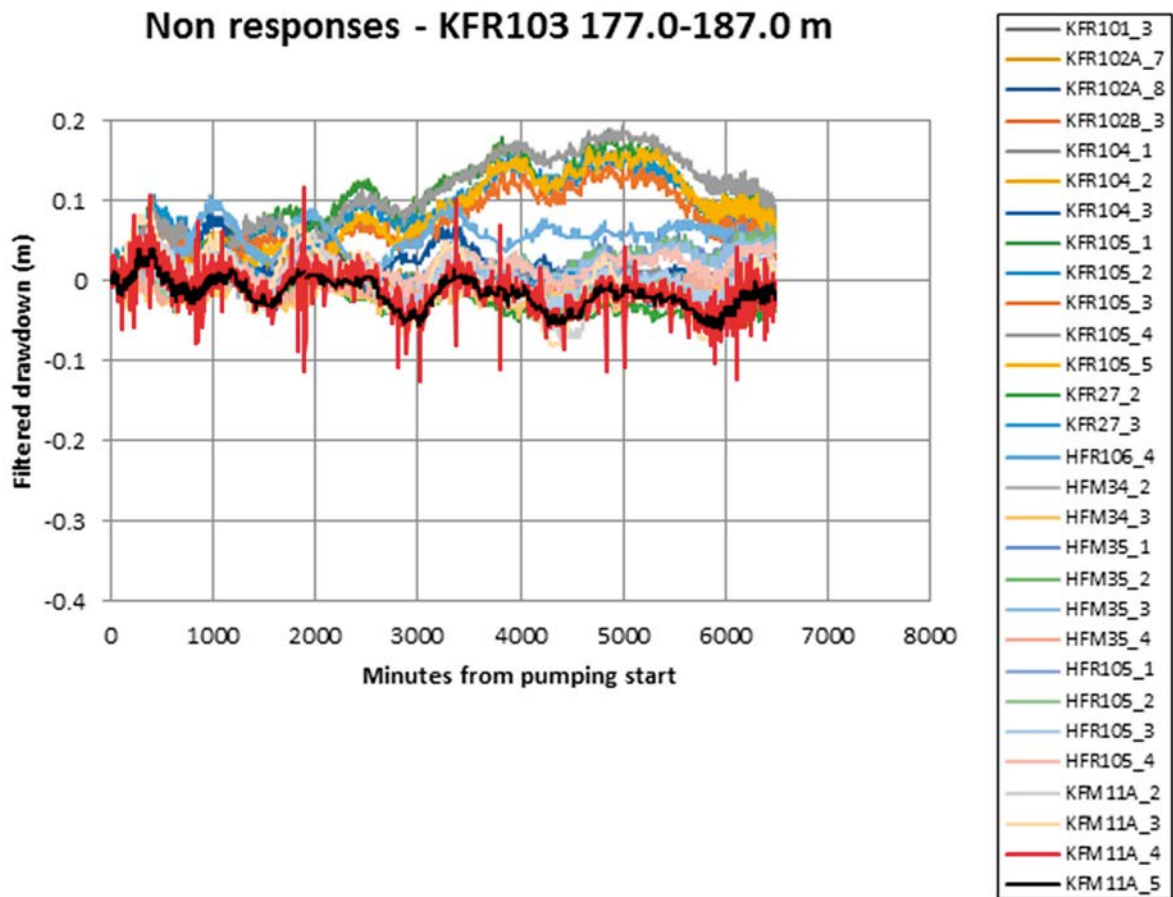


Figure A4-21. Filtered drawdown in observation sections not showing a response at the test in KFR103: 177.0–187.0 m.

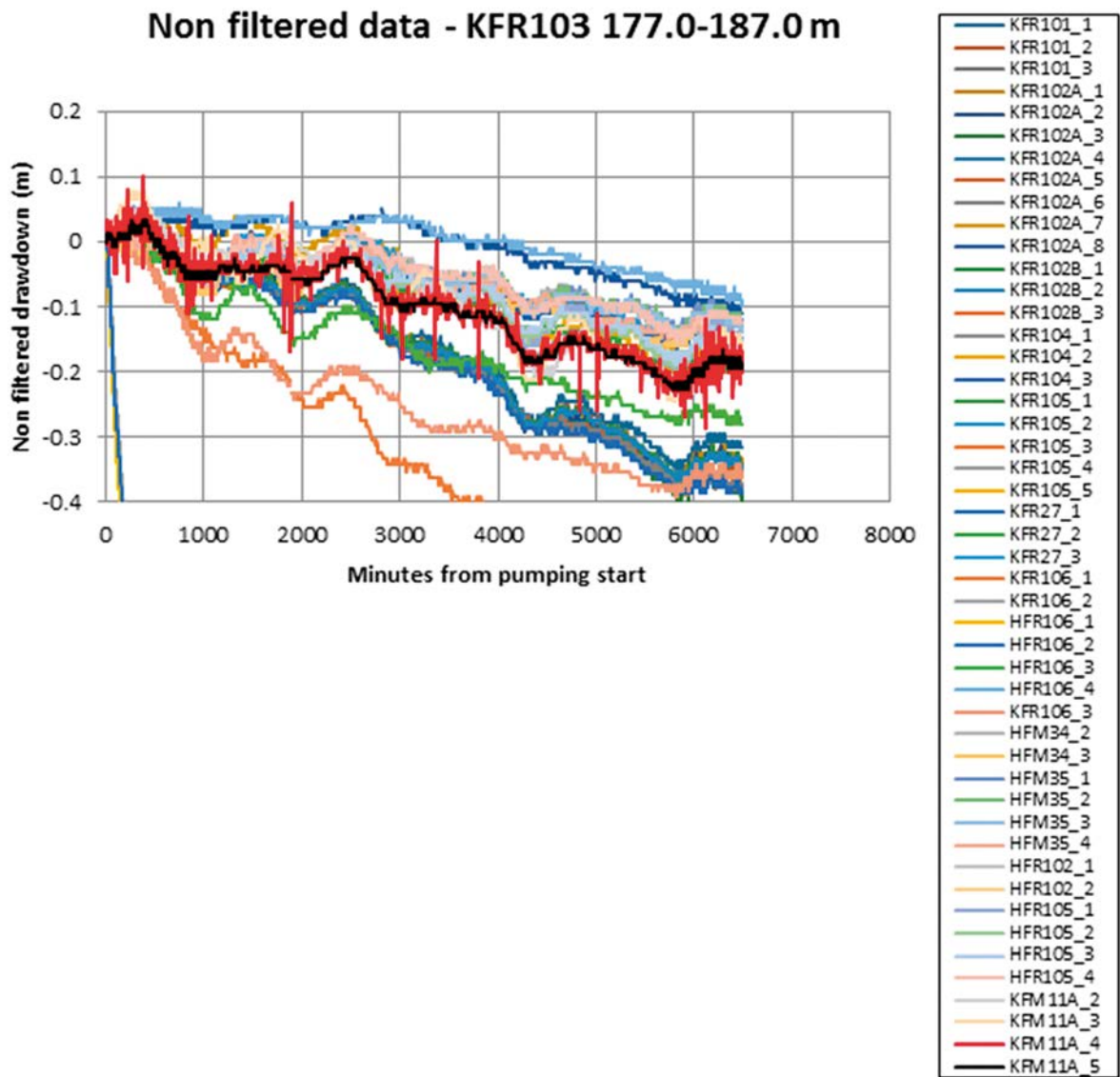


Figure A4-22. Non filtered data for all observation sections at the test in KFR103: 177.0–187.0 m.

A4.5 Filtered responses for test in KFR105: 120.0–137.0 m

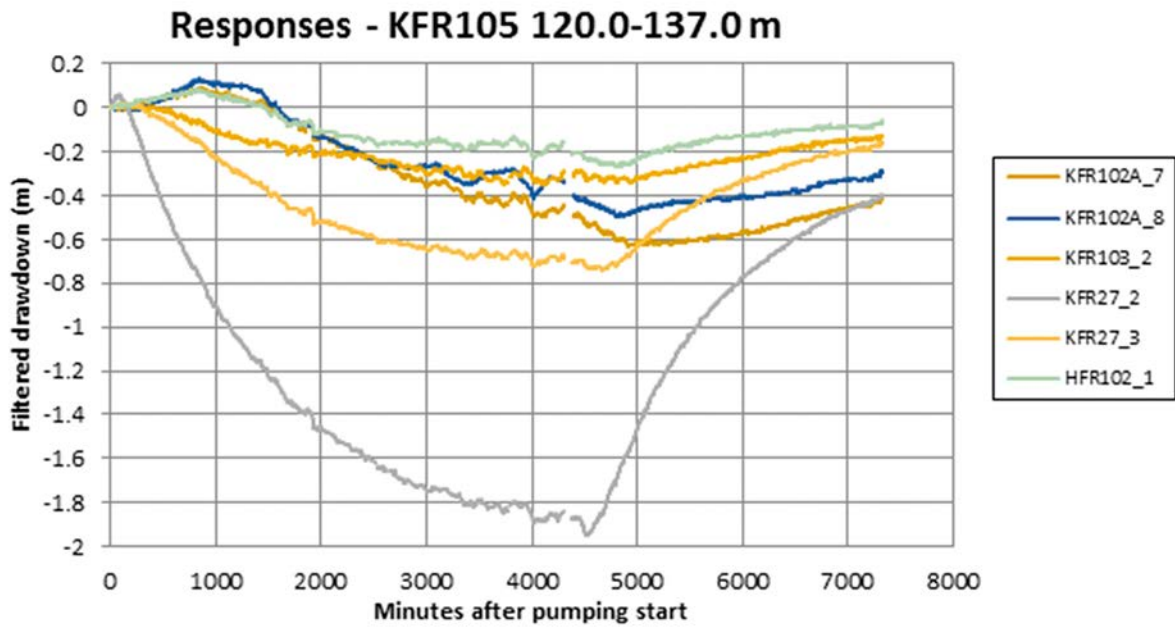


Figure A4-23. Filtered drawdown in observation sections showing a response at the test in KFR105: 120.0–137.0 m. Same figure in another scale in Figure A4-24.

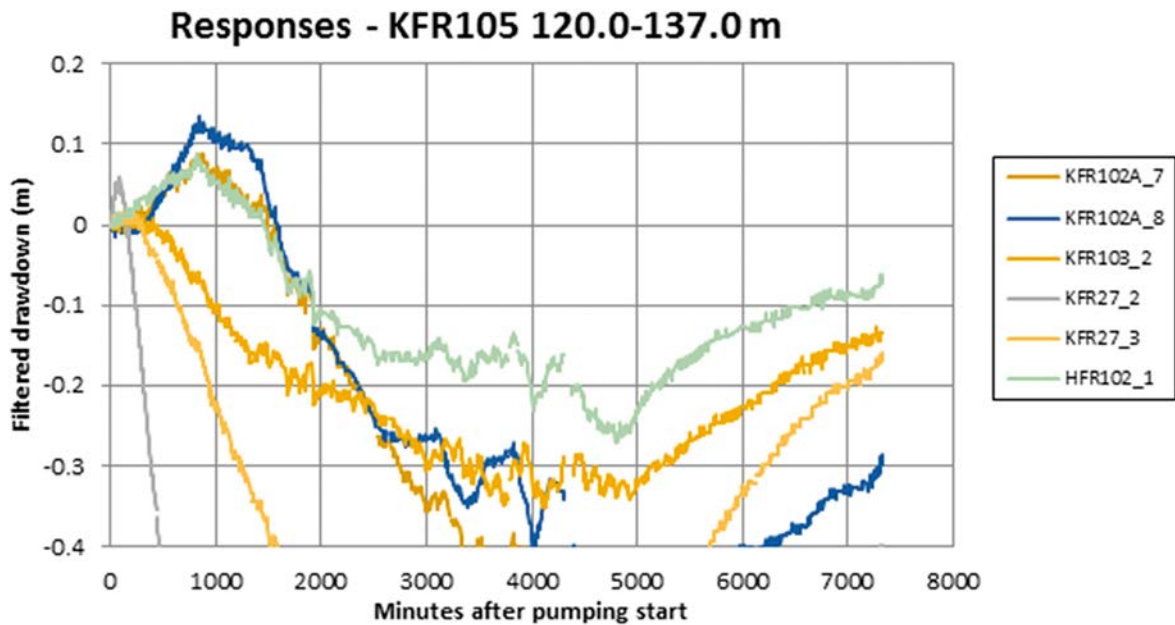


Figure A4-24. Filtered drawdown in observation sections showing a response at the test in KFR105: 120.0–137.0 m. Same figure in another scale in Figure A4-23.

Low confidence Responses - KFR105 120.0-137.0 m

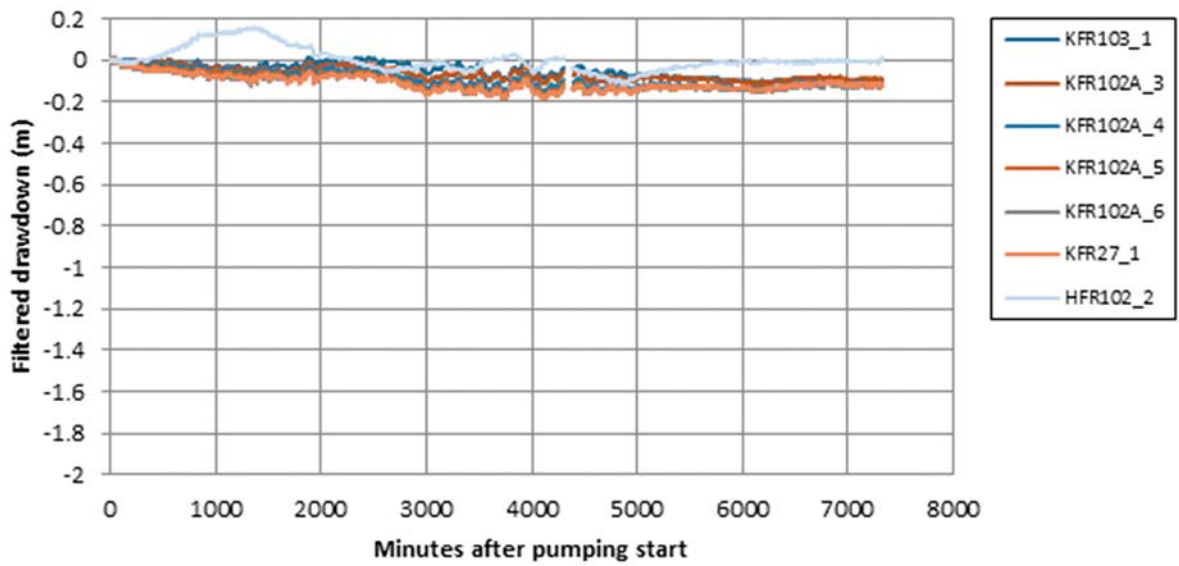


Figure A4-25. Filtered drawdown in observation sections showing a response with low confidence at the test in KFR105: 120.0–137.0 m. Same figure in another scale in Figure A4-26.

Low confidence Responses - KFR105 120.0-137.0 m

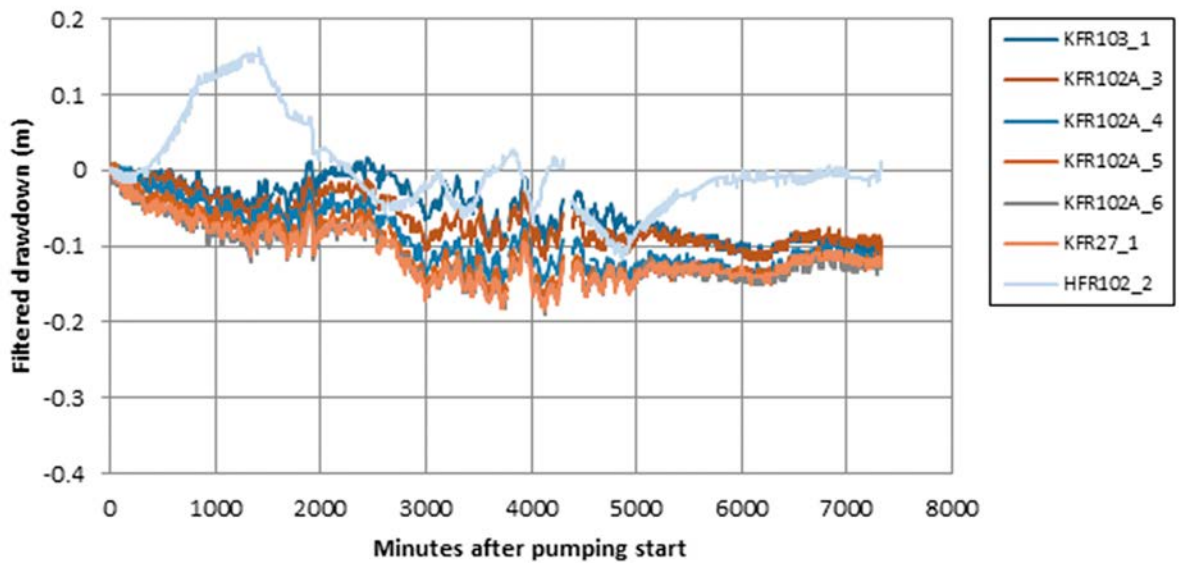


Figure A4-26. Filtered drawdown in observation sections showing a response with low confidence at the test in KFR105: 120.0–137.0 m. Same figure in another scale in Figure A4-25.

Non responses - KFR105 120.0-137.0 m

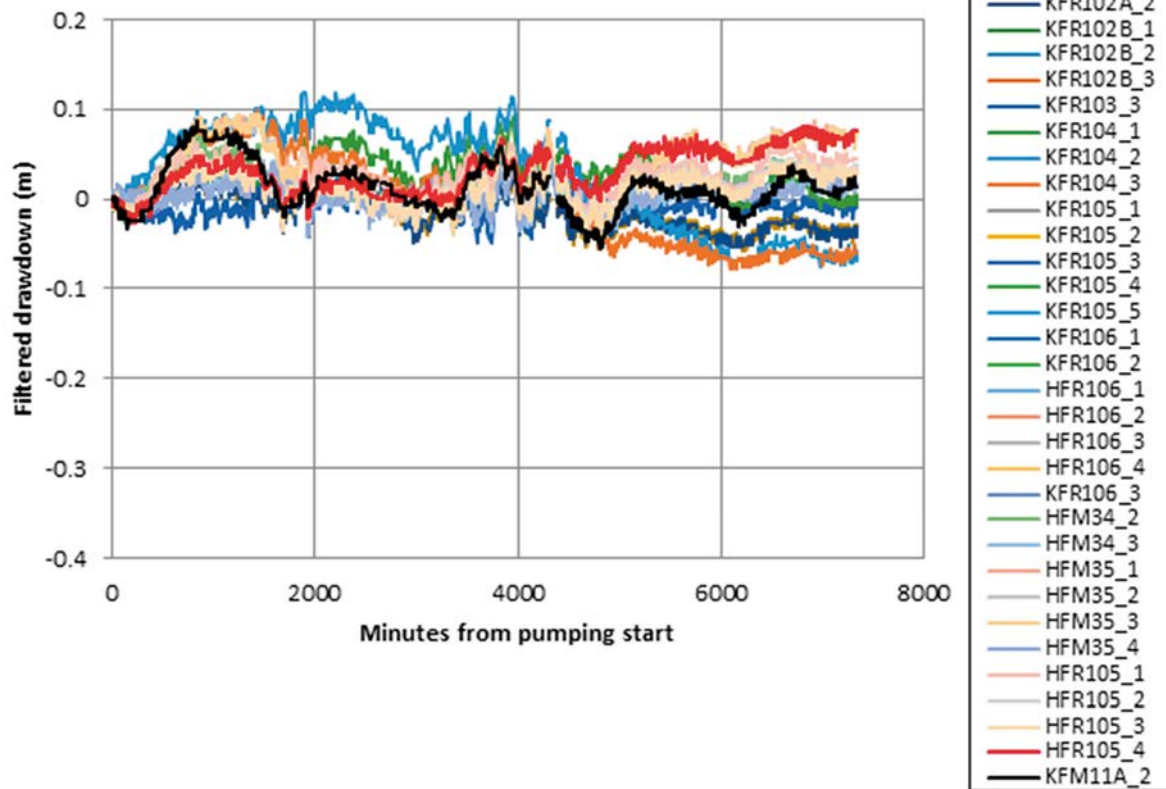


Figure A4-27. Filtered drawdown in observation sections not showing a response at the test in KFR105: 120.0–137.0 m.

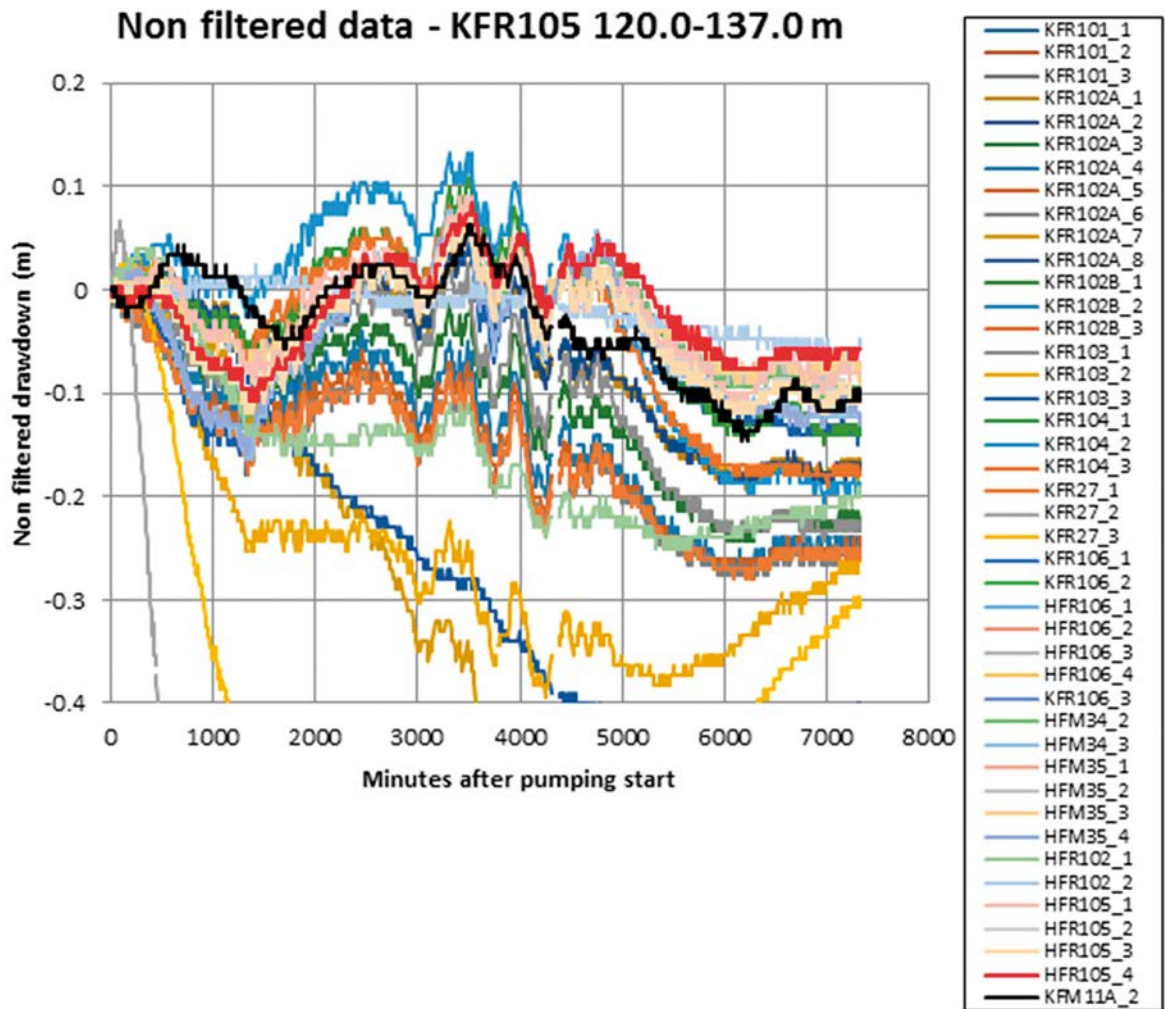


Figure A4-28. Non filtered data for all observation sections at the test in KFR105: 120.0–137.0 m.

SKB is responsible for managing spent nuclear fuel and radioactive waste produced by the Swedish nuclear power plants such that man and the environment are protected in the near and distant future.

skb.se